AN EXAMINATION OF THE ROLE OF OXYGEN IN THE WEAR OF FERROUS ALLOYS

VINOD K. SRIVASTAVA

AN EXAMINATION OF THE ROLE OF OXYGEN IN THE WEAR OF FERROUS ALLOYS

by

Vinod K. Srivastava, B.Sc., B.Sc.(Eng.), M.Sc. (Tribology)

A Thesis Submitted in Partial Fulfillment
of the Requirements for the Degree of
Doctor of Philosophy

Faculty of Engineering and Applied Science
Memorial University of Newfoundland

August 1974

St. John's Newfoundland

ABSTRACT

The wear of SAE 1080 steel under the conditions of unlubricated sliding is studied. The ranges of normal force and speed are 295-980 N and 0.193-1.544 m/s respectively. The specimen configuration adopted is of two coaxial hollow cylinders, 18.42mm mean diameter, rubbing at their annular end faces 2.54mm wide.

The environment of the rubbing surfaces is controlled by forcing air or oxygen-argon mixture between the specimens. The vibration in the machine is measured.

Wear debris particles are identified by x-ray diffraction and their size distribution determined. Wear surfaces are studied on an Optical and a Scanning Electron Microscope.

It appears likely that wear rate is governed by oxidation of an area at a little distance from the hot spot. A correlation has been found between the sliding speed which in turn affects the surface temperature with the wear rate. The surface topography is shown to be a function of speed.

In an environment of inert gas, the wear is of a severe type. When different mixtures of oxygen and argon gas are forced through the specimens, a significant change in the wear rate is observed.

The difference in mean temperature of the two rubbing specimens influences the wear rate. The specimen at higher temperature shows lower wear rate.

ACKNOWLEDGEMENT

The author expresses his sincere gratitude to his supervisor, Dr. J. Molgaard, for his careful guidance, interest and inspiration.

The technical assistance of Mr. R. C. Smith in X-Ray Powder Diffraction Work and Scanning Electron Microcopy, the frabrication of test rig by Mr. J. W. Tucker, Mr. R. A. MacLellan, Mr. S. V. Yetman and Mr. L. Spurrel of the Department of Technical Services, the assistance in experimental work by Mr. J. F. Conroy, Mr. W. J. Grenning and Mr. J. R. Haynes - undergraduate students, the typing by Miss C. Gardner and Miss L. Smith and the drafting by Mr. T. Dyer are gratefully acknowledged.

The author would also like to express his appreciation of the financial aid provided by Dr. J. Molgaard's National Research Council of Canada Grant, No. A-7095 and the Graduate Fellowship award by Dean F. A. Aldrich.

The provision of a home, away from home, by Mr. Kumud Acharya and his family helped considerably in accelerating the completion of the work.

TABLE OF CONTENTS

LIST OF FIGURES

LIST OF TABLES

NOTATION

a	Radius of Contact
A	Real Area of Contact
A_p	Arrhenius Constant for Parabolic Oxidation
A_L	Arrhenius Constant for Linear Oxidation
B	Constant
d	Distance along which a Wearing Contact is made
D_i	Inside Diameter of the Specimen
D_o	Outside Diameter of the Specimen
f	Coefficient of Friction
h	Thickness of the Wear Particle
K	Archard's Wear Coefficient
K^1	Quinn's K^1 Factor
l	Length of Wear Particle
L	Sliding Distance
N	Normal Load applied to the Specimens
P	Hardness
Q	Activation Energy for Linear Oxidation
Q_p	Activation Energy for Parapolic Oxidation
R	Gas Constant
t	time
T	Torque
V	Sliding Speed
V_W	Wear Volume

X	Deflection of the Galvanometer in U.V. Recorder
α	Pitch Cone Angle
γ	Strength Coefficient of Material
Θ	Temperature
Θ_A	Ambient Temperature
$\Theta_A + \Theta_B$	Total Bulk Surface Temperature
Θ_C	Contact Temperature
Θ_S	Source Temperature

CHAPTER 1

INTRODUCTION AND OBJECTIVES OF THE CURRENT RESEARCH

The majority of problems encountered in situations where two surfaces slide against each other, under the action of a normal load, are attributed to poor lubrication practice, wrong selection of materials, bearings and improper understanding of the sliding mechanism. Usually the breakdown of the sliding components takes place through wear, which manifests itself in a variety of ways and forms. The cost of replacing the worn components, their frequency of replacement and downtime of a machine because of wear problems are matters of serious concern for a variety of industries.

The need for machine components capable of withstanding much higher pressures, sliding speeds and temperatures cannot be fulfilled until a proper understanding of the mechanism of wear and its controlling factors has been developed. It will be true to say that for sliding components, some kind of lubricant is often present between the two rubbing surfaces. However, details of this wear process, because of the interaction between rubbing surfaces and the lubricant, are complicated and in order to develop a proper understanding of the wear process, it is necessary that the variables affecting the wear mechanism be reduced to a minimum.

If the mechanism of wear, without bringing the complications of the lubricant performance and its interaction to the sliding

surface, can be established, the problems of lubricated wear will be easier to solve. For the current investigation it was decided to concentrate on the study of the Unlubricated (or Dry) Wear.

In most sliding situations the environment of the sliding surfaces contains oxygen and a reaction of oxygen with the metal is part of the wear process. The frictional heat generated at the rubbing surfaces flows from the point of contact into both of the contacting bodies and, consequently, a temperature field is developed at the rubbing surfaces and within the rubbing bodies. The temperature field influences parameters like the structure of the rubbing materials, the interaction between the surfaces, topography and the formation of oxide at the rubbing surface.

As discussed in the following two chapters, it seems necessary in order to develop an understanding of the wear process, to pursue the following specific questions.

Is the wear rate governed by the hot spot oxidation or the general surface oxidation?

Is there a correlation between the mean surface temperature, the composition of wear debris particles and the composition and topography of the thin surface layer at rubbing interface of the specimen?

How does the partial pressure of oxygen, in an oxygen-inert gas mixture, influence the wear rate?

How does the wear rate of the rubbing specimens depend on the accessibility of gas?

Does the difference in mean surface temperature of the two rubbing specimens influence the wear rate? If it does, what is the extent of this effect?

In the following chapters, the background for this research will be discussed in some detail and the equipment, results obtained with it are described and discussed.

CHAPTER 2

CHOICE OF THE PROBLEM

2.1. General

In situations where interacting surfaces move relative to each other, breakdown of the sliding components is the major cause limiting the life and performance of the machinery. The breakdown often takes place through wear* which may be catastrophic, fast, slow, or very slow but finite. Thus, wear may be either destructive or acceptable within a given design, but even when acceptable, it may be more severe than desirable because of the frequency of part replacement.

Breakdowns, due to wear, can be avoided by sound lubrication design and practice. However, there are no established codes for the design of all sliding components. The design criteria for selecting standard sliding components come from the manufacturers of these components, who maintain guides for the selection of the components. The manufacturers guides are based on laboratory experiments, performed under controlled conditions of test variables. These components, when used in the actual service conditions, may undergo premature failure, and in applications with continuous and/or automated production or operation of plants, the breakdown of the single component may have serious economic consequences.

---

* Wear is defined as change in dimensions of the rubbing body and/or change in composition where change occurs at the mating surface.

Wear is a design and maintenance problem in most industries. However, in the following sections, its relationship to Ocean Engineering problems is illustrated.

2.2. Breakdowns in the Auxiliary Machines of Ships

Ships, when at sea, are isolated from their major sources of mechanical parts. Any breakdown of prime movers, running gears of the engine proves to be serious. Many mechanical components related to ocean trade are specially designed to meet the pecularities of ship's environment. In the design and practice of the marine lubrication, parameters like the ocean environment and seawater must be considered in addition to the other variables which are common to most other lubricating systems.

2.2.1. Examples of Bearing Failures in Marine Equipment

In the area of "Bearing-Failures", three reports have been published by the Naval Engineering Test Establishment, (NETE), Lasalle, Quebec. (Reports No. 1, 2 and 3). These reports resulted from a project raised by Canadian Forces Headquarters (CFHQ) for the NETE to investigate specific instances of the chronic bearing failures.

It was found that the factor which contributed the most to a high unreliability factor in bearing performance was an inadequate knowledge of the technology of the bearings and their lubrication.

2.2.2. Piston Ring and Cylinder Liner Wear

The last decade has been one of the intensive development in the marine engineering. It has seen the virtual disappearance of the naturally-aspirated direct drive diesel engines as propelling machinery for new ships; the emergence of direct driven supercharged diesel engines as predominant prime mover, and an ever increasing demand, on the part of users, for higher efficiency and output power.

A variety of scavenging systems are employed in conjunction with exhaust gas driven turbo chargers operating on either pulse or constant pressure driven systems to achieve the higher efficiency, power and smaller weight to power ratio.

The much higher mean and maximum pressures and temperatures encountered with turbo charging brought ring and liner wear into the forefront of serious problems on almost all marine engines. Wear of piston rings and cylinder liners increases the clearance between the two; causing a pressure drop in the cylinder due to leakage, and thus a reduction in the output power of the engine. Increased oil consumption, sooty exhaust and contamination of the crank case oil with combustion products, are few of the other affects of ring and liner wear. These effects cause the wear to propagate and many other consequences follow: like the breakdown of the lubricant film, scuffing of the ring and the introduction of unnecessary vibration in the system.

In fishing vessels the trend for next several years seems to be towards high powered, high speed, marine diesel engines which have lower cost per horse power and high durability level. (Palmer, 1970)

2.3. Area of the Needed Research

There is a need for reliable, medium and high speed, both two cycle and four cycle diesel engines with smaller weight to power ratio and relatively higher efficiency for use in all kinds of vessels - from large ocean going ships to small outboard motor boats, including ferries, tugs, fishing boats and naval vessels.

An important factor affecting the life and performance of marine diesel engines is the piston ring and cylinder liner wear. While the use of chromium plated piston rings, improved temperature control and the use of modern oils have reduced the corrosive wear to small proportions, the wear of cylinder liners and the piston rings which arises from the interaction between hot spots of two surfaces in relative motion is still a problem, limiting the performance of diesel engines.

The mechanism of ring and liner wear is not completely understood and, in fact, the present knowledge of the operation of piston rings is not sufficient to enable them to be designed to meet any precise quantitative performance characteristics. The operation of the rings is affected by a number of interacting factors, such as pressure, piston speed, temperature, contact area, structure of the rubbing materials, surface topography, hardness, vibration in the system and environment (both around the machine and at the wearing interface).

The direction in which these parameters affect the wear rate is more or less established within certain limited ranges but no one knows the mechanisms by which these parameters effect the wear rate.

The use of laboratory tests has met with limited success in the prediction of actual service life. Before a satisfactory scale can be established for transferring the small scale laboratory experiments to actual service conditions, proper understanding of the fundamental aspects of individual parameter need to be established.

Thus, the problem is to develop a proper understanding of the mechanism of wear and its controlling factors. This is also true of wear in many other types of machinery.

The high rise in temperature at sliding contacts has been known for some time. There have been some investigations involving the measurement of temperature actually occurring at the asperity contacts. The effects of surface temperature on the wear of Diesel Engine Cylinder and Rings have been studied by some workers, Nault, Lander and Edgar, (1954); Sreenath and Venkatesh, (1970); Neale, (1971). There is still some considerable uncertainty about the details of the wear process, with the interaction between rubbing surfaces and the lubricant present further complicating the already unclear picture of the wear of cylinder and rings.

The general picture is that steep temperature gradients are found through the walls of a cylinder or liner at areas adjacent to combustion chamber because the high temperatures and pressures and extreme turbulence of the gas in these areas cause high rates of heat flow into the relatively cool walls. The metal temperatures are influenced by the wall thickness and the coolant temperature as well as by the conductivity of metal.

In the majority of cases, the wear of piston rings and the cylinder bore occurs initially at the top ring, which has the highest peak pressure and temperature. The damage generally spreads to the other rings and also to the surface of the piston.

The wear of piston rings and cylinder liners is an example of wear processes where the environment of the sliding surfaces contains oxygen and the reaction of oxygen with metal is part of the wear process.

The mechanism of this wear process needs investigation and indeed is subjected to study at the present time, as discussed in the following chapter. The expectation is that the considerable body of knowledge existing now on the oxidation of metals can be usefully applied to the understanding of this type of wear process.

CHAPTER 3

EXISTING THEORIES OF WEAR

3.1. General

During the relative motion of two bodies, sliding on one another, heat is generated in a thin surface layer as a result of the deformation of material involved in the formation and breakdown of frictional bonds. The heat flows from the point of contact into both of the contacting bodies and consequently a temperature field is developed at the rubbing surface and within the rubbing bodies. The temperature field in the two bodies may be either symmetrical, ie. the temperature gradients are the same in both specimens at the same distance from the rubbing surface, or asymmetrical.

In either case the temperature field influences the parameters like the surface structure of the rubbing materials, interaction between the surfaces, topography, hardness and formation of the oxide at the rubbing surface.

The following sections contain a brief survey of the studies of the wear of ferrous alloys where reaction of oxygen with metal plays a part.

3.2. Survey of Literature

Fink and Hoffman (1932) observed that under certain conditions, a wear rate could be reduced by running the test in an inert atmosphere and assumed that, in air, the surfaces are chemically activated by rubbing together and form oxides which by penetrating and destroying the coherence of metal, cause wear particles to be detached.

Kerridge (1955) explained a mild wear process as a three stage mechanism involving the transfer of metal, its conversion to oxide and removal of oxide to give loose wear products. The wear debris particles were identified as α-Fe_2O_3 and α-$Fe_2O_3 \cdot nH_2O$.

Kerridge and Lancaster (1957) studied a severe type of wear and suggested that the wear process occurs in two distinct stages, namely the removal of metal from wearing surfaces by transfer and the formation of wear debris particles from a transferred layer on the opposing surface. It was found that the rate of transfer of metal determines the wear rate while Kerridge (1955) previously maintained that for mild wear, the rate determining factor is the oxidation rate.

Archard and Hirst (1957) observed back transfer from one rubbing surface to the other and then back to the original surface in the equilibrium state of wear. The transferred material was wholly or partially oxidized.

Lancaster (1957) observed that a reduction in wear rate was associated with an increase in contact resistance because of the formation of an oxide film.

Cocks (1957) designed an experiment to study the role of atmospheric oxygen at high speed of rubbing. The formation of oxide was confirmed by a dropping of the coefficient of friction to low values. At low loads wear was found to be due to metallic welding, whereas at high loads, the wear process was one of oxide disintegration. The wear debris particles were identified at α-Fe_2O_3.

Johnson and his co-workers (1957) found that at higher velocities of sliding, a black powder (identified as FeO) was produced. It was noticed that Fe_3O_4 prevents surface damage while Fe_2O_3 induces severe wear and welding.

Yoshimoto and Tuskizoe (1958) postulated that the mechanism of wear is dependent on the real area of contact. Wear was classified as being mechanical wear, Fe_2O_3 film wear or Fe_3O_4 film wear. Oxidation during wear was assumed to follow a linear oxidation law and wear was assumed to be taking place entirely from within the continuous oxide film.

Welsh (1965) found that the wear rate and type of wear is more a function of the load, rather than the rubbing speed. Three transition loads were identified at which changes from one form of wear to the other takes place. Any reduction in the wear rate was accompanied by the formation of the oxide debris particles. The extent and the type of surface oxidation that can occur affects the type of wear taking place.

Molgaard and Grosberg (1967) noticed that an oxide layer of very small thickness was always present between rubbing bodies and the division of heat between the rubbing surfaces was markedly affected by the oxide layer.

Earles and Powell (1967-a) found that, depending on the load and the rubbing velocity, either a continuous or near continuous oxide film is present between the rubbing surfaces. These oxide films are detached leaving the metallic substrate, producing wear debris particles. The time history of the formation of oxides at a rubbing surface was in line with the time history of wear. The steady state coefficient of friction was observed to be a function of (Load) $^{1/2}$x (speed).

Earles and Kadhim (1967) observed that for unlubricated sliding at high speeds between a copper (pin) and steel (disc) surfaces, a continuous oxide layer is formed on the disc track with increasing normal load. The coefficient of friction was shown to decrease with load and sliding speed and a function of (Load) $^{1/2}$x speed.

Earles and Powell (1967-b) noticed that if load is kept constant and speed is varied the wear rate first increases with speed and then decreases, the maximum value being associated with the region in which the effect of surface breakdwon is most pronounced. The sliding wear rate was observed to be dependent on both the specimen and the track surface condition.

Earles, Hayler and Powell (1970) measured the surface temperature of pin and predicted the total surface temperature by considering the heat flow through an idealised single asperity tip and from existing

theories of Jaeger (1942), Archard (1959) and Barber (1967). The friction coefficient and transitions in sliding process were shown to be related to the predicted total temperature.

In order to estimate a criterion for the formation of wear debris particles, Earles and Powell (1968) found that the oxide layer generated by sliding, builds up to a critical thickness before becoming detached from the substrate for form a wear particle.

Clark, Pritchard and Midgley (1968) investigated the mild wear of various steels sliding unlubricated in dry CO_2. The wear debris particles were entirely oxides, α-Fe_2O_3 and Fe_3O_4. The wear rate was postulated to depend on the type of oxide at the rubbing surface. Fe_3O_4 was assumed to provide a protective layer at the surface and hence reducing the wear rate.

deGee (1967) showed that, in general, relatively thick films inhibit adhesion between sliding surfaces and thus reduce friction and wear. If a reduction in the availability of oxygen results in the formation of monolayer films, adhesion is increased.

Quinn (1962) observed that mild wear of unlubricated steel specimens principally involves the oxidation of newly exposed metal at hot-spot temperature between the contacting asperities.

Quinn (1968) demonstrated the advantage to be gained from using Electron Microscopy and X-Ray Diffraction in studies of unlubricated sliding. He confirmed a consistent mechanism of wear through thermal and/or mechanical fatigue. A correlation was noticed between the temperature of oxidation, indicated by presence of certain oxides in wear debris and the temperature expected to occur at the contacting asperities (Quinn, 1971).

In the following section, the models of wear proposed by Archard (1953, 1968) (and modified by Finkin (1964) and Rowe (1968)), Suh (1973, 1974), Yoshimoto and Tsukizoe (1958), Quinn (1962, 1967, 1969 and 1971) and Earles (1967-a, 1967-b and 1971) are briefly described.

3.3. Wear Models

3.3.1. Archard's Model

Archard (1953, 1968) assumed that the contact process consists of making and breaking of junctions. This is shown in Fig. 3.1. Consequently the distance of interaction of a single interacting asperity is only the length of the junction. The real area of contact of contacting surfaces, as distingulshed from the apparent or geometrical area of contact, is the instantaneous sum of the areas of all junctions.

For convenience, it is assumed that the junction consists of a circle of radius a, resulting in contact area, πa^2. The asperity interaction may or may not produce a wear particle, but if it does, it is further assumed that the depth of the wear particle is proportional to a. Thus the volume, δVw, of the worn particle is proportional to a^3, and the sliding distance, δL, in which the event has occurred, will be proportional to the size of contact, a.

Expressing wear rate in terms of volume removed per unit sliding distance, the contribution of this event to the total wear rate, is $(\delta Vw/\delta L)$ and is proportional to a^2, (ie. to δA). Thus, the contribution

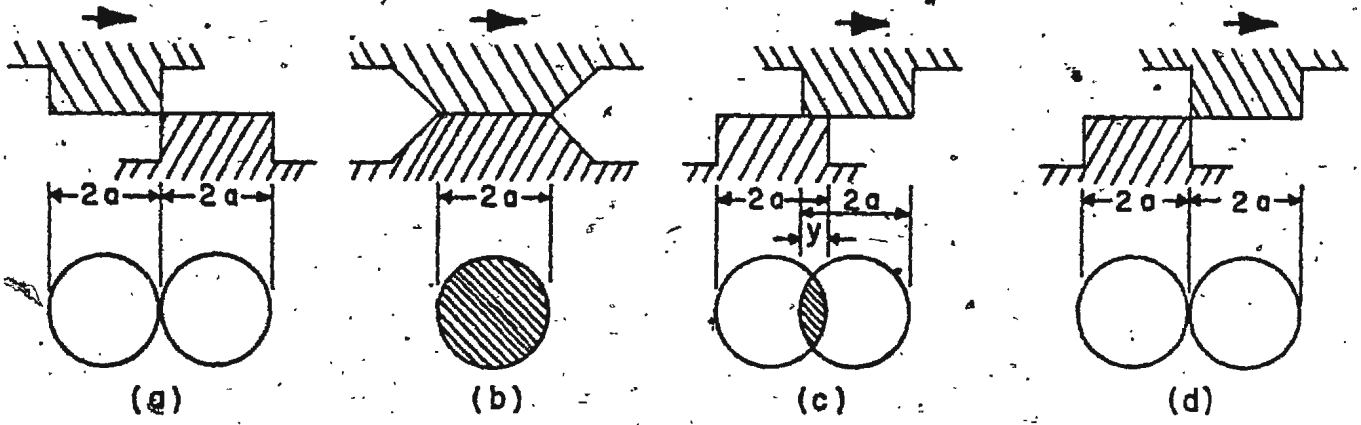

(a) APPROACH OF JUNCTION FORMING ASPERITIES
(b) MAXIMUM CONTACT AREA OF RADIUS "a"
(c) AFTER SLIDING THROUGH A DISTANCE "y"
(d) AFTER SLIDING THROUGH A DISTANCE "2a"

FIG- 3·1

IDEALISED REPRESENTATION OF ARCHARD'S MODEL OF CONTACT IN SLIDING SURFACES

of each event to the total wear rate is proportional to its contribution to the total true area of contact. More specially, if one assumes that particles are hemispherical, of radius, a, and that $\delta L = 2a$ then

$$\frac{\delta Vw}{\delta L} = \frac{\delta A}{3}$$

This model does not concern itself with the mechanics leading to the particle formation. It relates wear to the total area of contact, and assuming contact to be entirely plastic and the wear particles to be hemispherical in shape, states.

$$V_w = \frac{KNL}{3P}$$

where Vw is the wear volume, N is normal load, L is sliding distance, P is flow pressure (hardness) of the softer of the two contacting materials, and K is wear coefficient which is generally interpreted as probabilities of an asperity interaction giving rise to a wear particle.

Finkin (1964) examined the shape of the wear particles for common metals and found significant differences. 'K' really lumps together the probabilities of wear particle formation and factors concerning the shape of wear particles.

Rowe (1968) derived an expression which relates wear coefficient, K, to the probability of wear particle formation, P, and mean thickness-to-length ratio of the wear particle, (h/l). In its modified form, this relation may be written as

$$K = 2 \left(\frac{h}{l}\right) P$$

This equation contains all assumptions of Archard model.

2.3.2. Suh's Model

Suh proposed a model for the wear of metals under low speed sliding conditions which was presumed to be different from the generally accepted adhesion models.

According to Suh's model, the ultimate failure of the surface due to gross wear is caused by the following mechanisms:

- "Plastic deformation of the surface layer due to the traction exerted by friction at the surface.
- Subsurface void and crack formation due to the plastic deformation, especially around large inclusions and secondary phase particles.
- Subsequent crack propagation and void growth, which eventually link up with neighbouring cracks and voids to form long sub-surface cracks along a direction nearly parallel to the surface.
- Formation of loose wear particle wear sheets when the sub-surface cracks shear to the surface."

3.3.3. Yoshimoto and Tsukizoe's Model

Yoshimoto and Tsukizoe are among the more recent authors to consider, in detail, an oxidation process as part of a wear mechanism. By assuming a model which represents the profile curve of metal surface, Yoshimoto and Tsukizoe calculated the number and size of individual area of contacts. The wear depends on real area of contact and it occurs entirely from within the continuous oxide film. Every contact

produces a wear particle., The oxidation rate was assumed to follow a linear oxidation law.

3.3.4. Quinn's Model

Quinn's model of wear is based on the Archards' wear equation

$$W = K^1 \cdot A$$

where W is the wear rate (measured in terms of volume removed per unit sliding distance), K^1 is K^1 factor and A is the real area of contact between the sliding surfaces..

The K^1 factor is visualised as being the probability of producing a wear particle during an asperity encounter. It is assumed that on the average, $1/K^1$, asperity encounters are necessary (at a given asperity contact) for a critical oxide film of thickness (ξ_c) to be built up before it becomes detached to form a wear particle. It is further assumed that the total time (t) to produce a wear particle of thickness (ξ_c) is the sum of all the ($1/K^1$) individual encounters.

Wear of metal surfaces occurs when the oxide layers, formed at the few but relatively large areas of real contact, become fatigued, crack and flake off. As soon as one of the interfacial contacts is finished, another is fully established, so that at all times during the period of established wear rate, the real area of contact is subjected to oxidation at contact temperature. This assumption implies that one can equate the total volume of oxide formed at the real area of contact with the total volume of wear formed during the time of an established equilibrium wear rate.

By assuming a parabolic dependance of oxide growth per unit area upon time, Quinn has developed an expression for K^1.

$$K^1 = \frac{d \cdot A_p \, e^{-(Q_p/R\Theta_c)}}{\xi_c^2 \cdot \rho^2 \cdot V}$$

where d is the distance along which a wear contact is made, A_p is the Arrhenius Constant for parabolic oxidation, Q_p is the activiation energy for parabolic oxidation, R is the gas constant, Θ_c is the constant temperature, ξ_c is the thickness of wear particle, ρ is the density of oxide and V is the sliding speed.

Quinn maintains that "If one assumes appropriate values for Q_p, A_p, ξ_c and d, together with experimentally determined values of Θ_c, it is possible to predict the K^1 factor and thence the wear rate. There are, however, too many 'adjustable' parameters especially Q_p and A_p for this theory to be acceptable in the form evolved so far".

3.3.5. Earles's Model

A simple steady state model has been chosen with contact between sliding surfaces occuring at only one asperity (See Fig 3.2). This asperity is assumed to remain continuously in contact with the opposing surface until an oxide wear particle is formed. The process is then repeated with another asperity.

The real sliding process consists of series of collisions between asperities of the opposing surfaces because neither can be considered as smooth. Consecutive collisions for a given asperity may be infrequent

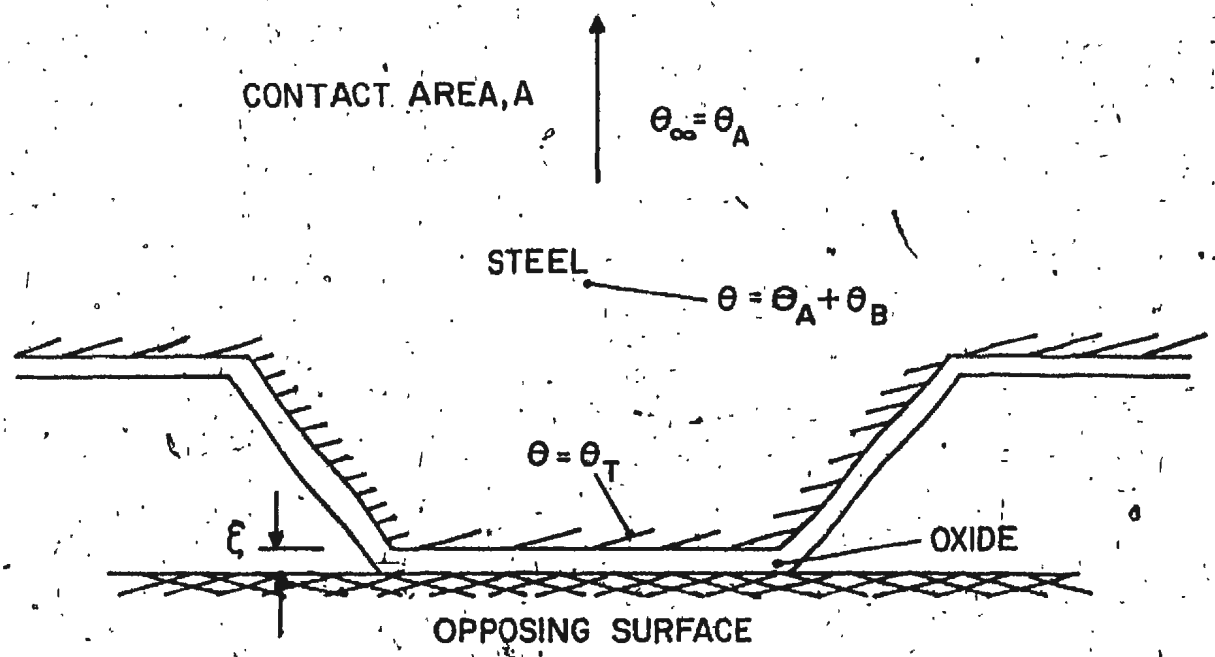

FIG. 3-2
EARLE'S ASPERITY CONTACT MODEL

so that the time spent with the asperity at total bulk temperature is much greater than that at total temperature at the asperity tip.

"The total bulk temperature is representative of the effective surface temperature controlling the wear mechanism."

The oxide layer generated by sliding builds up gradually to a critical thickness before becoming detached from the substrate to form a wear particle. The oxide can fail either by cracking, when the stress in oxide exceeds a critical value, or by blistering, when the adhesion strength of oxide/substrate interface is exceeded.

For the formation of a wear particle, impact of asperities is necessary, ie. failure will not be by a mechanism of static oxidation alone. A salient feature of the model proposed by Earles is the inclusion of the variation of the deformation resistance of metals as a function of temperature, according to the expression

$$P = P_o \exp(\gamma/(\Theta_A + \Theta_B))$$

The value of P is taken as 3 x (Yield Stress corresponding to total bulk surface temperature of the pin, $(\Theta_A + \Theta_B)$). γ is the strength constant for the material.

Assuming a linear dependance of oxidation rate on time

$$\xi = (\frac{AL}{B})t$$

(where ξ is the oxide film thickness built up in time t, AL is the Arrhenius constant and B is a constant in equation).

Earles has developed the following equation for the wear rate:

$$(\frac{N}{W}) = \frac{P_o \cdot B}{AL} \cdot \exp((\frac{Q}{R} + \gamma)/(\Theta_A + \Theta_B))$$

where N: normal load

W: wear rate

P_o & γ : as defined earlier are hardness and strength constant for material respectively.

A_L : Arrhenius constant for linear oxidation

Q: Activation energy

R: the gas constant

ε $(\Theta_A + \Theta_B)$: total bulk surface temperature of pin.

CHAPTER 4

DESIGN CRITERIA FOR THE RESEARCH EQUIPMENT

All the experiments were carried out under the conditions of unlubricated sliding. This is because:

-A lubricant adds an additional variable which is left out during this first stage of a longer term studies. The equipment can however be used with a lubricant, with some modifications.

-There are sliding components where rubbing takes place under dry conditions and design criteria for minimum wear of rubbing surfaces are not yet established.

In the following sections, a discussion of the factors which influenced the design of Wear Test Rig are presented.

4.1. Symmetry - Mechanical and Thermal

A symmetrical temperature field is one in which temperature gradients are the same in both specimens at the same distance from the rubbing surfaces.

Most reported studies of unlubricated wear have been carried out in thermally asymmetric situations, which simulate the conditions encountered in field applications. It is intended that this test rig can duplicate such situations to some extent.

However, when there is thermal asymmetry, the wear process differs on the two surfaces as is evident in the common occurrance that the wear rate of one of the two rubbing surfaces is significantly greater than the wear rate of the other surface. The interpretation

of the wear process on either surface is not complete unless the state of both specimens is taken into account.

The interpretation should be simpler, in a formal sense, if both specimens are completely identical, not only in geometry and material, but also in thermal conditions. (In fact, this condition adds some subtlety to an interpretation in that, on the average, whatever is postulated to occur on one surface is equally likely to occur on the other.)

4.2. Constant Contact Pressure

The mean contact pressure between two specimens was kept constant during a run. This was achieved by having constant wear land and by using dead weight loading. Dead weight loading was preferred against spring loading, because of the ease of application and low stiffness, which, however, can be increased through viscous damping through a variable restrictor (valve) on the hydraulic line.

4.3. Vibration

In the ideal case, vibration should be completely eliminated from the test rig. However, minimization of vibration was an important design criteria.

4.4. Variable Stiffness

A review of literature indicates that one of the reasons for inconsistencies in wear results is the stiffness of various test rigs.

The proposed wear rig has the provision where stiffness is not varied, rather variable damping is provided.

4.5. Environment Control

Since the main object of the present experiment is to study the role of oxygen in the wear of steel, it was important to design a gas supply system where gases can be mixed in desired proportions. The gas mixture is forced to the wearing contact area. This makes sure that the environment between the two test specimens, as well as around the specimens, is controlled.

4.6. Recording

Load, frictional torque, mean temperature of contact surface, gas pressure, wear of specimens and vibration are measured continuously.

CHAPTER 5

CHOICE OF MATERIAL USED

In this section, the considerations that lead to the choice of material used in these experiments are given.

The criteria for selection of the material were:

It should be representative of materials used for machinery parts requiring good wear resistance.

It should show simple metallurgical changes which can be correlated to the temperature attained by test samples during rubbing.

It should form more than one oxide so that the oxides found in wear debris can provide indications of the temperature during wear.

An eutectoid iron-carbon alloy meets these conditions as its structure is completely pearlitic, when annealed. Iron forms three oxides FeO, Fe_3O_4 and Fe_2O_3 of which FeO only forms above about 570°C. Carbon steels are also a very common material for sliding components of machinery.

An additional indication of temperature fluctuations experienced by the material during wear, can perhaps be obtained from the hardness of the material at different depths below the surface, since this material can be quench hardened and tempered. Work hardening could, however, be a complication, so hardness values can only be interpreted in conjunction with observations of structure.

The material used was Atlas Alloys Alpha-8 steel, which had the following analysis (supplied by the steel company).

	%
C	0.82
Mn	0.20
P	0.014
S	0.023
Si	0.18
Fe	Rest

The steel was supplied in the form of cylindrical rod 57mm in diameter and 1.5m long. From this rod, 50mm long sections were cut. These cylindrical bars were annealed by putting them in furnace at 825°C. for 6 hours and then allowing them to cool slowly in the furnace. Test specimens were made from these annealed bars.

The structure of the steel, in the annealed state, was completely pearlitic (Ref. Photograph 5.1 and 5.2).

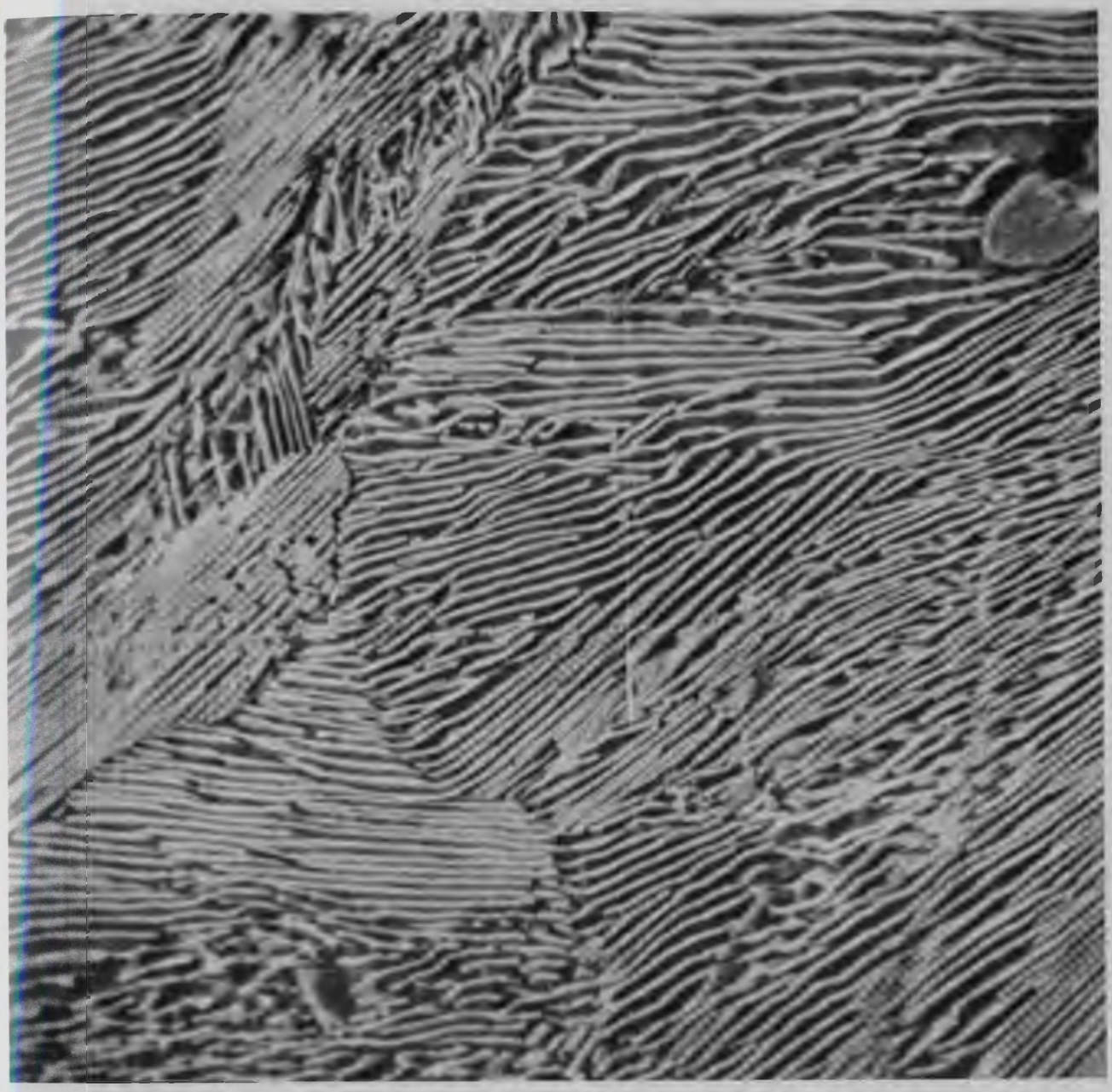

STRUCTURE OF THE STEEL IN THE ANNEALED STATE (x 2400)

PHOTOGRAPH NO. 5.1

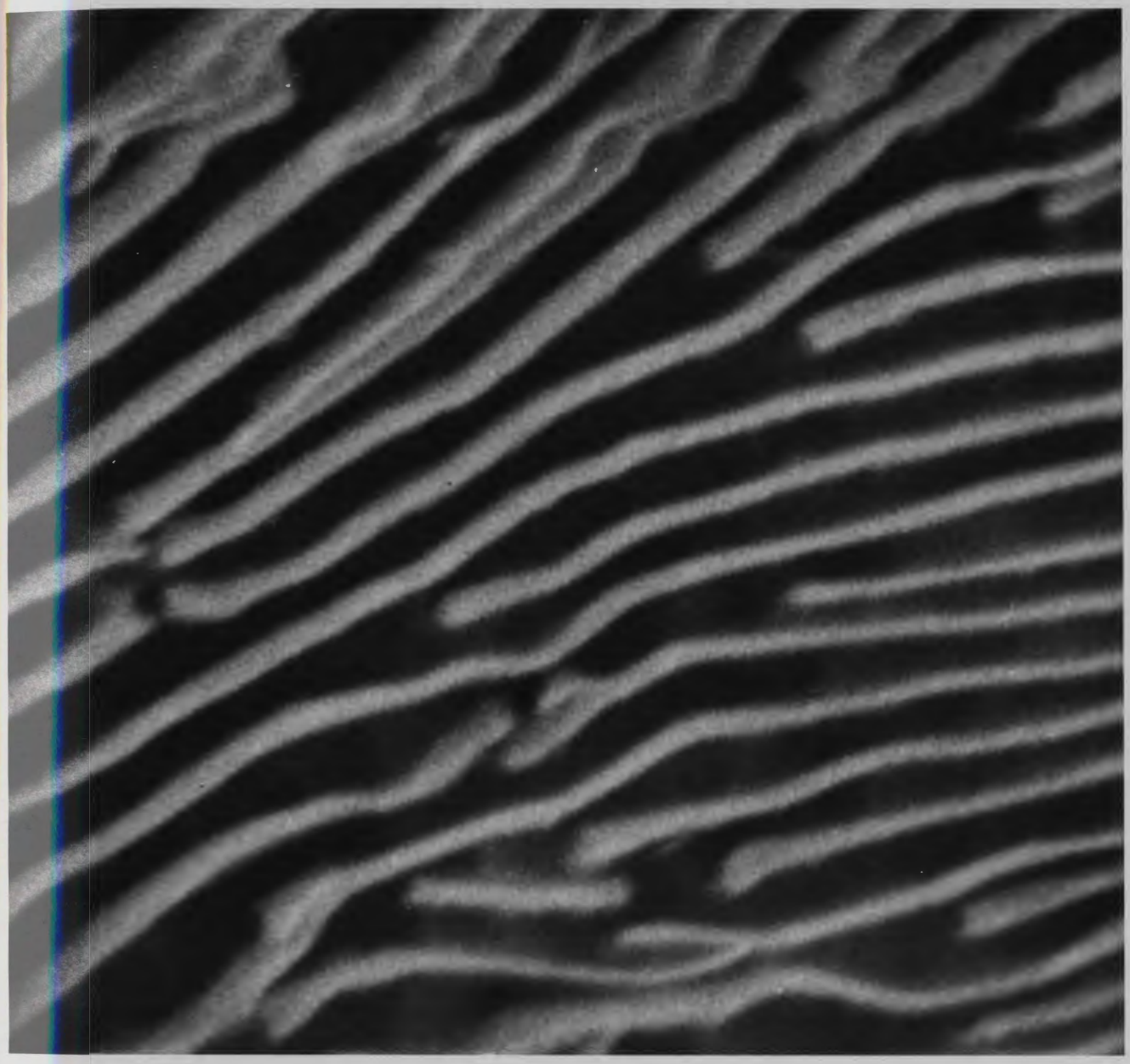

STRUCTURE OF THE STEEL IN THE ANNEALED STATE (x 12000)

PHOTOGRAPH NO. 5.2

CHAPTER 6

DESCRIPTION OF EQUIPMENT

6.1. General

The equipment consists of the specimens being studied, a mechanical means for holding the specimens and rubbing them together, a system for mixing and supplying gas mixtures to the rubbing interface and the devices for collecting wear debris and monitoring forces, temperatures, vibration and displacement due to wear at the specimens.

The items are described in the following, section by section, including some aspects of the stages by which development of the equipment took place, a development mainly to overcome mechanical problems and meet the design requirements of stiffness and low levels of vibration.

Readers who are not concerned with the details of all portions of the equipment and its development may nevertheless find the sections marked by asterisks of revelance to the discussion of the experimental result.

*6.1.1. Specimen Configuration

The specimen configuration adopted is of two coaxial hollow cylinders, rubbing at their annular end faces. This configuration is shown in Fig. 6.1.

This is the only configuration which permits continuous contact between identical specimens. It also has the advantage that a

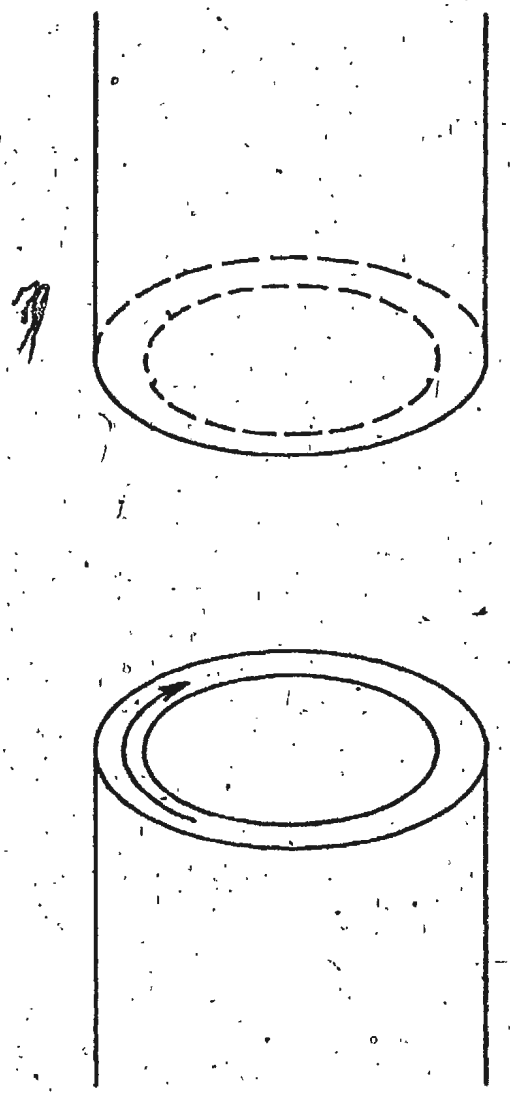

FIG. 6-1
SPECIMEN CONFIGURATION
(SCHEMATIC)

gas-mixture can be fed between the specimens, via the rubbing interface, controlling the environment of the rubbing surfaces (See Fig. 6.2).

Fig. 6.3 illustrates very schematically the layout of the specimens, specimen holder, shaft and loading devices.

Each specimen is attached to a holder. The general design for a specimen holder is a block of carbon steel to which the specimen is fastened. Heating elements are embedded in the carbon steel block so that the effective ambient temperature of the specimen can be varied and controlled. The heating block is mounted to a stainless steel portion of holder, where the stainless steel is chosen for its low thermal conductively to act as insulator. The next section of each specimen holder has facilities for a coolant, to protect the rest of equipment from the heat generated in the specimens or in the block heaters.

Details of the specimen holders are given in the following sections describing the development of the equipment. The stationary specimen holder, in particular, was developed through several stages of testing and redesign.

*6.1.2. Rotating Specimen Holder

The holder for rotating specimen was mounted on a collet chuck. Power leads, thermocouples and coolant is brought through the hollow head stock shaft as indicated in Fig. 6.4. Electrical connections are made via a slip ring assembly supplied by Graphite Metallizing Corporation, New York.

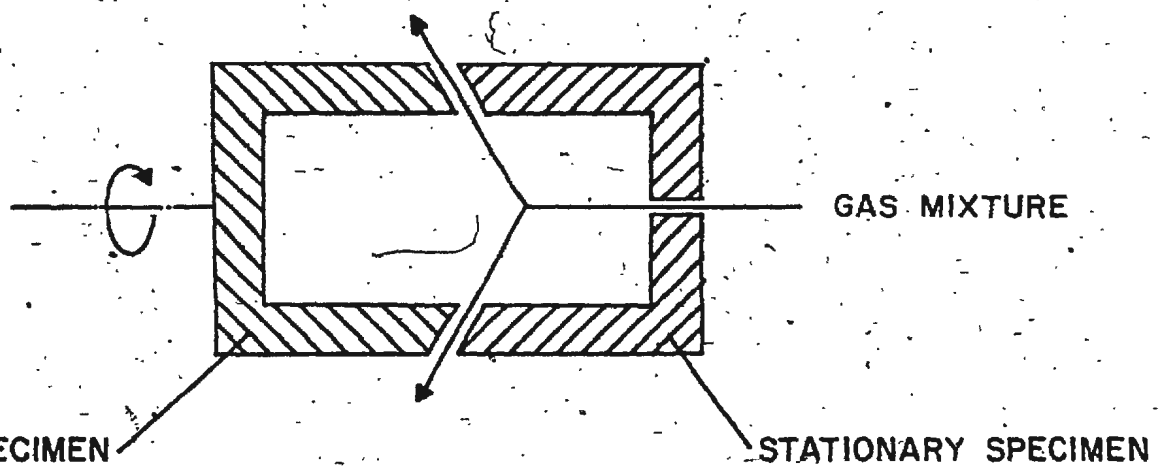

FIG · 6·2
ENVIRONMENT CONTROL
(SCHEMATIC)

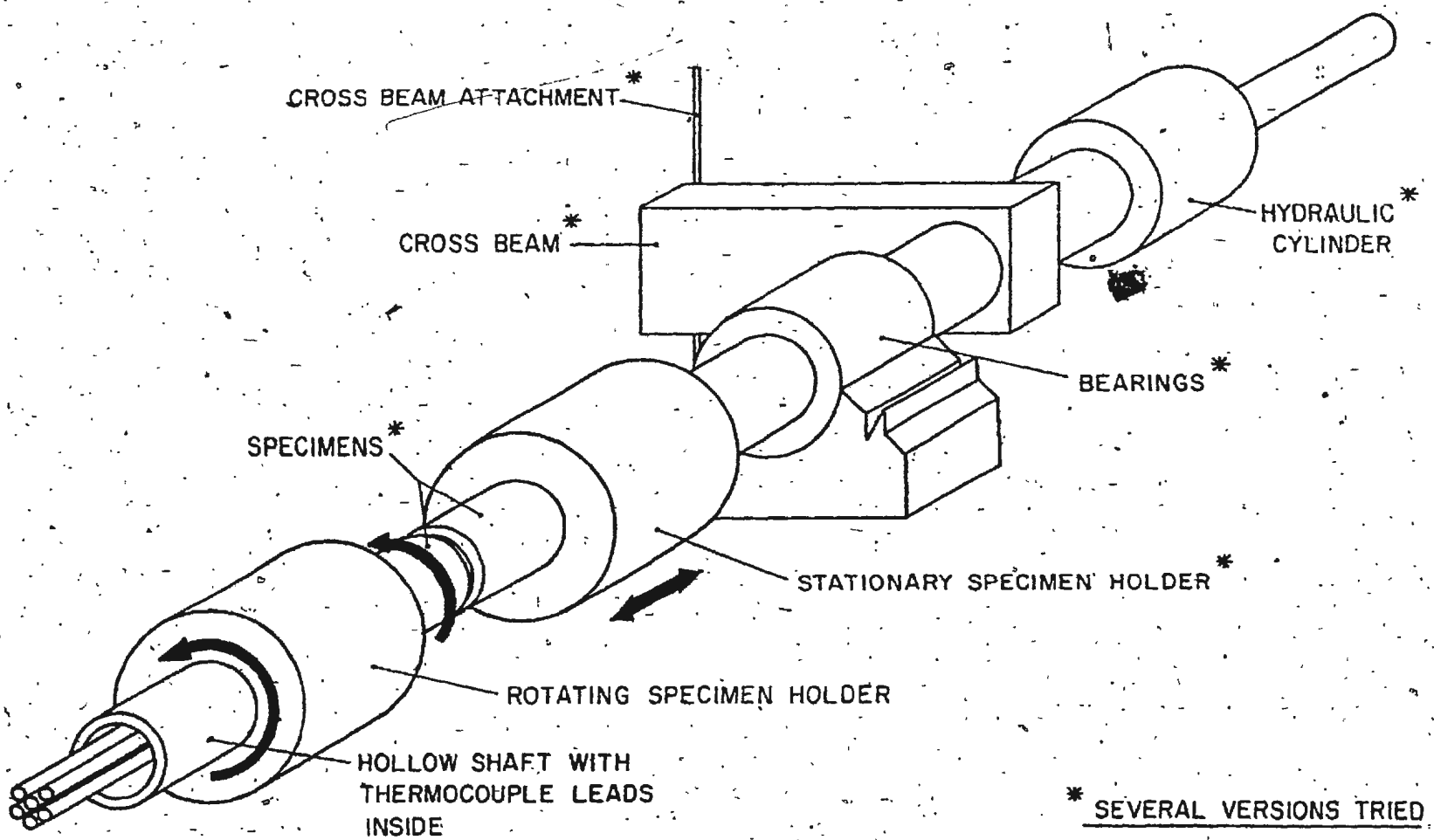

FIG· 6·3

DIAGRAMMATIC LAYOUT OF SPECIMEN, SPECIMEN HOLDERS & SPECIMEN HOLDER SHAFT CROSS BEAM AND HYDRAULIC CYLINDER

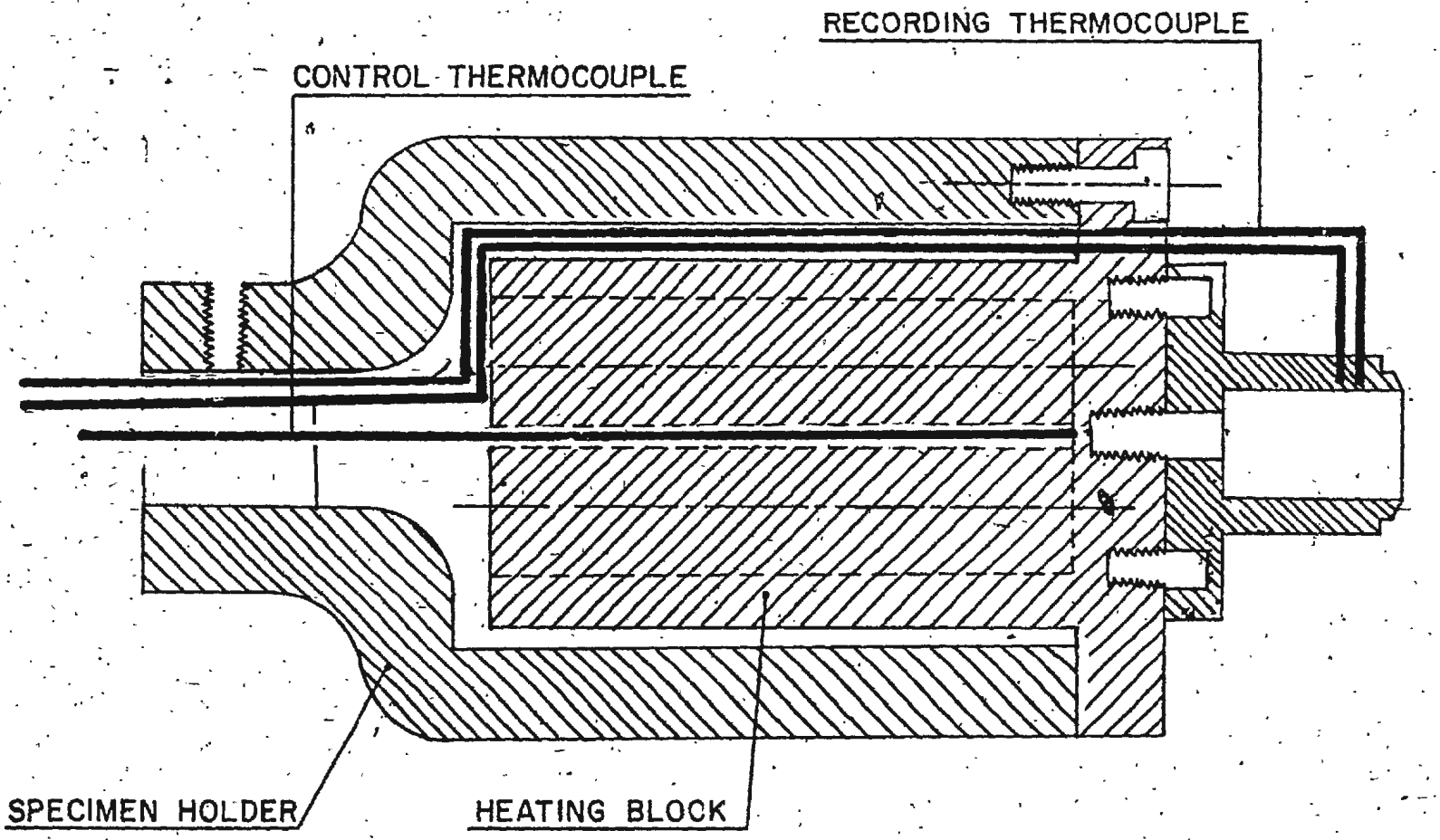

FIG·6·4

ROTATING SPECIMEN HOLDER

Two of the thermocouples are inserted into the rotating specimen at different distances from contact surface to permit estimation of the average contact temperature. A third thermocouple is embedded in centre of heater block to permit control of block temperature with automatic power controllers on the power supply to the heaters.

6.1.3. Stationary Specimen Holder

6.1.3.1. General

The specimen holder is mounted on a shaft which is located in bearings permitting both axial movement and rotation. The load between the specimen is provided by a hydraulic cylinder acting in line with the shaft. A cross beam is attached to the shaft. The cross beam is constrained to prevent rotation of the shaft. The force transmitted to the cross beam is the indication of torque due to the frictional force at the contacting surfaces of stationary specimen.

6.1.3.2. Initial Version

6.1.3.2.1. Specimens

The specimens were made from annealed Atlas Alpha-8 steel. The specimen configuration adopted was of two coaxial hollow cylinders 50mm outside diameter and 38mm inside diameter, rubbing at their annular end faces (6mm wear land width). The end faces were polished flat by using emery paper of decreasing number.

6.1.3.2.2. Specimen Holder

Details of stationary specimen holder are shown in Fig. 6.5.

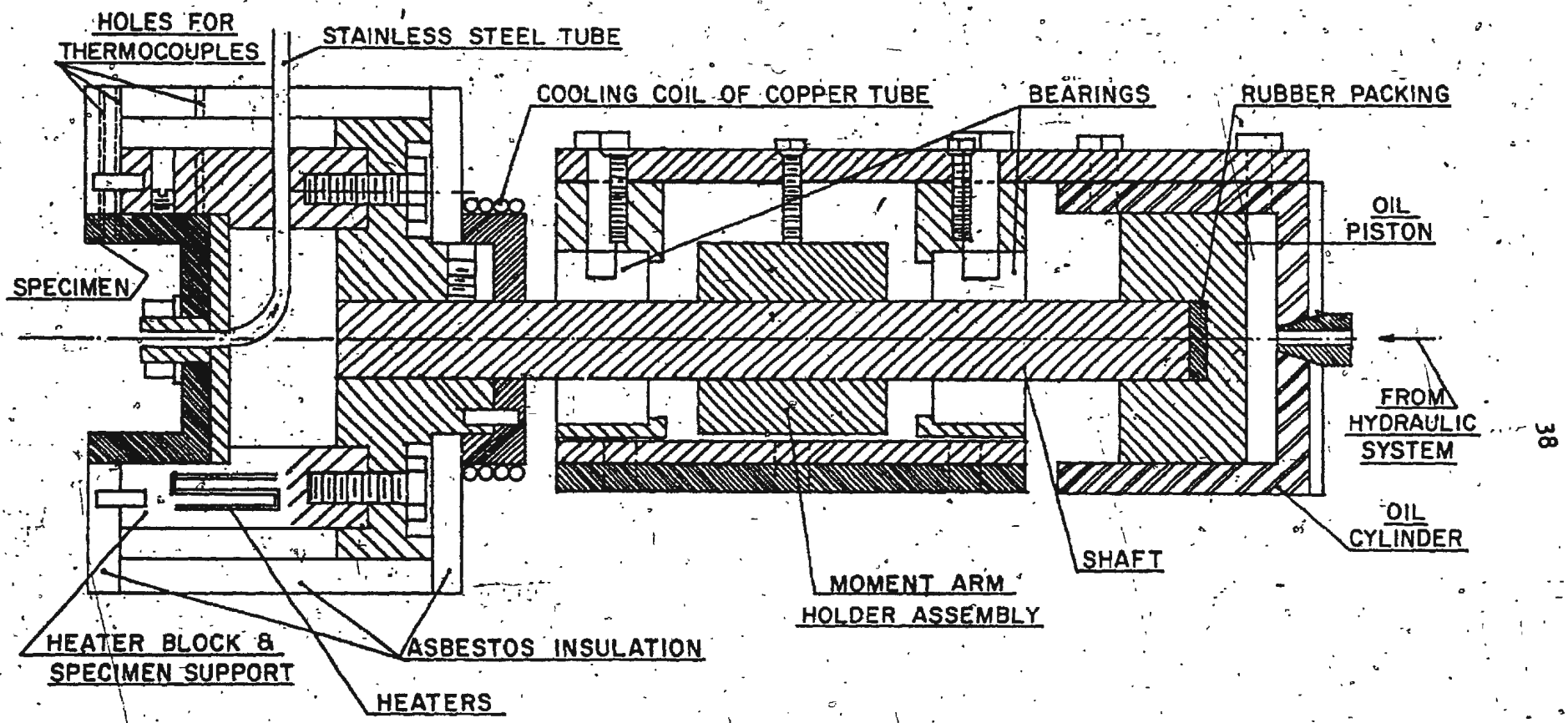

FIG·6·5

INITIAL VERSION OF THE STATIONARY SPECIMEN HOLDER

The specimen holder was made from a block of stainless steel and the specimen was mounted on the base place. The specimen was held in place by a 5mm set screw sitting on a flat on the specimen and by a 14mm nut and a lock washer tightened on the base plate bolt.

The specimen holder was fastened to the loading shaft by a specimen holder coupling which was made of stainless steel.

6.1.3.2.3. Specimen Heater

Eighty two holes, each 2.80mm in diameter and 25mm long were drilled in the specimen holder. Degussit Al23 (made by Degussa, Frankfurt) oxide ceramic tubing 2.70mm outside diameter, 1.70mm inside diameter, 30mm long and open at both ends were cemented in the holes.

Kanthal type A heater wire (made by The Kanthal Corporation, Connecticut) 1.03mm in diameter and 2m long was fed through Degussit tubing. Ends of Kanthal wire were welded to controlled power supply (See Fig. 6.5 and Photograph 6:11).

Initially the loading shaft was made from stainless steel-30355, 16mm in diameter and 200mm long. The shaft was secured to the specimen holder by a 3mm set screw sitting on a flat on the shaft. During rubbing, the screw used to get loose causing the specimen holder to twist relative to shaft.

The shaft was then modified to have threaded end. The specimen holder was modified to accommodate the threaded shaft. The threads were left handed to provide tightening during rubbing. However, the tortional vibrations produced during rubbing used to

loosen the shaft. The shaft was further modified and in this version, a locking collar was provided next to the threads. A torque of 150Nm was applied to tighten the shaft in specimen holder. This seemed to be the remedy until the shaft broke near the collar.

An examination of the fracture surface revealed that the failure was caused by fatigue as shown in the photograph 6.6.

In the next version the shaft had a flanged end which was bolted to the specimen holder. The circumferential crack developed in the shaft, close to fillet, can be seen in photograph 6.7.

For all these experiments, the nominal static load between two specimens was 490N. However, the analysis of normal load records showed zones of shock loading with loads exceeding 4900N. The frequency of load fluctuation was about 570 Hz and the stationary specimen holder assembly was vibrating at frequencies up to 4000 Hz.

It was believed that when the shaft hits the piston in the hydraulic cylinder, a shock load is produced. A Garlock Rubber piece (packing material), 3mm thick, glued to the rear end of shaft reduced the observed shock loads.

Through several stages of modification, the present design evolved, which is described below.

6.1.3.2.5. Aligning Bearings

Initially two linear Ball Bushings (made by Thomson Industries; No. XA 101824) were used to align and locate the

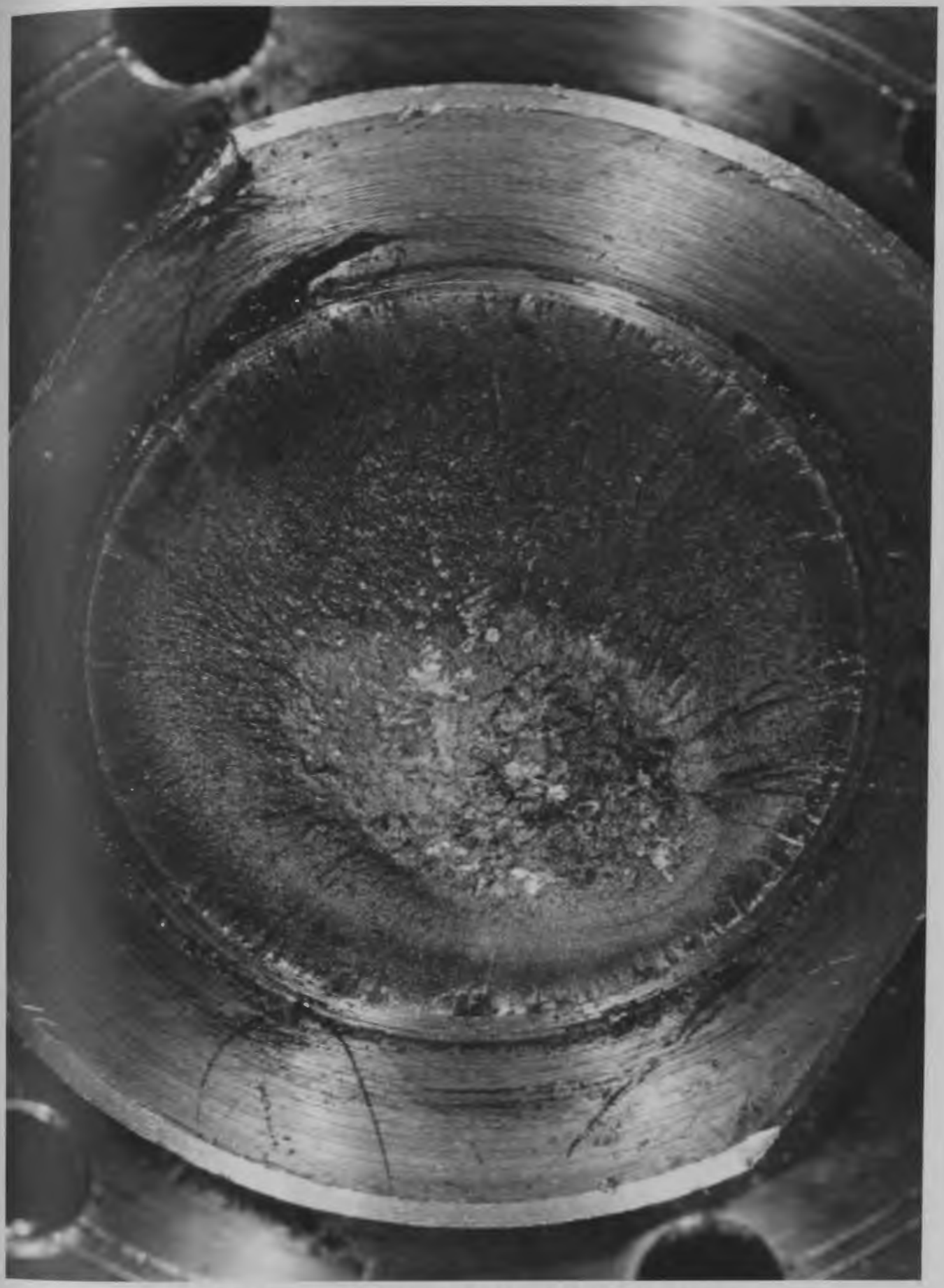

FRACTURE SURFACE, EARLY SPECIMEN SHAFT

PHOTOGRAPH NO. 6.6

STATIONARY SPECIMEN SHAFT WITH FLANGE

PHOTOGRAPH NO. 6.7

loading shaft. The bushings were retained in a brass housing and the housing was clamped to the top plate. However, the rotation between the bushing and shaft, provided by torsional vibration during rubbing, caused the balls in the bushing to rub against the sides of ball retainers. The rubbing action of balls produced wear and hence misalignment in the load axis. Once the load axis was changed, an additional torque was introduced at the wearing surface, causing further misalignment.

These bearings were replaced by a single Bearium metal bushing (supplied by Bearium Metal of Canada with following composition - virgin copper 70%, straits tin 8%, processed lead 22%) 90mm long and 16mm inside diameter. The bushing was retained in a mild steel block and block was clamped to top plate. In photograph 6.8 two versions of bearing are shown.

6.1.3.2.6. Cross Beams

The cross beam was made from medium carbon steel plate (113mm long x 13mm wide x 3mm thick). One end of the beam was attached to the moment arm holder clamped to the shaft while the other end was sitting between two ball point supports. These supports were provided by ball bearings sitting in 6mm diameter bolts. The bolts were secured to the stationary specimen holder assembly by a moment arm bracket.

The bending stresses produced in the beam were recorded by mounting two resistance strain gauges on the beam.

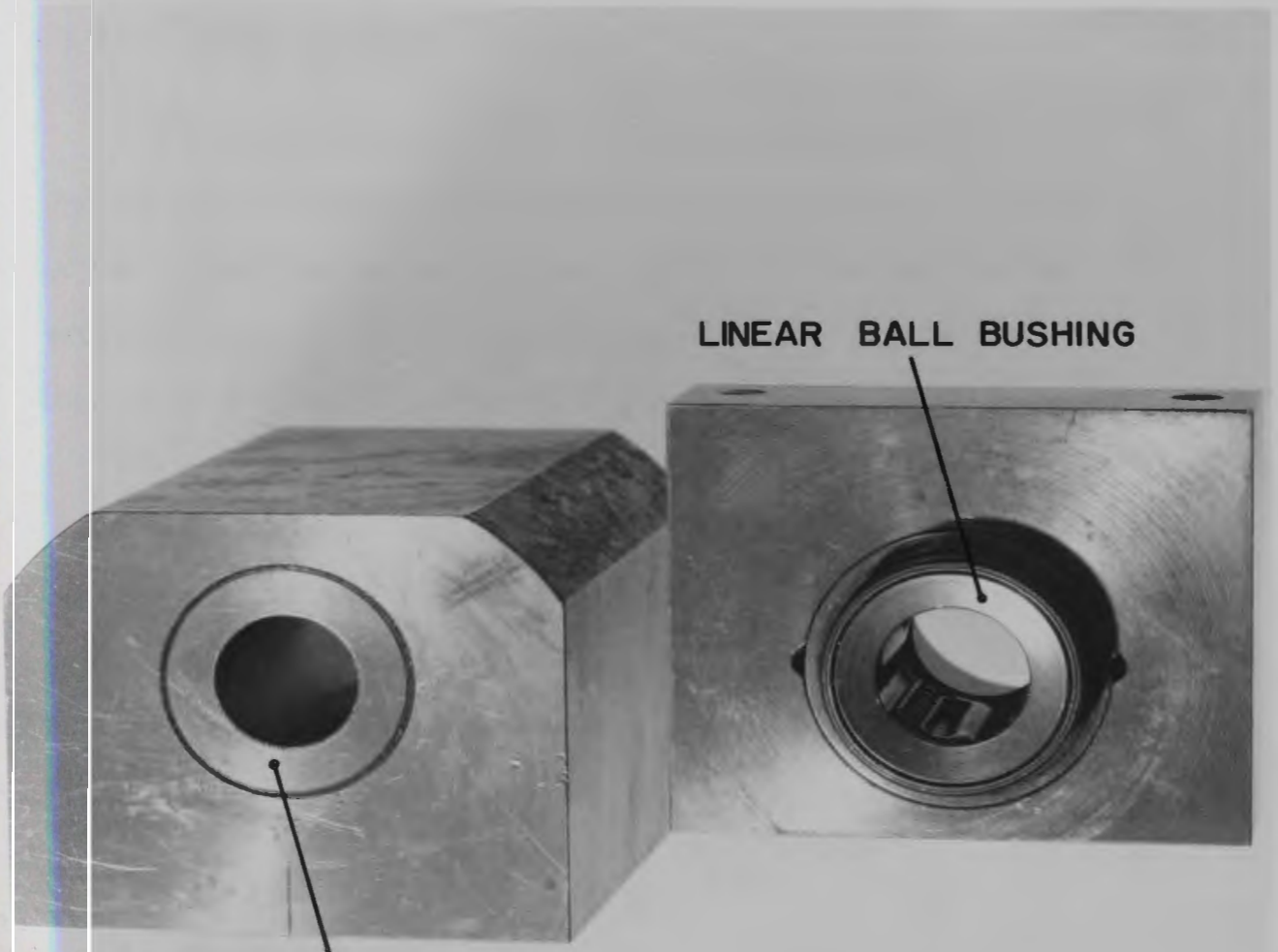

TWO VERSIONS OF THE BEARING

PHOTOGRAPH NO.6.8

This method of restraining the moment arm produced fatigue scars in the balls and indentations were noticed in the beam. Also, it was noticed that the cross beam shows buckling in transverse direction.

6.1.3.2.7. Support Blocks

The specimen holder, heater block, loading shaft piston and hydraulic cylinder were clamped to the top plate. The top plate was supported to the bearing housing bracket by six 3mm diameter machine screws. In photograph 6.9 the initial version of top plate and bearing housing bracket is shown.

The top plate and the bracket were clamped to the carriage of the lathe machine. In Fig. 6.10 details of the rear end support are shown. Front end support was provided by two rectangular pillars (25mm x 25mm x 200mm) and a clamping plate. A torque of 100N-m was used on each bolt for tightening. The supports, clamping plate, nuts and lock washers are shown in photographs 6.11 and 6.12.

*6.1.3.3. Present Version

6.1.3.3.1. Specimens

The specimens are made from annealed Atlas Alpha-8 steel.

Engineering drawings of the specimens are given in Figs. 6.13 and 6.14. The specimen configuration adopted is of two coaxial hollow cylinder 20.96mm outside diameter and 15.87mm

TOP PLATE & BEARING HOUSING BRACKET (EARLY VERSION)

PHOTOGRAPH NO. 6.9

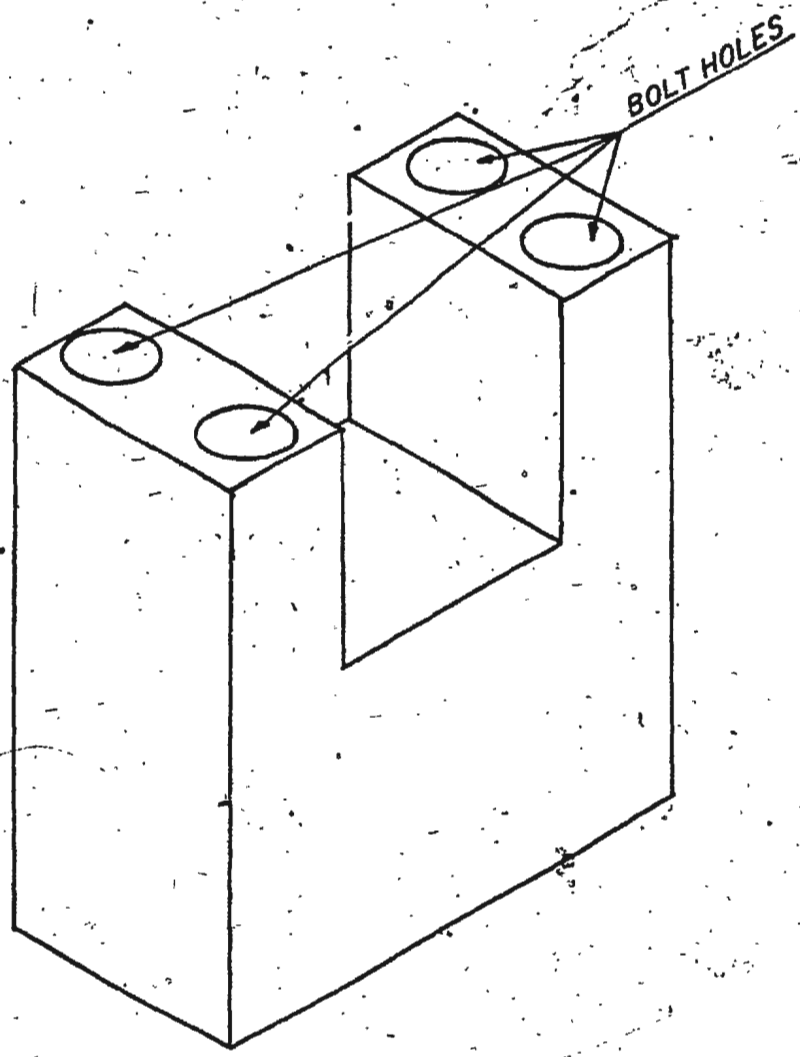

FIG. 6.10
REAR END RIGID SUPPORT

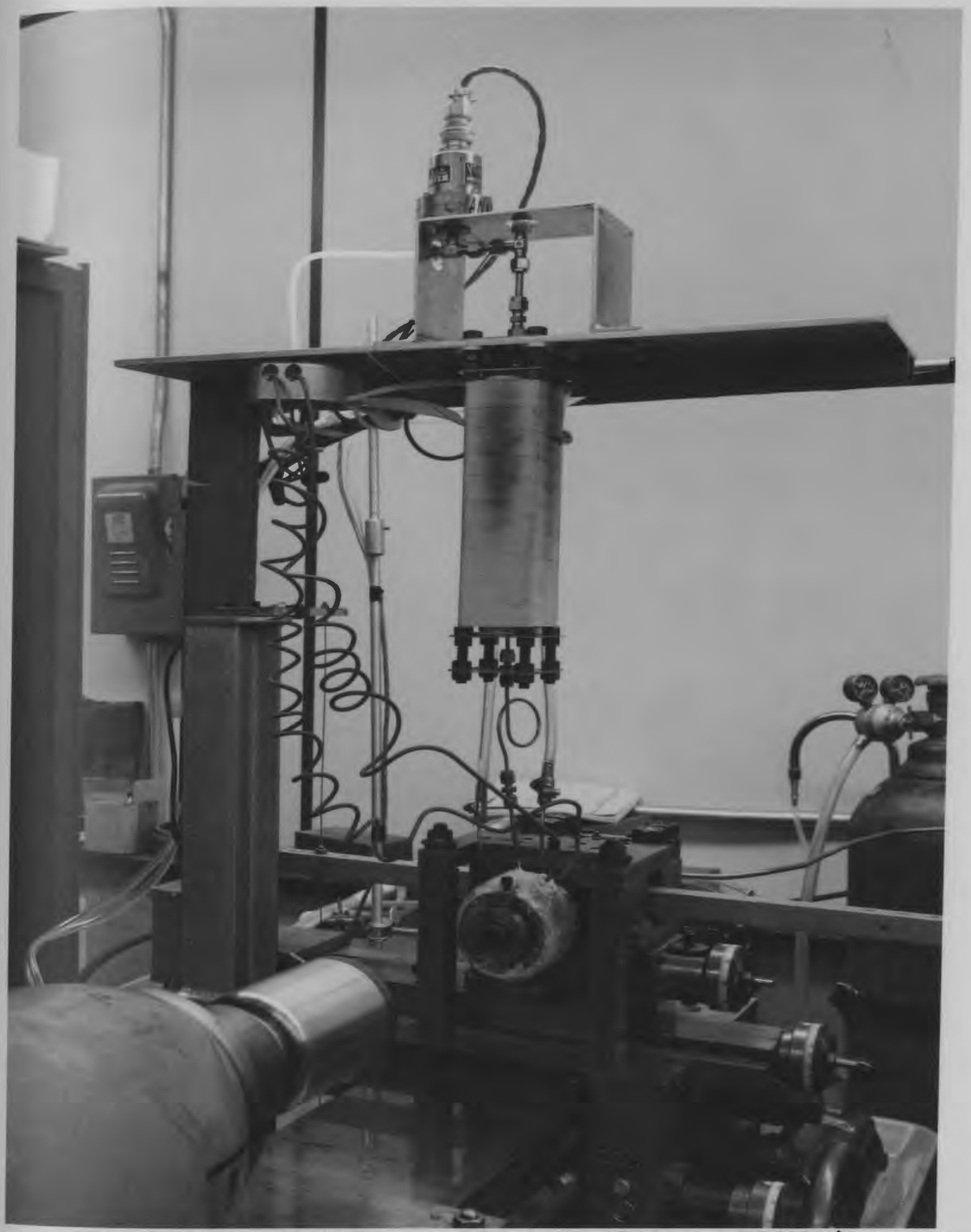

STATIONARY SPECIMEN HOLDER UNIT (EARLY VERSION)

PHOTOGRAPH NO· 6·11

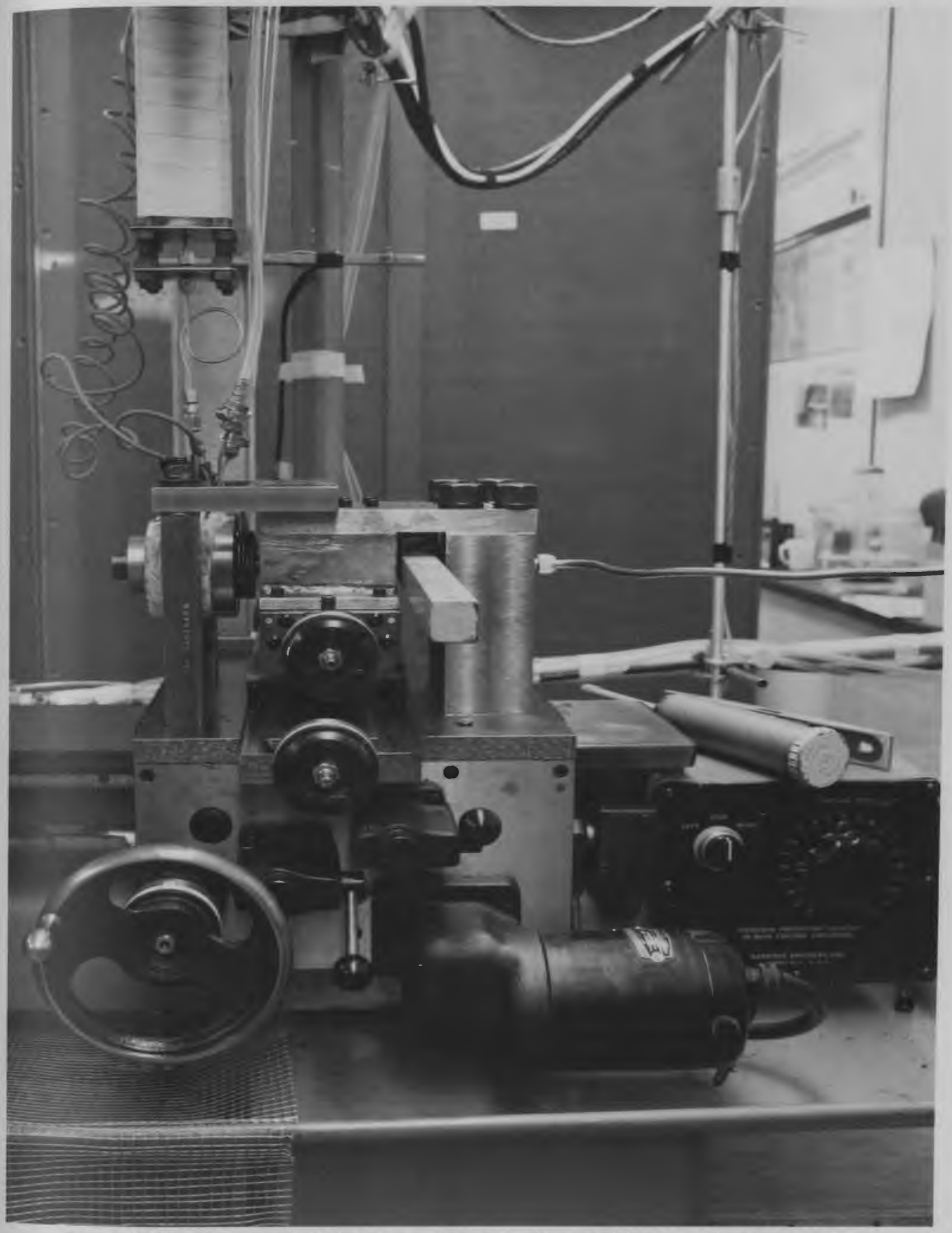

STATIONARY SPECIMEN HOLDER UNIT (EARLY VERSION)

PHOTOGRAPH NO. 6.12

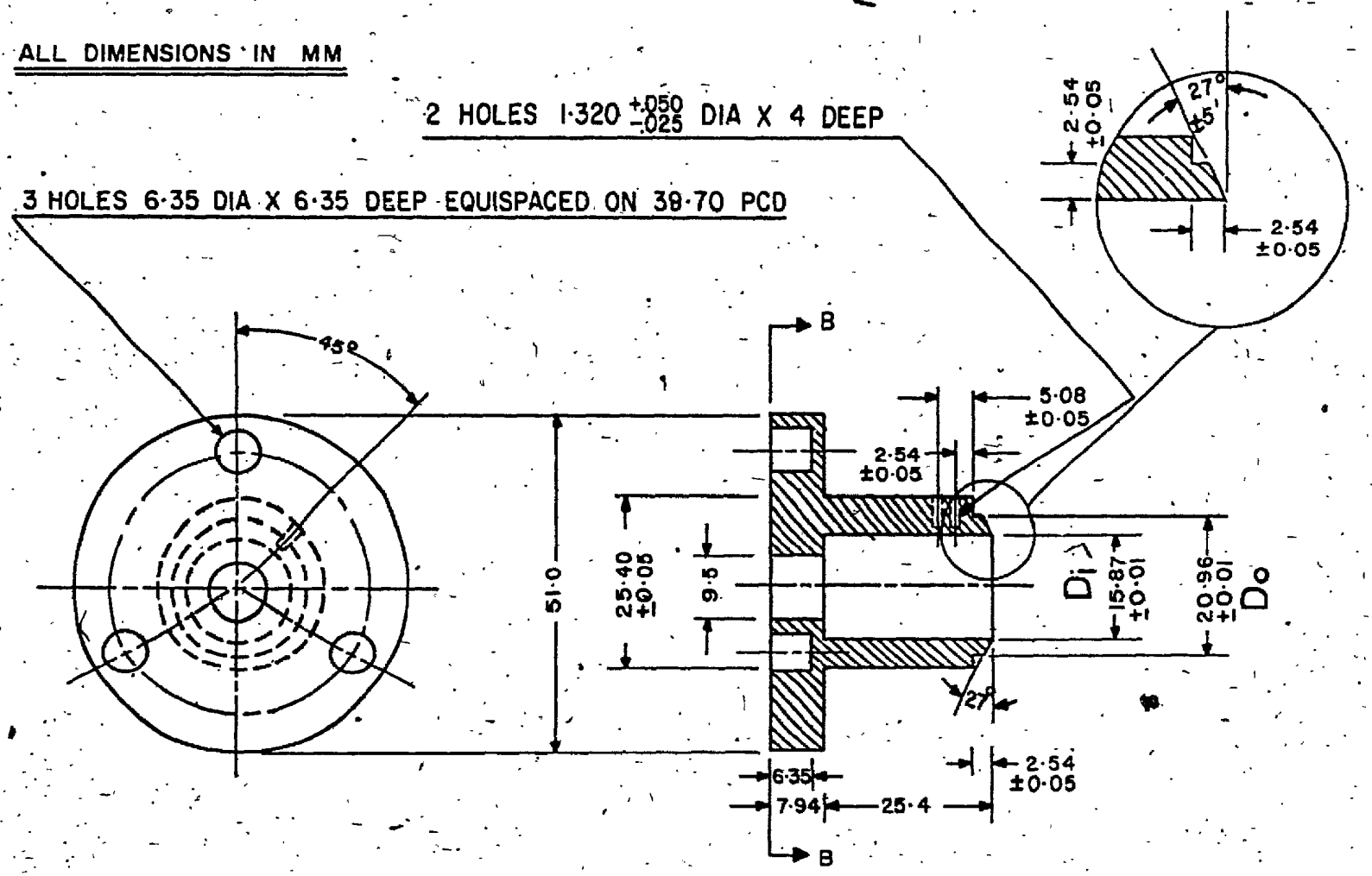

FIG. 6·13
ROTATING SPECIMEN

ALL DIMENSIONS IN MM

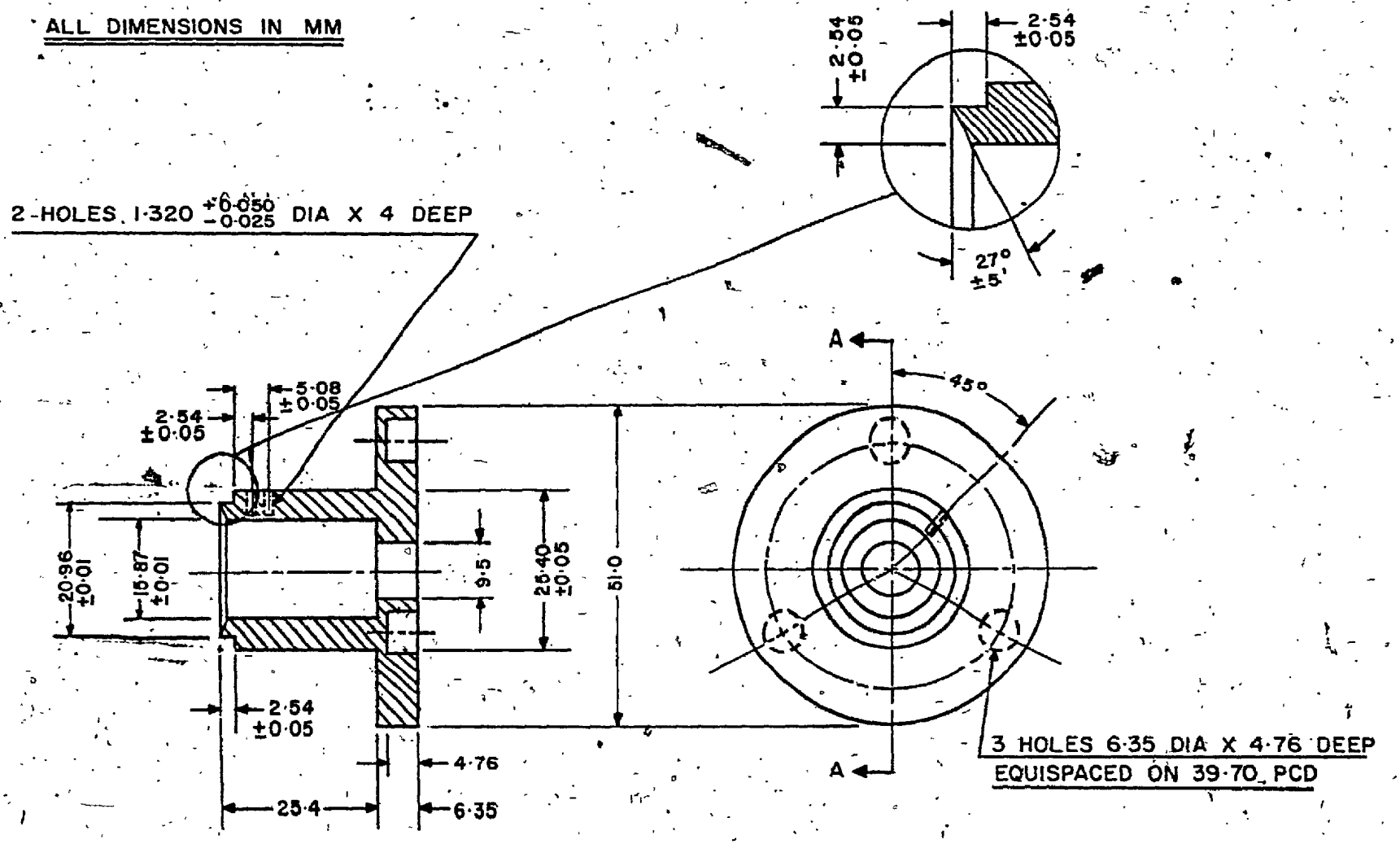

CROSS SECTION A-A

PLAN VIEW

FIG· 6·14

STATIONARY SPECIMEN

inside diameter with sloping end faces (slope of 27° from vertical) where rubbing takes place. The end faces are polished using emery papers of decreasing number.

Two thermocouples are inserted into the specimens at different distances from the contact surface to permit estimation of the average contact temperature.

6.1.3.3.2. Specimen Holder

A schematic diagram of the Wear Test machine is given in Fig. 6.15. Since the rotating specimen holder did not give any trouble during the initial runs, the stationary specimen holder and heater block are made similar to the rotating specimen holder and heater block (See photograph 6.16).

A thermocouple is embedded in the centre of the heater block to permit control of the block temperature with automatic power controllers.

6.1.3.3.3. Loading Shaft

The loading shaft is made from a cylindrical block of stainless steel (303), 70.75mm in diameter and 250mm long. Since the current version is a development of the initial version and the bearing housing bracket, cross beam and hydraulic piston were designed for the initial version, the shaft is stepped to fit in the available space.

The specimen holder is clamped to the loading shaft by six 8mm dia. x 63.5mm long, UNF bolts.

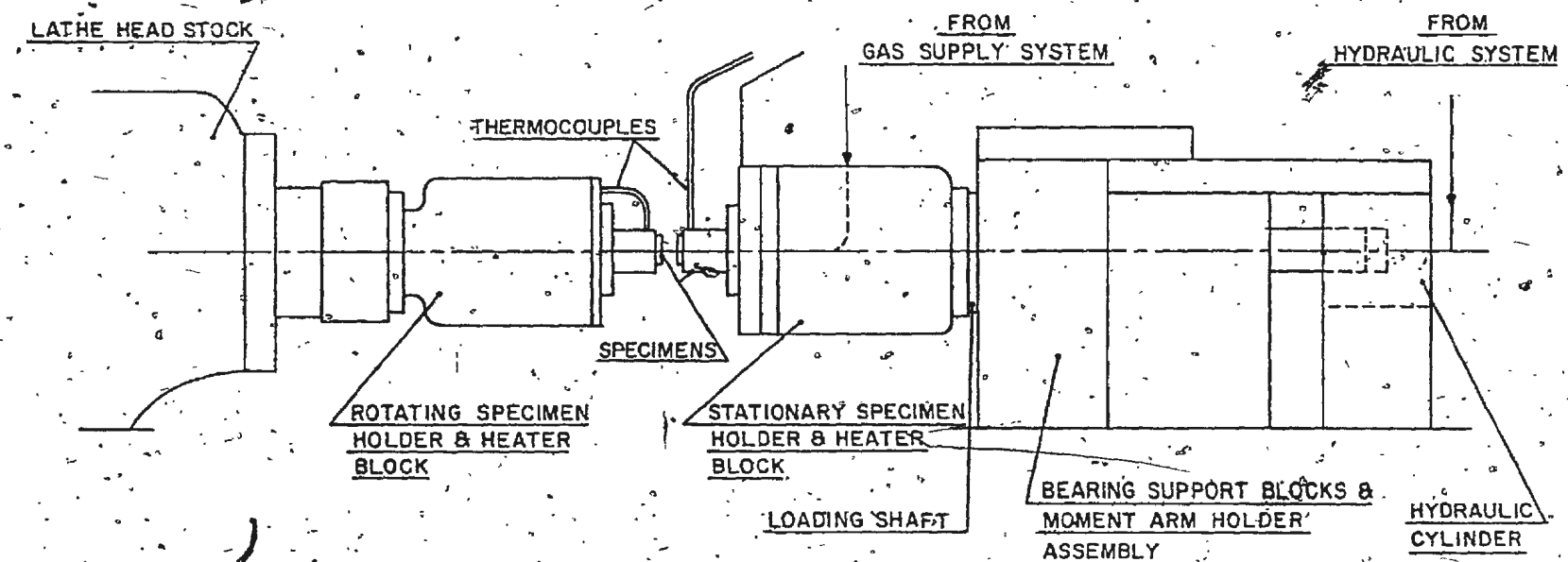

FIG. 6-15

SCHEMATIC DIAGRAM OF WEAR TEST MACHINE

SPECIMENS & THE SPECIMEN HOLDERS(FINALVERSION)

PHOTOGRAPH NO. 6.16

6.1.3.3.4. Bearings

The loading shaft is located in two brass bearings, the main bearing and the aligning bearing. The main bearing, 69.85mm in inside diameter and 95.25mm in outside diameter x 76.20mm long, is retained in a mild steel block, which also acts as the front end support. The aligning bearing is made by drilling a hole 31.75mm in diameter, in a brass block. The brass block is secured to the top plate by six 6mm diameter x 31.75mm long UNF bolts.

A circumferential groove and an axial groove is cut in the bearings. The grooves pass through an oil supply opening and the axial groove stops short of the end of the bearing. Moly Slip (made by Slipco Chemicals, Canada) was used as lubricant between the shaft and the bearings. The oil supply opening is connected to an oil reservoir which provides a gravity head.

6.1.3.3.5. Cross Beam

The earliest version of cross beam was sufficiently flexible for its deflection to be measured with strain gauges to indicate the frictional torque. As mentioned, this was soon replaced with a massive and stiff beam, which is clamped at its mid-point to the stationary specimen holder shaft.

The cross beam is made from a mild steel flat bar 38mm thick, 25mm wide and 660mm long. The bar is reinforced in the centre by two 50mm x 50mm square and 5mm thick plates. Two holes, at right angles to each other, are drilled in the bar.

The bigger hole, 25mm in diameter, is drilled along the width of bar, to accommodate the loading shaft and the smaller hole, along the thickness of bar, is drilled and tapped for 8mm diameter UNF set screw. The shaft is secured in place by a set screw sitting on a flat on the shaft.

One end of cross beam is attached to a vertical length of pianowire, connected at each end to steel cantilevers mounted on a vertical steel I-Beam (See photograph 6.17). Each cantilever carries strain gauges.

The pianowire is tensioned so that both cantilevers are strained towards the cross beam. Frictional torque generated at the stationary specimen is transmitted as a vertical force to the pianowire, reducing the deflection of one cantilever while increasing the deflection on the other.

On the other hand, axial movement of the stationary specimen, changes the deflection of the cantilevers in the identical sense (both strains increasing, or both decreasing) and the length of the pianowire is such that the net axial force on the stationary specimen holder shaft, due to the pianowire, is insignificant relative to the axial forces applied via the hydraulic cylinder.

6.1.3.3.6. Support Blocks

The top plate and bearing housing bracket is clamped to the carriage of lathe machine by front end and rear end support blocks. Details of these blocks are shown in Figs. 6.10 and 6.18.

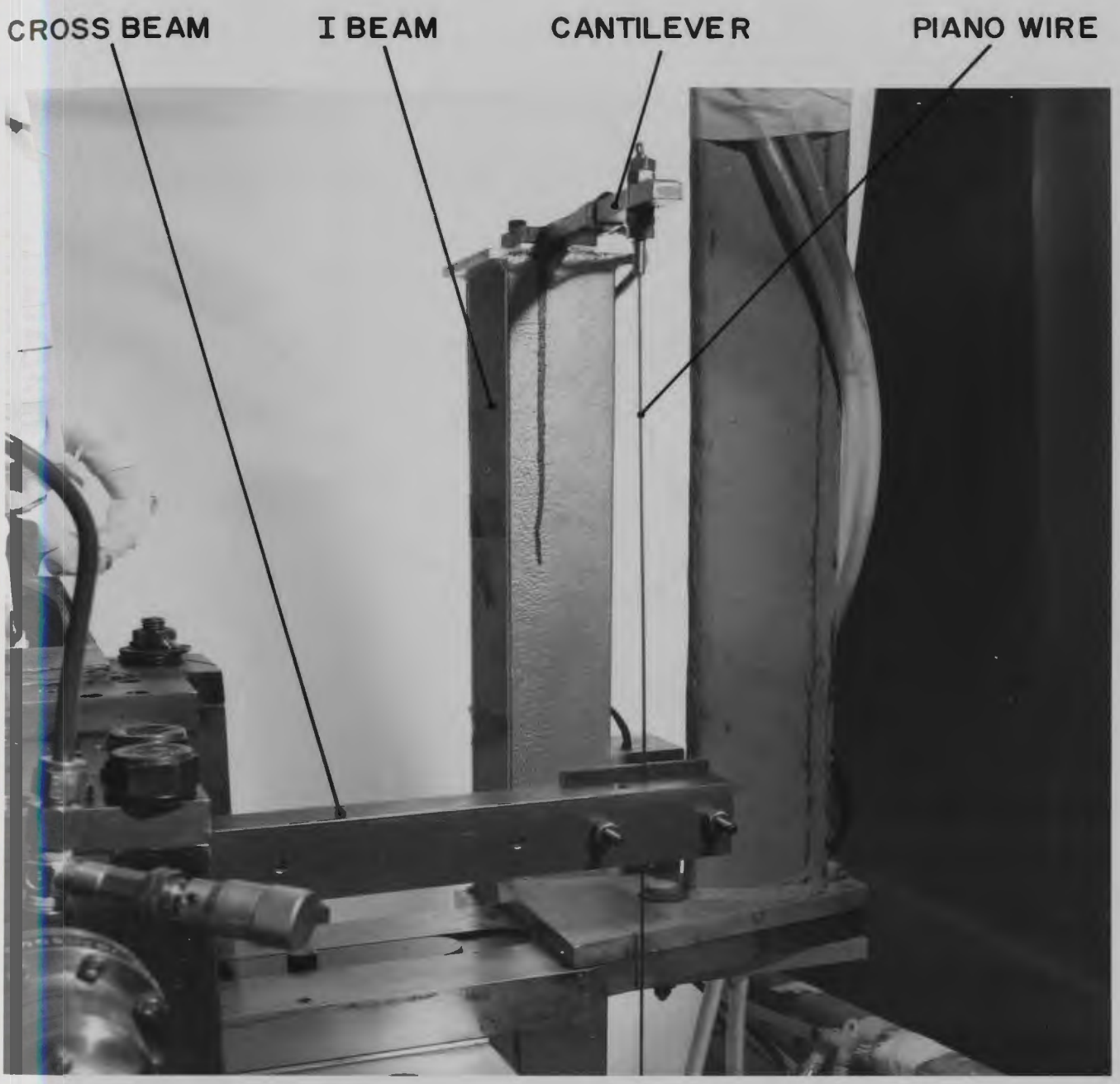

DETAILS OF CROSS BEAM CONSTRAINT (FINAL VERSION)

PHOTOGRAPH NO. 6.17

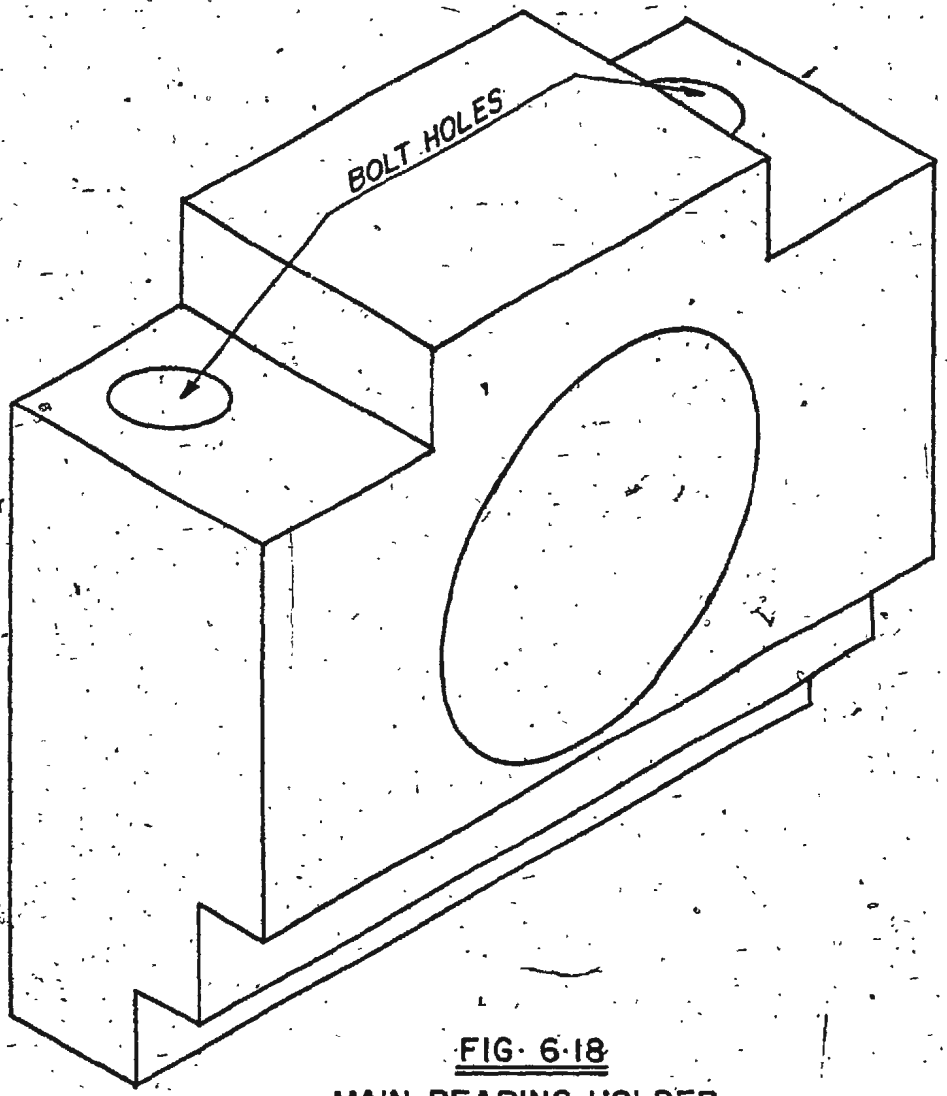

FIG· 6·18

MAIN BEARING HOLDER

FRONT END RIGID SUPPORT

6.2. Gas Supply System

*6.2.1. General

The block diagram of gas supply system is shown in Fig. 6.19. The input to the system is commercially available compressed argon and oxygen gas and the output is a mixture of argon and oxygen gas of desired composition, at a predetermined pressure, temperature and flow rate.

The commercial gases are purified and mixed in desired proportions in the gas mixing chamber. The gas mixture is fed to the stationary specimen and there is provision for heating the gas mixture before it enters the specimen.

The gas supply system has been divided into five subsystems, details of which are given below (Ref. Figs. 6.20 and 6.21).

6.2.2. Gas Purification System

The composition of gases was provided by the manufacturers: Canadian Liquid Air.

composition of argon gas:

argon	99.995%
oxygen	< 10 ppm
moisture	< 10 ppm
carbon di oxide	< 0.5 ppm
methylene	< 0.5 ppm

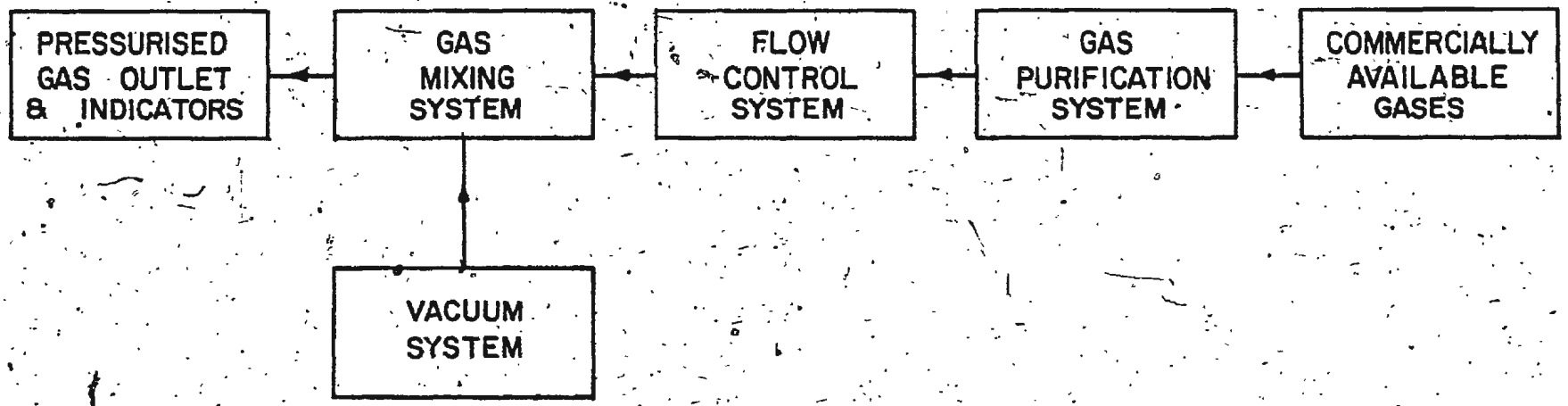

FIG·6·19
BLOCK DIAGRAM OF GAS SUPPLY SYSTEMS.

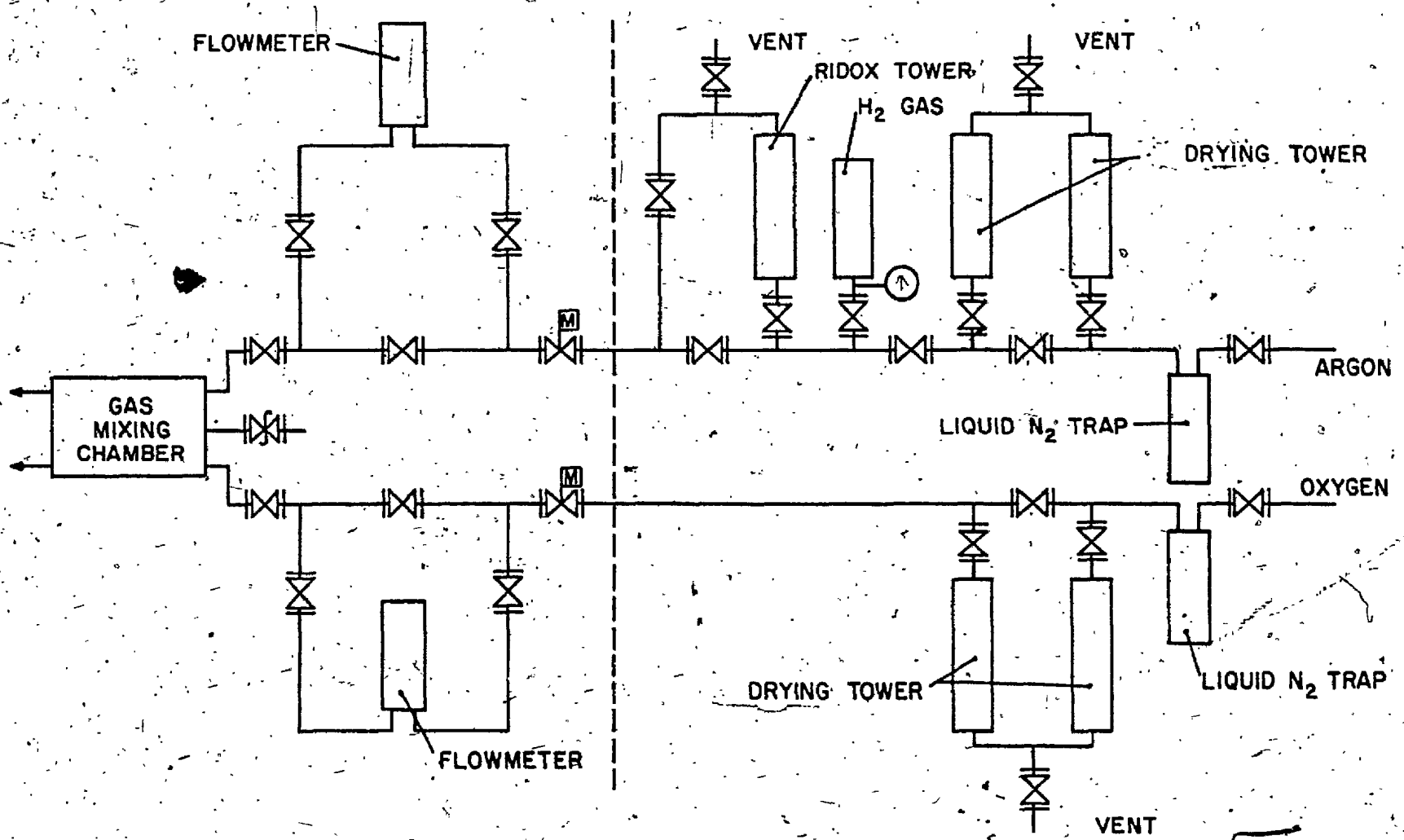

FIG· 6·20

SCHEMATIC DIAGRAM FOR GAS PURIFICATION AND FLOW CONTROL SYSTEMS

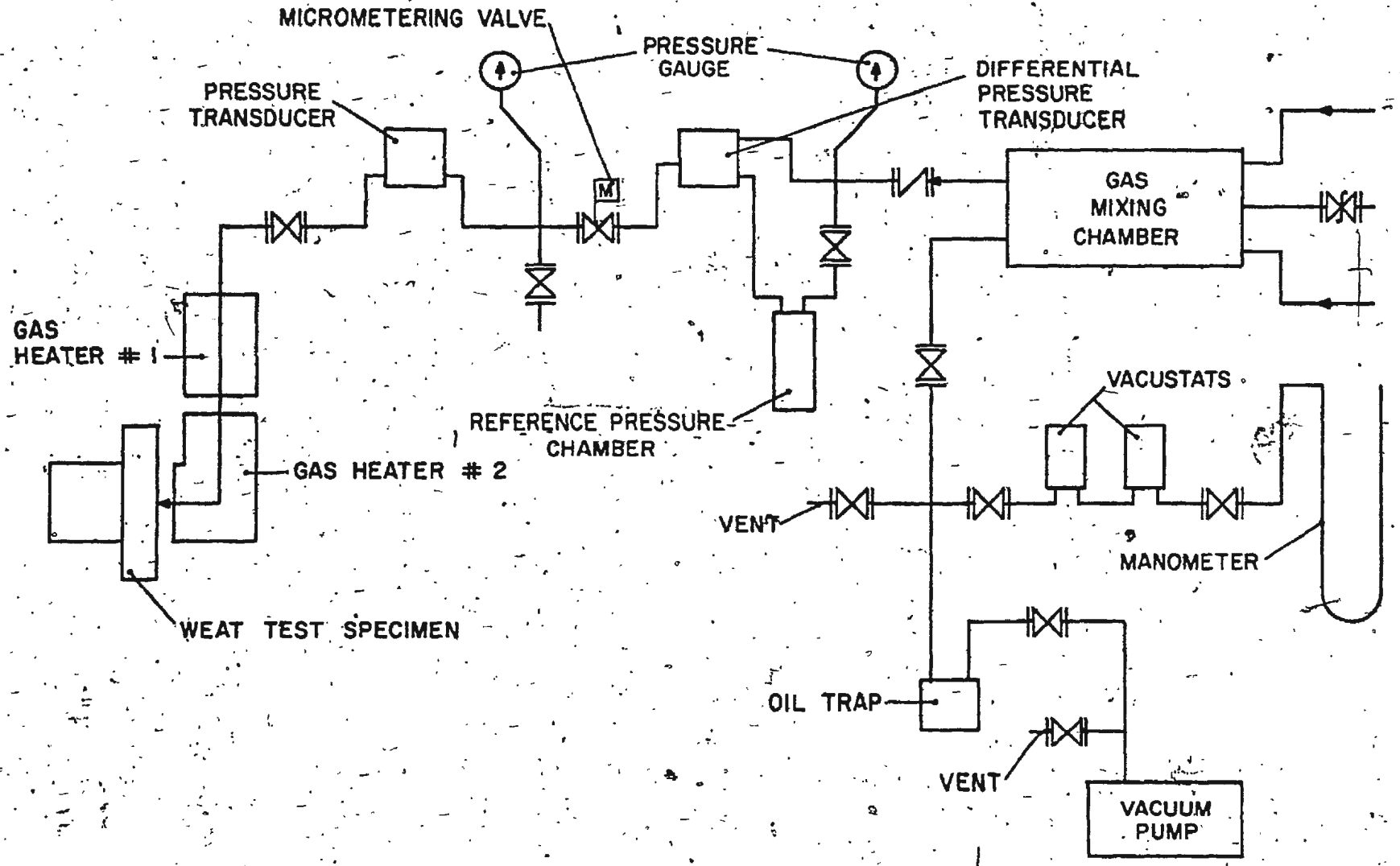

FIG·6·21

SCHEMATIC DIAGRAM FOR PRESSURIZED GAS OUTLET INDICATORS & VACUUM SYSTEM

composition of oxygen gas:

oxygen	99.5%
moisture	<210 ppm
carbon di oxide	<0.5 ppm
methane	<0.5 ppm

The purpose of the purification system was to remove all unwanted constituents (hydrocarbons, moisture and solid particles held in suspension) from the gas, as well as oxygen from the argon (when oxygen free argon is needed).

6.2.2.1. Liquid Nitrogen Traps

Their function was to precipitate out any hydrocarbons present in the oxygen and argon gas.

6.2.2.2. Drying Towers

Both the oxygen line and the argon line have identical drying towers. The main purpose of these towers is to remove water vapour and suspended solid impurities from oxygen and argon gas.

The drying towers are constructed in two sections, to make maximum use of available space and to facilitate the filling of towers with drying materials.

The towers are placed on a by pass to the supply line so that, if the need be, the drying towers can be isolated. The flow is controlled by a series of Nupro Valves (made by Swagelok). The upper valve marked vent in Fig. 6.20 is used when drying towers are regenerated.

The contents of each tower are placed in a definite order. Approximately 50mm of fibreglass wool is placed at the base of tower. This prevents any material from falling into the line and also filters out the solid particles held in suspension in the gas. Following next is approximately 75mm of molecular sieves (Type 4-A, Aluminum Sodium Silicate, 1.5mm pellets, supplied by B.D.H. Chemicals Limited, Poole, England) which filters out any remaining hydrocarbons in the gas. Next, 450mm of Silica Gel (self indicating type, about 6-20 mesh, manufactured by B.D.H. Chemicals Limited, Poole, England) is placed on top of molecular sieve to remove the moisture present in the gas.

The tower is equipped with an external heater which can raise the temperature of tower to about 100°C. (tested till 150°C.) to allow for regeneration of silica gel. Finally there is 50mm of fibre glass wool to prevent any material from being blown in the line.

Both the towers were filled with identical materials.

6.2.2.3. Ridox Tower

The function of the ridox tower in the system is to remove oxygen from argon gas. The Ridox Reagent (supplied by Fisher Scientific Company) is dark gray, irregular shaped grannules (8-14 mesh). Ridox retains oxygen by chemical reaction with the metal to form metal oxide. The regeneration process is essentially a reduction of metal oxide back to the metal. Reduced ridox has a light red cast which gradually turns dark gray upon oxidation.

The ridox reagent as supplied by the manufacturers was in the oxidized state and it was reduced before first use. Reduction is carried out in the following way:

The ridox reagent in the tower is heated to 200°C.

A regeneration gas of 4-6 volume percent hydrogen, remainder argon is fed through the Ridox tower.

Reduction is continued for two hours and then the container is purged with oxygen free argon gas.

A positive pressure of argon gas is impressed on the ridox reagent tube.

After reduction, the ridox reagent removes oxygen from argon gas by simple passage through the reaction container. The time between regeneration is determined by the size of the ridox container. From a knowledge of oxygen content of argon gas and the on-stream time of unit, the time for regeneration of ridox can be determined.

6.2.3. Flow Control System

It is of utmost importance that there is almost absolute control over the flow of pure argon and oxygen gas into mixing chamber. The flow control system (see Fig. 6.20) has been designed for this specific purpose. The two supply lines are almost identical in every sense.

The gas enters from gas purification section to flow control section through a fine metering valve (Nupro BM series supplied by Swagelok) with venier control. The purpose of this

valve is to make minute changes in the flow rate that would otherwise be unattainable by means of regular needle valves.

Each line is designed with two routes. The gas can enter the chamber either through a direct line or through a bypass line. The bypass line is used during mixing of gases and also in situations where continuous flow of gas is required. The bypass line allows the gas to flow through a rotameter which gives a visual readout of the flow rate.

The Rotameters (Show-Rate 150, supplied by Brooks Instrument Limited, Pennsylvania) selected for the present experiment, can be used over a wide range of flow rates (0-0.0764 Litres/minutes of argon gas at 1.03 Kg/mm^2 pressure and 20°C. to 0-2.215 Litres/minute) by interchanging the tubes and floats.

6.2.4. Gas Mixing System

6.2.4.1. General

The gas mixing system consists of a gas mixing chamber and mixing chamber enclosures.

6.2.4.2. The Gas Mixing Chamber

The purpose of this chamber is to provide space to mix argon and oxygen gas and to provide storage facilities for mixing gases.

On the input side, in addition to the controlled argon and oxygen gas line, a safety valve, set at 10.5Kg/mm^2, is included. The safety valve guards against over pressurizing the lines. On

the output side, a vacuum line and a pressurized gas outlet line are attached.

The chamber has been constructed of a 150mm diameter thick walled stainless steel pipe 925mm in length with spherical shape ends and has been tested up to a pressure of 700N/mm^2 at room temperature.

The gas mixing chamber can be degassed and evacuated before filling it with gases. For degassing the chamber, a heater has been designed from 1,950mm of No. 15 Kanthan Type A heater wire.

6.2.4.3. The Mixing Chamber Enclosure

The purpose of this enclosure is:

(i) To supply support and protection for the mixing chamber.

(ii) To provide a convenient method of arrangement for the heating element.

(iii) To help the mixing chamber.

The enclosure has been constructed of a 10mm thick Transite sheeting. Its approximate dimensions are 1125mm x 350mm x 330mm. The enclosure has been designed in two sections, the bottom or box of the enclosure and the top of the enclosure. In the box of the enclosure there are six 10mm transite support brackets which provide support for the chamber and the heater wire is fed through the holes in these brackets.

To monitor the temperature of gas mixing chamber, a chromel-alumel thermocouple has been inserted permanently between the flange of safety jacket and the wall of the mixing chamber.

The chamber enclosure and mixing chamber are insulated by using 50mm batts of fibreglass wool, layers of asbestos paper and aluminum foil.

6.2.5. Vacuum System

The vacuum system (see Fig. 6.21) has been designed specifically to evacuate the mixing chamber prior to filling it with argon and oxygen gas. The system is capable of evacuating the chamber to 0.001 torr of pressure.

The pressure is monitored by means of a U-Tube manometer and two vacustats (supplied by Edward High Vacuum Limited, Sussex, England). One vacustat has the range of 1 to 0.01 torr and the other has a range of 1 to 0.001 torr.

The system is also equipped with a sampling line which permits analysis of gases in chamber to be made at any stage.

6.2.6. Pressurized Gas Outlets and Indicators

6.2.6.1. General

After the gases have been mixed in the required relative amounts in the mixing chamber, the mixture is transported to the wear test specimen. In designing a system to do this, three factors had to be considered.

The need for a rapid method of resetting the flow rate.

The need for a method of continuously recording the fluctuations in flow rate.

The need for heating and controlling the temperature of gas mixture entering the wear test specimen interface.

6.2.6.2. Record of Pressure and Flow Control

Low flow rates from a pre-filled mixture in the mixing chamber can be estimated by comparing the pressure in chamber with the pressure of a volume of gas trapped in a reference pressure chamber (see Fig. 6.21).

A differential pressure transducer (supplied by Viatran Corporation; Range 0-35N/cm^2.D) measures the difference in pressure between the reference chamber (at fixed pressure) and the gas mixing chamber (variable pressure). The output of the differential pressure transducer can be recorded on a Southern Instrument multi channel ultra voilet recorder. Also, installed in the line is a 350N/cm^2 pressure dial gauge (supplied by AMETEK/U.S. Gauge) which gives a readout of the actual pressure in the mixing chamber.

To control the flow rate of the mixture of gases entering the specimen interface, a Nupro BM Series Micro Metering Valve with Venier Handle has been installed in the line. This valve enables rapid resetting of the flow rate.

After the gas has been passed through the fine Micro Metering Valve, it passes through the final stages of monitoring of pressure. In this stage of monitoring a 140N/cm^2 pressure dial gauge (supplied by AMETEK/U.K. Gauge) and a Gas Pressure Transducer (supplied by Viatran Corporation, Range 0-210N/cm^2 absolute) are used. The output of the transducer can be recorded

on the multi channel ultra violet recorder.

Flow rate of the mixture of gases entering the specimens is determined from a calibration curve correlating the position of vernier handle in Micro Metering Valve, the back stream pressure (pressure of gas mixture in cylinder) and the gas mixture pressure between the specimens.

6.2.6.3. Gas Heater

The gas heater has been designed and constructed to raise the temperature of the argon and oxygen gas mixture from room temperature to a temperature of 600°C - the estimated maximum of the mean surface temperature.

The gas mixture passes through a 1500mm length of 3.25mm outside diameter stainless steel tubing wound in a coil of 60mm diameter. The coil is placed on a mild steel circular core, 62.5mm in diameter and 115mm long. The coil and core assembly are wrapped in asbestos paper and the entire unit is kept in a tubular heater (68mm inside diameter and 145mm long; power output 1000 Watts at 110V). Any vacancy between the gas coils, core and heating element was filled with alundum cement.

The heater unit is supported on two semicircular support brackets and the entire unit is enclosed in a rectangular box made of transite.

A thermocouple is embedded in the centre of the mild steel core to permit control of the core temperature with automatic power controllers on the power supply to heaters.

To compensate for heat loss from the heated gas mixture, while the gas is being transported from the heater to the specimen interface, the supply line leading from the heater to the specimen was wrapped with a heating tape (Heater No. 2 in Fig. 6.21). The power supply to the heating tape was controlled by a variable voltage source.

*6.3. Debris Collection

During initial experiments the wear debris were collected under the rubbing specimens. A debris catcher was made for this purpose, however, most of the debris seemed to be airborn and did not fall directly below the specimens.

The weight of the debris collected was roughly 25% of the weight lost by specimens. This indicated the need for more efficient debris collection.

A schematic diagram for wear debris collection is shown in Fig. 6.22. A plexiglass rectangular box with two clearance holes on opposite faces for the specimen holders is fastened to the bed of lathe machine. The box is made in two sections, a top half and a bottom half, hinged together. This facilitates the insertion and removal of the wear debris catcher which is kept under the specimens.

A 10mm diameter hole is drilled in the top face of the box and a straight polypropylene connecting tube is secured in the hole.

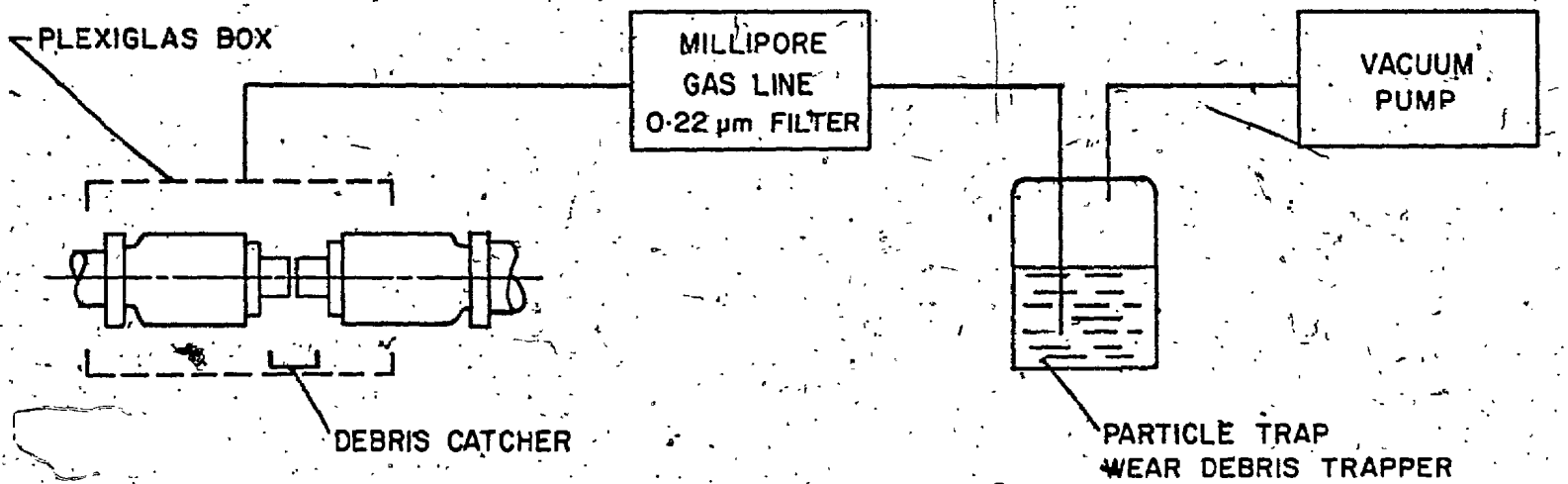

FIG· 6·22

SCHEMATIC DIAGRAM FOR WEAR DEBRIS COLLECTION

The plexiglass box is connected to a vacuum pump (Little Giant, supplied by Fisher Scientific Company) through a 0.22mm filter held in a Millipore Gas Line Filter (manufactured by Millipore Corporation) and Gas Washing Bottle (supplied by Fisher Scientific Company). The gas washing bottle is half filled with liquid paraffin.

The suction created by the vacuum pump near the hole in the top face of the plexiglass box causes the air around the specimen and the specimen holder to flow towards the pump. Airborn debris is carried by this flowing air and is deposited on the filter paper. Debris particles which are smaller than 0.22mm are trapped in the liquid paraffin in the gas washing bottle.

The debris particles which are not airborn are collected in the wear debris catcher kept under the specimens.

6.4. Measuring Systems

6.4.1. Normal Load

*6.4.1.1. General

The schematic diagram for the hydraulic system is shown in Fig. 6.23.

The oil reservoir is filled with SAE 30 oil (supplied by Imperial Oil Limited) and filtered compressed air is fed into the reservoir. The air forces the oil into the pressure cylinder of the constant pressure cell (supplied by Norwegian Geotechnical Institute, Oslo, Norway) through an oil filter. The constant

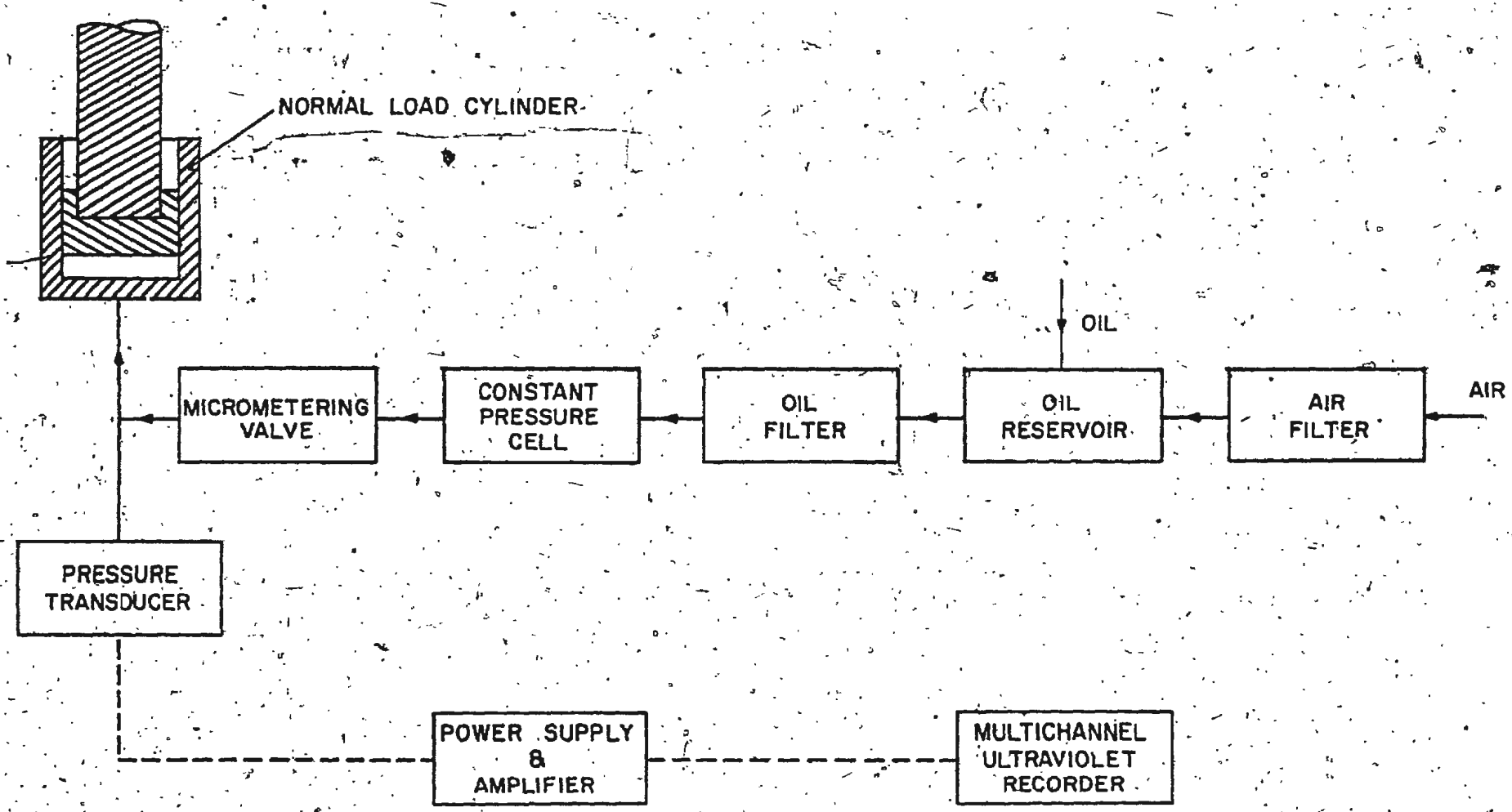

FIG·6·23

BLOCK DIAGRAM FOR HYDRAULIC SYSTEM

pressure cell maintains a constant oil pressure in the hydraulic line from the cell to the hydraulic piston and cylinder assembly. A micrometering valve (supplied by Swagelok) with vernier handle can be adjusted to provide a variable damping in the hydraulic line. Output from the micrometering valve is connected to the piston and cylinder assembly. The pressure of the oil in the hydraulic cylinder is recorded by a pressure transducer (supplied by Viatran Corporation, New York).

6.4.1.2. Air Filter

The compressed air (pressure 10.5N/cm^2) is filtered by Rego Filter and Pressure Regulator (supplied by Bastian-Blessing Company).

6.4.1.3. Oil Reservoir

The oil reservoir is made from a glass tube 110mm diameter and 175mm long. The reservoir has two inputs, one for oil and the other for the compressed filtered air. There are two outputs, one is connected to the oil filter and the other is connected to drain to empty the reservoir.

6.4.1.4. Oil Filter

Oil from the reservoir is filtered by MF-Millipore filter (0.22mm pore size, supplied by Millipore Corporation) held in a Millipore gas line filter holder.

6.4.1.5. Constant Pressure Cell

The purpose of this unit is to maintain a constant oil pressure within the hydraulic cylinder in the piston and cylinder assembly. The main components of this apparatus are a loaded piston (made of stainless steel, area 200 sq. mm) and a bushing (made of brass) attached to the top of a vertical cylinder filled with oil. In principle it operates exactly opposite to the principle of an hydraulic jack.

In principle the constant pressure cell creates a constant pressure in the hydraulic line. The piston in the constant pressure cell moves when the piston in the normal load cylinder moves, and as oil leaks out of the system. However, due to the inertia of the system, particularly of the piston in the constant pressure cell and of the weights supported by the piston and also due to viscous damping in the hydraulic line, the pressure in the line can fluctuate markedly during rapid movements of the pistons.

The cell is made in two sections, the upper half which acts as an oil reservoir and the sealed lower chamber where constant pressure is maintained. A needle control valve provides the connection between the two sections.

The pressure is maintained as long as the loaded piston does not reach the end of its travel. When the piston nears the end of travel, the needle control valve is opened and the loaded piston is pulled upwards. The oil from the reservoir flows into the cell chamber. A needle valve is then closed and system maintains a constant pressure.

The bottom plate of the cell rests on a steel ball and is held in position by three bolts which pass through compression springs. This arrangement provides a means of adjusting the vertical axis of piston, which is important for the reduction of friction between the piston and bushing.

The cell is provided with a loading platform which is attached to a yoke. Between the yoke, which is made of aluminim to decrease its weight, and the piston is another ball for eliminating horizontal forces on piston.

A large plexiglass cylinder is used to cover the entire constant pressure cell and protect it from dust. (See Fig. 24)

6.4.1.6. Micrometering Valve

The micrometering valve with a vernier handle can be adjusted to provide a variable damping in the hydraulic line and can, thus change the axial dynamic stiffness of the stationary specimen.

6.4.1.7. Piston and Cylinder Assembly

The purpose of the piston and cylinder assembly, acting in line with the shaft, is to provide constant nominal load between the wear test specimens.

The piston is made of brass and has an area of cross section of 200 sq. mm. The cylinder is made of stainless steel. Both parts are carefully honed to the same tolerance as loading piston and bushing in the constant pressure cell (about 25μm).

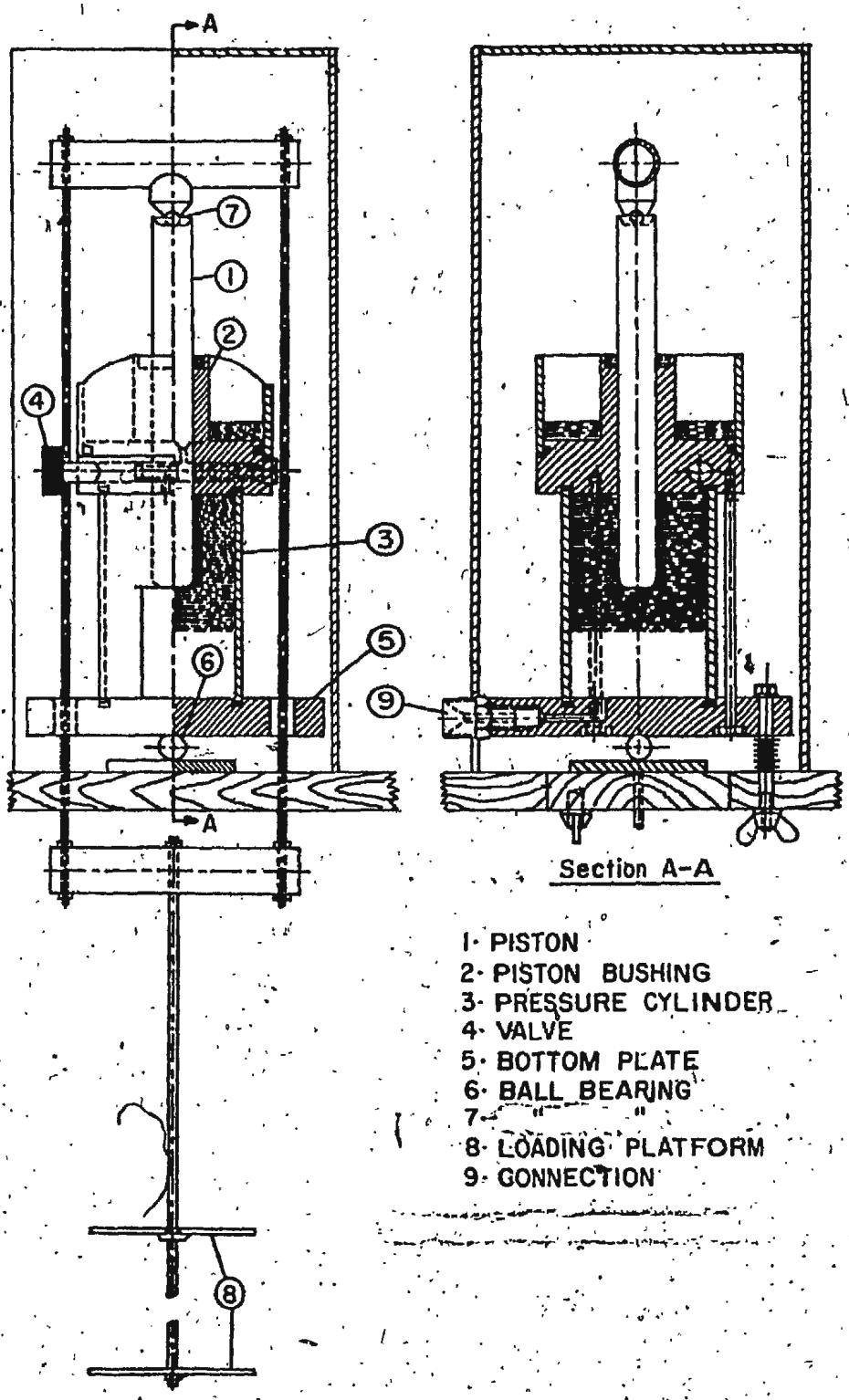

FIG. 6.24

CONSTANT PRESSURE CELL

A 26mm diameter and 18mm long hole is drilled in one end of the piston. The end of the loading shaft (carrying the specimen holder assembly at the other end) sits in this hole. A Garlok rubber piece, 6mm thick, is glued to the end of the shaft to absorb shock loads generated at the specimen surfaces, which seemed to be caused by brief episodes of welding.

For bleeding any trapped air from the hydraulic cylinder, a bleeder screw has been provided. The bleeder screw sits in a 6mm diameter UNF tapped hole on the top face of the hydraulic cylinder.

6.4.1.8. Pressure Transducer

6.4.1.8.1. General

As mentioned, rapid fluctuations can and do occur in the oil pressure, about the mean pressure set by the constant pressure cell. Therefore, the cell pressure is measured by a pressure transducer, which can record dynamic signals up to 3000 Hz. The output of the transducer can be recorded on the multichannel ultra violet recorder.

6.4.1.8.2. Calibration of the Pressure Transducer

The transducer was calibrated by placing loads in an increasing order of magnitude from no load to 147N load on the loading platform of the constant pressure cell. The output of the transducer was amplified and the amplified output was recorded on the ultra violet recorder using a SMI/S galvanometer (supplied by Southern Instruments). The galvanometer has a natural frequency

of 1600 Hz.

The loads were then removed from the pan, in the same step as they were placed while loading, and output was again recorded.

The calibration curve for the hydraulic pressure transducer is given in Figs. 6.25 and 6.26.

6.4.2. Frictional Torque

6.4.2.1. General

The details of the cross beam, pianowire and cantilever used for the measurements of frictional torque generated at the stationary specimen surface are given in section 6.3.3.3.5.

Each cantilever carries two resistance strain gauges. The details of the strain gauges are given below.

Manufacturer: KYOWA Electronic Instrument Company Limited, Tokyo, Japan

Type	KFC - 5 - C1 - 11
Lot No.	923-054
Gauge Length	5mm
Resistance	120.2 ± 0.3 ohm
Gage Factor	2.12 ± 1.5%

6.4.2.2. Strain Gauge Circuit

The schematic diagram of the strain gauge circuit used for the measurements of the Frictional Torque is given in Fig. 6.27. The gauges are connected as a four-active-arm bridge to provide

SCANNING ELECTRON MICROGRAPH OF WORN SPECIMENS

LOAD 490 N

SPEED 0.965 m/s

ROTATING SPECIMEN

x 2200

PHOTOGRAPH 9.33

SCANNING ELECTRON MICROGRAPH OF WORN SPECIMEN

LOAD 490 N

SPEED 0.965 m/s

WITH 0.02% O_2

ROTATING SPECIMEN

x 2200

PHOTOGRAPH 9.34

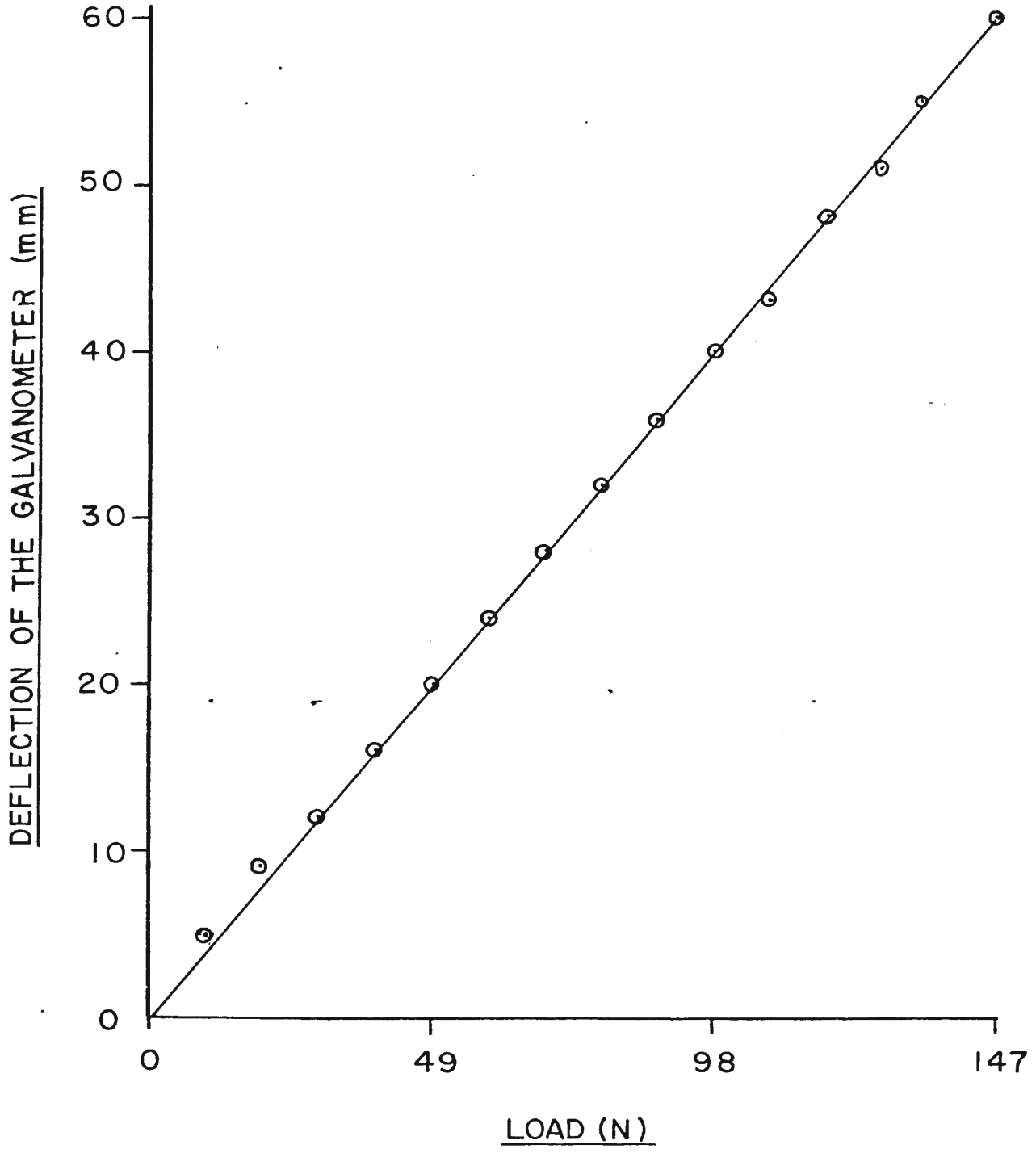

FIG· 6·25

CALIBRATION CURVE FOR THE HYDRAULIC PRESSURE TRANSDUCER (USING TYPE SMI/S GALVANOMETER AND AMPLIFIER)

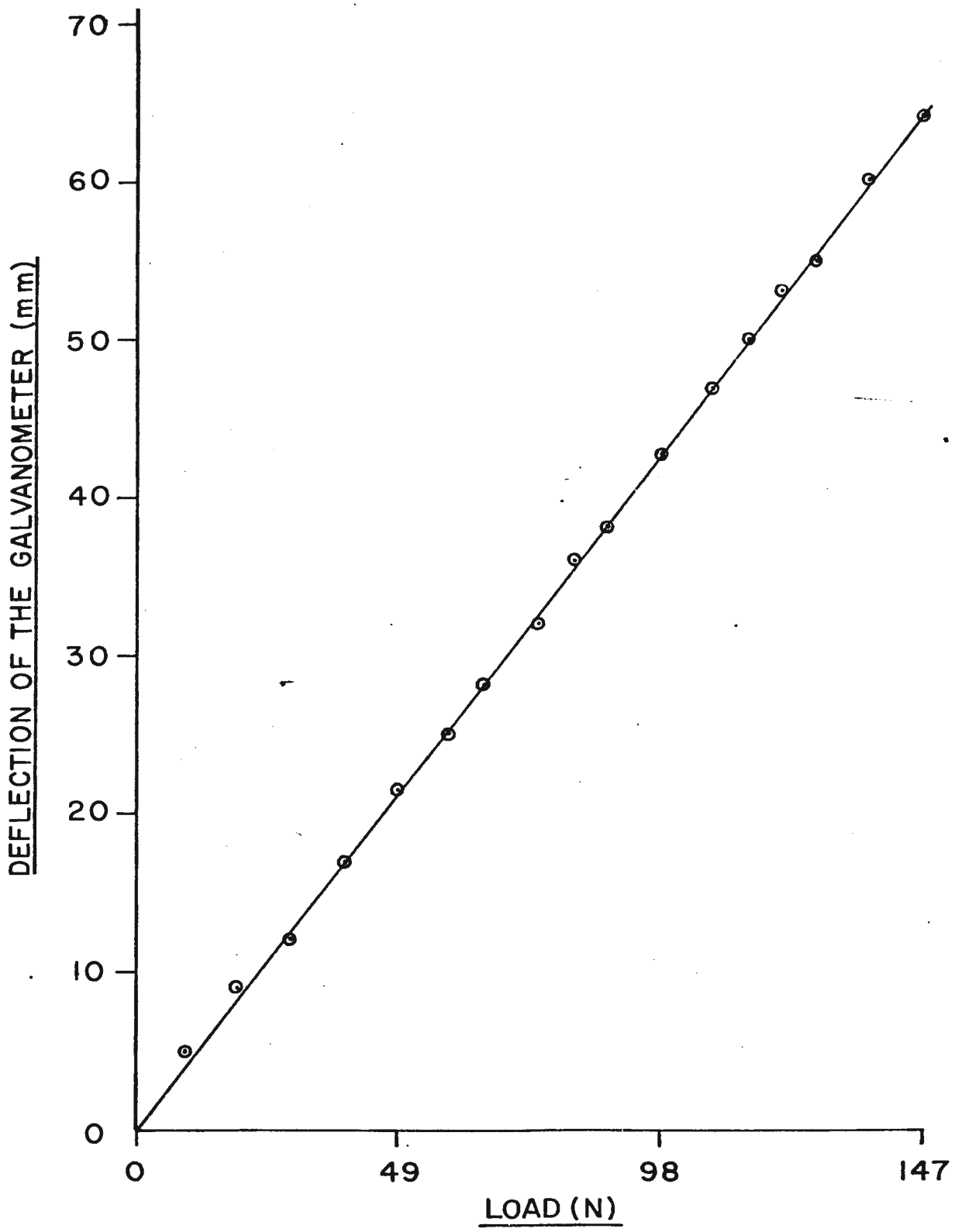

FIG· 6·26

CALIBRATION CURVE FOR THE HYDRAULIC PRESSURE TRANSDUCER (USING TYPE SMI/L GALVANOMETER)

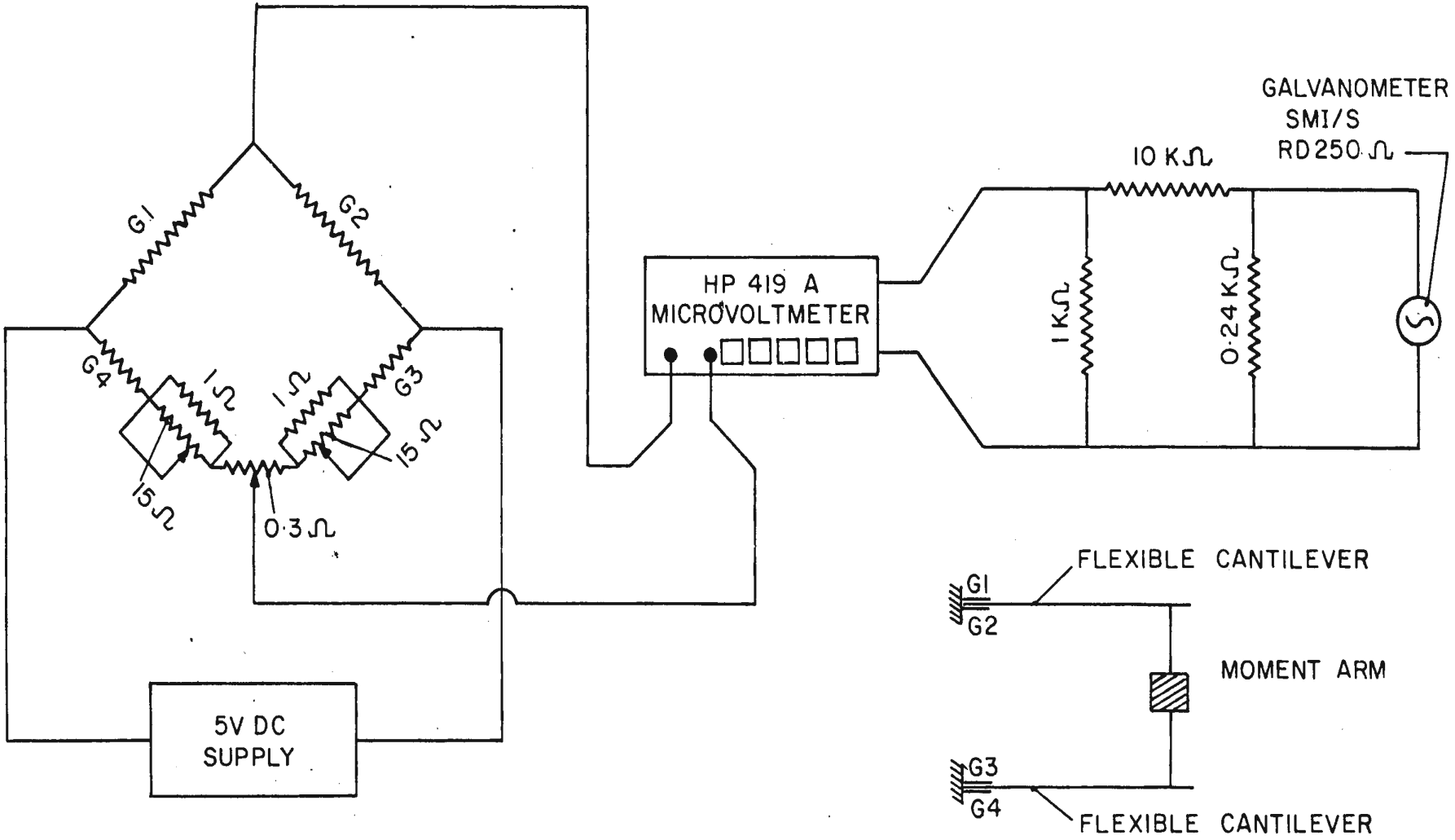

FIG·6·27

STRAIN GAUGE CIRCUIT FOR FRICTIONAL TORQUE MEASUREMENTS

four times the bridge output of a one-active-arm bridge as well as to compensate for thermal effects. An additional advantage of this arrangement is the fact that strain produced in the gauges, because of motion of cross beam along the axis of the shaft, does not affect the output voltage of the bridge. In other words, the output of the strain gauge bridge, is a measure of the frictional torque alone.

The output of the strain gauge circuit is amplified by a Hewlett Packard Model 419A DC Voltmeter. The amplified output can be recorded on a multichannel ultra violet recorder. A SMI/L galvanometer (supplied by Southern Instruments, natural frequency 160 Hz) is used to record the output.

6.4.2.3. Calibration of the Strain Gauges

The strain gauges were calibrated under static conditions.

A known torque was applied to the stationary specimen by suspending weights from it. The schematic drawing for this set-up is shown in Fig. 6.28. The torque was increased in steps of 260N.mm from no torque to 3900N.mm of torque. The output of the bridge was recorded on the ultra violet recorder. The torque was then decreased in the same steps and the output was recorded.

The calibration curve for the strain gauges is given in Fig. 6.29.

*6.4.2.4. Caluclation of the Coefficient of Friction between two Specimens during Rubbing from the Frictional Torque Measurements

The specimen contact is analogous to the contact at a cone clutch.

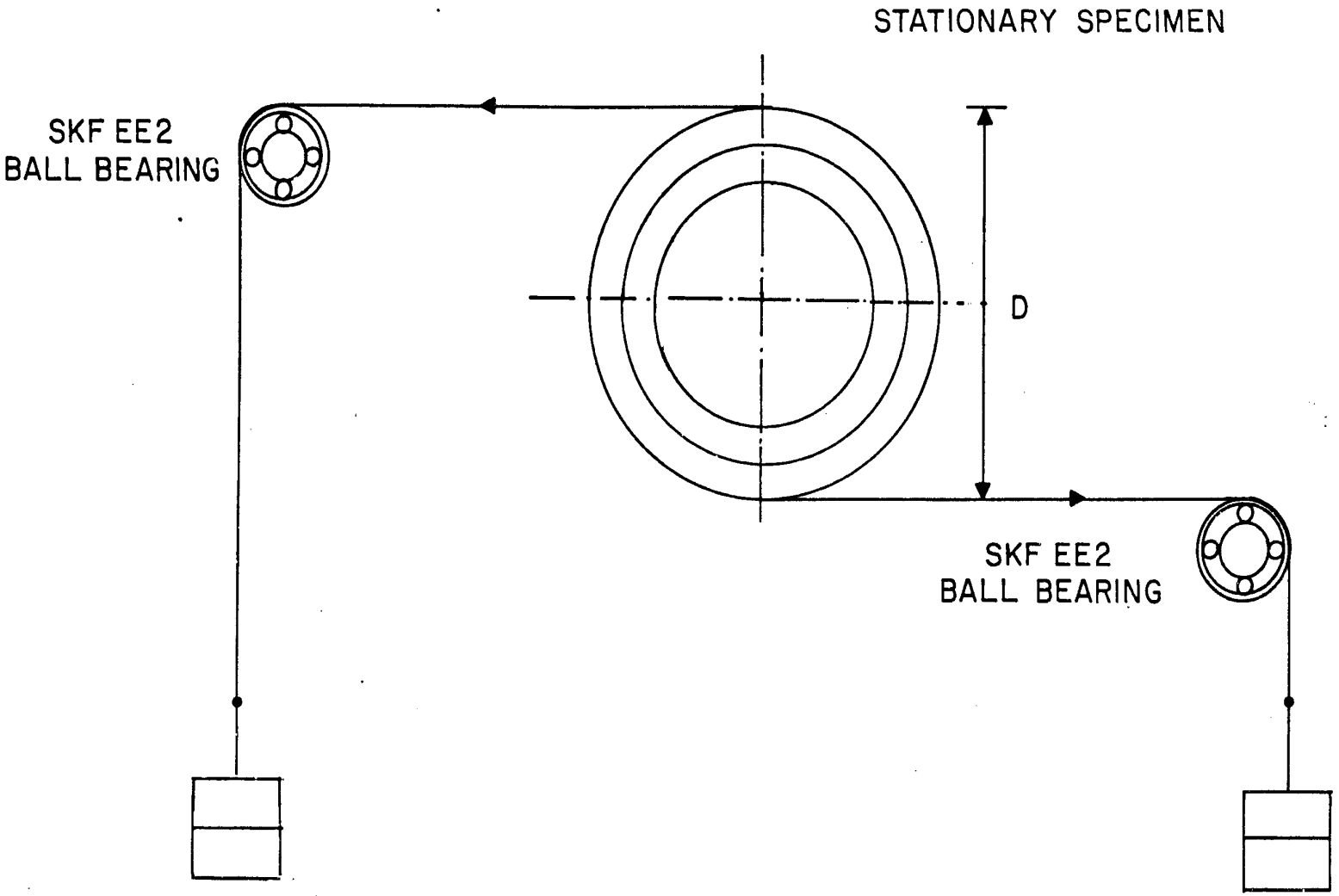

FIG· 6·28

SCHEMATIC FOR APPLYING TORQUE ON THE STATIONARY SPECIMEN FOR STRAIN GUAGE CALIBRATION

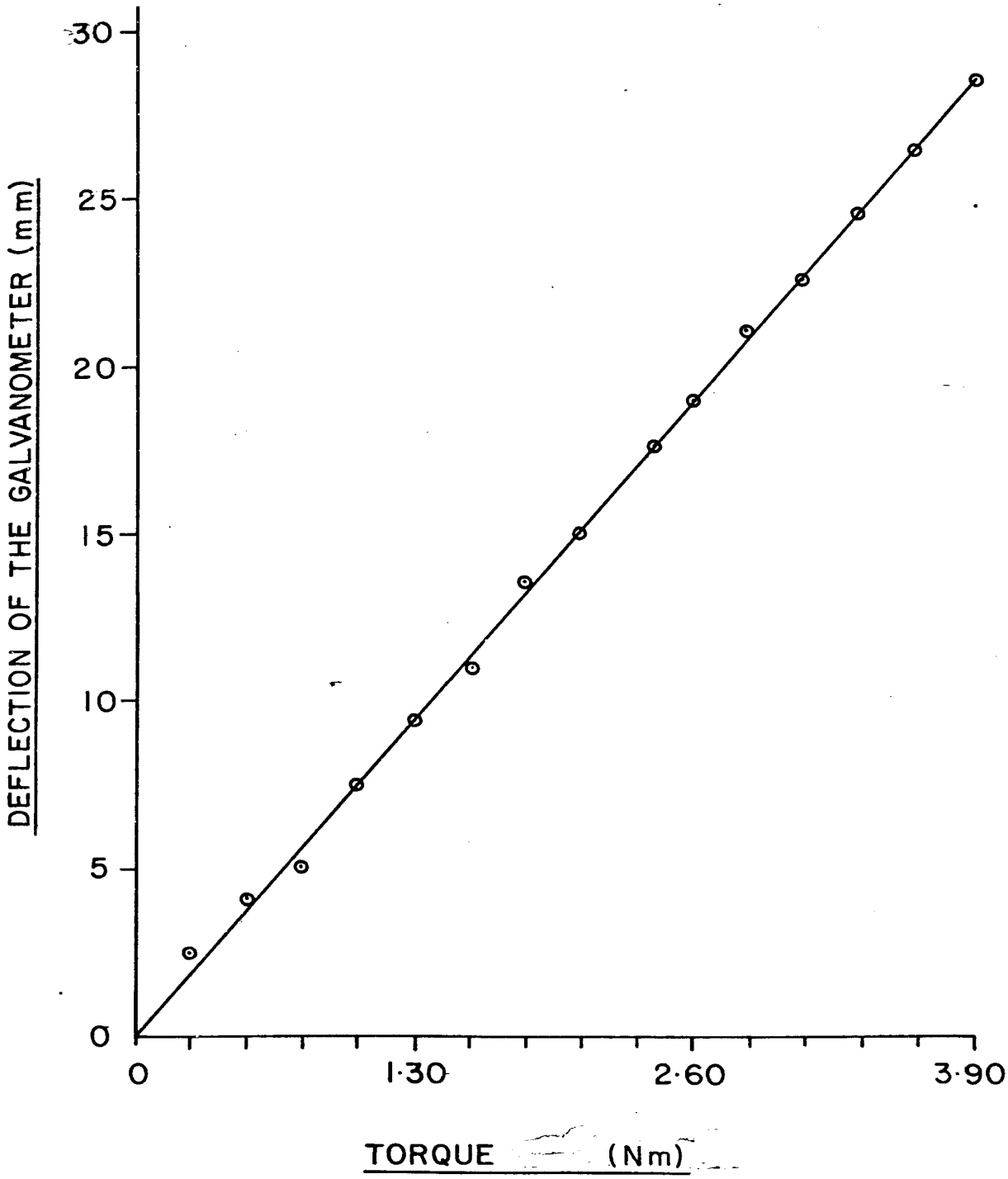

FIG· 6·29

CALIBRATION CURVE FOR THE STRAIN GAUGES USED FOR THE TORQUE MEASUREMENTS

During rubbing the contact is made between Do=20.95mm and Di=15.88mm (see Fig. 6.13). The torque produced at the interface ($\bar{T}$) is given by

$$T = \frac{N.f}{\sin\alpha} \left[1/3 \left(\frac{Do^3 - Di^3}{Do^2 - Di^2}\right)\right] \qquad (6.1)$$

where N: normal load applied to the specimens
f: coefficient of friction
α: pitch cone angle (63^o)

From equation (6.1)

$$T = 10.40 \quad Nf \qquad N.mm \qquad (6.2)$$

From the calibration curve for the strain gauges the torque applied to the stationary specimen (T in N.mm) is related to the deflection of galvanometer (X in mm) by the equation

$$T = 136.82 \quad .X \qquad (6.3)$$

From equations 6.2 and 6.3, the coefficient of friction is

$$f = 13.15 \quad .\frac{X}{N} \qquad (6.4)$$

Thus, the friction coefficient between the two rubbing specimens can be directly calculated from the output of the strain gauges.

6.4.3. Surface Temperature

The average surface temperature of the specimens is estimated by inserting two thermocouples at different distances from the contact surface. In photograph 6.30, the thermocouples in the rotating specimen are shown.

The thermocouples were supplied by Thermo Electric Canada. The specifications of the thermocouple are given below.

Type: chromel (+), Alumel (-)

Sheathing: stainless steel, 600mm immersion length

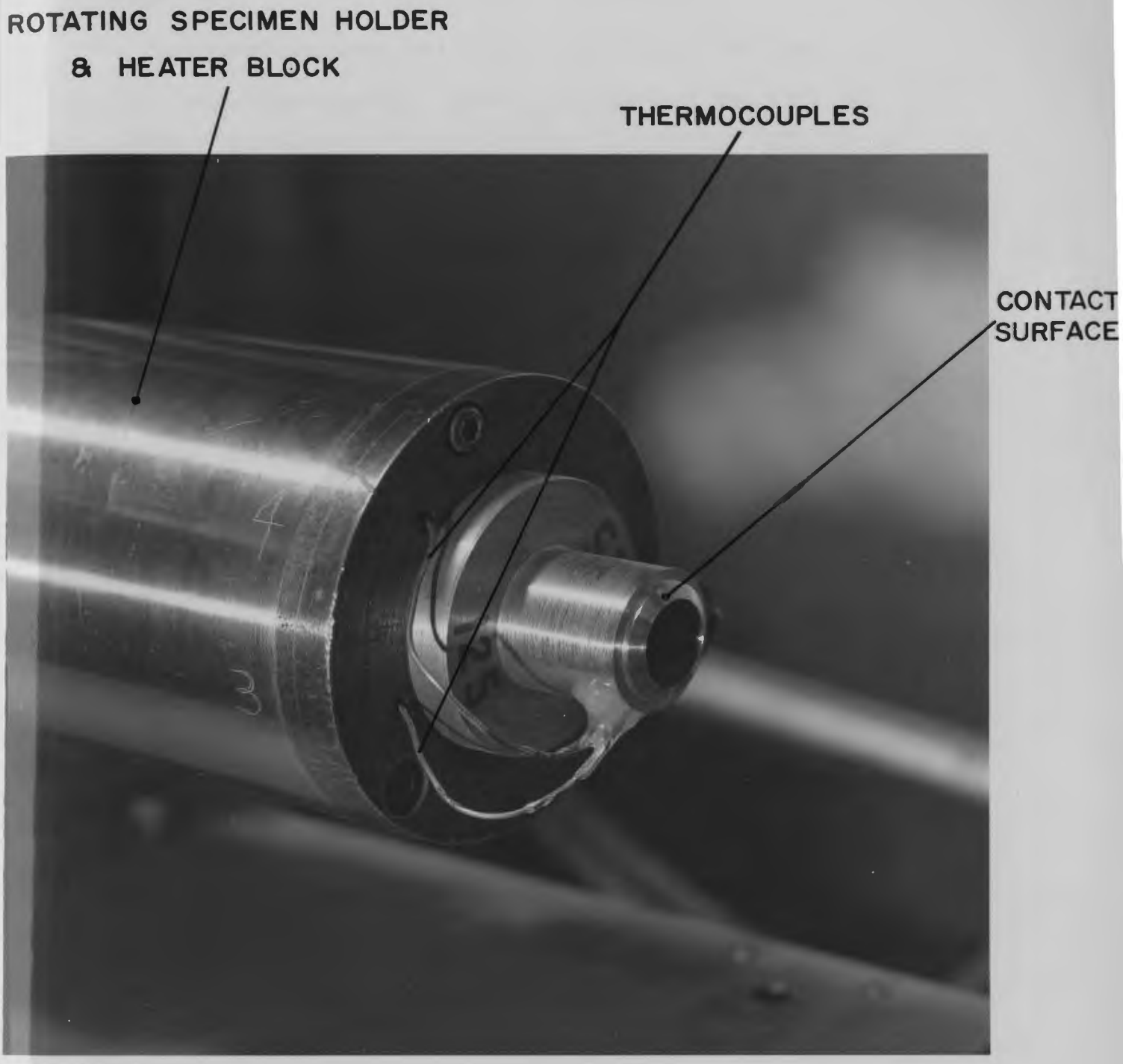

ROTATING SPECIMEN & HOLDER
(SHOWING THERMOCOUPLES)

PHOTOGRAPH NO. 6.30

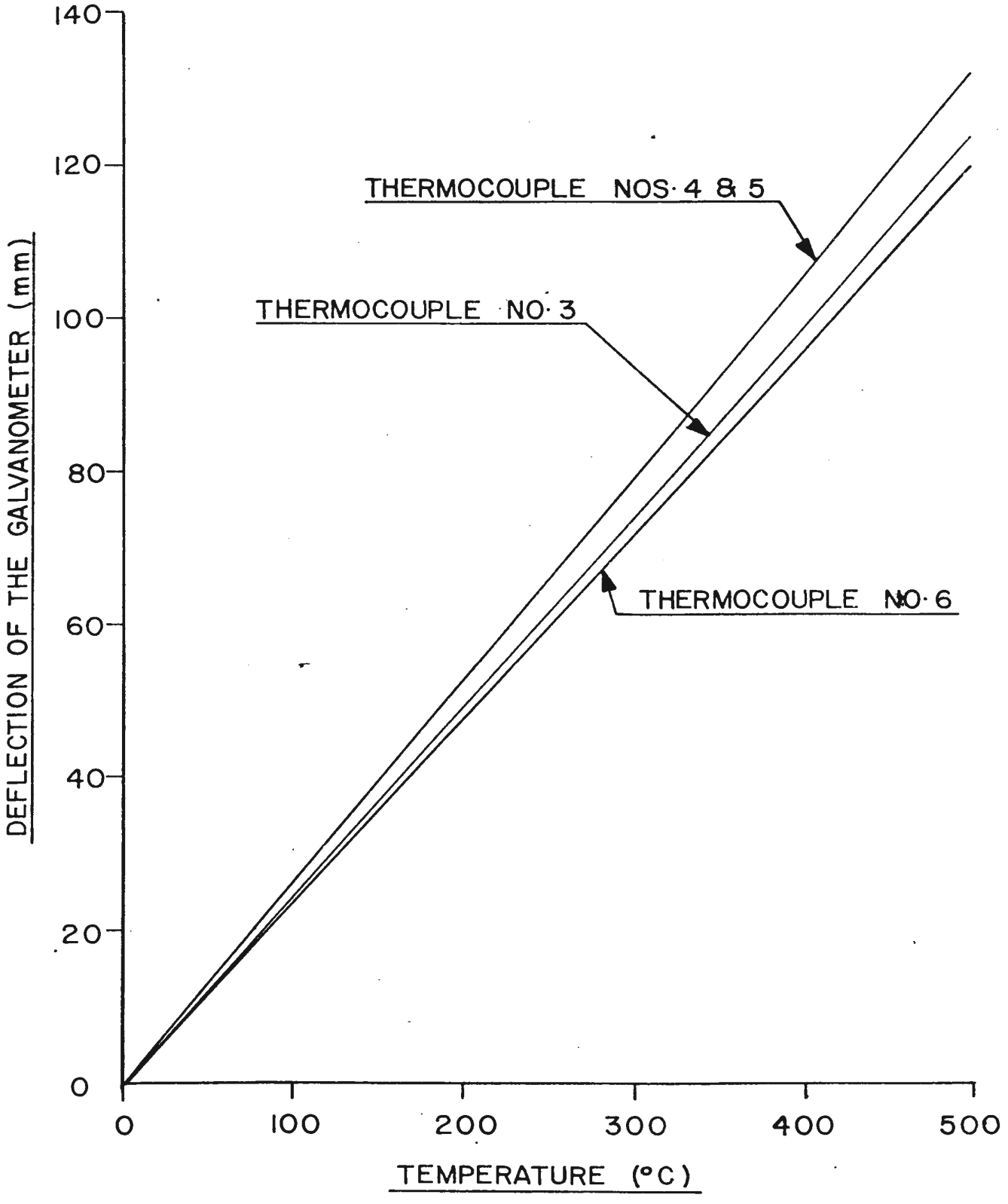

FIG. 6.31

CALIBRATION CURVE FOR THE THERMOCOUPLES

6.4.4.2. Balancing of the Rotating Parts

The schematic diagram of the setup used for dynamic balancing of the rotating parts is shown in Fig. 6.32. All the equipment were supplied by Bruel & Kjaer, Copenhagen, Denmark.

The Accelerometer (Type 4339) was placed on the main bearing of the lathe head stock. The accelerometer was connected to the Frequency Analyser (Type 2107) through a vibration Pick-Up Preamplifier (Type 2625). The frequency analyser was set to a frequency corresponding to the speed of rotation of the lathe machine.

The output from the frequency analyser was used to trigger the Motion Analyser (Type 4911) ensuring a reasonably clean triggering waveform.

The method of balancing the rotating part was similar to the one described in the book "Application of B & K Equipment to Mechanical Vibration and Shock Measurements", (1972), supplied by Bruel & Kjaer.

The balance weights are shown in Photograph 6.33.

6.4.4.3. Power Spectral Density Measurements

The block diagram for the power Spectral Density measurements is illustrated in Fig. 6.34.

The Frequency Analyser (Type 2107) is connected to the Level Recorder (Type 2306) and to the Accelerometer (Type 4339) with preamplifier (Type 2625). A -3dB/octave filter is connected directly to the terminals marked "EXTERNAL FILTER" in the frequency Analyser. The -3dB/octave filter provides the correction, to be

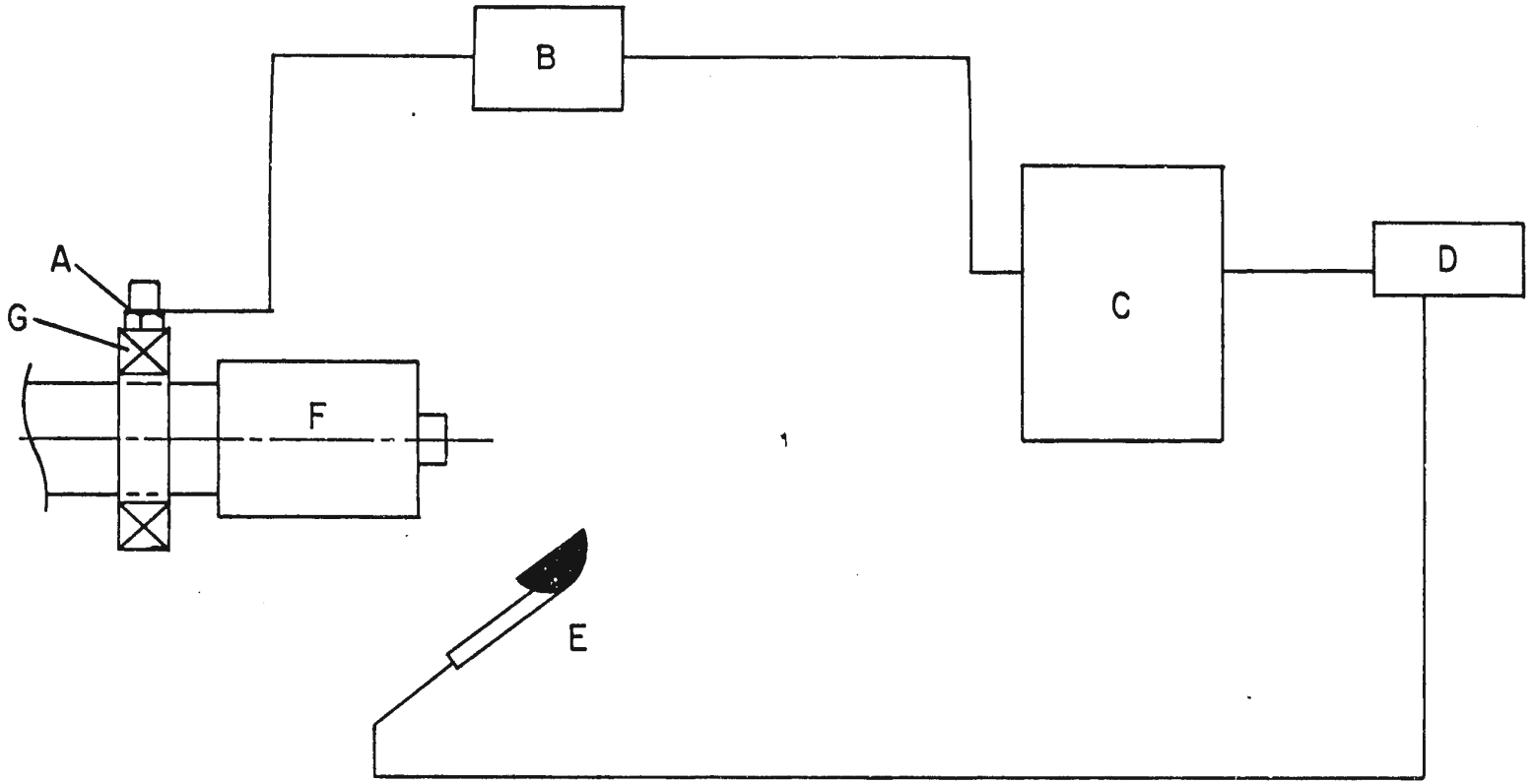

A- ACCELEROMETER
B- VIBRATION PICK-UP PREAMPLIFIER
C- FREQUENCY ANALYSER
D- MOTION ANALYSER
E- STROBOSCOPE
F- ROTATING PART TO BE BALANCED
G- BEARING OF THE LATHE

FIG· 6·32

SCHEMATIC DIAGRAM OF THE BRUEL & KJÆR UNIT USED FOR DYNAMIC BALANCING OF THE ROTATING PARTS

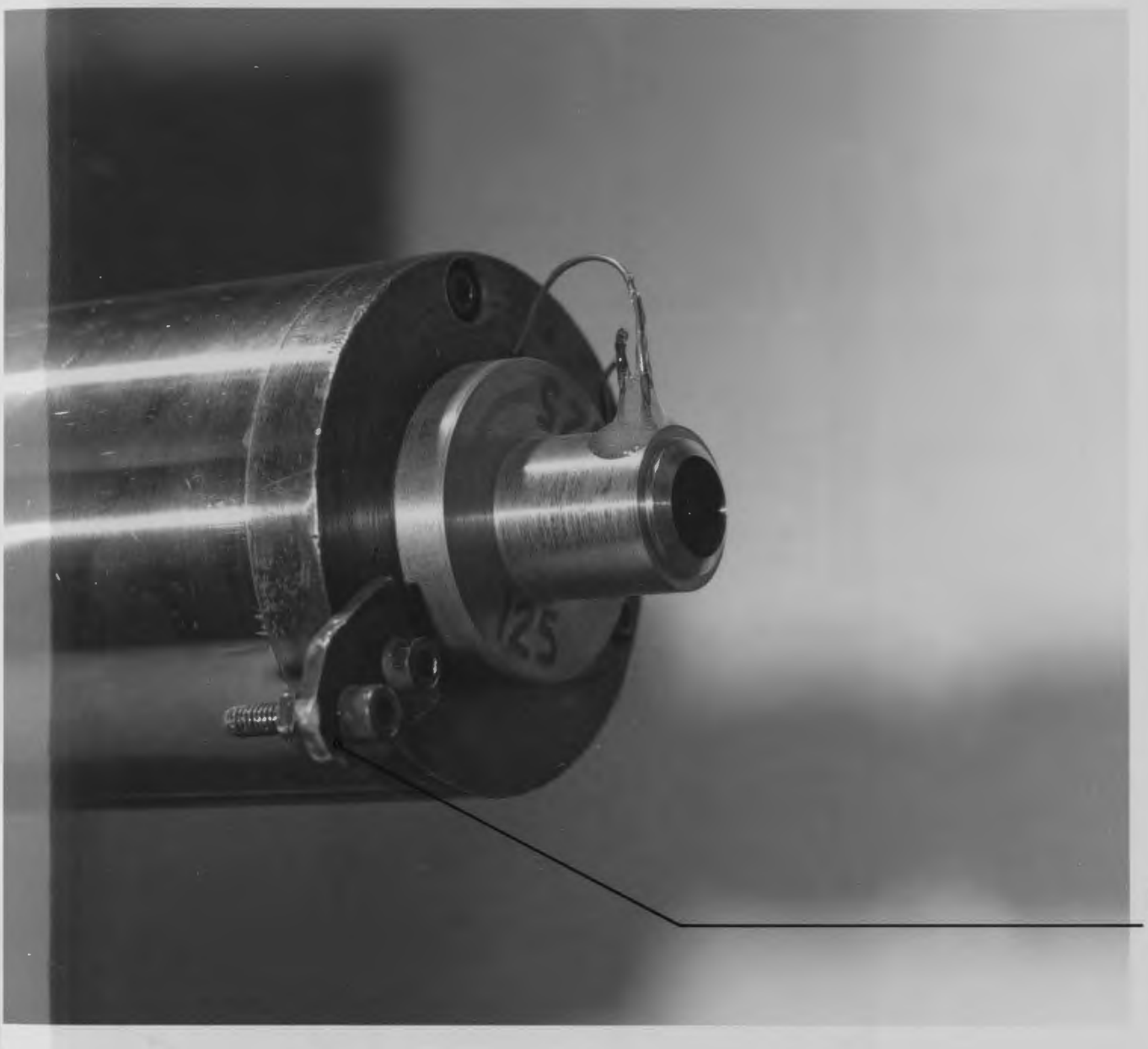

ROTATING SPECIMEN & HOLDER
(SHOWING BALANCE WEIGHT)

PHOTOGRAPH NO. 6.33

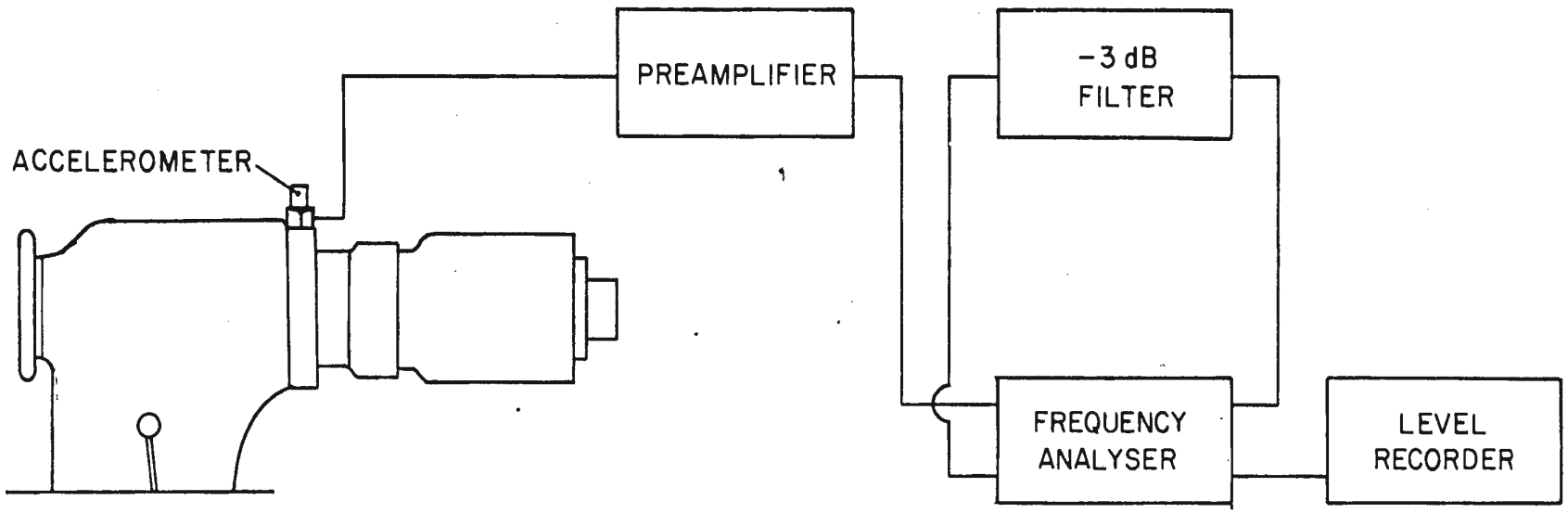

FIG· 6·34

BLOCK DIAGRAM FOR VIBRATION – POWER SPECTRAL DENSITY MEASUREMENTS

made to the measured spectrum, to obtain a power spectral density diagram.

In order to keep the statistical error in the Power Spectral Density measurements within 10%, the following settings of the control knobs were used:

Frequency analyser:

Octave selectivity "Max" (Effective bandwidth 8%)

Level Recorder:

Writing speed	80mm per sec.
Paper speed	3mm per sec.
Drive shaft speed	12 RPM

The Power Spectral Density of the vibration in the rig was recorded at six different locations, three on the stationary specimen holder assembly side and three on the rotating specimen holder side (on the lathe head stock).

The experimental setup for the power spectral density measurements is shown in the Photograph 6.35.

*6.4.5. Displacement of the Specimen

The displacement of the specimen, during wear, was recorded by a Linear Displacement Transducer (supplied by Schaevitz Engineering) mounted against a polished face plate on the moment arm. The moment arm is attached to the loading shaft to which the specimen is attached.

The output of the transducer is recorded on a DC Recorder (supplied by Bausch and Lomb).

The transducer was calibrated by applying a known displacement to the core of transducer, by a micrometer, and noting the output.

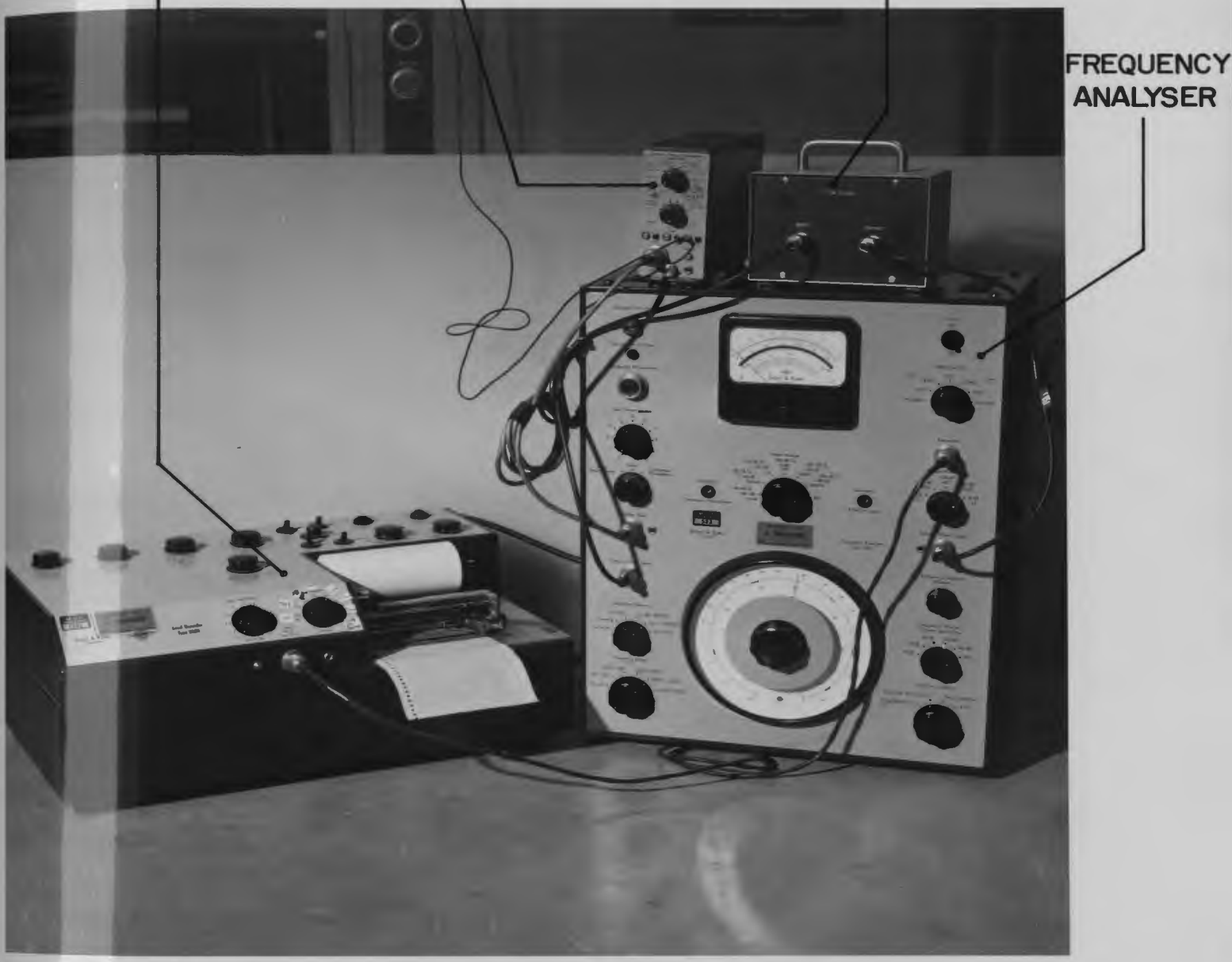

VIBRATION ANALYSER

PHOTOGRAPH NO. 6.35

The schematic diagram for specimen displacement measurements is shown in Fig. 6.36.

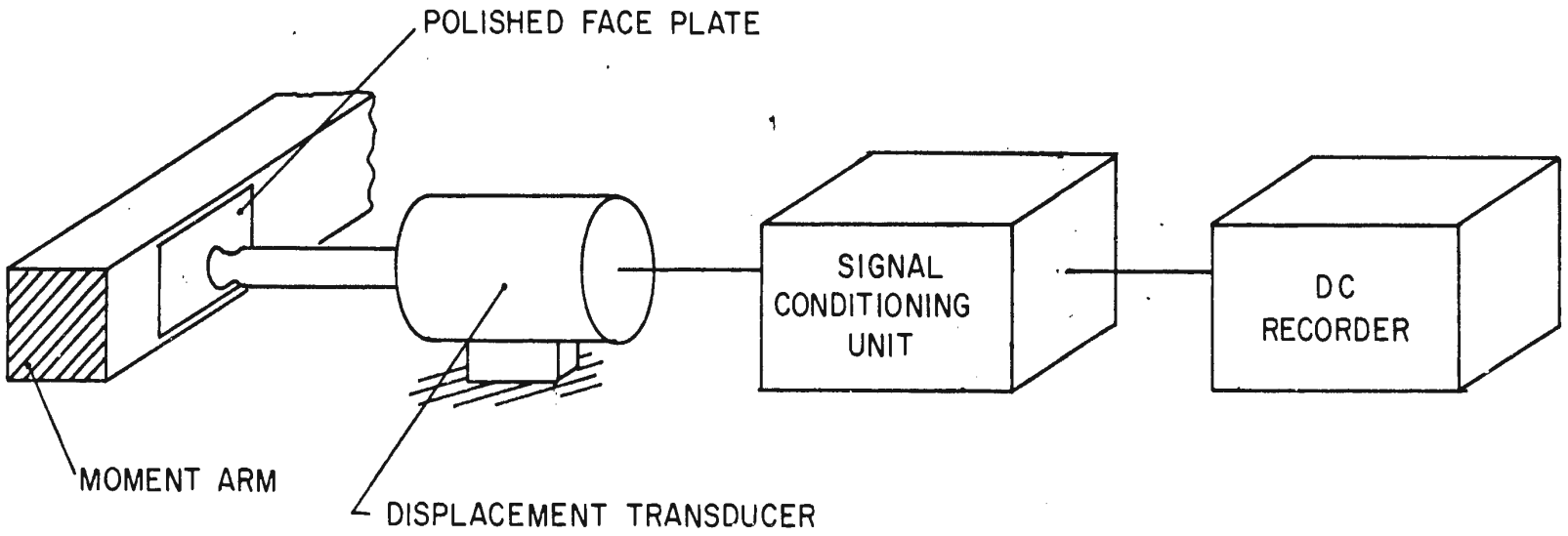

FIG· 6·36

SCHEMATIC DIAGRAM FOR SPECIMEN DISPLACEMENT MEASUREMENTS

CHAPTER 7

MEASUREMENT OF PARAMETERS AFTER RUBBING

7.1. Weight Loss

The test specimens were weighed before and after each run. The difference in the two weights, ie. the weight lost by the specimens, was a measure of the wear of the specimens.

A Gram-Atic Electronic Balance (supplied by Fisher Scientific Company, Sensitivity 0.0001g) was used for weighing the specimens.

The specimens were cleaned in acetone in an ultra-sonic bath for at least half an hour before they were weighed.

7.2. Surface Topography and the Embedded Wear Debris Particles

Each test specimen was used for three wear tests. After each test the specimen was refaced and polished to provide a new wear surface for the next test.

In order to examine the topography of the worn surfaces, a two-stage technique was developed to make replicas of the surface.

The replica medium for the first stage replicas was 10% solution of Cellulose Acetate in acetone. For the second stage replicas, 8% solution of Poly Vinyl Alcohol in water was used.

The wear debris particles transferred from the worn specimen to the second stage replica was examined with a Scanning Electron

Microscope (Cambridge Stereoscan Mark II, made by Kent Cambridge, England) for composition, shape and size.

7.3. Analysis of the Wear Debris Particles

7.3.1. Identification

The constituents of the wear debris particles were identified by a X-Ray Powder Diffraction Unit (made by Siemens, Germany) using a Debye-Sherrer powder diffraction camera.

7.3.2. Size Analysis

The size distribution of the wear debris particles was determined on a Zeiss Micro-Videomat Unit (made by Carl Zeiss, Germany).

The particles were mounted on microscope slides using 0.5% Pro-texx mounting medium (supplied by Fisher Scientific Company) in xylene.

7.3.3. Shape Analysis

The shapes of the wear debris particles were examined on the scanning electron microscope. Use was made of an Energy Dispersive X-Ray Spectrometer (made by Kevex Corporation) and a count rate meter to identify the wear debris particles. It was possible to separate the metallic iron debris from the oxide debris.

7.4. Metallurgical Changes

The major items of equipment, a Metallurgical Microscope (Type MeF2 with Automatic camera and a Micro-hardness tester, made by Reichert,

Austria) and the Scanning Electron Microscope were used for observing the metallurgical changes in the worn specimens.

7.4.1. Topography of the surface

A general picture of the worn surface was obtained by looking at the surface at lower magnifications (up to x160) on the metallurgical microscope.

The metallurgical microscope is equipped with the usual facilities for the use of a polariser, analyser and the facilities for dark field and bright field illumination. This microscope is ideally suited for looking at the wear tracks, craters, large surface cracks and the wear debris particles embedded in the surface.

For more detailed investigation of the surface, the scanning electron microscope was used, where the worn surfaces were examined at higher magnifications (up to x20,000). The microscope has a provision whereby the specimen stage can be tilted, which permits the taking of stereo pictures. From a stereo picture, the thickness of the transferred layer or similar details can be determined.

7.4.2. Structural Changes

An annular piece was cut from worn specimens by cutting perpendicular to the specimen axis about 6mm from the rubbing surface.

The annular piece was further cut into two halves (see Fig 7.1). One half was used for examination of its worn surface. The other half was coated, by electroplating, with copper and nickel, then further cut into two quarters, which were mounted in bakelite for mettallographic study of cross sections through the material below the worn surface.

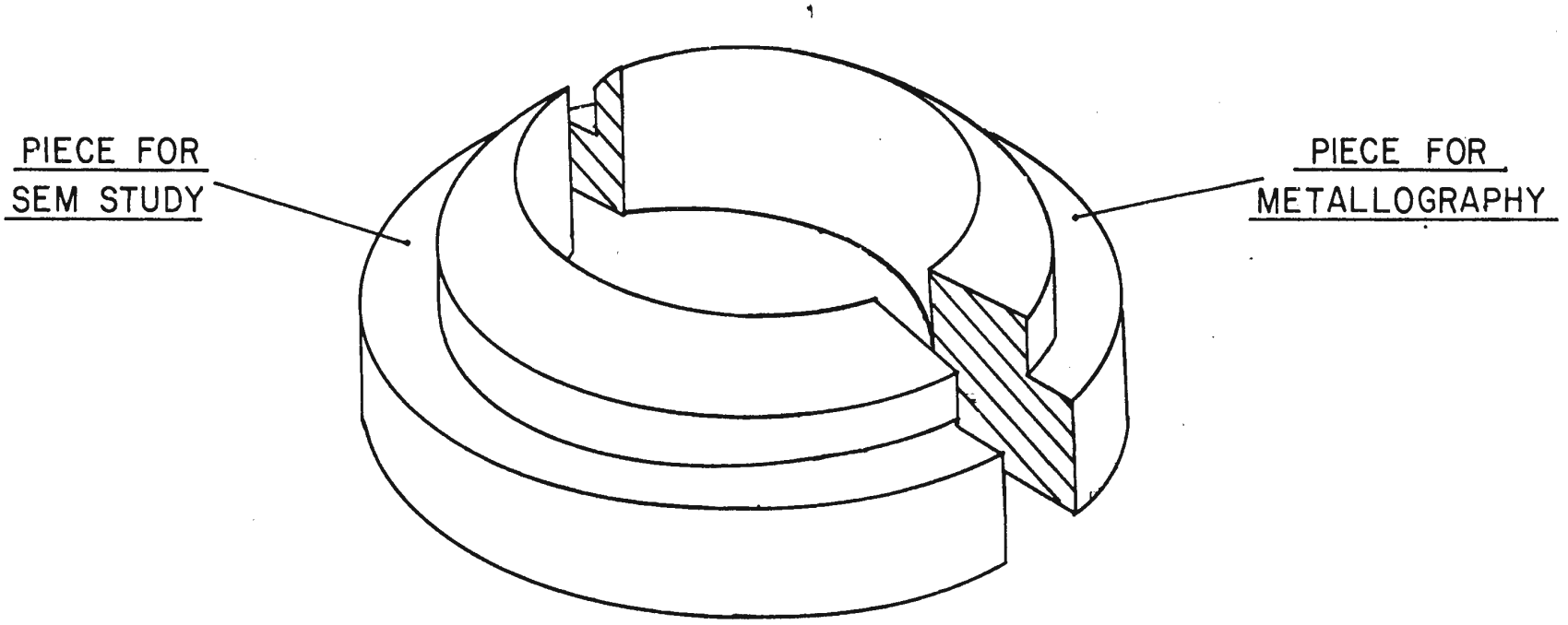

FIG· 7·1
CUTS FROM WEAR SPECIMENS FOR EXAMINATION

Fig 7.2 indicates the two cross sectional planes examined, one parallel to the sliding direction and one perpendicular to the sliding direction.

The mounted specimens were mechanically polished using different grades of emery paper and 0.25um grade diamond abrasive paste. The polished surfaces were etched in 2% Nital and the structure was examined on the metallurgical and the scanning electron microscope.

7.4.3. Microhardness Measurements

The hardness of the material at different depths below the wear surface was measured by a Microhardness Tester (made by Reichert, Austria) which can be fitted to the metallurgical microscope.

The polished and the etched specimens, prepared for examination of the structural changes were used for the microhardness measurements.

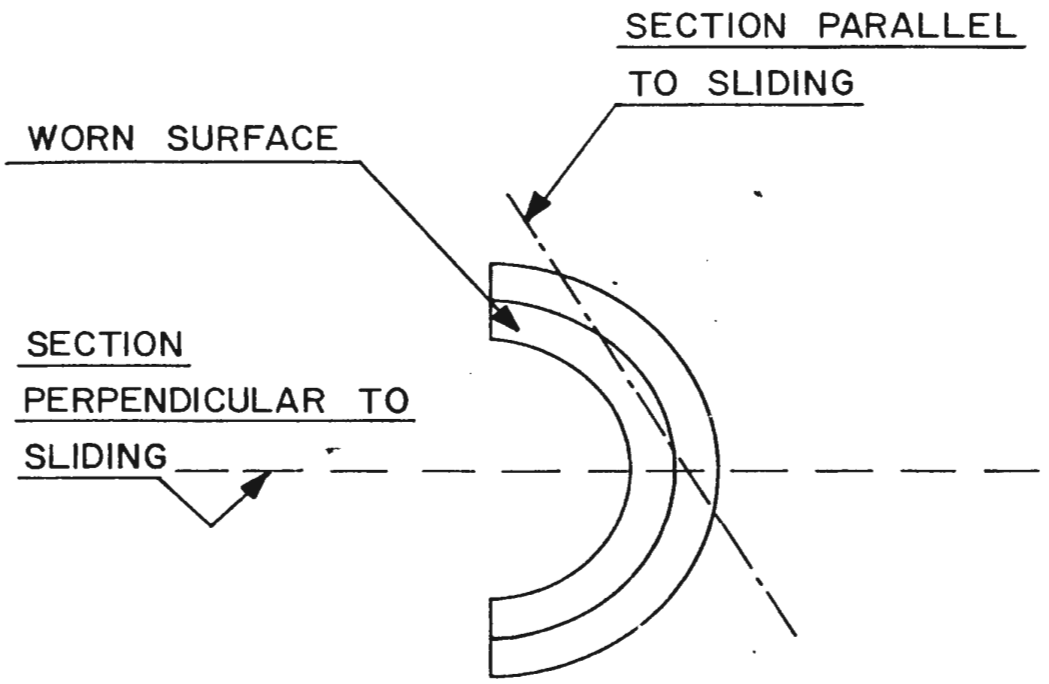

FIG· 7·2

PLAN VIEW SHOWING PLANES OF CROSS SECTION EXAMINED METALLOGRAPHICALLY

CHAPTER 8

THE WEAR TESTS

8.1. General

It is well known that load and speed can affect wear rates. The two parameters tend to affect the temperature of rubbing surfaces and, therefore, the rubbing is likely to be affected by the temperature alone.

On the test equipment being used in the present work, it is possible to vary these parameters within the following ranges:

Sliding Speed	0 - 3000 RPM (equivalent to 0 - 2.895 m/s for the specimens used)
Normal Load	0 - 1,960 N
Specimen Holder Temperature	20 - 600^{o}C

However, limited ranges of these parameters were used in the study.

In addition, it is possible to force air or gas mixtures between the specimen. The effect of this variable was also studied.

8.2. Effect of Speed on Wear Rate

In order to study the effect of sliding speed on wear rate, an initial series of experiments were carried out at various sliding speeds and normals as shown below without any gas flow, forced between the specimens:

Nominal load (N)	Sliding Speed (m/s)
295	0.965, 1.158 & 1.544
490	0.193, 0.386, 0.772, 0.965, 1.061, 1.158 & 1.544
980	0.772, 0.965, 1.158

Initially the experiments were conducted at a nominal load of 490N and sliding speeds of 0.193, 0.386, 0.772, 1.158 and 1.544 m/s. Increase in sliding speed gave a decrease in wear rate except between 0.772 and 1.158 m/s where a jump in the wear rate to a higher value was observed. A transition in the wear rate values was noticed in the range of 0.772 and 1.158 m/s. It was then decided to determine more precisely the speed where the increase takes place. Additional experiments were performed at the sliding speeds of 0.965 and 1.061 m/s. Indeed a transition was noticed at 1.061 m/s, where both high and low values of wear rate can occur. Higher wear rates were associated with the appearance of FeO (see Fig 9.2(a)).

The experiments at the two other loads, 295N and 980N were conducted in the speed range of 0.965 to 1.544 m/s and 0.772 to 1.158 m/s. The high vibration in the test machine corresponding to a load of 980N and a speed of 1.158 m/s indicated that any further increase in sliding speed at this load might cause a breakdown in the machine.

In all these experiments, it was noticed that about three quarters of the total weight of the wear debris particles were

collected inside the specimen.

8.3. Effect of a change of Specimen Holder Temperature

In the wear tests described in the previous section, for a load of 490N, the wear was found to decrease with an increase in speed from 0.193 m/s to 0.965 m/s. As noted above, at 1.061 m/s a scatter in the wear rate values was noticed. Some wear rates were roughly in the same order as the wear rate for 0.965 m/s, while others were quite high. In the wear debris of the experiments at 1.061 m/s, with high wear rates, FeO was noticed. It seemed likely that the appearance of FeO is associated with a jump in wear rate value.

Based on the oxidation theory, it can be assumed that once FeO appears, the significant temperature, ie. the temperature controlling the formation of this oxide which is about 570^{o}C. It was thought that a model for flow of heat could be postualted and verified using this fact.

A model for the distribution of heat from rubbing contact to the two specimens was postulated (described in Section 10.1.1.) and a second series of experiments were carried out to test the model.

The sliding speed and the mean normal load were kept constant at 0.965 m/s and 490N respectively. The specimen holder temperature was changed. At holder temperatures of 100^{o}C, 150^{o}C and 200^{o}C sets of experiments were performed, without gas flow.

8.4. Effect of Forcing Air through the Specimens

As noted in the objectives (refer to Chaper 1) we wished to study the influence upon wear of gas composition and its availability at its availability at the rubbing surfaces.

Unheated air was forced through the specimens at a supply pressure of 35×10^4 N/m^2 and flow rate of 75×10^{-6} m^3/s. The mean normal load was kept constant at 490N and speed was changed. Experiments were performed at sliding speeds of 0.193 m/s, 0.386 m/s, 0.772 m/s, 0.965 m/s, 1.061 m/s, 1.158 m/s and 1.544 m/s.

In a following series of tests air was preheated to 200^{o}C and was forced through the specimens at a flow rate of 75×10^{-6} m^3/s. Experiments were conducted at sliding speeds of 0.386 m/s, 0.772 m/s, 0.965 m/s and 1.158 m/s, keeping the load constant at 490N.

In a third series of tests corresponding to experiments without forced air, the load was changed to 295N and at sliding speeds of 0.965 m/s, 1.158 m/s and 1.544 m/s. The effect of forced air at a supply pressure of 35×10^4 N/m^2 and a flow rate of 75×10^{-6} m^3/s was studied.

Likewise, corresponding to earlier experiments without forced air, a series of experiments was conducted with a load of 980N, and with air at a supply pressure of 35×10^4 N/m^2 and a flow rate of 75×10^{-6} m/s, forced through the specimens. Sliding speeds of 0.772 m/s, 0.965 m/s and 1.158 m/s were used.

8.5. Effect of Gas Mixture on the Wear Rate

To pursue the question posed in the objectives (refer to Chapter 1), experiments were conducted with lower than atmospheric proportions of oxygen. The composition of the gas mixtures (%(V/V) oxygen in argon) used in all the experiments of this series were $0.02\%O_2$, $0.2\%O_2$ and $2.0\%O_2$.

The following combination of loads and sliding speeds were used:

Load (N)	Sliding Speed (m/s)
490	0.965 & 1.158
295	1.158

In addition to gas mixtures, pure argon was forced through the specimens as well, in the second series of experiments for this section.

The flow rate of the gas mixture for all these experiments was kept constant at 75×10^{-6} m^3/s and the gas supply pressure at 35×10^4 N/m^2.

CHAPTER 9

RESULTS

9.1. General

9.1.1. A Typical Test Procedure and Results

The description of a typical experiment , Dry Wear Test Experiment (DWTE) no. 40 is given in this section. All the other experiments were performed in a similar way, except the sets where air or various gas mixtures were forced through the specimens. For these sets the gas supply system was used, however, the rest of the experimental procedure was similar.

The distances of the thermocouple holes with reference to the contact surface on each specimen, was measured with a travelling microscope. The specimens were cleaned in acetone in an ultrasonic bath for at least half an hour and their weight determined.

The rotating specimen was then mounted on the rotating specimen holder and its position was adjusted so that the outer surface of the specimen ran true to within 25.4 μm (.0001 in.). The specimen was fastened in this position. The stationary specimen was attached to the stationary specimen holder and the lathe carriage was brought forward, guiding the contact surface of the stationary specimen to sit against the contact surface of the rotating specimen. The cup and cone configuration of the specimen surfaces (see Fig 6.13 and 6.14) permitted the self alignment of the specimens. At this stage

the stationary specimen was forced against the rotating specimen and the stationary specimen was clamped to the specimen holder.

Two thermocouples (T3 and T4 on the rotating specimen and T5 and T6 on the stationary specimen, T3 and T5 being nearer to the contact surface) were inserted into the specimen and were held in place by putting Five-minute Epoxy glue around the thermocouples on top of the specimens. Usually it took about half an hour before a satisfactory bonding was achieved.

The speed of the lathe machine was then set at the desired speed to within 0.1%. A stroboscope was used to check this speed. For Run DWTE 40 the speed was set to 400 RPM which correspond to a sliding speed of 0.386 ms^{-1} for the specimen configuration used for the tests.

All the electrical and electronic equipment (e.g. strain gauge circuits, amplifiers, transducers, displacement record, U.V. twelve channel recorder, B & K Vibration monitoring unit and the revolution counter, etc.) were switched on, and about three quarters of an hour of warm up time was given before the start of the actual experiment.

The hydraulic system was checked for any trapped air in the line. A high point vent was provided in the hydraulic line, which was opened to bleed any trapped air. Also, the bleeder screw on top of the normal load cylinder was taken out so that oil from the constant pressure cell could flow past the hydraulic line and out through the bleeder screw opening. This was done to make sure that no air was trapped in the line. The bleeder screw and the high point

vent were then replaced and the fittings were made tight.

The motor for paper drive on the U.V. Recorder was switched on and zero readings for thermocouples T3, T4, T5 and T6, strain gauges and normal load were recorded.

The wear debris catcher was kept under the specimen and two 0.22 μm filters were placed in the Millipore Gas line filters. The revolution counter was reset to zero and the cooling lines were turned on.

The stationary specimen was pressed against the rotating specimen and with the flow control valve, in the line between the constant pressure cell and normal load cyliner, fully open the loading shaft was moved backward, away from the rotating specimen, till the cross beam reached about the middle of space between the rear end support and the stationary holder assembly. This was important in order to provide space for the cross beam to move freely, both in the forward and reverse direction during the experiment. The flow control valve was then closed and the desired nominal load, 5kg for run DWTE 40 was placed on the load pan of the constant pressure cell. The dial reading indicating the longitudinal position of the carriage on the lathe was noted down and the carriage was moved backwards, so that the specimens were not touching. The main bearing and the aligning bearing of the stationary specimen holder assembly were flushed with Molyslip (Lubricating Oil) and the oil reservoirs were filled.

The wear test machine was then ready for the experiment. The brake from the lathe machine was removed and the lathe was running at

the preset speed. The carriage was brought forward till the dial reading indicating the position of the carriage reached the previously noted value. The carriage was locked in this position. At this stage the specimens were in contact. The paper drive on the recorders were switched on, the revolution counter was set to zero, the vacuum pumps in the wear debris particle collection line were switched on and then the flow control valve in the hydraulic line was opened so that the nominal load acted at the contact surface.

Experiment DWTE 40, was one of the experiments designed to study the effect of sliding speed on wear. The mean nominal load at the wearing surface was 490N and the sliding speed was set at 0.386 m/s. The specimens were not heated and air was not forced through the specimens. It was decided that for all the experiments with sliding speeds up to 1.061 m/s, the duration of experiments would be 30,000 revolutions, while for speeds of 1.158 m/s and 1.544 m/s the duration would be extended to 40,000 revolutions. The additional 10,000 revolutions were needed to allow for sufficient time to complete auxiliary tests (e.g. vibration monitoring).

On the one hand it was desired to have a complete record of all the variables (see Sec. 4.6.) throughout the run. On the other hand it was desired to have high frequency records of some of the variables (e.g. load). The U.V. Recorder is used because of its ability to follow high frequency signals. However, it would be expensive and cumbersome to have a high speed recording for a complete run, consequently, the oscillograph from the U.V. Recorder

was obtained at different intervals during the run. During some of the intervals the paper speed was high while in others it was low.

The intervals used were the same for all the runs and also the paper speed was predetermined. The following intervals and paper speed settings were used.

Revolutions on Counter when paper drive was switched on (in X1000)	Paper Speed on U.V. Recorder (inches per second)
Start	1.9
1	1.9
3	1.9
4	0.9
5	0.9
7	3.6
8	0.9
12	0.9
15	18.0
19	0.9
29	3.6
39 (For 1.158 m/s & 1.544 m/s only)	3.6

At 15000 Revs, the debris catcher was taken out and a new debris particle catcher was placed. To check the identification of the thermocouples on the chart, each thermocouple lead was shorted in turn.

The Vibration was recorded during the experiment at the predetermined locations as noted in Section 9.1.2.8. However, only five readings out of a desired six readings could be taken in most of the experiments due to a shortage of time.

When the counter read 29,500 Rev., the vacuum pump in the debris collection line was stopped and at 30,000 Rev. the experiment

was terminated by unlocking the carriage and moving it away from the rotating specimen. The oil control valve was closed and the lathe machine was stopped. All electronics was switched off. The cooling water was left on for at least two hours after stopping the experiment.

The wear debris particles collected inside the specimens were taken out and put in a petri-dish. The four lots of wear debris particles, two collected on the wear debris catcher, one collected on the Millipore filter and one from the inside of the specimen were weighed. (When there is sufficient gas flow between the specimens, no debris was found inside the specimen.)

The thermocouples were removed from the specimen, very cautiously and by using a sharp knife to peel off the epoxy glue from the glue-metal interface. The specimens were taken out from the holders and the first stage replica of wear surface was made as described in Section 7.2. The specimens were then cleaned in acetone in a ultrasonic bath and their weight determined.

Sections from the test samples were cut for metallurgical and topographic studies as described in Section 7.4.2.

Samples for the identification of the wear debris particles and the size analysis, were taken from the wear debris particles after the debris were weighed.

The measurement of weight loss and topography of the surface are fairly straight forward, and there is only one such measurement for each specimen in the run, where as numbers to characterize both

temperatures and vibration during the run, have to be derived from fairly complex sets of readings from several different locations.

Table 9.1. shows a typical format used for interpreting the galvanometer deflection on U.V. Oscillograph. The table contains the results from DWTE 40. The numbers inside the table, in the first row, represent the total galvonometer deflection, for the given function, at the given number of revolutions. The second row gives the net deflection which is obtained by subtracting the room temperature reading (initial position of the galvanometer) from the total galvanometer deflection. The third row represents the actual value of the function which is obtained from the calibration curves for that function. The two bottom rows in the table give the extrapolated surface temperature for the rotating and the stationary specimen surfaces. The procedure for extrapolating these temperatures is given in detail in Appendix A. The distances used in the calculation X_1, X_2, & X_3 were measured on specimens as

$X_1 = 0.075$ in.

$X_2 = 0.100$ in.

$X_3 = 0.100$ in.

By substituting these values in Eq^n. A-3 & A-5

$$\text{Text } P = T3 + 2.6125\ (T3 - T4)$$

& $$\text{Text } P' = T5 + 2.6125\ (T5 - T6)$$

Once T3, T4, T5 & T6 are known Text P - extrapolated surface temperature for the rotaing specimen and Text P' - extrapolated surface temperature for the stationary specimen can be determined.

TABLE 9.1

A TYPICAL RESULT - READ FROM U.V. OSCILLOGRAPH

DWTE: 40 DATE: 2.1.74 RPM: 400 DETAIL: Cold/No Air LOAD CYCLES: 510 HZ

REVOLUTIONS	INITIAL DEFL.	1K	3K	4K	5K	7K	8K	12K	15K	19K	
FUNCTION											
T3	0	24.5	27	29.5	30	29.5	30	34.5	34	34	Reading
		24.5	27	29.5	30	29.5	30	34.5	34	34	Deflection (mm)
		96	104	114	116	114	116	134	132	132	°C
T4	8	35	33	34.5	34	33.5	34	36.5	39.0	39.0	Reading
		27	25	26.5	26	25.5	26	28.5	31.0	31.0	Deflection (mm)
		95	103	108	107	106	107	117	127	127	°C
T5	15	25	42.0	42.0	43.0	43.0	44.0	43.0	44.0	43.5	Reading
		10	27.0	27.0	28	28	29	28	29	28.5	Deflection
		39	104	104	108	108	112	108	112	110	°C
T6	20	28.5	40.5	41.5	41.5	42	42.5	41.5	40	41.5	Reading
		8.5	20.5	21.5	21.5	22	22.5	21.5	20	21.5	Deflection
		34	84	87	87	89	91	87	83	89	°C
N	64	65	70-100	80-100	80-100	80-100	75-95	78-98	75-95	75-95	Reading
(Normal Load)		1	6-36	16-36	16-36	16-36	11-31	14-34	11-31	11-31	Deflection
			140-840	375-840	375-840	375-840	256-723	326-793	256-723	256-723	(N)
TQ	40.0	55.0	58.0	58.5	58.5	58.5	58.5	58.5	58.5	59	Reading
(TORQUE)		15.0	18.0	18.5	18.5	18.5	18.5	18.5	18.5	19	Deflection
		40	.48	.50	.50	.50	.50	.50	.50	.51	f
Text R (°C)		100	108	130	140	134	136	180	151	150	(150)
Text S (°C)		52	156	147	163	157	167	163	177	165	(165)

The number on the right hand bottom corner of the table, inside brackets, are the mean extrapolated surface temperatures. The method for calculating this mean value from the temperature distribution from 3000 revolutions to 30,000 revolutions is shown in Appendix B.

For the fluctuations in the normal load acting at the specimen interface, the minimum and the maximum values are read. Also when the paper speed was kept at 18 ips the frequency of load fluctuation was measured. The load was fluctuating at a rate of 510 cycles/sec.

The record of vibrations in the lathe machine for DWTE 40 is shown in Fig 9.1. The position of the accelerometer, various settings of the pre-amplifier, frequency analyser and level recorder are given on the graph. The X-axis is the frequency scale and the frequency of the peaks is written adjacent to the peak. The vibration reading goes back to zero level, each time the range is changed on the analyser. The Y-axis in Fig 9.1. is the B-power scale. The values of the divisions are written in $(g^2/HZ) \times 10^{-4}$. These readings are shown in Table 9.2. together with the linear of displacement (amplitude) calculated from them. The integrated power spectral density ($\sum_{20HZ}^{3000HZ} g^2/HZ$) of the vibration was determined by adding the areas under each peak over the range of 20HZ to 3000HZ. The calculated values are shown in the last column in Table 9.2.

The results of the X-ray diffraction are shown in Table 9.3. The wear debris particles were identified as α-Fe, α-Fe_2O_3 & Fe_3O_4.

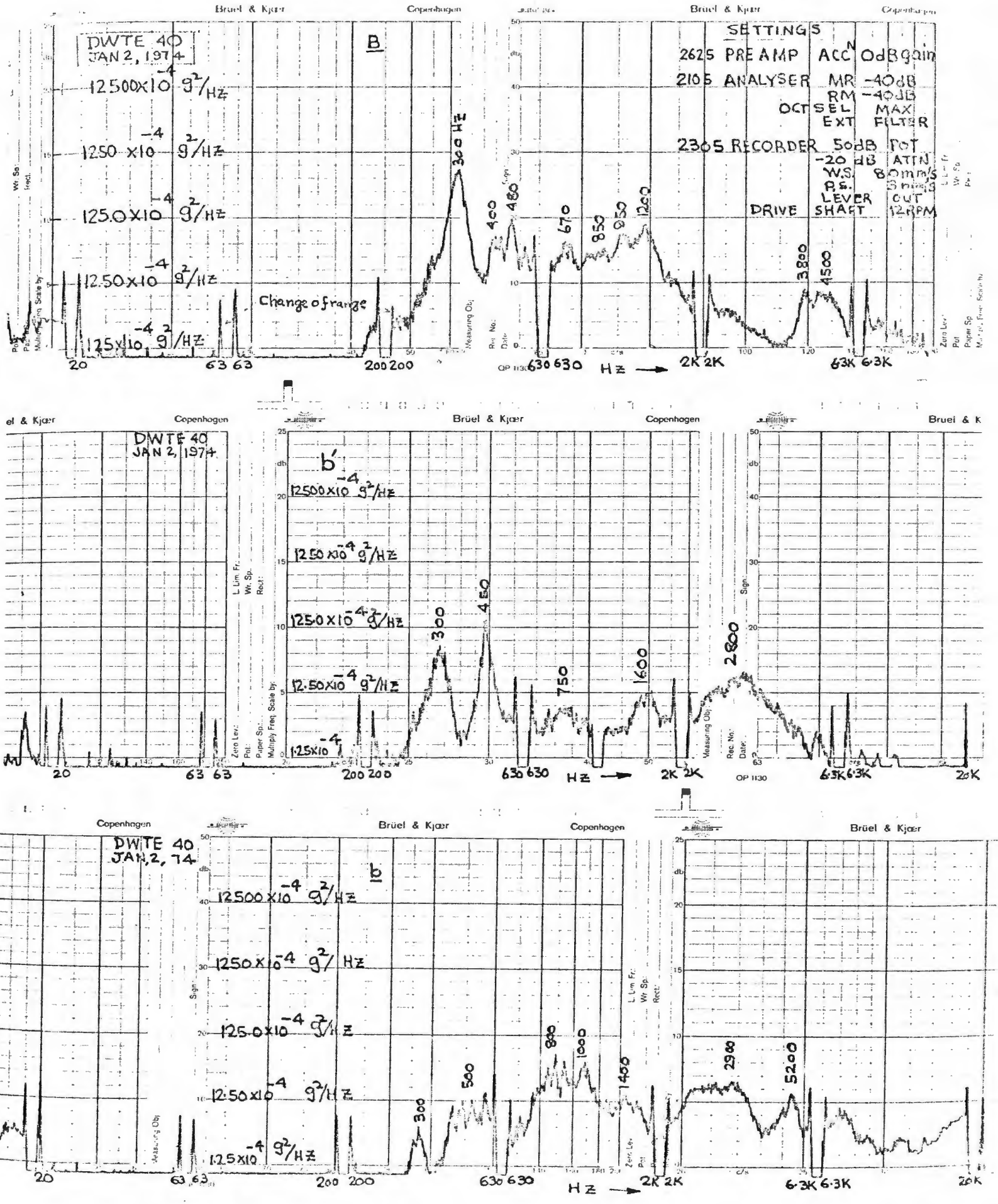

FIG 9.1

B&K VIBRATION RECORD

TABLE 9.2

TABULATION OF RESULTS FROM A VIBRATION RECORD

NOTE: 40

NOTE: 2.1.1974

P.S.D.

ACCELERATION

POSITION OF ACCELEROMETER	f	DIVISIONS ON GRAPH	POWER SPECTRAL DENSITY	DISPLACEMENT (AMPLITUDE)	INTEGRATED POWER SPECTRAL DENSITY
	HZ		$g^2/HZ \times 10^{-4}$	μm	g^2/HZ
B	300	27	625.9	239	4.0
	400	17	62.6	49	
	480	20	125.0	53	
	670	16	49.7	20	
	850	15	39.5	13	
	950	18	78.8	15	
	1200	19	99.2	11	
	3800	9	9.9	< 1	
	4500	9	9.9	< 1	
A	300	21	157.3	120	3.1
	400	17	62.6	24	
	500	21	157.3	56	
	675	13	24.9	14	
	800	16	49.7	15	
	980	15	39.5	10	
	1300	14	31.4	6	
	1700	18	78.8	6	
	2200	16	49.7	3	
b	300	6	4.9	21	0.64
	500	10	12.5	16	
	800	17	62.6	17	
	1100	16	49.7	11	
	1400	11	15.7	4	
	2900	13	24.9	2	
	5200	11	15.7	1	

TABLE 9.2 (Cont'd)

TABULATION OF RESULTS FROM A VIBRATION RECORD

TE: 40 (cont'd)

TE: 2.1.74

P.S.D.

ACCELERATION

POSITION OF CELEROMETER	f	DIVISIONS ON GRAPH	POWER SPECTRAL DENSITY	DISPLACEMENT (AMPLITUDE)	INTEGRATED POWER SPECTRAL DENSITY
	HZ		$g^2/HZ \times 10^{-4}$	μm	g^2/HZ
a	290	8	8.0	28	0.65
	480	16	48.7	33	
	825	14	31.4	11	
	1000	14	31.4	9	
	1300	15	39.5	7	
	1500	12	19.8	4	
b'	300	18	78.9	89	0.50
	450	22	198.0	73	
	750	8	7.9	7	
	1600	10	9.9	4	
	2800	12	24.9	2	

TABLE 9.3

400 rpm COLD SPECIMENS (No Air)

Sample No.	DWTE 40-1	Operator	J. F. Conroy
Film No.	133	Date	January 26, 1974
Radiation/Filter	CR/V	Identification	α-Fe, α-Fe_2O_3, Fe_3O_4
Collimation	Coarse		

Line No.	S	S/2	2	Remarks	d_{obs}	I/I_{10}	$d_{ref.}$	I/I_{100}
1	73.2	36.6	36.6°	αFe_2O_3	3.649	4	3.66	25
2	85.6	42.8	42.8°		3.140	1		
3	91.6	45.8	45.8°	Fe_3O_4	2.945	2	2.966	70
4	100.4	50.2	50.2°	αFe_2O_3	2.70	10	2.69	100
5	108.4	54.2	54.2°	Fe_3O_4 αFe_2O_3	2.515	10	2.53 2.51	100 50
6	112.8	56.4°	56.4°	Fe_3O_4	2.424	1	2.419	10
7	125.2	62.6	62.6°	αFe_2O_3	2.205	3	2.201	30
8	133.6	66.8	66.8°	Fe_3O_4	2.081	8	2.096	70
9	137.8	68.9	68.9°	α Fe	2.025	6	2.0268	100
10	154.8	77.4	77.4°	αFe_2O_3	1.832	4	1.838	40
11		84.9	84.9°	αFe_2O_3	1.697	6	1.690	60
12		91.5	91.5°	Fe_3O_4 αFe_2O_3	1.60	2	1.61 1.596	85 16
13		100.4	100.4°	Fe_3O_4 αFe_2O_3	1.492	7	1.483 1.484	85 35
14		103.7	103.7°	αFe_2O_3	1.456	5	1.452	35
15		115.9	115.9°	αFe_2O_3	1.352	1	1.349	4
16		121.8	121.8°	αFe_2O_3	1.311	3	1.310	20
17		130.5	130.5°	Fe_3O_4 αFe_2O_3	1.262	3	1.264 1.258	10 8
18		140.8	140.8°	αFe_3O_4	1.216	4	1.2112	20
19		156.8	156.8°	α Fe	1.170	3	1.1702	30

The distribution of the wear debris particles is given in Table 9.4. From this data, the distribution curve is plotted, as shown in Fig 9.14.

The studies of structural changes are described in detail in later sections of this chapter.

9.1.2. Wear Tests

Tables of the wear test results are enclosed in the Appendix C.

The results of the wear tests performed at a nominal load of 490N to study the effect of sliding speed, effect of specimen holder temperature, effect of forcing air, preheated air and various gas mixtures through the specimens are given in tables C-1 to C-21.

Table C-1 summarizes the wear rates, coefficients of friction, extrapolated surface temperature and their standard deviations, listed as mean values for each of the speeds used with unheated specimens and no air. Table C-2 lists values of above variables for each individual run. Table C-3 summarises the X-ray analysis and size analysis on debris particles. Table C-4 lists the displacement at the six lowest frequencies of vibration and integrated power spectral density for frequencies of 20 to 3000 HZ for each run of the series.

Table C-5, C-6, and C-7 are corresponding tables for runs during which specimen holder temperatures were changed. (Vibration was not recorded). Tables C-8, C-9, C-10 and C-11 record the results for unheated specimens with air flow of 75×10^{-6} m^3/s. Tables C-12 and C-13 record the results with preheated air. Vibration was not recorded and only one run was taken at one speed.

TABLE 9.4

PARTICLE SIZE ANALYSIS DATA

SAMPLE NO. 40 LOT 3 (Collected under specimen) OBJECTIVE x100

SLIDE NO. VS403 OPTOVAR x2.0

X✓	0	6	7.5	10	13	17	23	30	39	51	66	86	111
μm	0	0.50	0.64	0.85	1.11	1.45	1.96	2.55	3.32	4.34	5.61	7.31	9.44
1	152	144	141	120	74	48	25	10	3	2	1	1	0
2	147	144	140	123	90	57	32	22	11	2	1	0	0
3	155	150	148	135	102	65	32	19	6	2	1	1	0
4	132	126	124	110	73	49	29	24	12	5	1	1	0
5	175	170	165	153	103	75	41	19	11	6	4	1	1
6	261	248	240	216	149	83	42	22	11	5	3	1	0
7	163	158	155	137	98	58	27	13	6	4	3	2	1
8													
9													
10													
T	1185	1140	1113	994	689	435	228	129	60	26	14	7	2
%	100-R f	96 4 4	94 6 2	84 16 10	58 42 26	37 63 21	19 81 18	11 89 8	5 95 6	2 98 3	1 99 2	0.6 99.4 0.4	

TABLE 9.4 (cont'd)

PARTICLE SIZE ANALYSIS DATA

SAMPLE NO. 40 LOT 1 (on filter paper) OBJECTIVE x100

SLIDE NO. VS401 OBTOVAR x2.0

X_v	0	6	7.5	10	13	17	23	30	39	51	66	86	111
μm	0	0.50	0.64	0.85	1.11	1.45	1.96	2.55	3.32	4.34	5.61	7.31	9.44
1	132	108	87	56	43	28	19	15	10	7	4	2	0
2	130	104	77	53	37	31	26	16	14	12	8	2	0
3	141	125	104	68	46	39	37	31	13	11	6	3	2
4	129	111	97	60	49	40	30	26	17	15	10	3	3
5	159	137	108	73	55	37	31	30	21	14	7	4	2
6													
7													
8													
9													
10													
T	691	585	473	310	230	175	143	118	75	59	35	14	7
%		85	68	45	33	25	20	17	11	8.5	5	2	1
	100-R	15	32	55	67	75	80	83	89	91.5	95	98	99
	f	15	17	23	12	8	5	3	6	2.5	3.5	3	1

Tables C-14 to C-17 record the results with different gas mixtures at a sliding speed of 0.965 m/s. Tables C-18 to C-21 record the results with different gas mixtures at a sliding speed of 1.158 m/s.

Tables C-22 to C-24, C-25 to C-28, C-29 to C-32 list the results for unheated specimens and with a load of 295N, for no air, with air and gas mixtures respectively. (There were no vibration recordings with no air.)

Tables C-33 to C-35, C-36 to C-39 record the results at a normal load of 980N, with no air and with air respectively. Vibration was not recorded for the runs without air.

9.1.2.1. Effect of sliding speed on wear rate

In Fig 9.2.(a) the effect of the sliding speed on the wear rate (expressed as wear volume per unit distance) at a nominal load of 490N is shown. The three plots from bottom to top represent the wear rate of the stationary specimen, rotating specimen and the total wear rate respectively. The total wear rate was obtained by adding the wear rates of the stationary and the rotating specimen. When the speed was increased from 0.193 m/s to 0.965 m/s, a decrease in the wear rate values was noticed. At a speed of 1.061 m/s a scatter in the wear rate values was observed. Results from three tests out of a total of six performed at this speed, showed a jump in the wear rate to higher values while the remaining three were at the same level as wear value corresponding to the sliding speed of

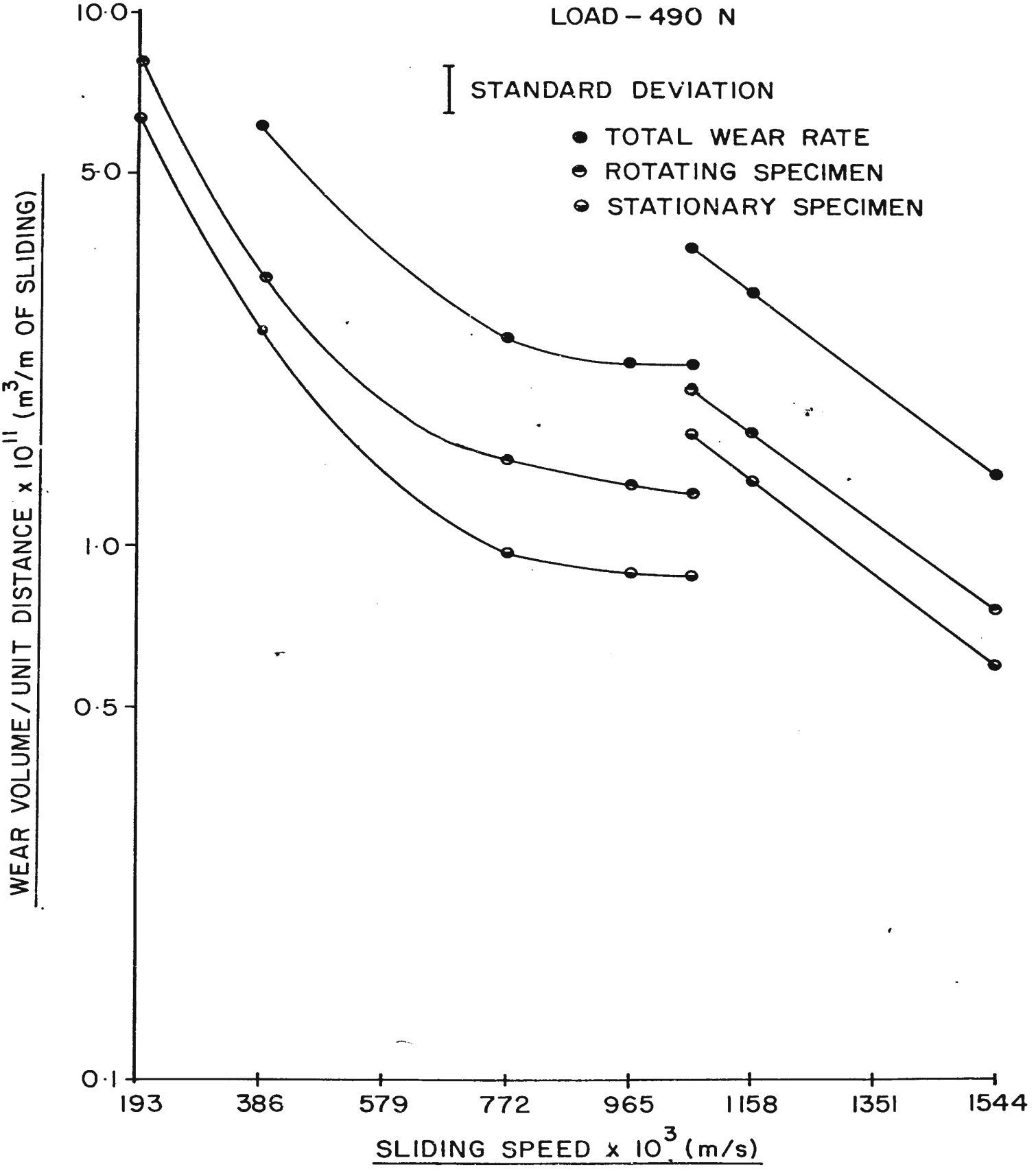

FIG·9·2(a)

EFFECT OF SLIDING SPEED ON WEAR RATE

0.965 m/s. The wear debris particles from the experiments at the speed of 1.061 m/s and with higher wear rate were identified as α-Fe, Fe_3O_4, α-Fe_2O_3 and FeO, while the identification of debris particles from the experiments at the 1.061 m/s and with lower wear rate revealed the presence of α Fe, Fe_3O_4 and α-Fe_2O_3 only. No FeO was noticed, even in a trace form.

When the sliding speed was increased to 1.158 m/s, the wear rate was lower than the higher of the two sets of wear rates measured at 1.061 m/s. A further increase in speed to 1.544 m/s caused the wear rate to decrease again.

The mean values and the standard deviation of the wear rate are given in table C-1 while results of individual tests are tabulated in table C-2. The deviation was determined for all the wear rate measurements relative to the mean wear rate of the tests at a given speed. These deviations were expressed as a ratio of mean value and a standard deviation (ratio) was calculated from all the deviation values so determined. This standard deviation is shown in the graph.

As mentioned in the section 9.1.1. all the experiments up to a sliding speed of 1.061 m/s were carried out for a constant number of revolutions (30,000 Revs.) and hence for a constant distance of sliding. The experiments at the two higher speeds 1.158 m/s and 1.544 m/s were carried out for 40,000 Revs., the distance of sliding was same for these two experiments. However, the time for wear was different for different speeds. In tables C-1 and C-2 the mean values

and the standard deviation of the wear rate expressed as wear mass per unit time and the results of individual tests are given. In Fig 9.2.(b), the effect of sliding speed on wear rate (expressed as wear mass per unit time) is shown. An increase in the sliding speed from 0.193 m/s to 0.772 m/s caused the wear rate to decrease. However, the decrease is not as prominent as in Fig 9.2(a). With an increase in speed to 1.061 m/s, the wear rate showed an increase. The highest wear rate was noticed at the sliding speed of 1.061 m/s, for the experiments where FeO appeared in the wear debris particles. Beyond this speed the wear rate decreased with an increase in the speed.

9.1.2.2. Effect of a change of specimen holder temperature

A jump in the wear rate seemed to be associated with the appearance of FeO in the wear debris particles. A model for the distribution of heat from rubbing contact to the two specimens was postulated (described in Section 10.1.1.) and a set of experiments were carried out to test the model.

The sliding speed and the mean normal load were kept constant at 0.965 m/s and 490N respectively. The specimen holder temperature was changed. At the holder temperatures of 100^{o}C, 150^{o}C and 200^{o}C six sets of experiments were performed, two at each temperature. The results of these tests are given in tables C-5 and C-6. With an increase in the holder temperature, the wear rate showed an increase, however, a jump in the wear rate to a higher value can be seen at a holder temperature of 200^{o}C. The wear rate value is in the range of wear rate corresponding to a sliding speed of 1.061 m/s, with

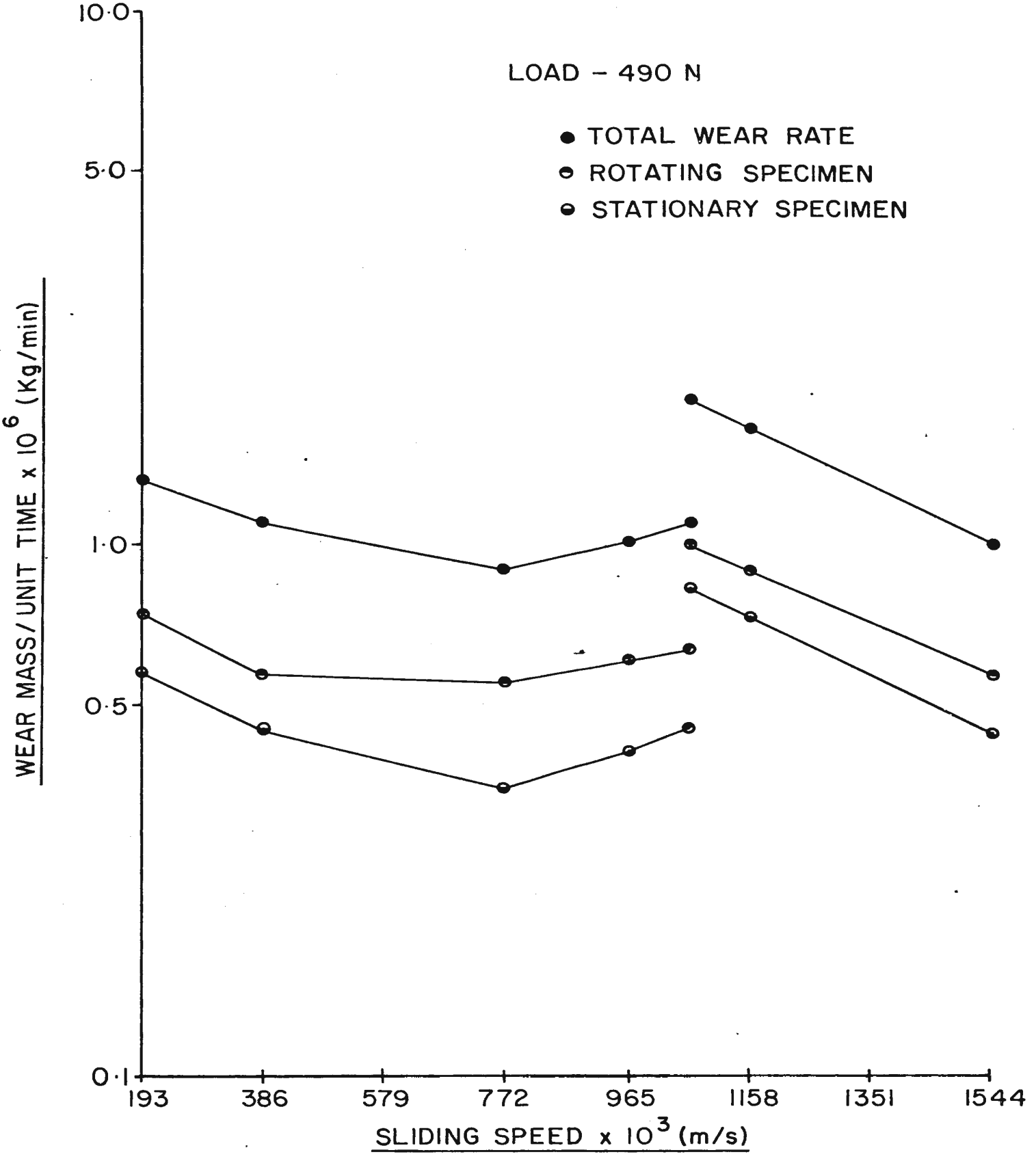

FIG·9·2 (b)
EFFECT OF SLIDING SPEED ON WEAR RATE

FeO in wear debris particles. The identification of the wear debris particles revealed the presence of FeO in the experiments with holder temperature of 200°C. At 100°C and 150°C temperatures, the FeO was absent.

9.1.2.3. Effect of Load on the Appearance of FeO

In the experiments described so far, the nominal load was kept constant at 490N. To investigate the effect of load on the appearance of FeO, experiments at two other loads were carried out, one at a load of 295N and speeds of 0.965 m/s, 1.158 m/s and 1.544 m/s and other at a load of 980N and speeds of 0.772 m/s, 0.965 m/s and 1.158 m/s.

The results of these experiments are given in tables C-22, C-23, C-33 and C-34. FeO appeared at the sliding speed of 1.158 m/s irrespective of the loads applied.

9.1.2.4. Effect of Forcing Air through the Specimens

9.1.2.4.1. With a Nominal Load of 490N

The effect of forcing air through the specimens for a nominal normal load of 490N and for various sliding speeds is shown in Fig 9.3.(a).

It should be noted that a small correction is applied to the wear rate values plotted, to allow for the reduction in normal load between the specimens due to the pressure of the air or gas mixture between the specimens. Typically, the air pressure was 10.5×10^4 N/m^2, reducing the load by 20N or 4% of the nominal load of 490N. The plotted wear rate values are 4% greater than the measured values.

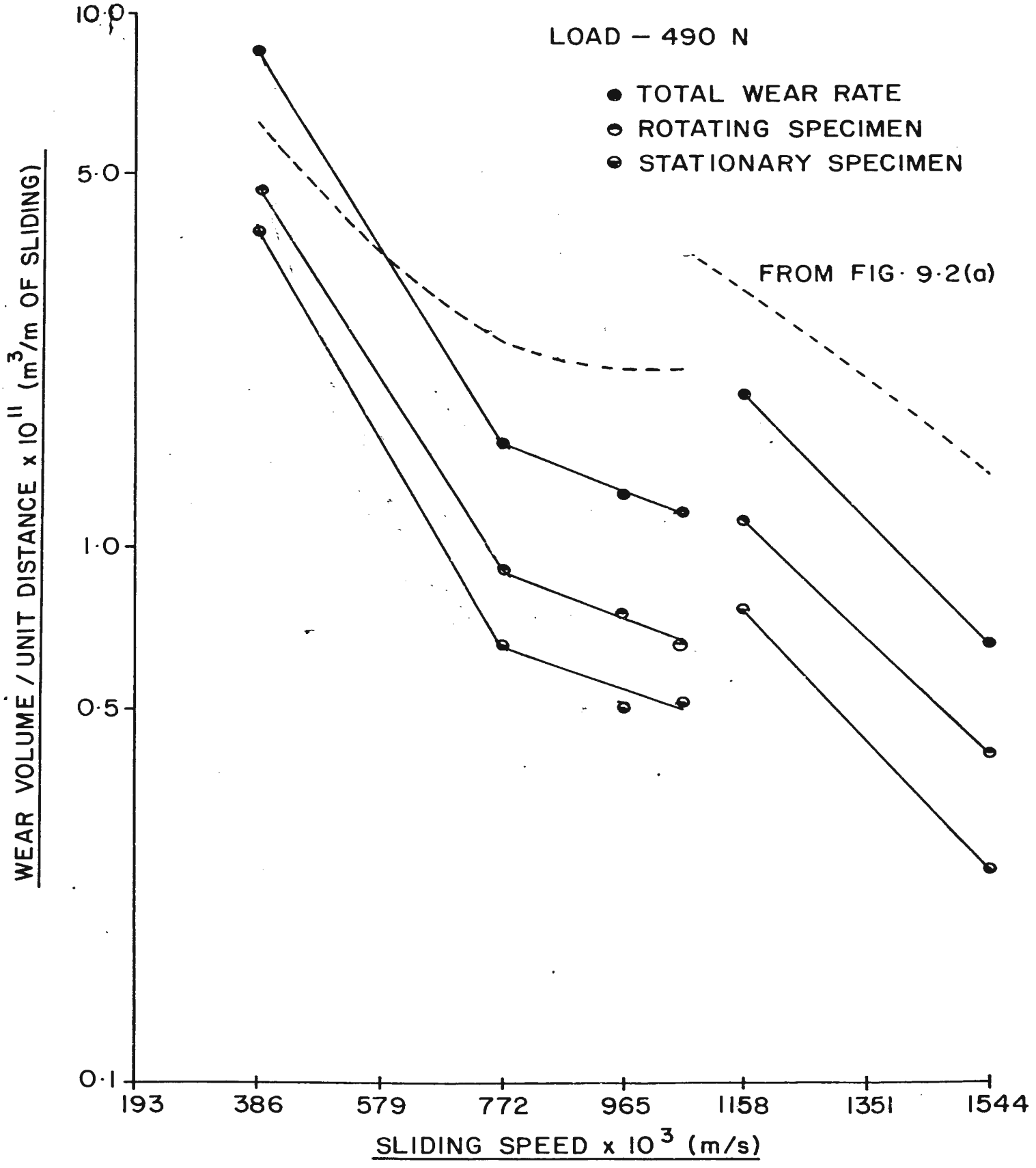

FIG· 9·3(a)

EFFECT OF FORCING COMPRESSED AIR ON WEAR RATE VERSUS SLIDING SPEED RELATION

The flow rate of air was kept at 75 x 10^{-6} m^3/s for all the experiments. The general pattern of the sliding speed and wear rate relationship is the same as shown in Fig 9.2.(a), with two differences. First the wear rate values are different and second the jump in the wear rate value occurs at a sliding speed of 1.158 m/s and not at 1.061 m/s as observed previously.

At a speed of 0.193 m/s, severe wear of the specimens was observed giving rise to an extremely high wear rate. At a speed of 0.386 m/s the wear rate was higher in the experiments with air than without air. For speeds greater than 0.386 m/s the effect of air was to reduce the wear rate.

The mean values and the standard deviation of the wear rate are given in Tables C-8 and C-9.

In Fig 9.3(b), the wear rate is expressed in terms of wear mass per unit volume and the effect of forcing air through the specimens is shown. There now appears to be two transitions in the graph, one at a speed of 0.772 m/s and other at 1.158 m/s. For comparsion purposes, the total wear rates of the specimens (for experiments without air) are shown in dotted line.

The mean values and standard deviation of the wear rate are given in Tables C-8 and C-9.

The effect of preheating air to 200^{o}C before it is forced through the specimens is shown in Fig 9.4. The nominal load and the flow rate of air were kept at 490N and 75 x 10^{-6} m^3/s respectively. The results of the wear test are tabulated in Table C-12.

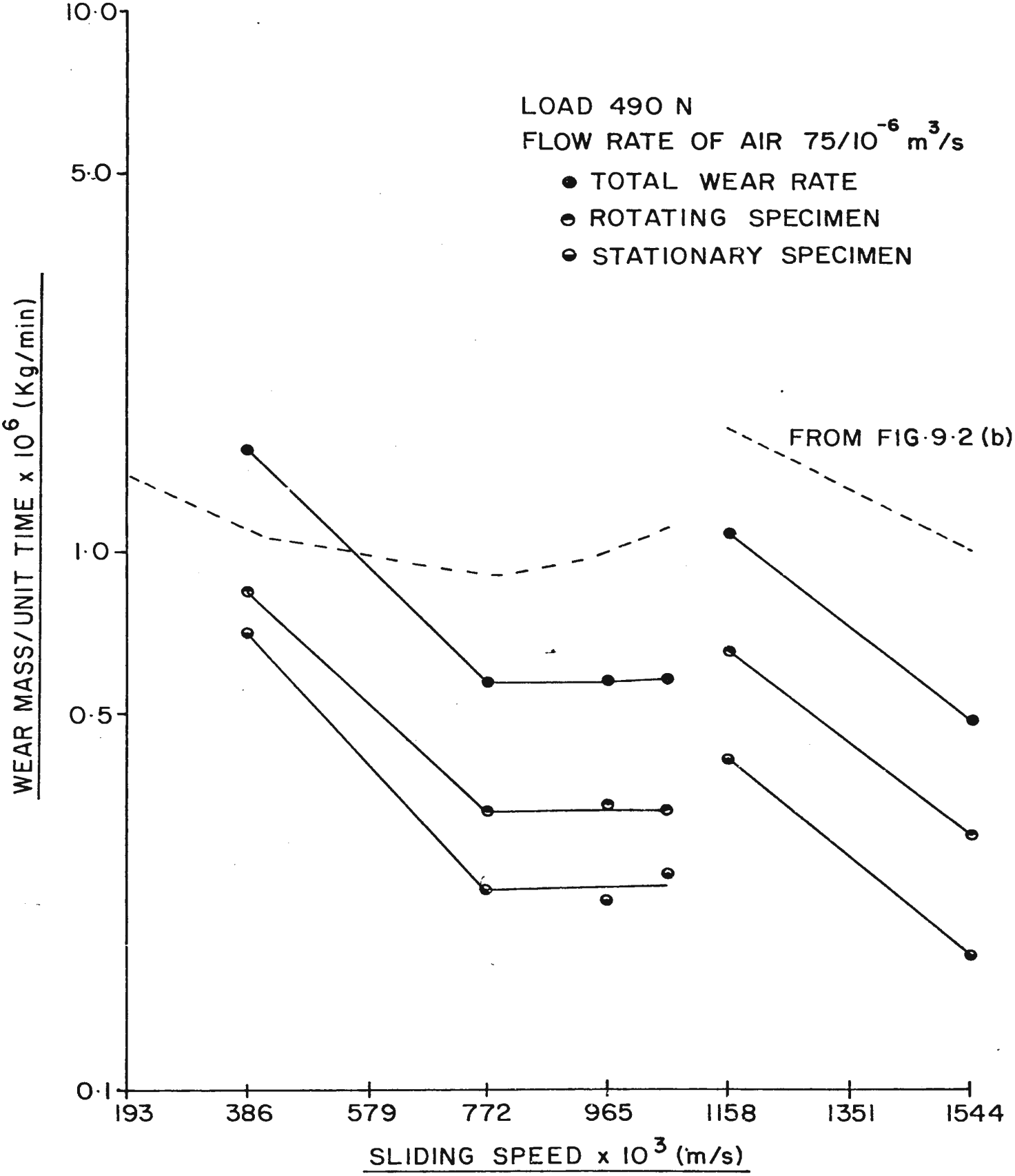

FIG·9·3(b)

EFFECT OF FORCING COMPRESSED AIR ON WEAR RATE VERSUS SLIDING SPEED RELATION

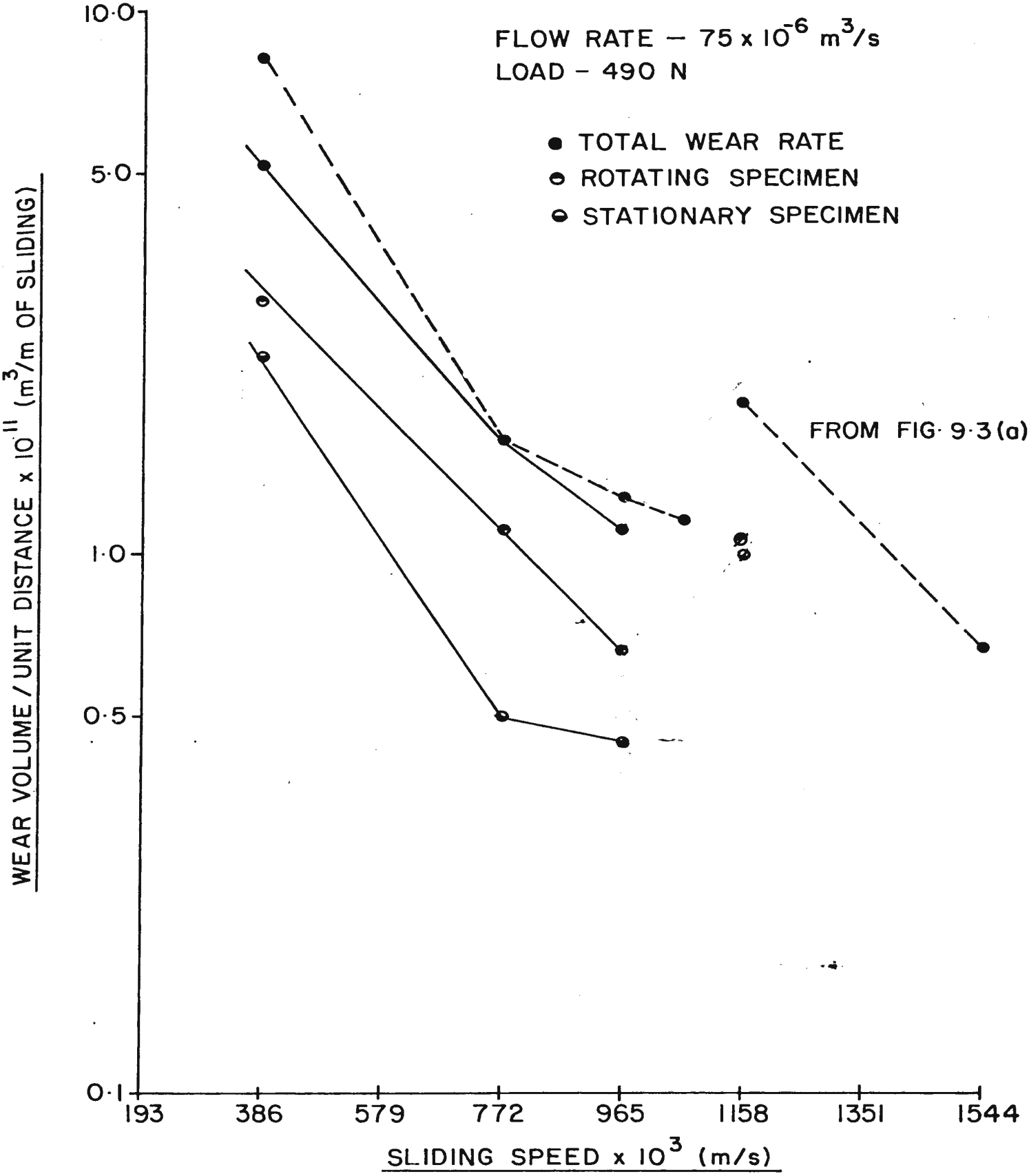

FIG. 9·4
EFFECT OF PREHEATING AIR TO 200°C

The pattern of the wear rate values are nearly the same as shown in Fig 9.3.

9.1.2.4.2. With a Nominal Load of 295N

In Tables C-25 and C-26, the mean values and the standard deviation of the wear rate and results of the individual tests are given. The flow rate of air was kept constant at 75×10^{-5} m^3/s while the sliding speed was varied. Experiments were performed at sliding speeds of 0.965 m/s, 1.158 m/s and 1.544 m/s. The effect of forcing air through the specimens seems to decrease the wear rate at all the three speeds. No change is noticed in the composition of wear debris particles because of the forced air. FeO appears at 1.158 m/s for the experiments with or without air. No FeO is noticed at 0.965 m/s.

9.1.2.4.3. With Nominal Load of 980N

The mean values and the standard deviation of the wear rate and results of the individual tests are given in tables C-36 and C-37. With a constant nominal load of 980N and flow rate of air of 75×10^{-6} m^3/s experiments were performed at three different sliding speeds, 0.772 m/s, 0.965 m/s and 1.158 m/s. A decrease in the wear rate values is noticed at all the three different speeds with compressed air forced through the specimens. FeO appears at the sliding speed of 1.158 m/s.

9.1.2.4.4. Effect of Load on the Appearance of FeO for Experiments with Air Forced through the Specimens

The effect of load on the correlation between appearance of FeO and sliding speed is shown in Fig 9.5., using results obtained at 295N, 490N and 980N, with an air flow rate of 75×10^{-6} m^3/s as described in the earlier sections. For these loads, FeO appeared at a sliding speed of 1.158 m/s irrespective of the load. The same correlation exists between the appearance of FeO and sliding speeds for runs without forced air.

9.1.2.5. Effect of Gas Mixtures on Wear Rate

9.1.2.5.1. With a Nominal Load of 490N

The results of the wear tests performed to study the effect of gas mixtures at a constant load of 490N and sliding speed of 0.965 m/s are given in Tables C-14 and C-15. With pure argon the coefficient of friction was recorded as about 1.7 and there was metal to metal transfer to a considerable extent between the test objects. The stationary test specimen showed an increase in weight after wear and the metal transferred from the rotating specimen on to the stationary specimen surface could be easily seen. The forces were too high to continue the tests for very long, for fear of damage to the equipment. Very little debris particles were formed.

The effect of gas composition, a mixture of oxygen and argon, is shown in Fig 9.6. The values for 20% oxygen content were obtained

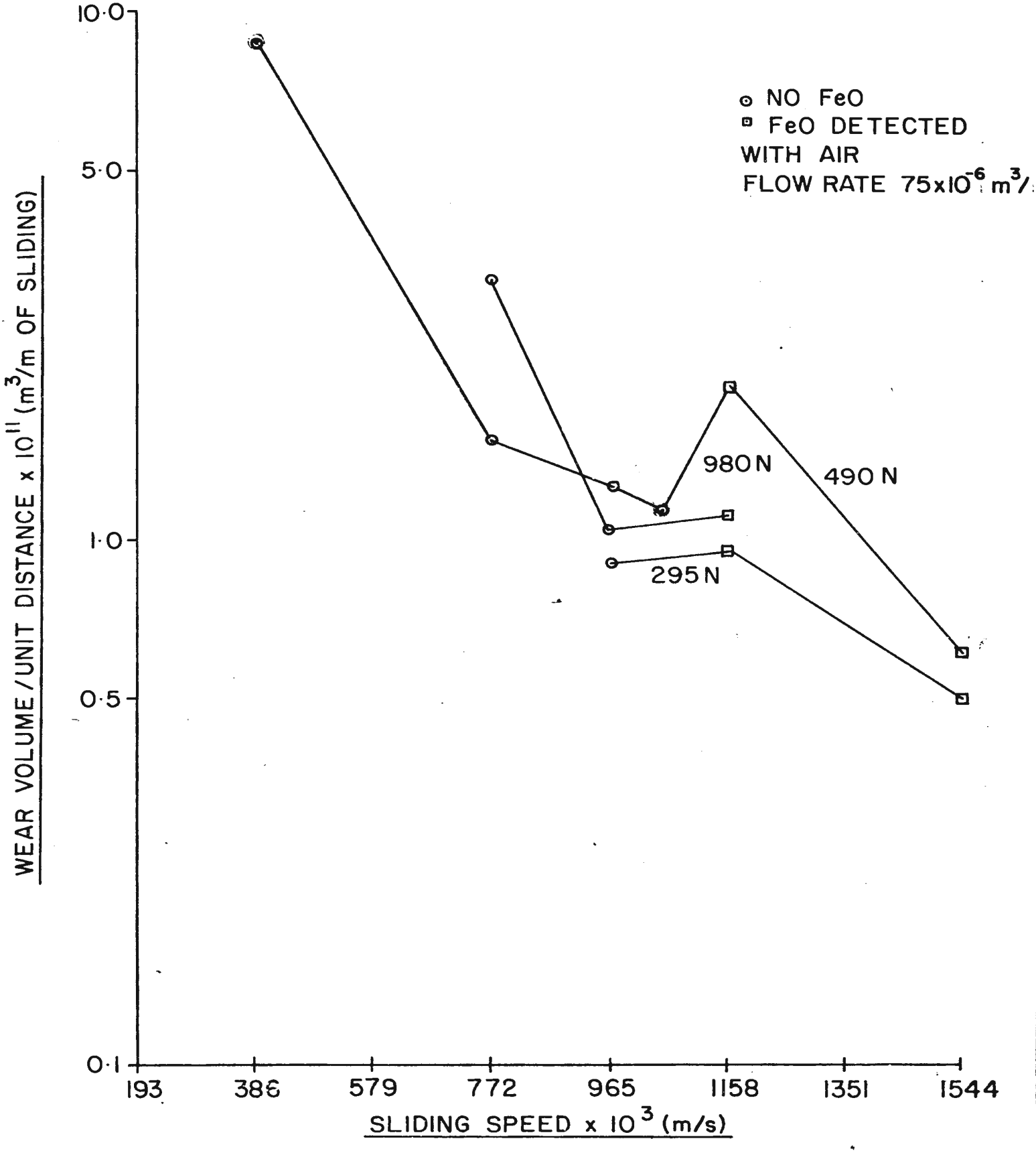

FIG·9·5

EFFECT OF LOAD ON APPEARANCE OF FeO FORMATION

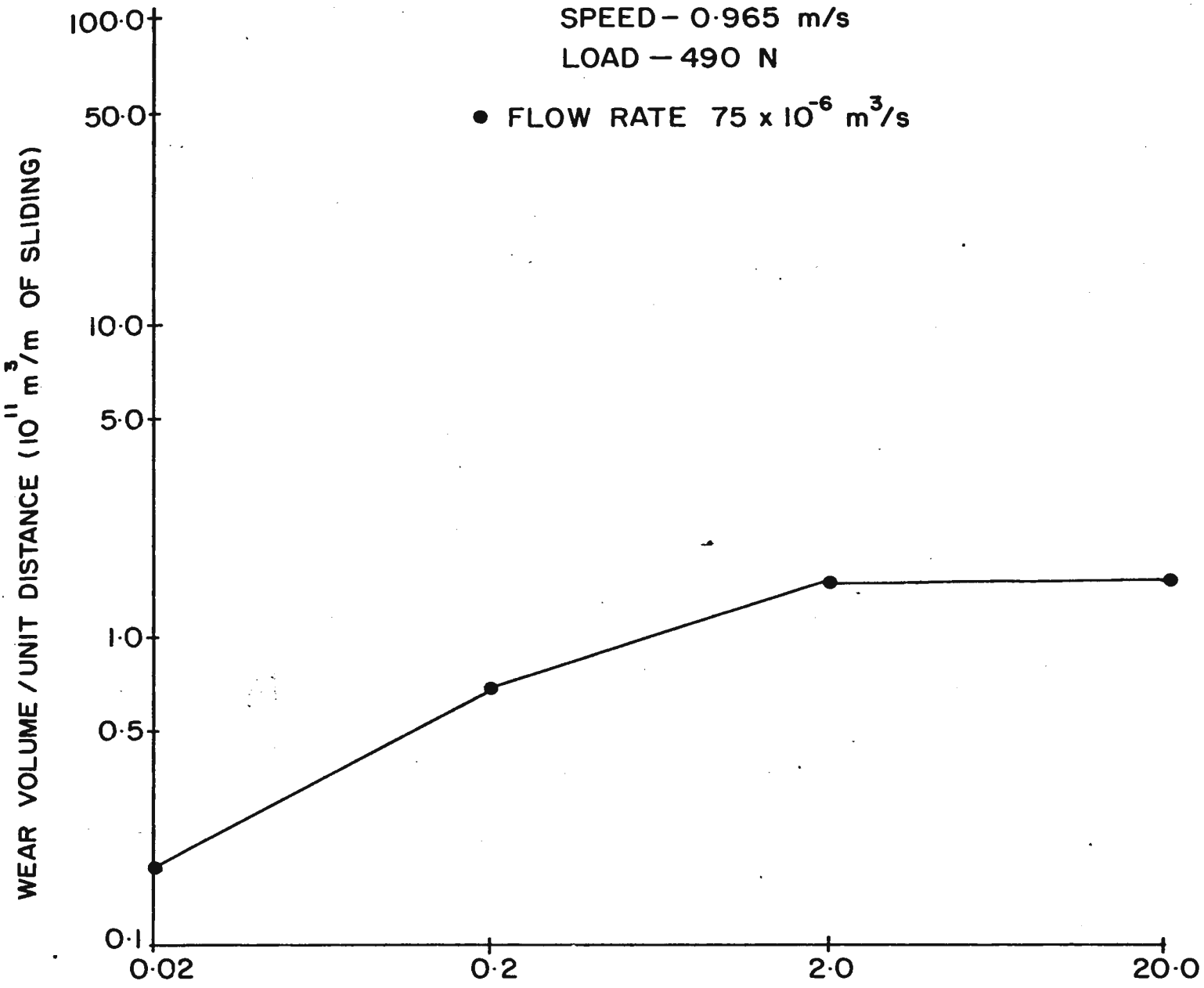

FIG· 9·6

EFFECT OF GAS MIXTURE ON WEAR RATE AT 490 N & 0·965 m/s

using air. The effect of decreasing the oxygen content is very little until the content is 2%. From 2% down to .02% oxygen, decreasing oxygen content decreases the wear rate. There is an increase in coefficient of friction with decreasing oxygen content.

The results of the experiments performed at a sliding speed of 1.158 m/s with a nominal load of 490N, to study the effect of gas mixtures are given in tables C-18 and C-19. With pure argon, the coefficient of friction was recorded as 1.6, however, unlike the experiment with the sliding speed of 0.965 m/s, no gain in weight of the stationary specimen was noticed. Wear rate was fairly high and at the end of experiment the outermost surfaces of the contact surface of the specimen were different from the inner surface. Indications were that oxygen from the outside was pumped inside the specimen giving a polished outer surface. The inner surface showed metal transfer and scuring marks.

The effect of the gas composition is shown in Fig 9.7. The pattern of the wear is same as for the 0.965 m/s experiments. The wear rate values are higher, however, the effect of decreasing oxygen content is very little until the content is 2%. From 2% down to 0.02% oxygen decreasing oxygen content decreases the wear rate. There is an increase in the coefficient of friction with decreasing oxygen content.

9.1.2.5.2. <u>With a Nominal Load of 295N</u>

In Tables C-29 and C-30, the results of the tests performed to

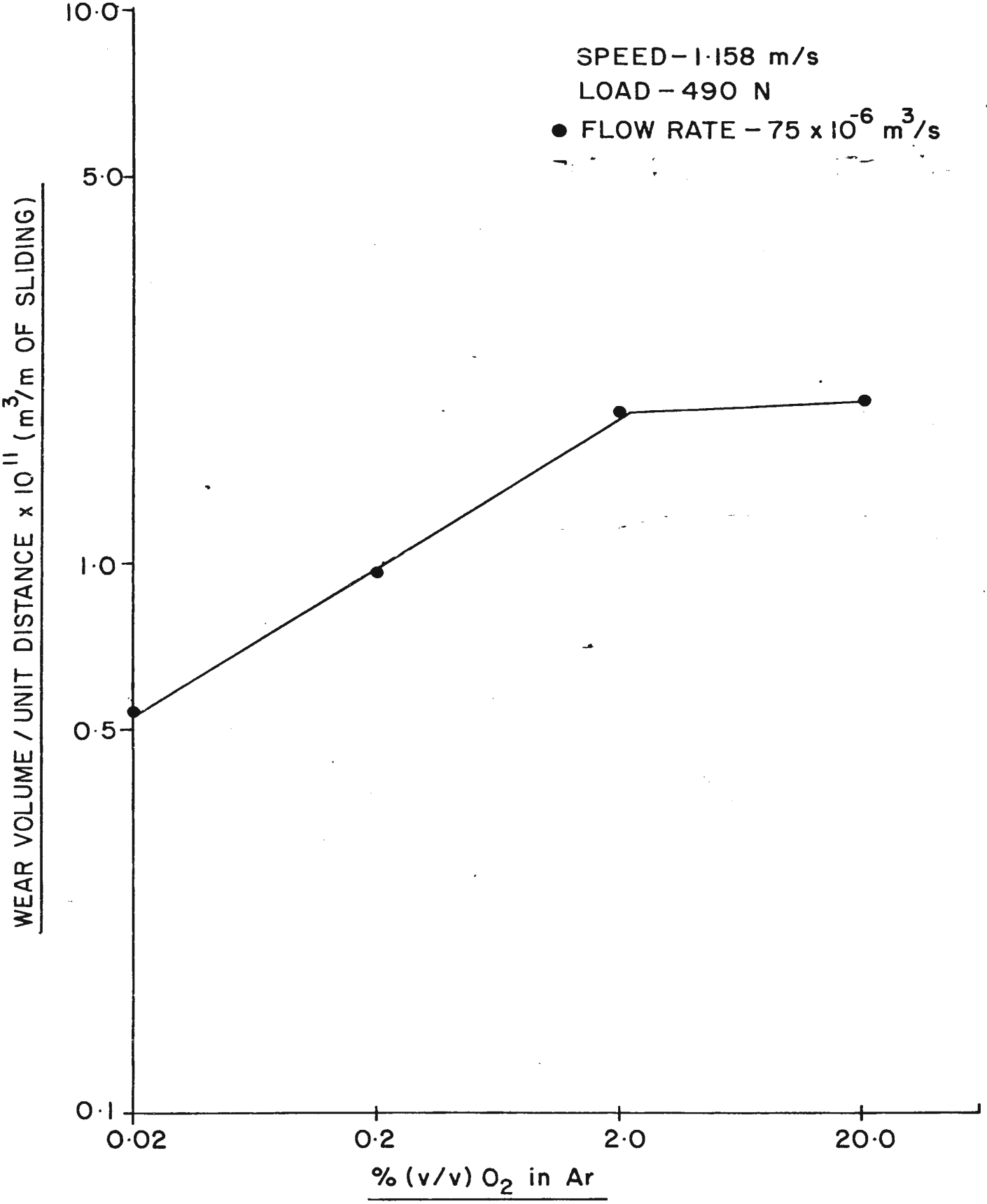

FIG·9·7

EFFECT OF GAS MIXTURE AT 490 N AND 1·158 m/s

study the effect of different gas mixtures forced through the specimens are given. The nominal load was kept constant at 295N and the sliding speed at 1.158 ms^{-1}.

With pure argon, metal to metal transfer to a considerable extent between the specimens was noticed. The coefficient of friction was recorded as about 1.75. The effect of the gas mixture was to reduce the wear rate with diminishing oxygen content. The coefficient of friction showed an increase with decreasing oxygen content.

The effect of gas mixture on wear rate is plotted in Fig 9.8.

9.1.2.6. Coefficient of Friction

The values of the coefficient of friction are included in the table of results given in Appendix C. For each experiment, the coefficient of friction was determined and in this section the general trend is being discussed.

The mean values of the coefficient of friction between the two rubbing specimens are shown in Table 9.5. For unheated specimens with or without air forced through the specimens, the pattern of the coefficient of friction versus sliding speed variation is similar to the wear rate versus sliding speed variation. With an increase in sliding speed up to 0.965 m/s, the coefficient of friction decreases with speed. An increase in sliding speed from 0.965 to 1.158 m/s results in a jump of coefficient of friction to a higher value. For speed of 1.544 m/s, the coefficient of friction shows a lower value than that for 1.158 m/s.

The effect of forcing air through the specimens seems to increase the coefficient of friction at lower speeds up to 0.386 m/s, and decrease at higher speeds up to 1.544 m/s.

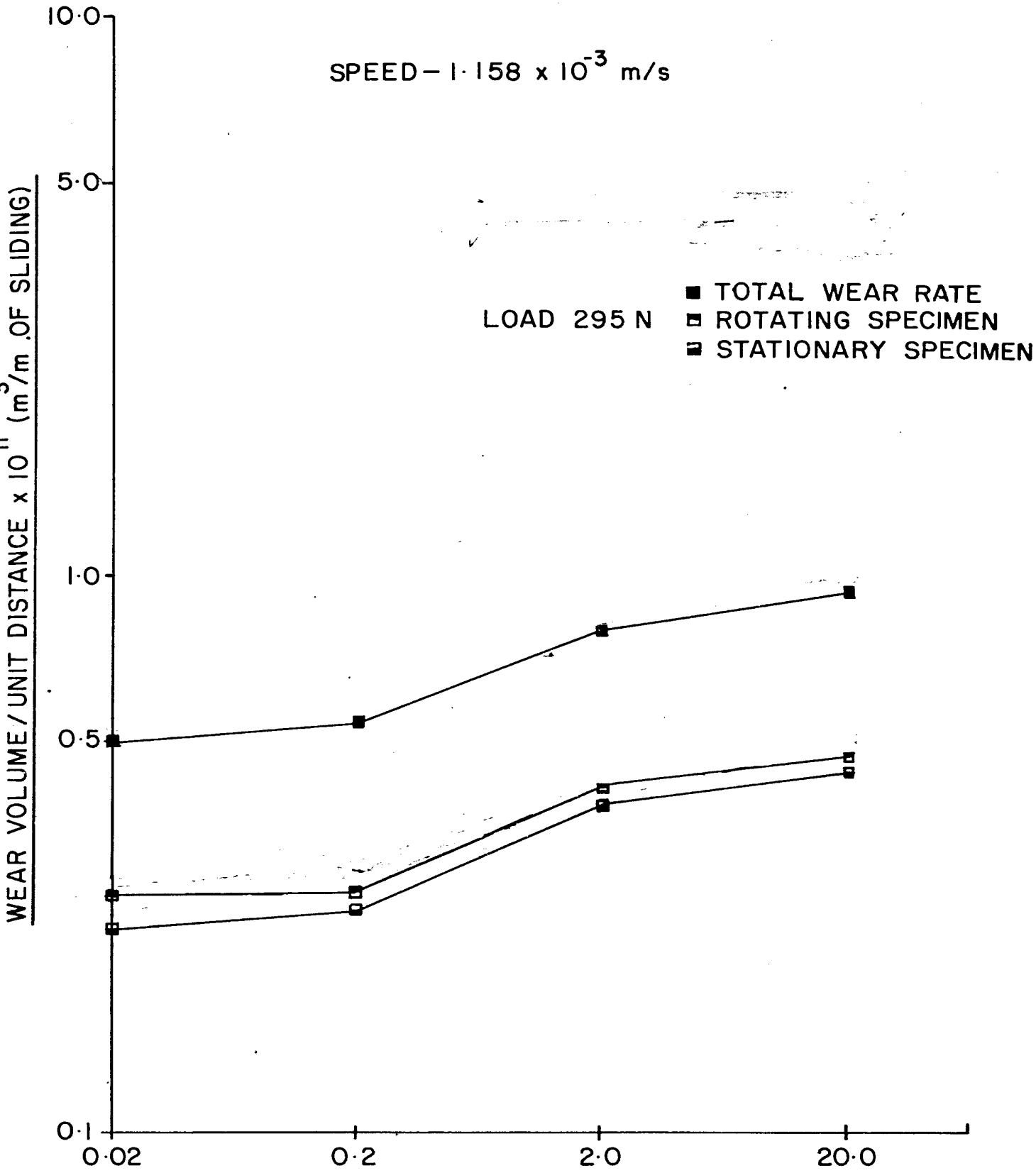

FIG 9·8

EFFECT OF GAS MIXTURE ON WEAR RATE

TABLE 9.5

SPEED (ms^{-1})	0.193	0.386	0.772	0.965	1.061	1.158	1.544	
								LOAD (N)
UNHEATED SPECIMENS				0.37		0.64	0.55	295
NO AIR	0.55	0.51	0.44	0.46	0.45-0.62	0.65	0.58	490
DIFFERENT LOADS & SPEEDS			0.46	0.48		0.70		980
UNHEATED SPECIMENS				0.39		0.45	0.40	295
WITH AIR	0.70	0.55	0.40	0.45	0.45	0.50	0.46	490
DIFFERENT LOADS & SPEEDS			0.42	0.47		0.63		980
UNHEATED SPECIMENS						1.75		Ar
DIFFERENT GAS MIXTURES						0.60		0.02% O_2
LOAD 295N						0.48		0.2% O_2
						0.37		2.0% O_2
UNHEATED SPECIMENS								
DIFFERENT GAS MIXTURES				1.65		1.60		Ar
LOAD 490 N				0.54		0.64		0.02% O_2
				0.51		0.60		0.2% O_2
				0.48		0.54		2.0% O_2

RESULTS OF THE COEFFICIENT OF FRICTION MEASUREMENT

When Argon is forced through the specimens, the coefficient of friction is the highest. With an increase in the oxygen content of the Oxygen-Argon gas mixture, the coefficient of friction shows a decrease.

9.1.2.7. Mean Surface Temperature

The values of mean extrapolated surface temperatures for each individual experiment are given in the table of results on Appendix C.

The mean values of the mean extrapolated surface temperature of the rotating specimen are shown in Table 9.6. With an increase in the sliding speed an increase in the surface temperature is noticed. The effect of forcing air through the specimens seems to reduce the temperature. However, this can be attributed to lower coefficients of friction between the specimens.

In an atmosphere of inert gas, the surface temperature is the highest. When the Oxygen content of the Oxygen-Argon gas mixture is increased, the mean surface temperature shows a decrease.

The extrapolated surface temperatures of the stationary specimen were higher than the rotating specimen by about 10 to 25^{o}C but with the same trend.

The variation of the mean extrapolated surface temperature with the sliding speed for rotating specimen is shown in Fig 9.9.

TABLE 9.6

SPEED (ms^{-1})	0.193	0.386	0.772	0.965	1.061	1.158	1.544	
								LOAD (N)
UNHEATED SPECIMENS				140		195	207	295
NO AIR	105	150	225	250	240-320	300	310	490
DIFFERENT LOADS & SPEEDS			330	450		600		980
UNHEATED SPECIMENS				135		175	180	295
WITH AIR	80	115	205	230	225	275	280	490
DIFFERENT LOADS & SPEEDS			300	440		550		980
UNHEATED SPECIMENS						.375		Ar
DIFFERENT GAS MIXTURES						290		0.02% O_2
LOAD 295 N						246		0.2% O_2
						290		2.0% O_2
UNHEATED SPECIMENS				400		400		Ar
DIFFERENT GAS MIXTURES				305		355		0.02% O_2
LOAD 490 N				290		340		0.2% O_2
				260		310		2.0% O_2

MEAN (EXTRAPOLATED) SURFACE TEMPERATURE (^{o}C)

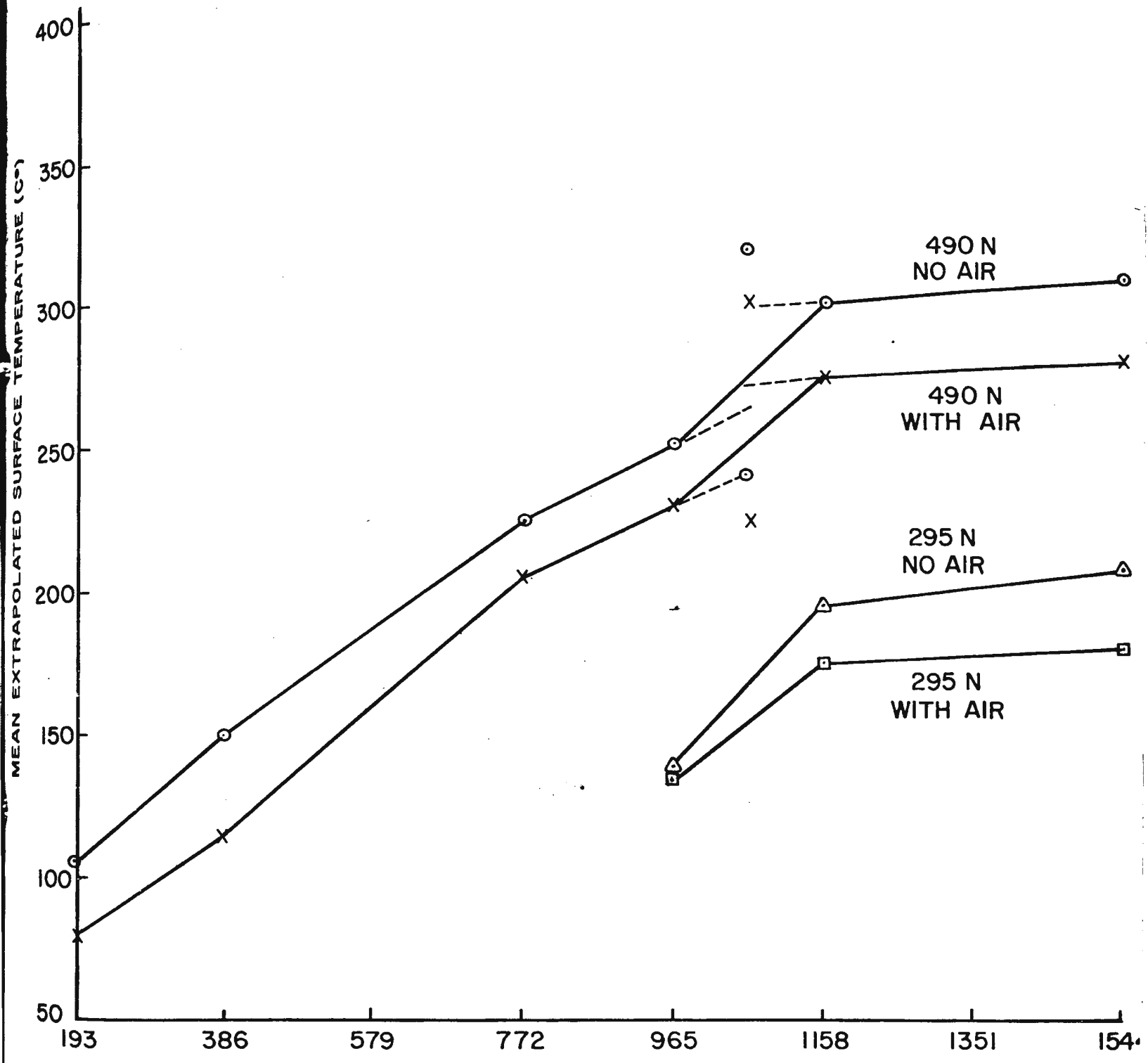

FIG. 9.9

VARIATION OF MEAN EXTRAPOLATED SURFACE TEMPERATURE WITH SLIDING SPEED FOR ROTATING SPECIMEN

9.1.2.8. Effect of Load, Sliding Speed and Gas Mixture on Vibration

The vibration of the wear test machine was measured at six different locations as shown in Fig 9.10. Vibration in the axial direction were recorded at locations B'and b' on the main bearing of the lathe machine headstock on the rotating specimen side and on the normal load cylinder on the stationary specimen side respectively. Vibration in the horizontal and the vertical mode was recorded at A & B for the rotating specimen side and at a and b for the stationary specimen side.

The vibration was recorded in power spectral density units. From these values, the linear displacement (amplitude) of vibration and the integrated power spectral density was calculated.

The linear displacements (amplitudes) at the lowest frequencies of vibration, and the integrated power spectral density, are tabulated in Appendix C - Table of Results. The largest amplitudes occur at the lowest frequencies.

The highest amplitude of vibration was recorded as 280 um (.001 in.) for DWTE 22 at location B - Load 490N, sliding speed 0.193 m/s without air. The amplitude usually was an order lower than this value. There doesn't seem to be any correlation between the amplitude of vibration and the sliding speed, normal load or gas mixture. For any individual test run the linear displacement was higher for the rotating specimen side than the stationary specimen side. Also, the axial vibration amplitude was usually higher than the horizontal and vertical vibration.

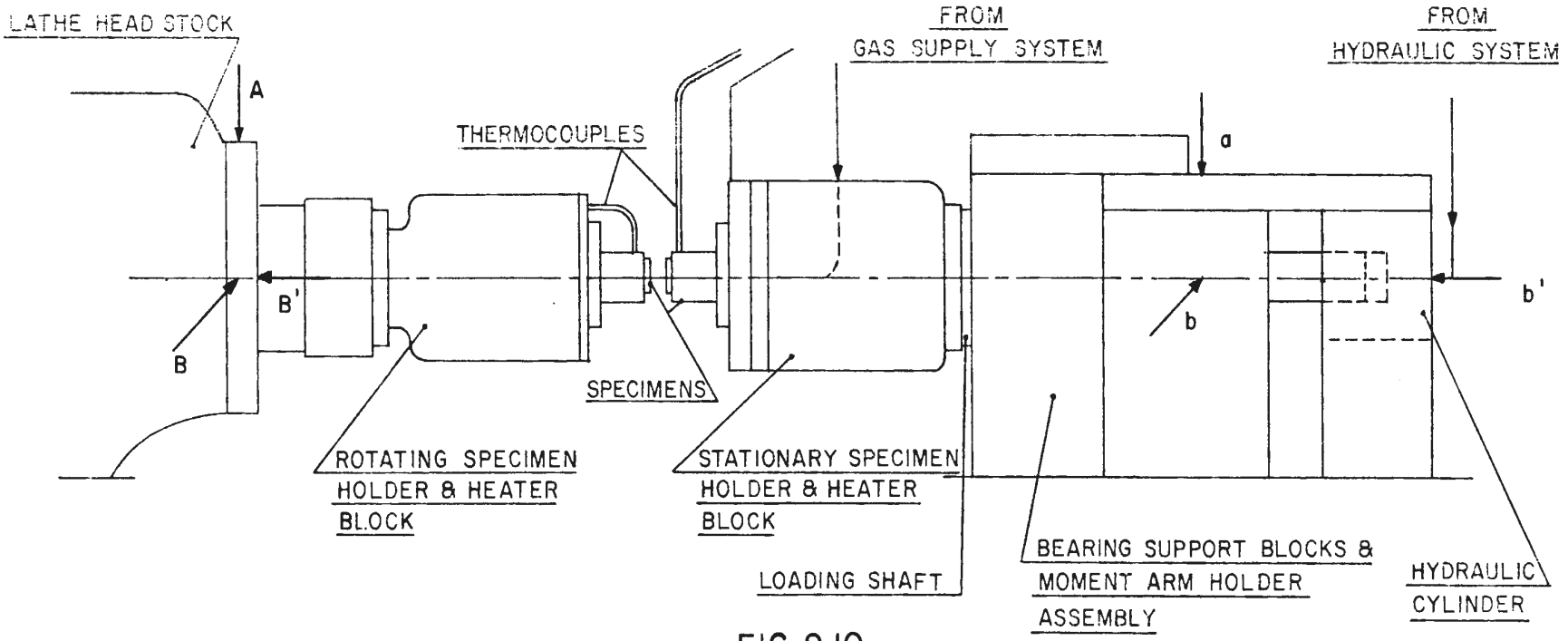

FIG·9·10

SCHEMATIC DIAGRAM OF WEAR TEST MACHINE

SHOWING LOCATIONS OF THE ACCELEROMETER

The integrated power spectral density over the range of 20HZ to 3000HZ shows a correlation with the mean normal load, sliding speed and the composition of the gas mixture.

In Fig 9.11., the effect of increasing the mean normal load at a constant sliding speed of 1.158 m/s is shown. An increase in the mean normal load, caused an increase in vibration, except at location B where horizontal vibration of the headstock was recorded.

Fig 9.12. shows the effect of sliding speed on vibration. No significiant change is noticed, except the dip in B' curve corresponding to 1.158 m/s. In Fig 9.13. the effect of gas mixture on vibration is shown. A decrease in the oxygen content was found to reduce the vibration.

9.1.3. Analysis of the Wear Debris Particles

9.1.3.1. Identification

The results of X-Ray analysis are given in Appendix C - Table of Results and have already been referred to in previous sections. In Table 9.7. the most common results for the composition of the wear debris particles are summarized.

α-Fe was always present in the wear debris particles, irrespective of the experimental conditions.

FeO appeared at the sliding speed of 1.061 m/s for the experiments with unheated specimens and no air. When air was forced through the specimens, FeO appeared at 1.158 m/s. For the specimen holder temperature, of 100^{o}C and 150^{o}C, no FeO was noticed; however, FeO was

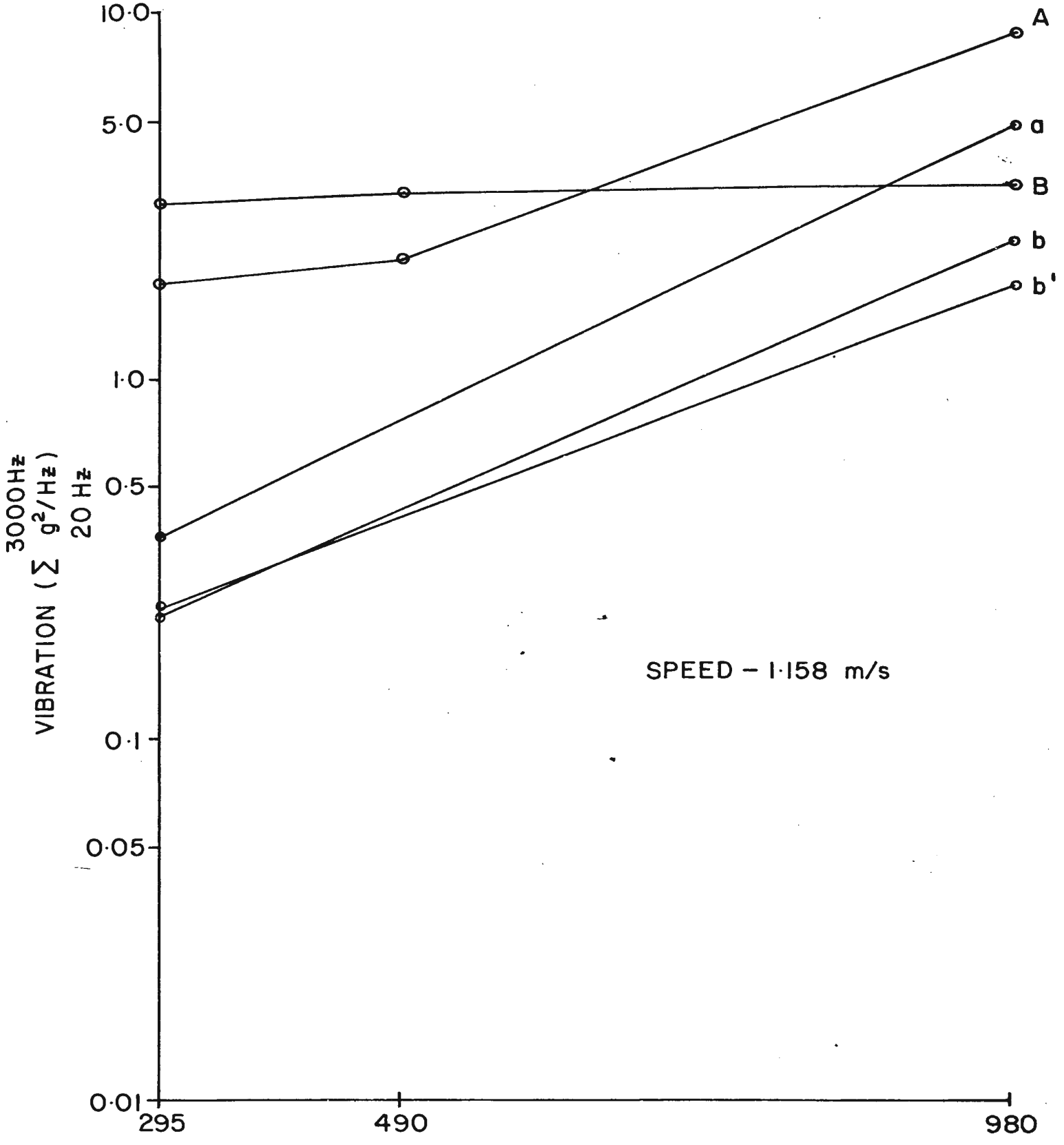

FIG· 9·11

EFFECT OF LOAD ON VIBRATION

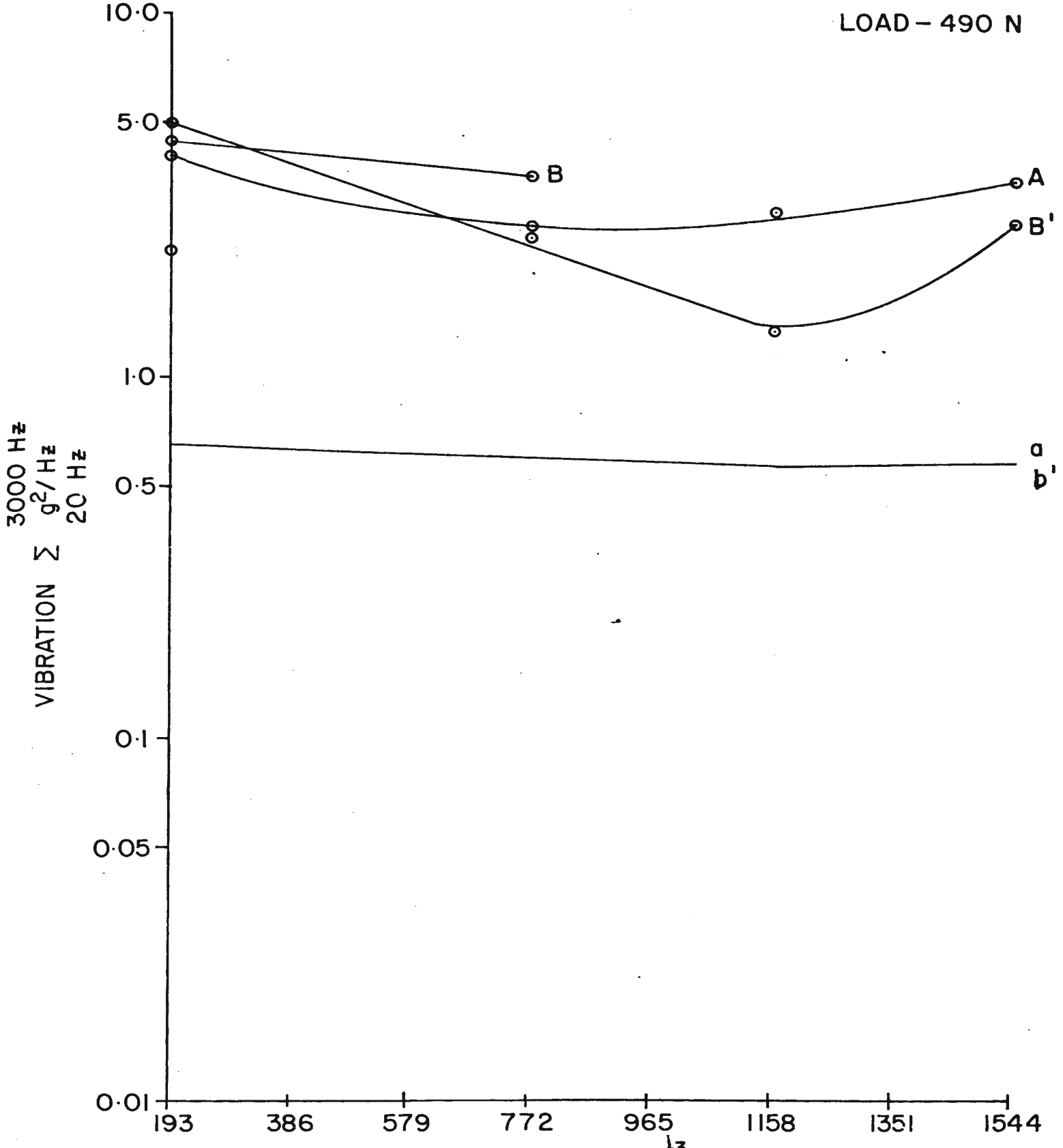

FIG·9·12

EFFECT OF SLIDING SPEED ON VIBRATION

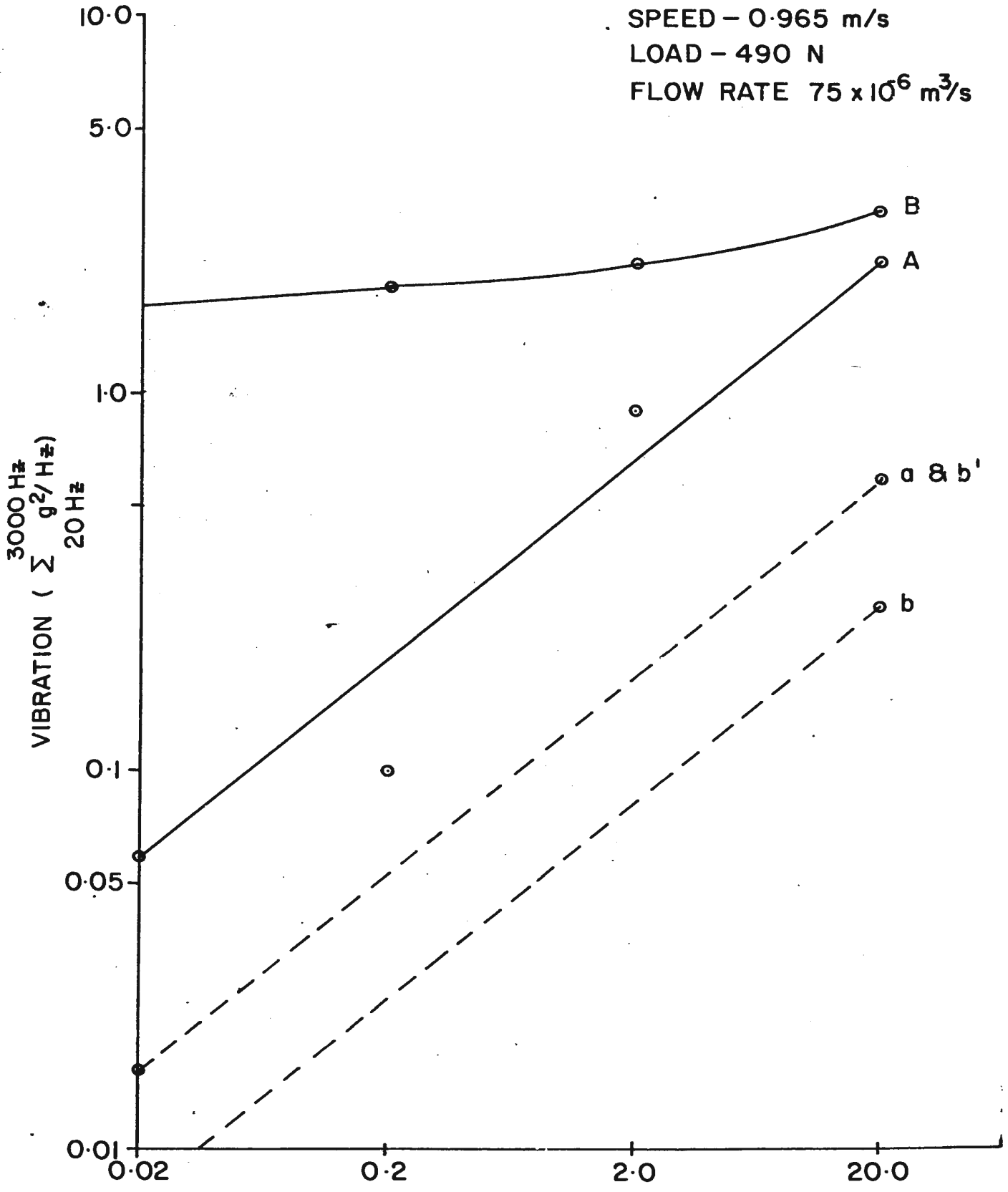

FIG·9·13

EFFECT OF % (v/v) O_2 in Ar ON VIBRATION

TABLE 9.7

SPEED (ms^{-1})	0.193	0.386	0.772	0.965	1.061	1.158	1.544	
LOAD x98 (N)	3 5 10	3 5 10	3 5 10	3 5 10	3 5 10	3 5 10	3 5 10	
UNHEATED SPECIMENS		T	x x	T x x	x	x x x	x x	Fe_3O_4
NO AIR	x	x	x x	x x x	x	x x x	x x	Fe_2O_3
DIFFERENT LOADS & SPEEDS					T*	x x x	x x	FeO
	x	x	x x	x x x	x	x x x	x x	Fe
UNHEATED SPECIMENS		T	x	x x	x	x x	x x	Fe_3O_4
WITH AIR	x	x	x	x x	x	x x	x x	Fe_2O_3
DIFFERENT LOADS & SPEEDS						x x	x x	FeO
	x	x	x	x x	x	x x	x x	Fe
				11.52 x 100°C				
HEATED SPECIMENS				x x x				Fe_3O_4
NO AIR				x x x				Fe_2O_3
LOAD 490 N, SPEED 0.965 ms^{-1}				x				FeO
				x x x				Fe
				2.2.02		%(V/V)O_2 in Ar		
UNHEATED SPECIMENS				x x				Fe_3O_4
DIFFERENT GAS MIXTURES				x				Fe_2O_3
LOAD 490 N				T*x x				FeO
				x x x				Fe

RESULTS OF X-RAY ANALYSIS

T: Traces found
T*: Transition

present at 200°C.

In the experiments where different gas mixtures were used - corresponding to a load of 490N and a speed of 0.965 m/s, for 2% O_2 the consituents present were α-Fe, α-Fe_2O_3 and Fe_3O_4 and traces of FeO. For 0.2% O_2 mixture, the wear debris particles were entirely αFe, FeO and Fe_3O_4 while for 0.02% O_2 the debris particles were entirely αFe and FeO.

9.1.3.2. Size Analysis

Typical results of the size analysis of the wear debris particles are given in Figs 9.14 to 9.18.

In Figs 9.14 and 9.15 the distribution curves for wear debris particles collected under the specimen and on the filter paper are shown. The distribution curve, for the particles from the filter paper, is skewed to the left indicating a larger number of fine particles.

In Figs 9.16 and 9.17 the effect of sliding speed on the size distribution is shown. At the higher speed, finer particles were obtained.

In Fig 9.18., the effect of forcing air through the specimen is shown. The debris examined were collected under the specimen.

The median and the standard deviation of the particle sizes are tabulated in Appendix C - Table of Results, for most of the experiments.

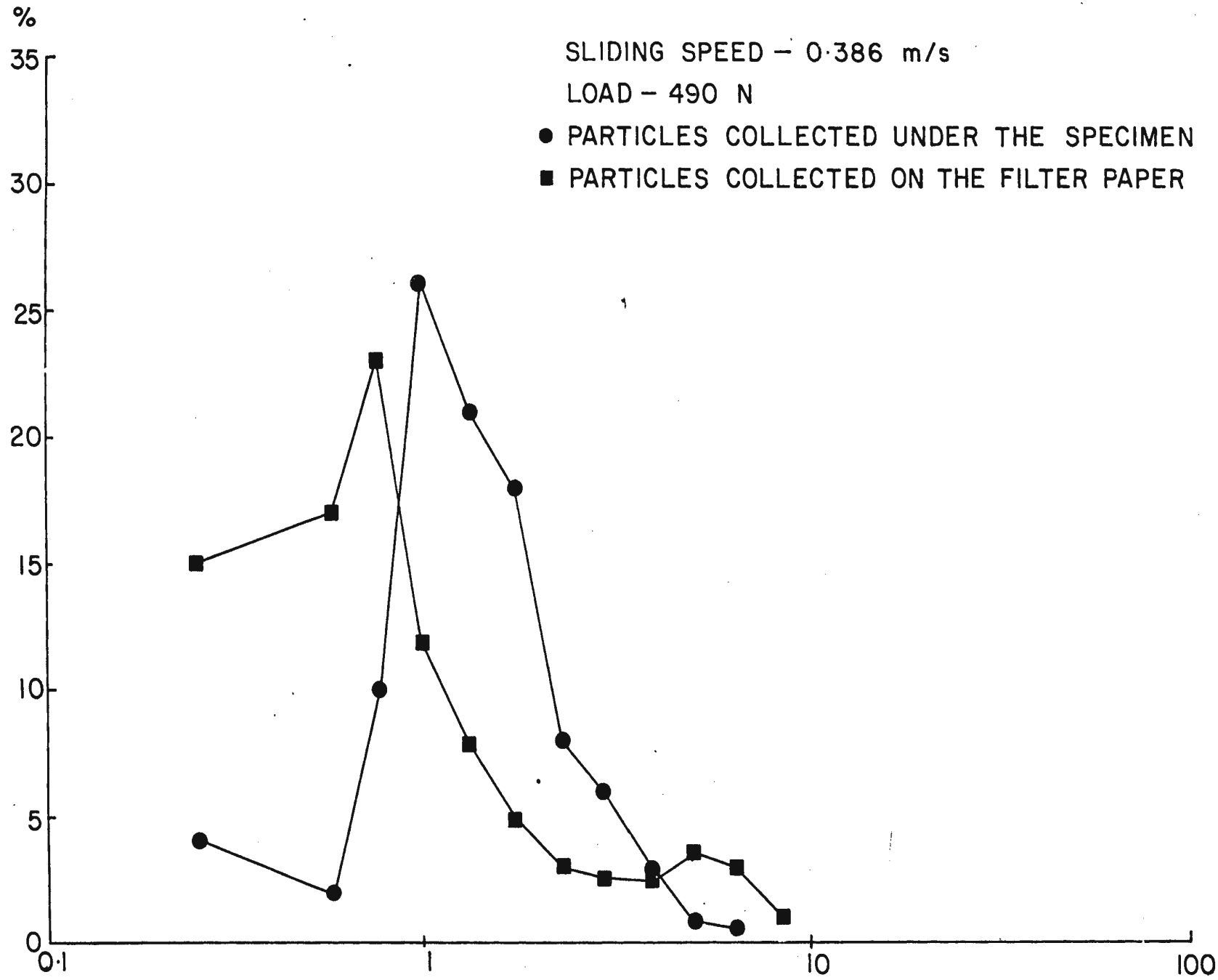

FIG·9·14

DISTRIBUTION CURVE FOR WEAR DEBRIS PARTICLES

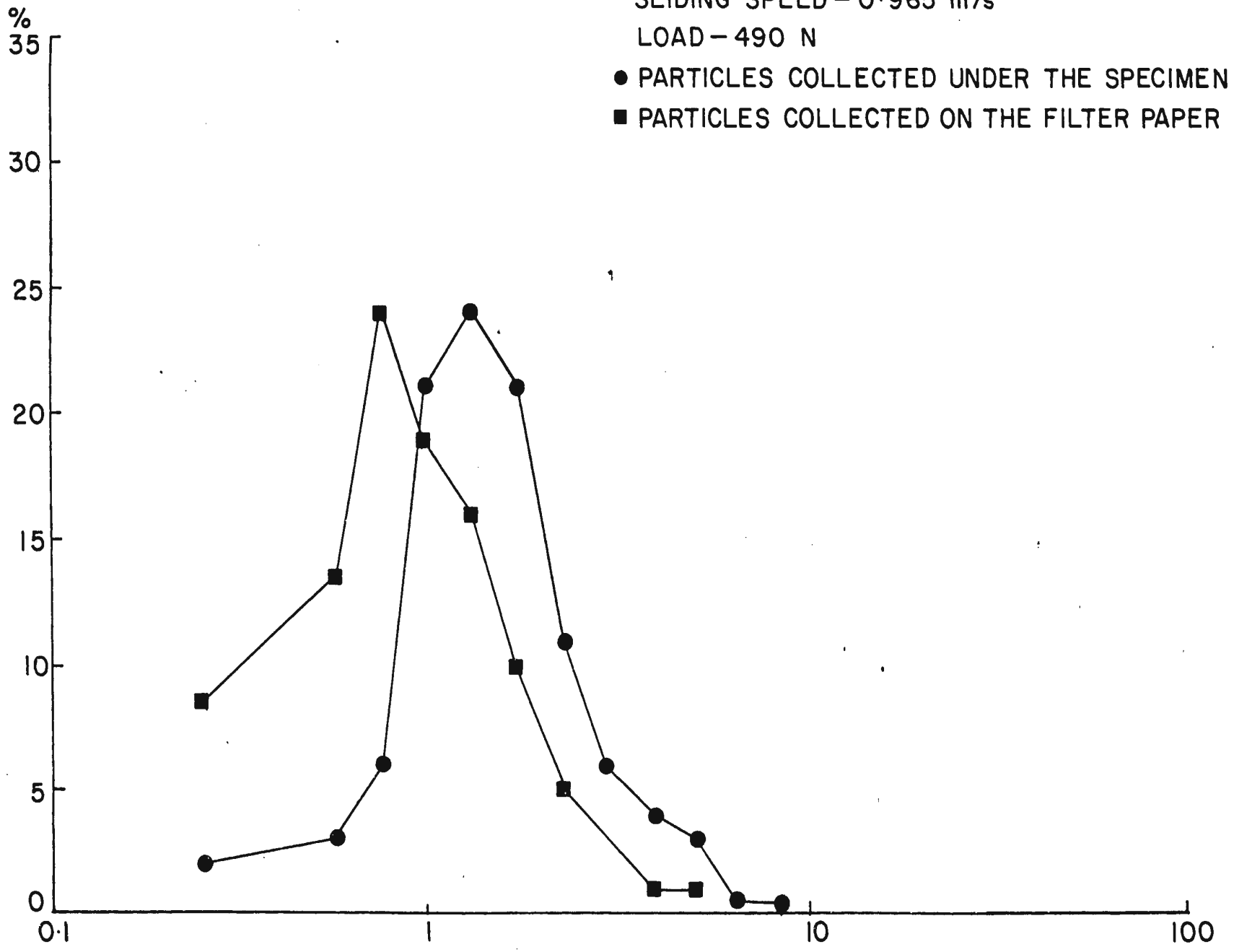

FIG·9·15

DISTRIBUTION CURVE FOR WEAR DEBRIS PARTICLES

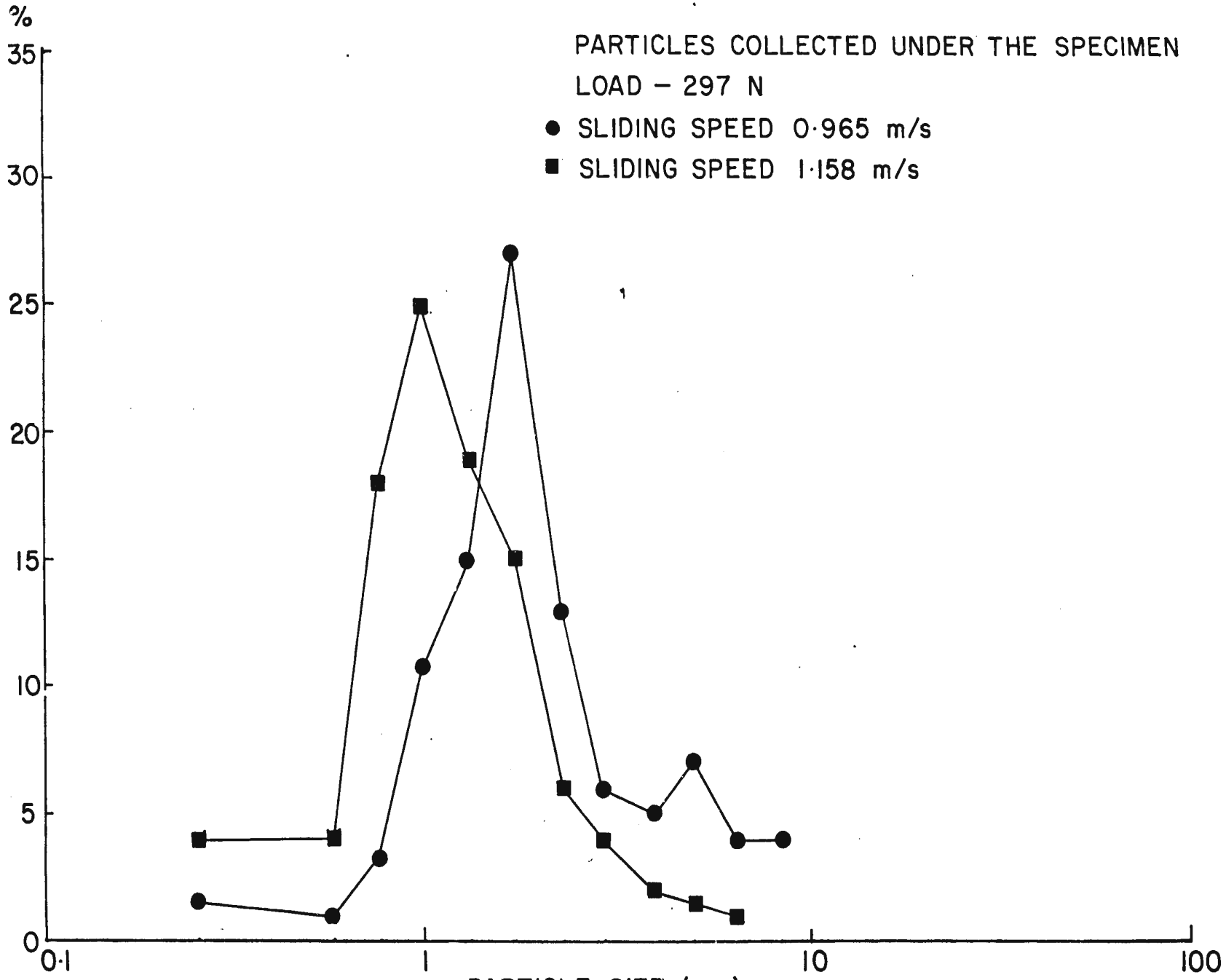

FIG·9·16

DISTRIBUTION CURVE FOR WEAR DEBRIS PARTICLES

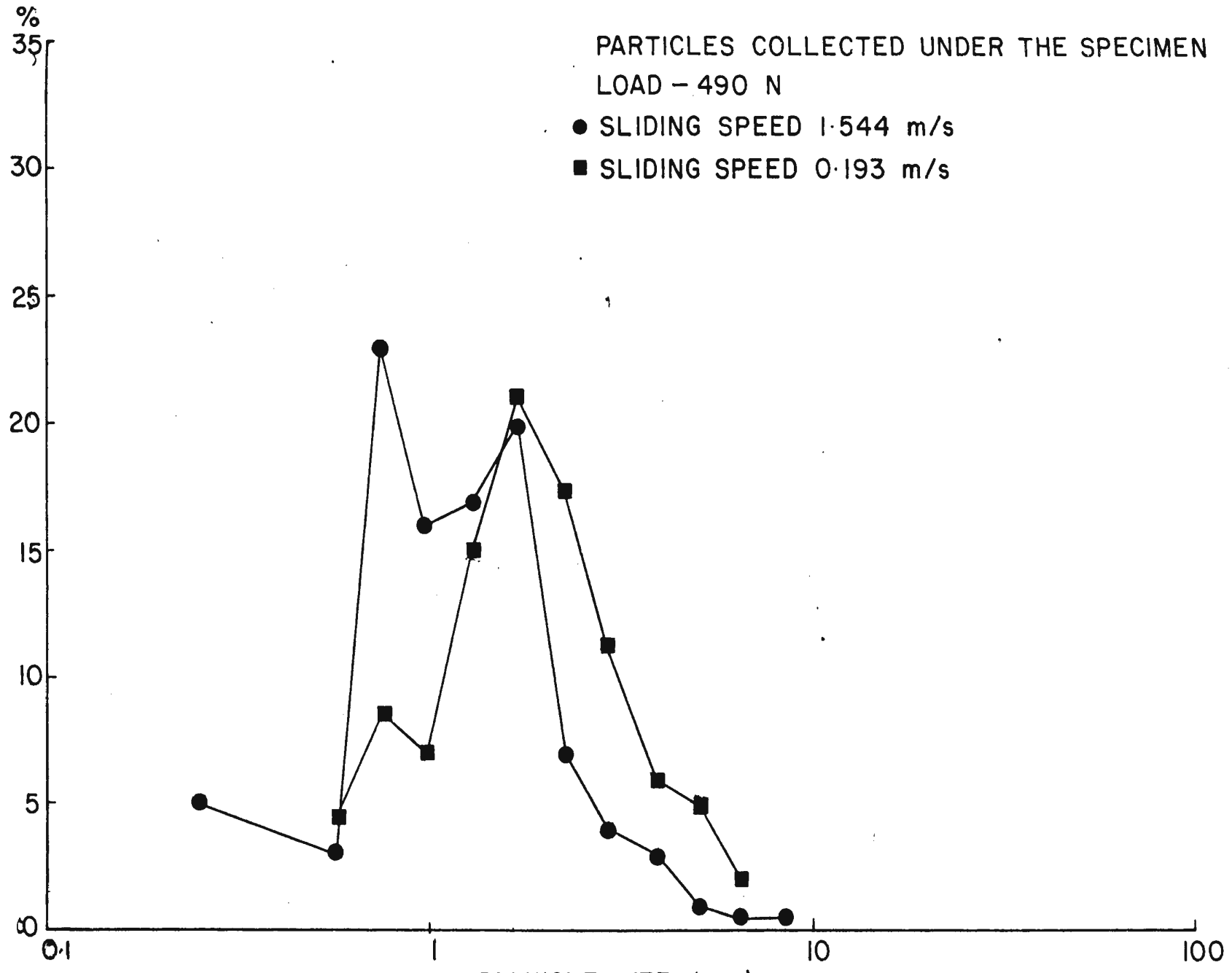

FIG· 9·17

DISTRIBUTION CURVE FOR WEAR DEBRIS PARTICLES

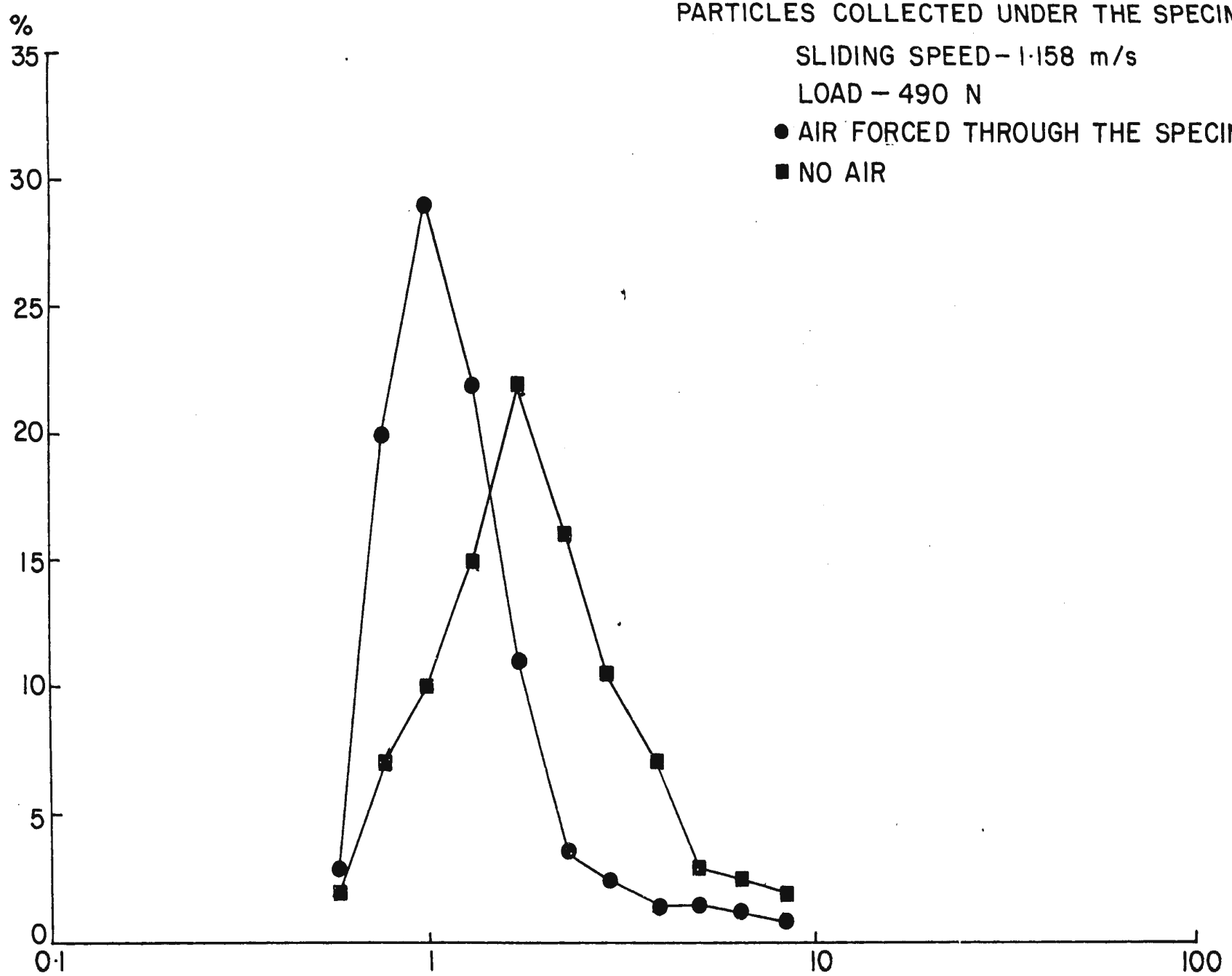

FIG· 9·18

DISTRIBUTION CURVE FOR WEAR DEBRIS PARTICLES

9.1.4. Metallurgical Changes

9.1.4.1. Topography of the Surface

In photographs 9.19 to 9.26, a general picture of the wear surface is given. These photographs were taken on the metallurgical microscope using polarised light. An interesting feature of these photographs is the presence of a layer of transferred oxide film on the wear surface. In photographs 9.19. and 9.20. cracks in the transferred layer and wear debris particles sitting in the wear grooves can be seen. The surface topography for both the specimens are similar.

At 1.158 m/s (photograph 9.21) patches of transferred layer on a lower substrate can be seen. At 0.193 m/s (photograph 9.22) oxides on surface can be seen. With 2% oxygen (photograph 9.23) patches of the transferred layer and rough lower surface can be seen. With 0.2% oxygen (photograph 9.24) the entire surface is smeared with a transferred layer. In photograph 9.25, typical of a load of 980N, a transferred layer with a hole in it can be seen. The hole seems to have been formed by the flaking off of part of the layer from this region. In photograph 9.26, typical of a load of 295N, the transferred layer is less continuous, leaving an irregular surface profile.

Photographs 9.27 to 9.34 were taken on the Scanning Electron Microscope at a tilt of 30^{o} of the specimen holder stage. In addition, photographs were taken at the same location with a holder tilt of 50^{o} (in most cases). This enabled relative heights to be estimated by the parallax effects.

OPTICAL MICROGRAPH OF THE WORN SPECIMEN

LOAD 490 N

SPEED 1.1544 m/s

WITH AIR

ROTATING SPECIMEN

x 180

PHOTOGRAPH 9.19

OPTICAL MIRCOGRAPH OF THE WORN SPECIMEN

LOAD 490 N

SPEED 1.544 m/s

WITH AIR

STATIONARY SPECIMEN

x 180

PHOTOGRAPH 9.20

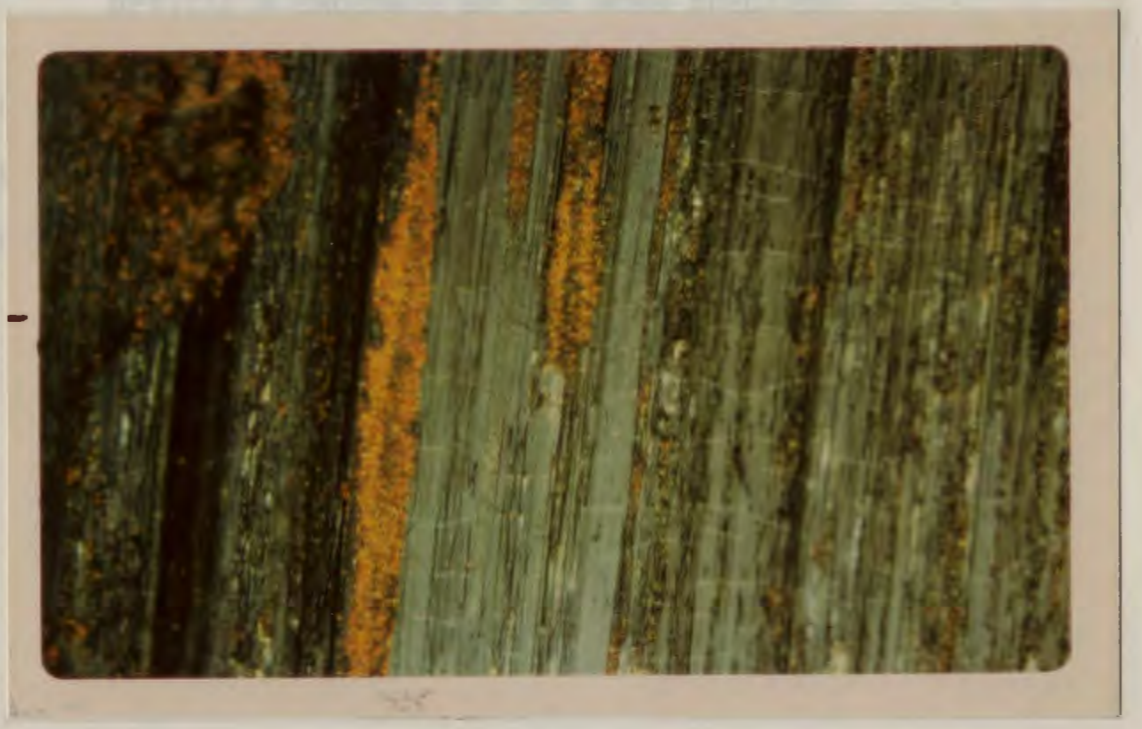

OPTICAL MICROGRAPH OF THE WORN SPECIMEN

LOAD 490 N

SPEED 1.158 m/s

WITH AIR

ROTATING SPECIMEN

x 180

PHOTOGRAPH 9.21

OPTICAL MICROGRAPH OF THE WORN SPECIMEN

LOAD 490 N

SPEED 0.193 m/s

ROTATING SPECIMEN

x 180

PHOTOGRAPH 9.22

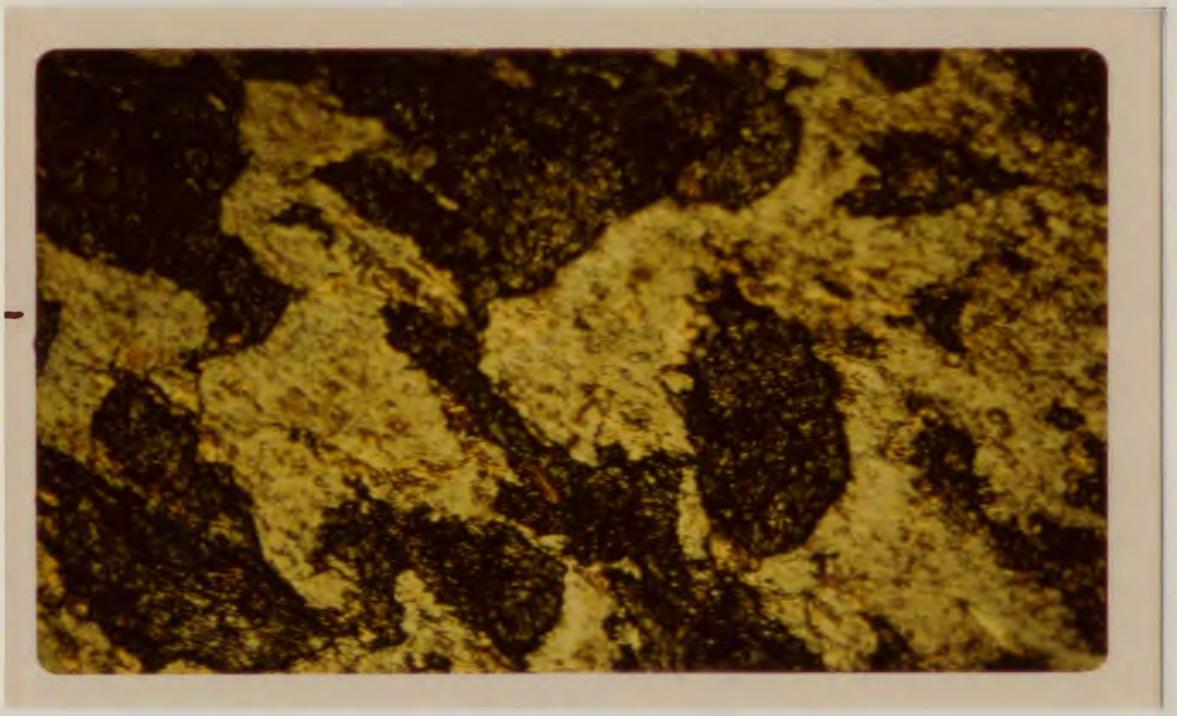

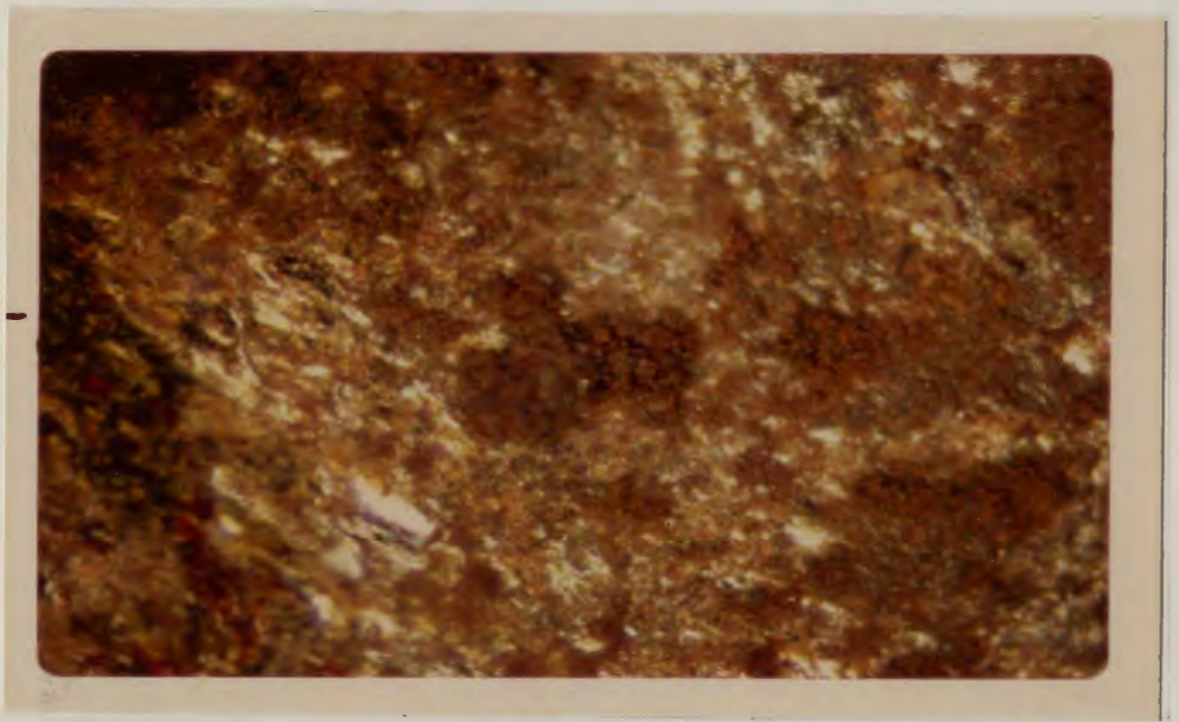

OPTICAL MICROGRAPH OF THE WORN SPECIMEN

LOAD 295 N

SPEED 1.158 m/s

WITH 2% O_2

STATIONARY SPECIMEN

x 180

PHOTOGRAPH 9.23

OPTICAL MICROGRAPH OF THE WORN SPECIMEN

LOAD 295 N

SPEED 1.158 m/s

WITH 0.2% O_2

STATIONARY SPECIMEN

x 180

PHOTOGRAPH 9.24

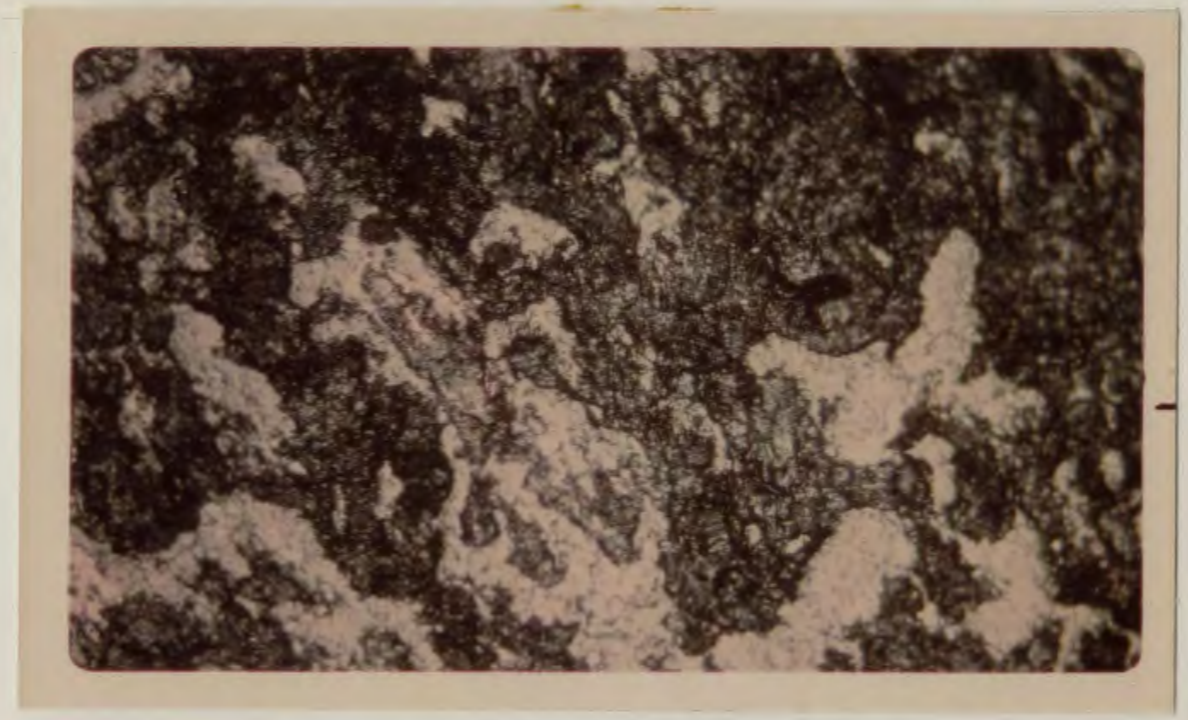

OPTICAL MICROGRAPH OF THE WORN SPECIMEN

LOAD 980 N

SPEED 0.965 m/s

WITH AIR

ROTATING SPECIMEN

x 180

PHOTOGRAPH 9.25

OPTICAL MICROGRAPH OF THE WORN SPECIMEN

LOAD 295 N

SPEED 1.544 m/s

WITH AIR

ROTATING SPECIMEN

x 180

PHOTOGRAPH 9.26

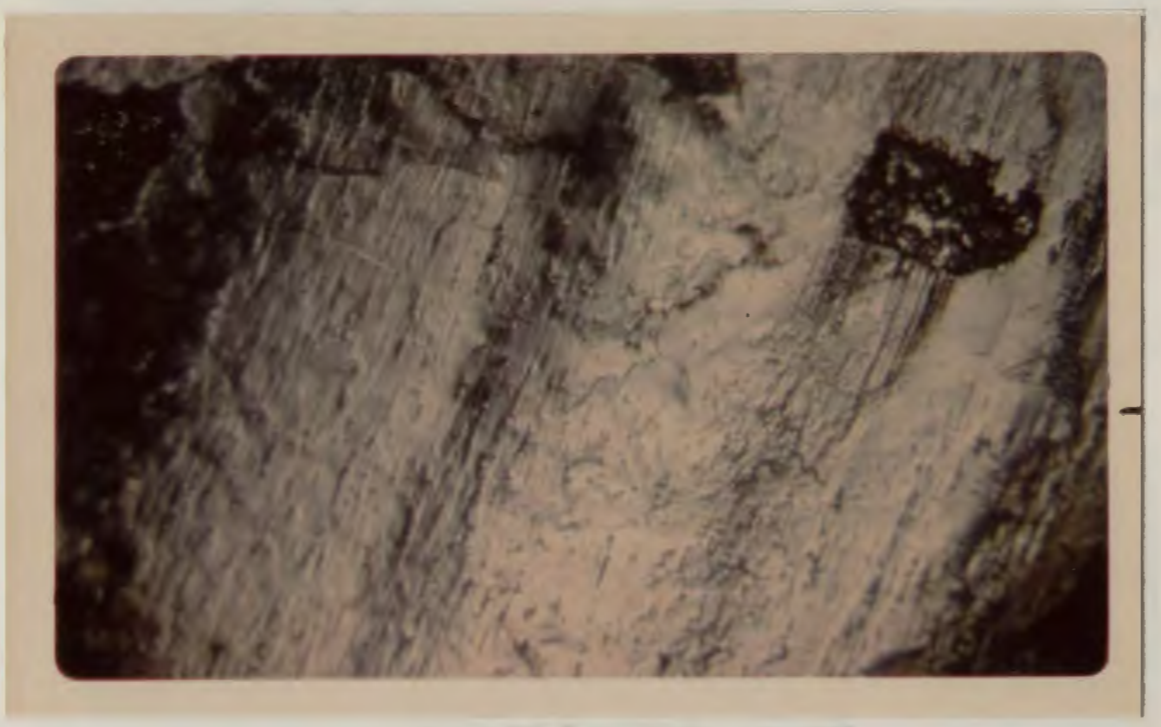

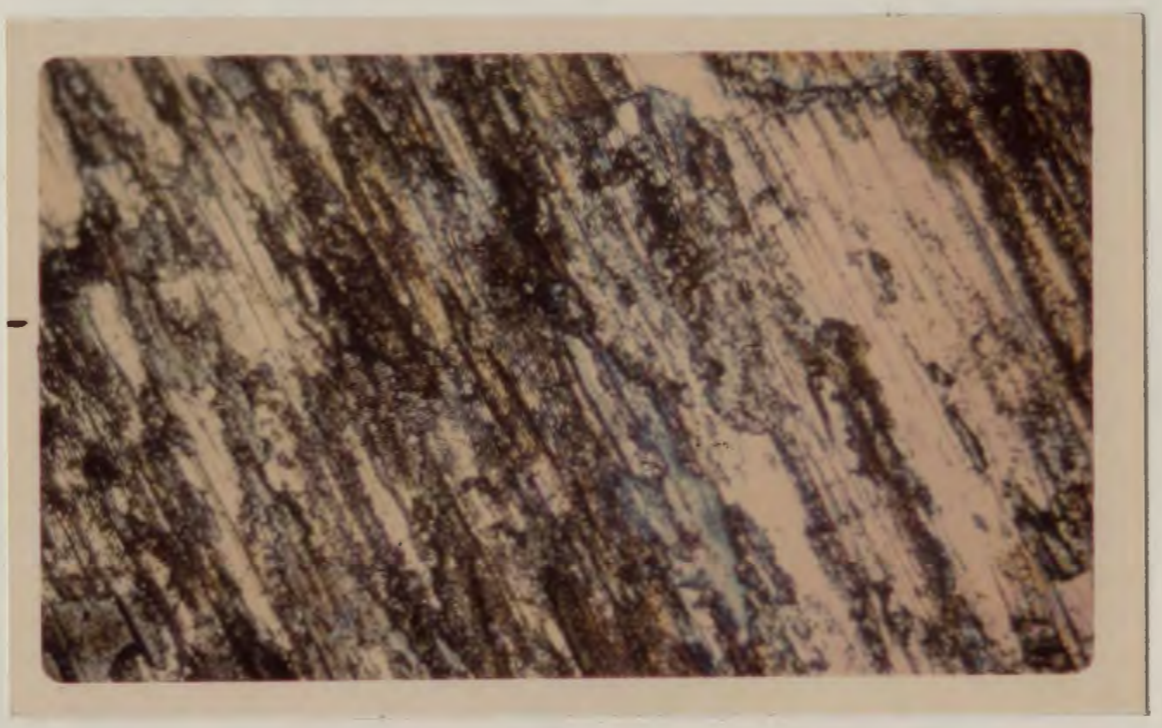

Photograph 9.27 gives a general picture of the surface. The location where photograph 9.28 was taken is shown in the picture.

In photograph 9.28, two zones of the transferred layers sitting on the surface are shown. The cavity formed is full with wear debris particles. Two spherical wear debris particles are sitting in the cavity.

Count rates obtained with the x-ray energy dispersive analyser set on the FeKα radiation were lower than for pure iron, atall locations shown in photograph 9.28, suggesting that all the visible material was oxide, both transferred layers and the substrate, as well as the debris particles.

Photograph 9.29 gives a general view of the surface. The locations where photographs 9.30, 9.31 and 9.32 were taken are marked on the photograph. In photograph 9.30, a lower surface of the specimen with grooves in it can be seen. A transferred layer, presumably oxide, is sitting on top of the surface. The wear grooves on the surface of specimen is inclined at 10^{o} to the wear mark on top of the oxide film. Probably, transverse vibration is responsible for this pattern. In photograph 9.31, a transferred oxide layer on the surface is shown. The thickness of this layer near the bottom of photograph was estimated to be 7 um. Also the photograph shows a cleavage plane in the front from which part of the layer has been removed.

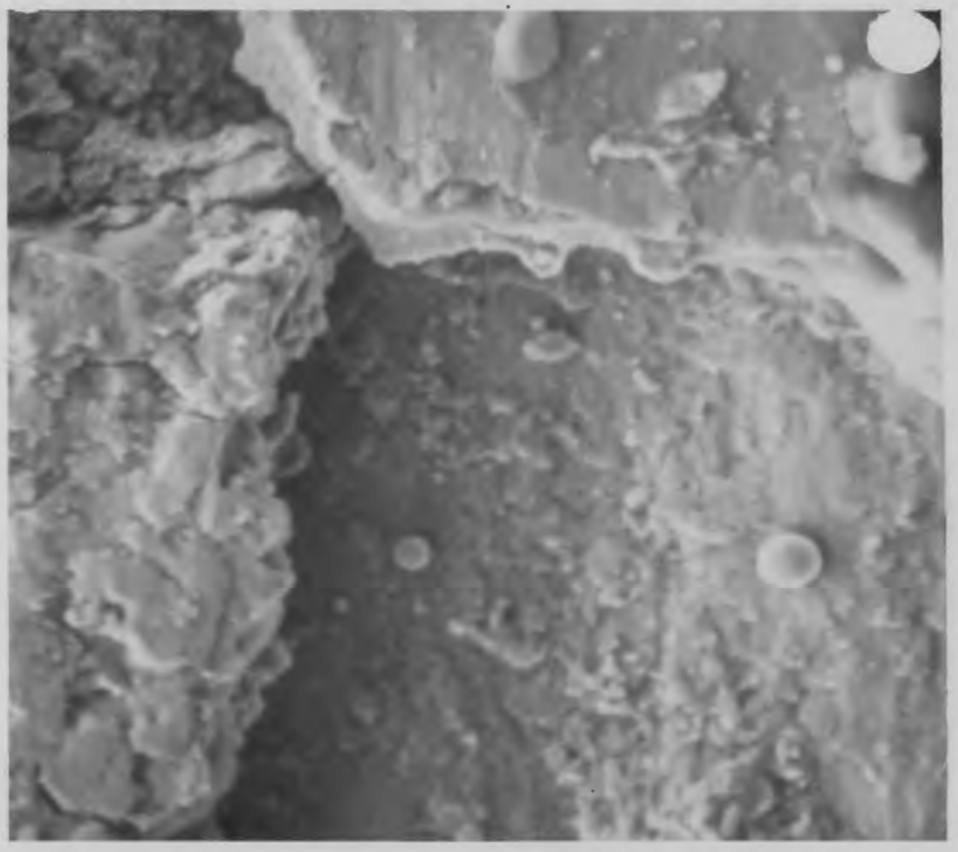

SCANNING ELECTRON MICROGRAPH OF WORN SPECIMENS

LOAD 490 N

SPEED 0.965 m/s

ROTATING SPECIMEN

x 220

PHOTOGRAPH 9.29

SCANNING ELECTRON MICROGRAPH OF WORN SPECIMENS

LOAD 490 N

SPEED 0.965 m/s

ROTATING SPECIMEN

x 2200

PHOTOGRAPH 9.30

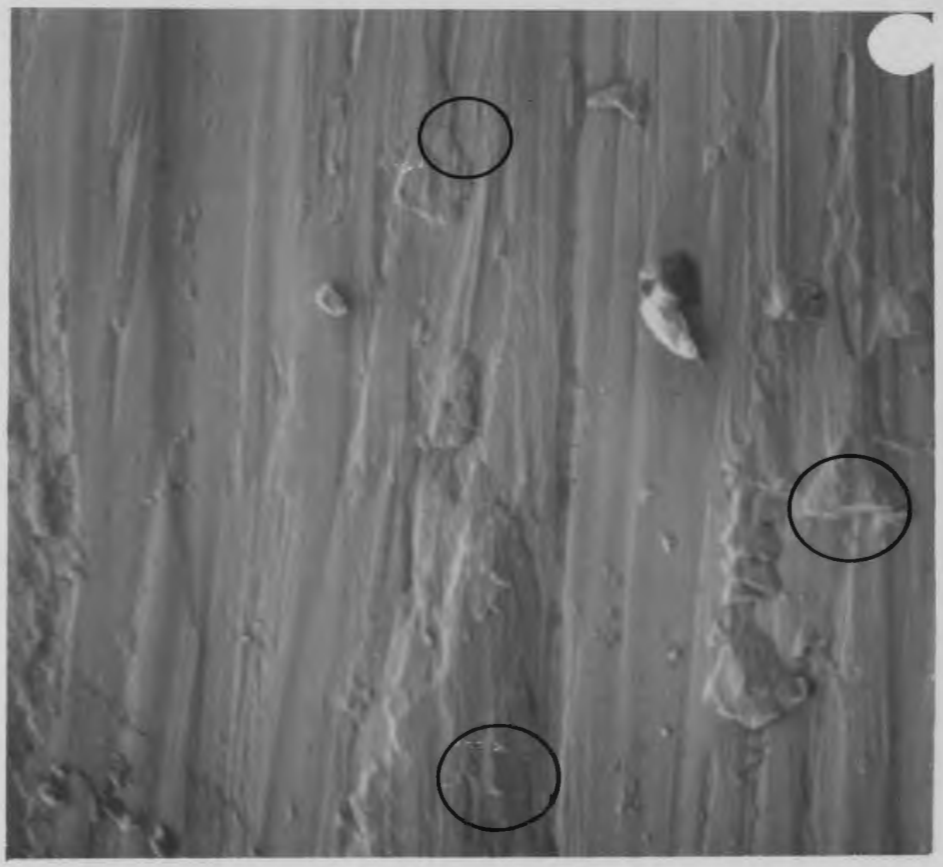

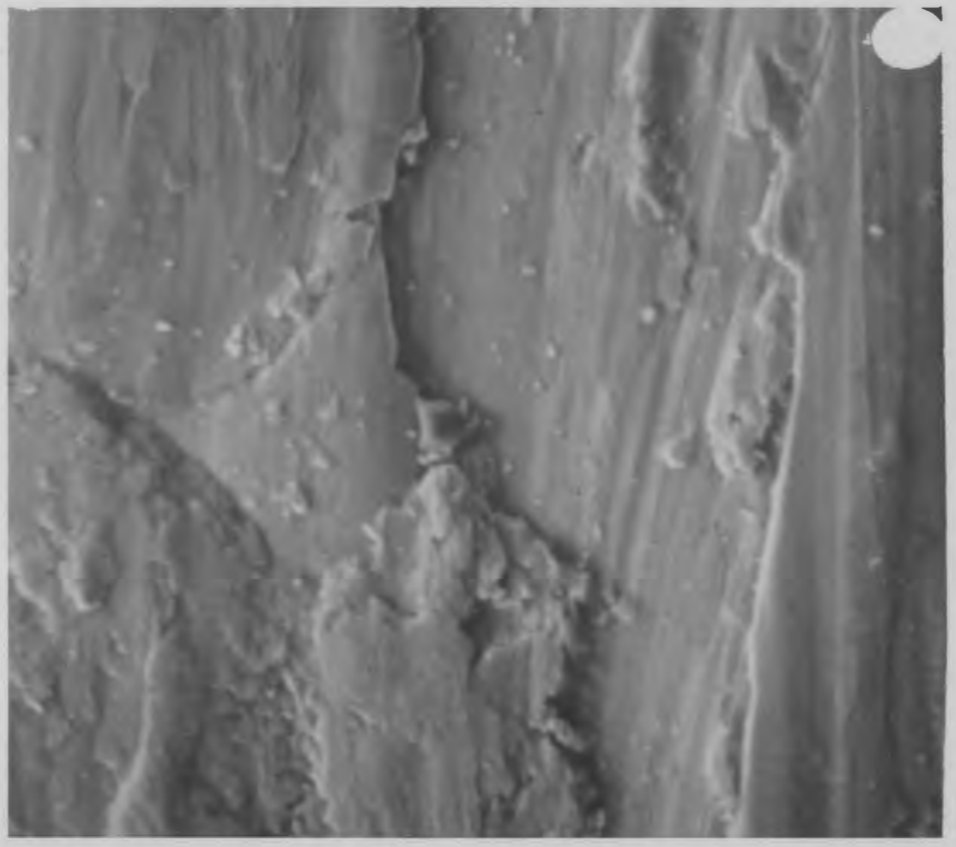

SCANNING ELECTRON MICROGRAPH OF WORN SPECIMEN

LOAD 490 N

SPEED 0.965 m/s

ROTATING SPECIMEN

x 2200

PHOTOGRAPH 9.31

SCANNING ELECTRON MICROGRAPH OF WORN SPECIMEN

LOAD 490 N

SPEED 0.965 m/s

ROTATING SPECIMEN

x 2200

PHOTOGRAPH 9.32

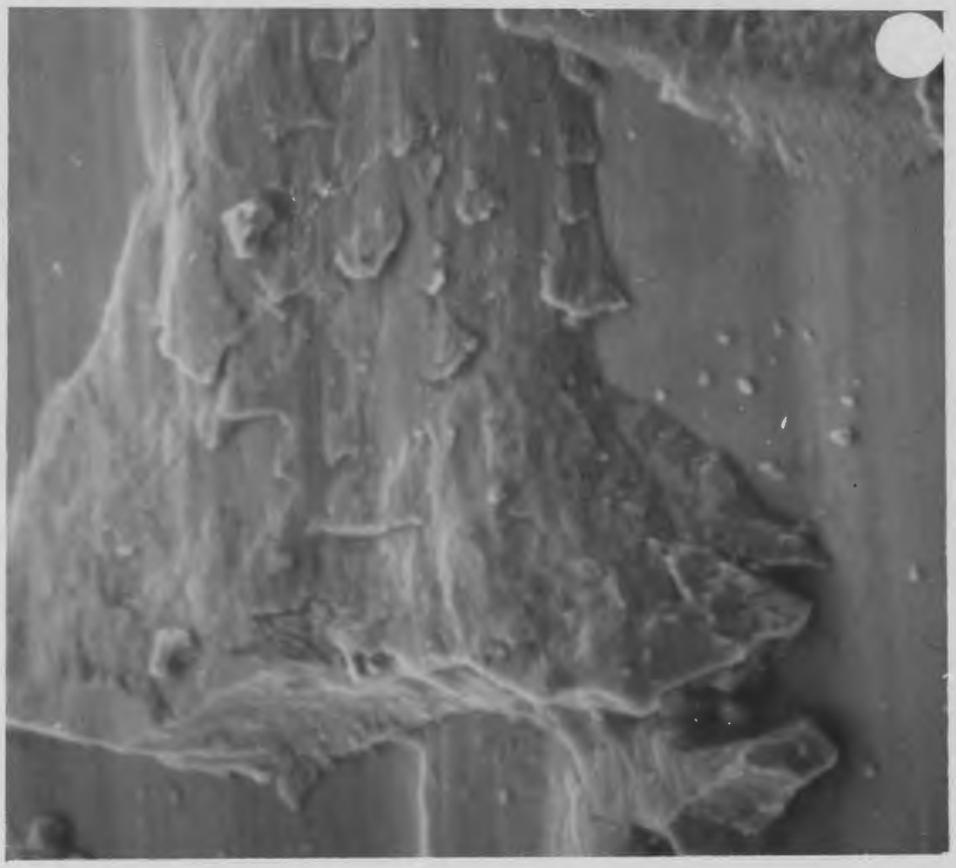

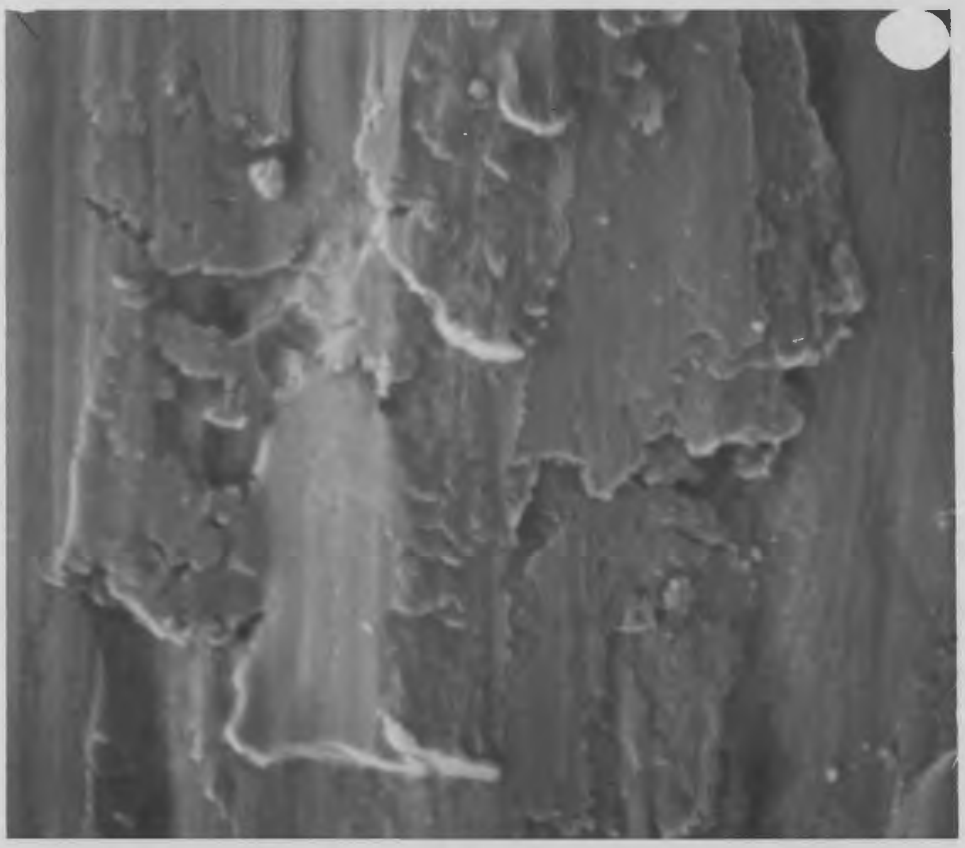

Photograph 9.32 shows the laminations. At the right and left edges of the picture, the substrate can be seen and different thicknesses of the apparently transferred oxide are piled up one on top of the other. The thickness of layers measured near ends from where they have been removed was found to be 1 μm.

Photograph 9.33 shows cracks formed in the transferred layer and the wear debris. These cracks must have been formed after the experiment was stopped. Even the smallest amount of shear force can break open the debris.

In photograph 9.34, wear debris particles of unusual shape can be seen sitting on the transferred layer. These were right at the edge of wear surface.

9.1.4.2. Structural Changes

Structures of the worn specimens are shown in optical micrographs 9.35 and 9.36 and in scanning electron micrographs 9.37 to 9.42, taken on the cross sectional plane of the specimen parallel to the sliding direction.

Photograph 9.35 shows a transferred layer, probably oxide, sitting on top of the deformed specimen surface.

Surface deformation is shown in photographs 9.36 to 9.39. The striking feature of these photographs is the pattern of material flow, near the wear surface, parallel to the direction of sliding similar to that described by Dautzenbert (1973). The white area in photograph 9.36 is probably ferrite, formed by the decarburisation of steel near

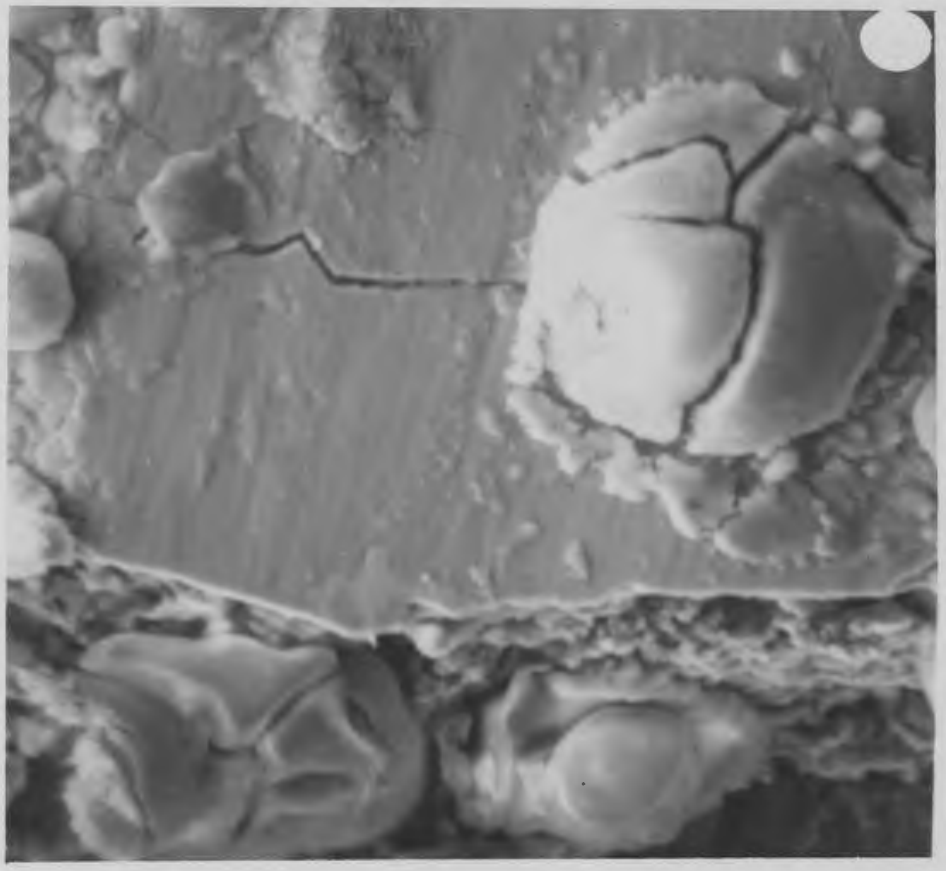

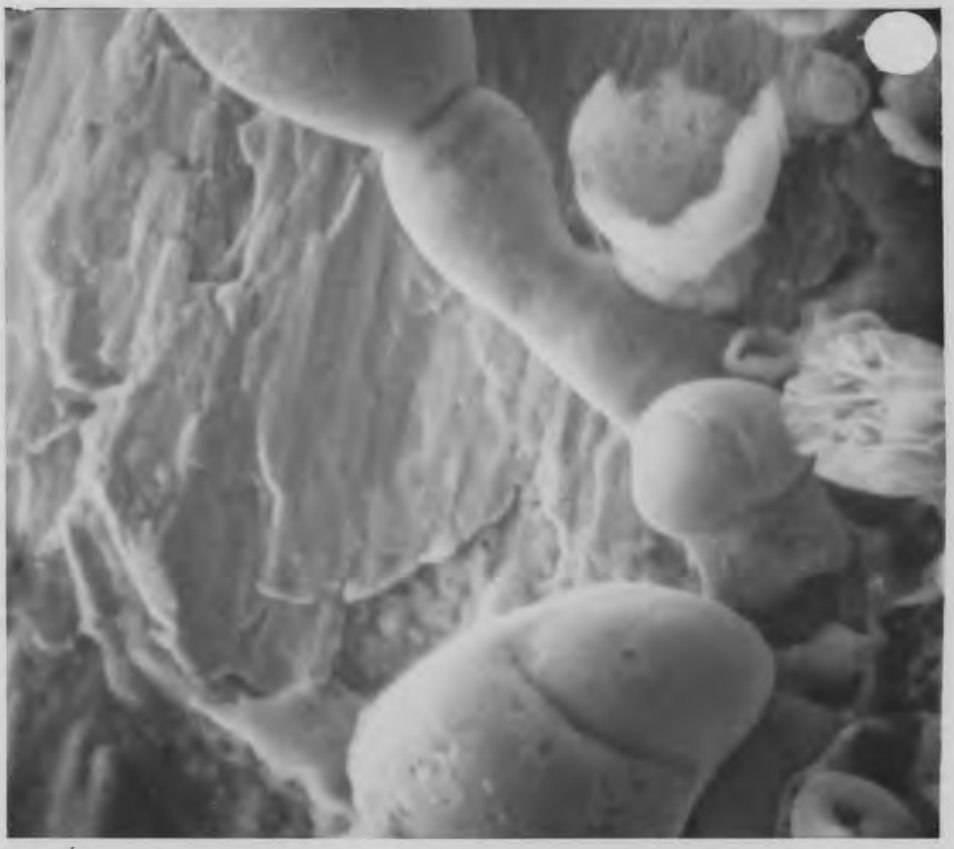

OPTICAL MICROGRAPH OF WORN SPECIMEN

LOAD 490 N

SPEED 1.158 m/s

ROTATING SPECIMEN

x 720

PHOTOGRAPH 9.35

OPTICAL MICROGRAPH OF WORN SPECIMEN

LOAD 490 N

SPEED 1.158 m/s

STATIONARY SPECIMEN

x 720

PHOTOGRAPH 9.36

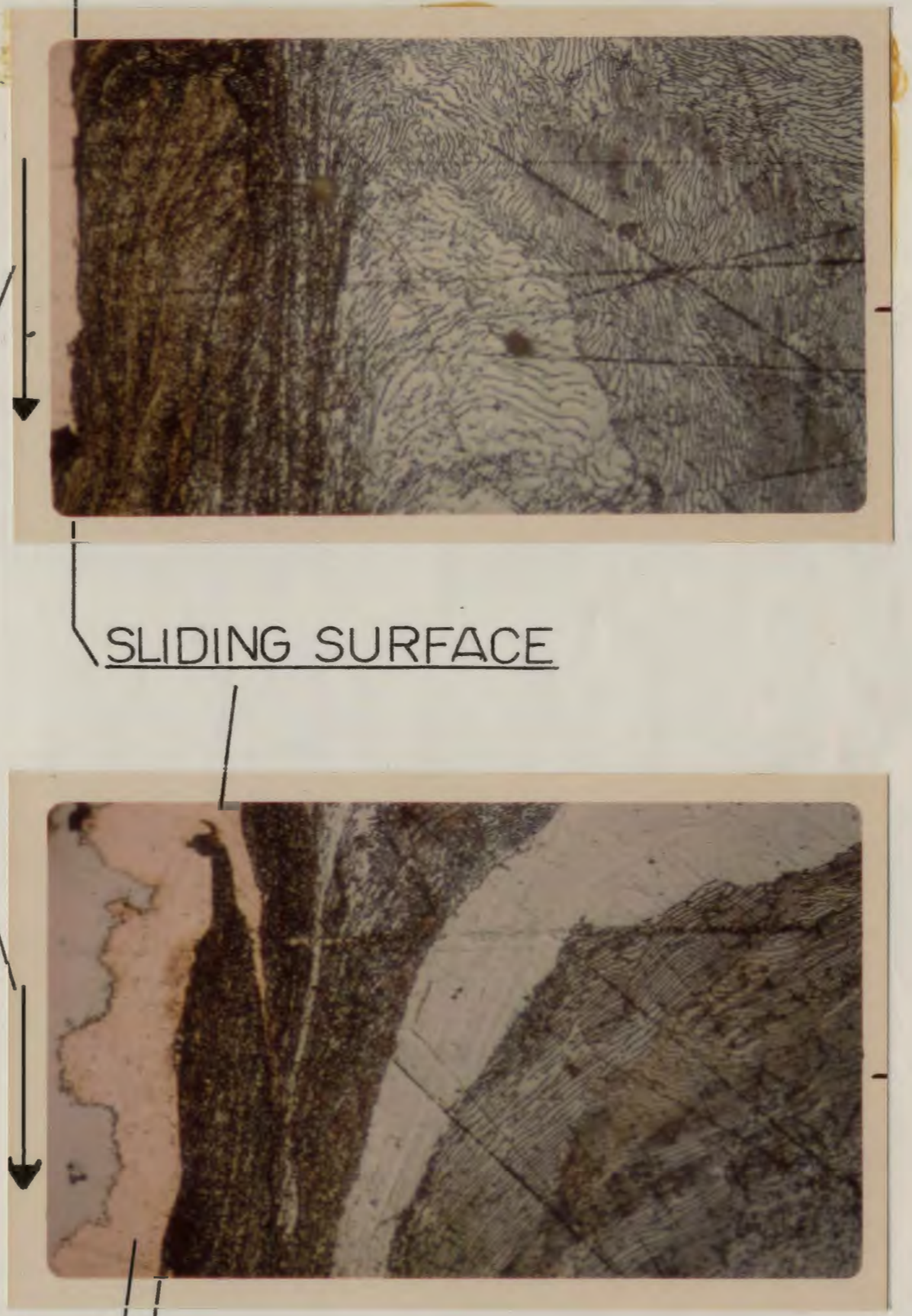
SLIDING DIRECTION
SLIDING SURFACE
Cu

the wear surface. The transferred layer, to the left of picture can be seen sitting on the wear surface. Copper plated on to the specimen, prior to mounting for sectioning (to support the specimen edge) has filled the space between the transferred layer and the specimen surface.

Photograph 9.37 shows the deformed pearlite structure. The flow pattern can be seen in photograph 9.38. Photograph 9.39 shows a broken pearlite structure. The direction of pearlite in the undeformed specimen was parallel to the bottom edge of the picture. The undeformed lamellar pearlites are shown in photographs 5.1 and 5.2. In photographs 9.40, 9.41 and 9.42, cracks below the surface are shown.

9.1.4.3. Microhardness Measurements

Two sets of the microhardness measurements are plotted in Figs 9.43 and 9.44. The general pattern of the microhardness values for most of the test are similar. Two transitions in the microhardness plots were noticed, first transition about 75 μm away from the wear surface and the second transition about 150 μm away. Up to 75 μm away from the surface, the hardness was found to show a rapid decrease with increase in the distance. A change in slope takes place at 75 μm and after 150 μm the hardness was the same as for the bulk material.

Invariably, the stationary specimen was harder than the rotating specimen in the first transition zone, which could explain the generally lower wear rate values for stationary specimens in the wear tests previously described.

SCANNING ELECTRON MICROGRAPH OF WORN SPECIMEN

LOAD 490 N

SPEED 1.158 m/s

WITH AIR

ROTATING SPECIMEN

x 5500

PHOTOGRAPH 9.37

SCANNING ELECTRON MICROGRAPH OF WORN SPECIMEN

LOAD 490 N

SPEED 1.158 m/s

WITH AIR

ROTATING SPECIMEN

x 1950

PHOTOGRAPH 9.38

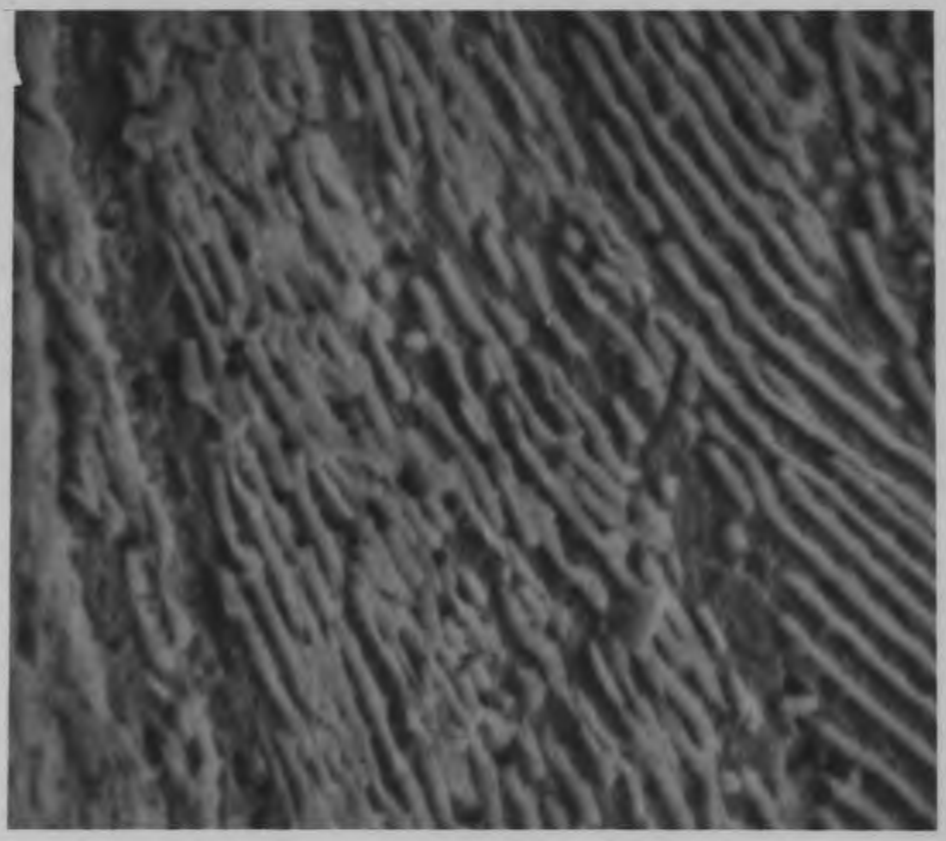

SCANNING ELECTRON MICROGRAPH OF WORN SPECIMEN

LOAD 490 N

SPEED 1.159 m/s

WITH AIR

ROTATING SPECIMEN

x 7000

PHOTOGRAPH 9.39

SCANNING ELECTRON MICROGRAPH OF WORN SPECIMEN

LOAD 980 N

SPEED 1.158 m/s

WITH AIR

ROTATING SPECIMEN

x 700

PHOTOGRAPH 9.40

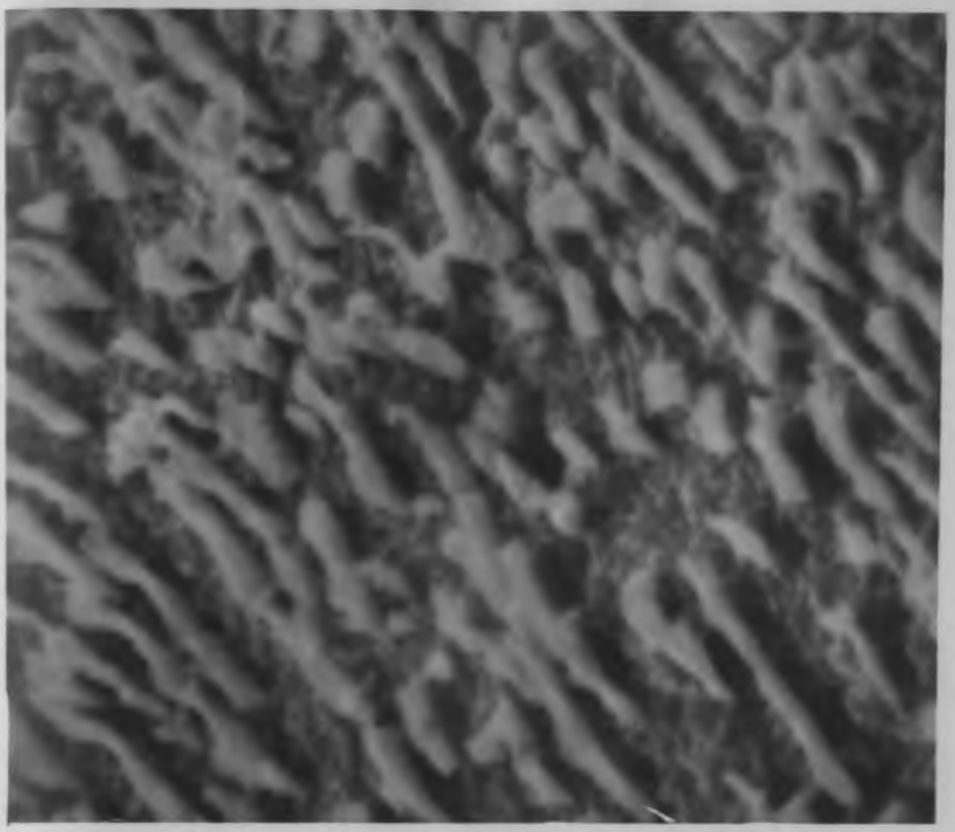

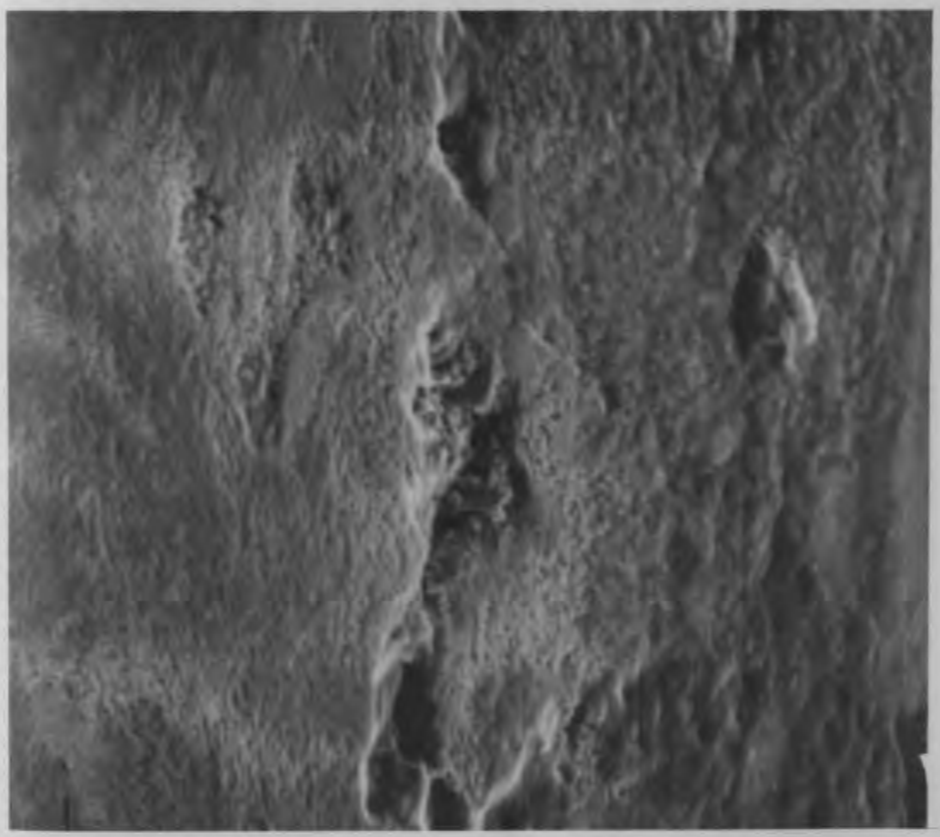

SCANNING ELECTRON MICROGRAPH OF WORN SURFACE

LOAD 490 N

SPEED 0.965 m/s

WITH AIR

ROTATING SPECIMEN

× 3500

PHOTOGRAPH 9.41

SCANNING ELECTRON MICROGRAPH OF WORN SURFACE

LOAD 490 N

SPEED 0.965 m/s

WITH AIR

ROTATING SPECIMEN

× 350

PHOTOGRAPH 9.42

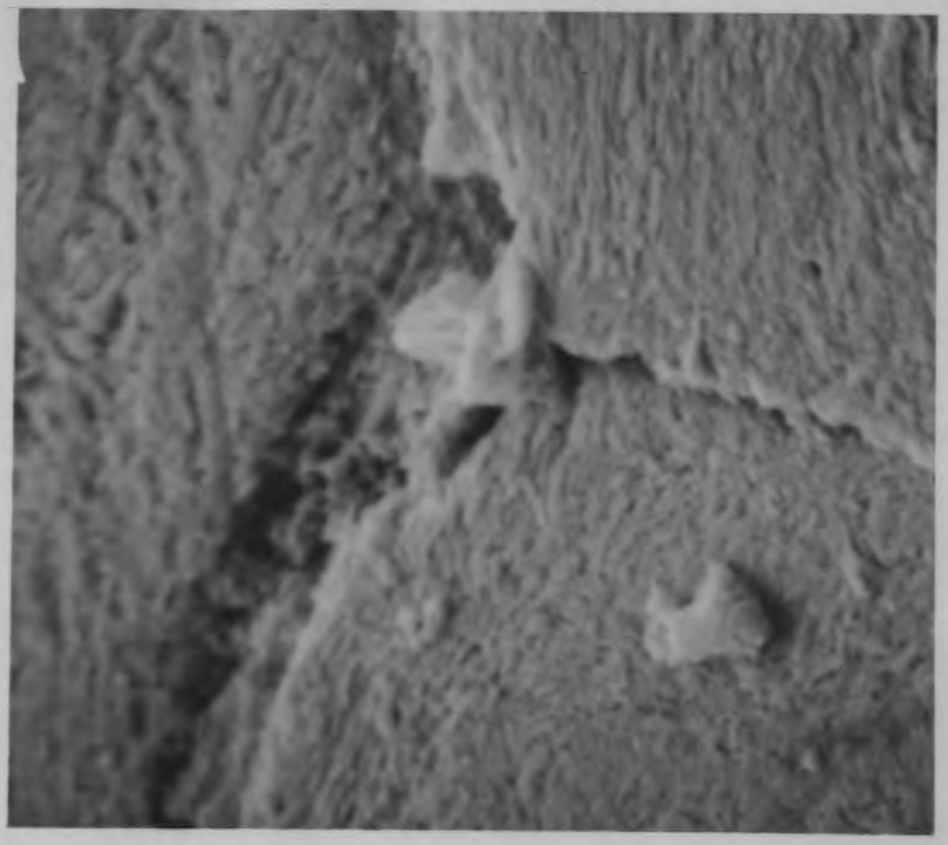

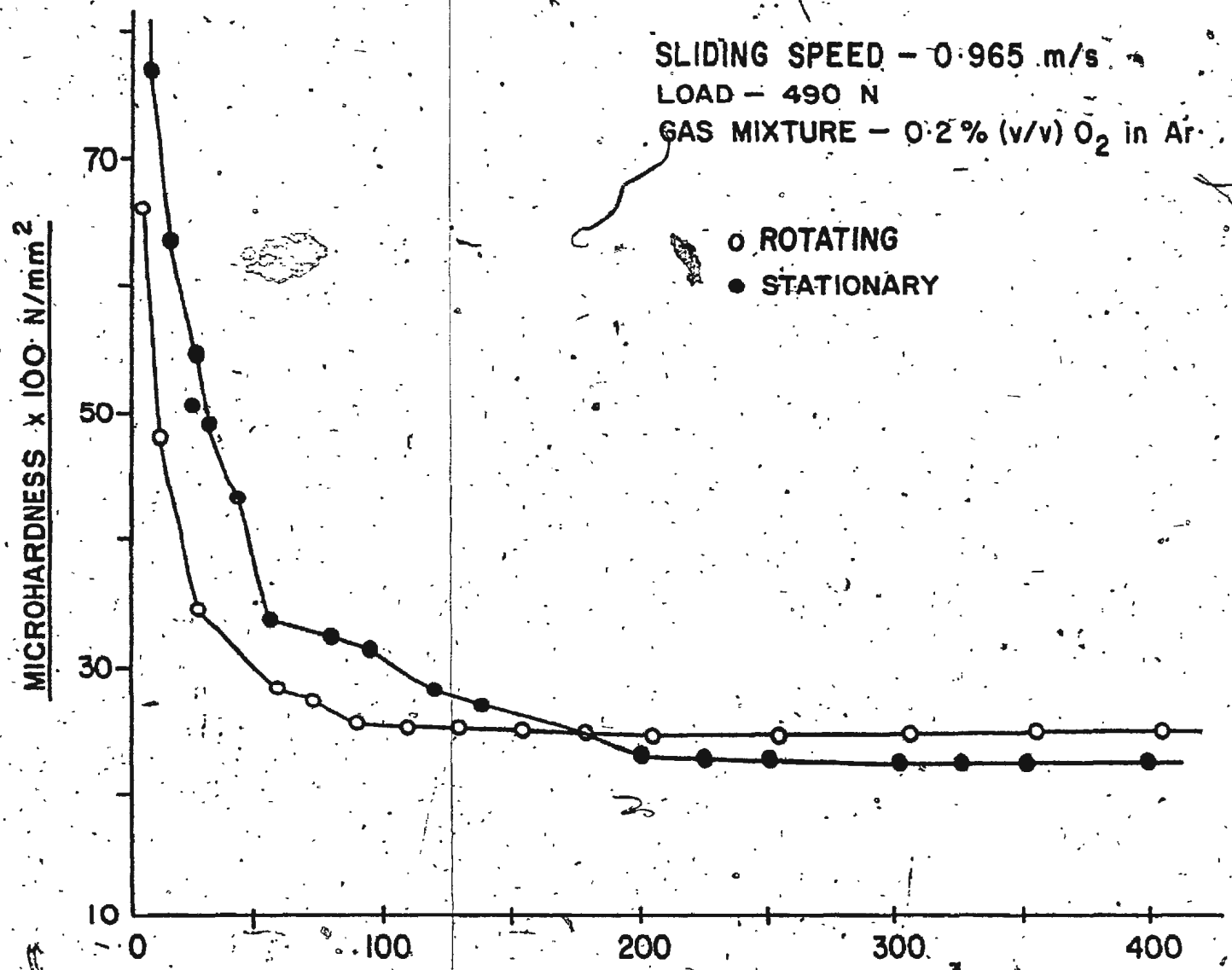

FIG·9·43

MICROHARDNESS PLOT

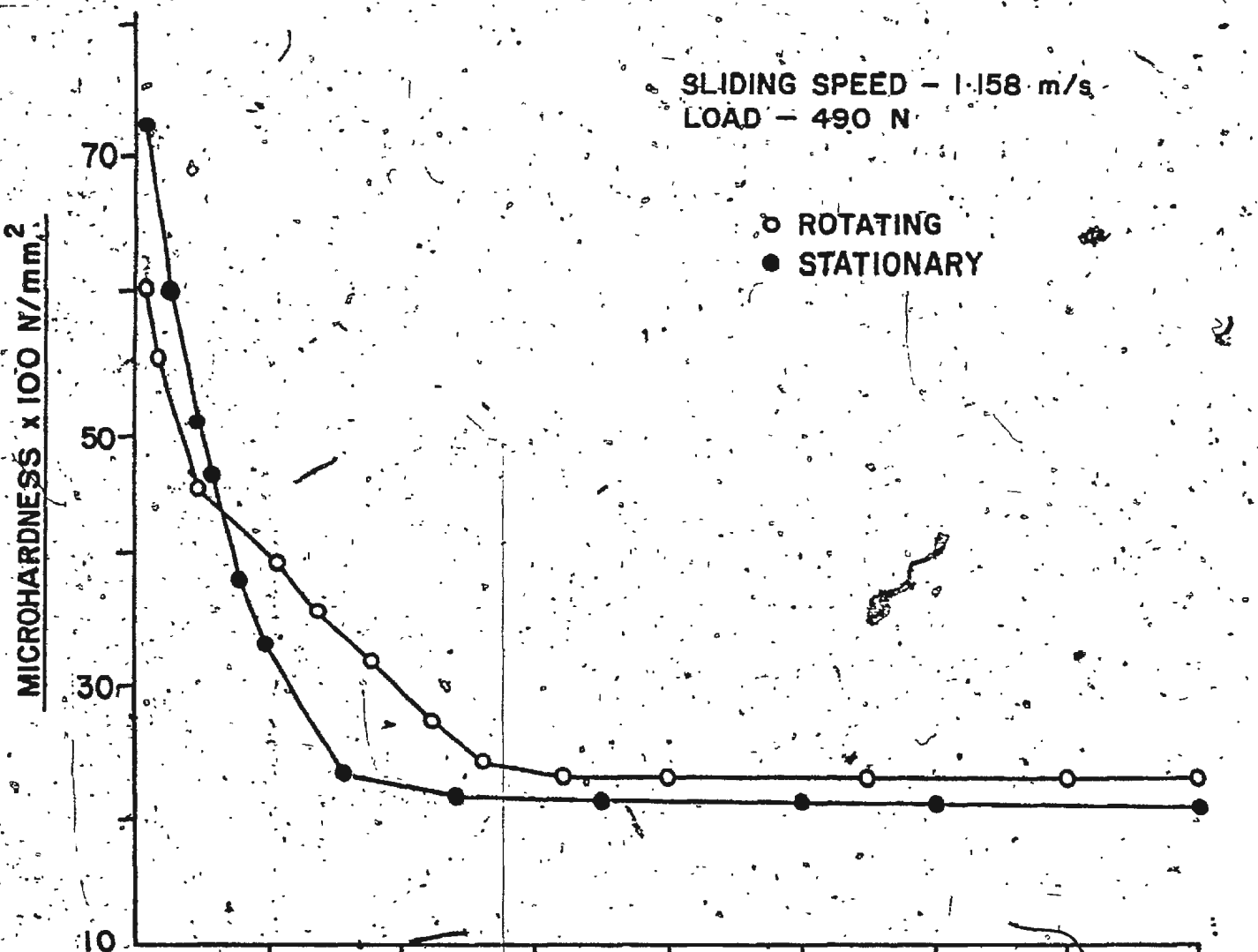

FIG· 9·44

MICROHARDNESS PLOT

A hard surface layer has been noted before, some times seen as a 'white layer', (eg. Welsh (1965), Eyre (1971)). In these tests the surface layer did not etch white, but is obviously hard. The structure of this layer has not been investigated any further in the work reported here.

CHAPTER 10

DISCUSSION OF RESULTS

10.1 General

The results of experiments performed at a nominal load of 490N to study the effect of the sliding speed, indicated that with an increase in the sliding speed the wear rate decreases until wustite, FeO, appears in the wear debris particles. Once the wustite appears the wear rate jumps to a higher value but any further increase in the sliding speed causes the wear rate to decrease again.

For the experiments where FeO just appears it can be assumed that the source temperature, i.e. the temperature of the locations at which FeO is produced, has reached 570°C. The findings that at a sliding speed of 0.965 m/s no wustite was noticed while at 1.158 m/s wustite was always present, and the wear rate showed an abrupt increase, indicated the need for a thorough investigation in the speed range of 0.965 m/s and 1.158 m/s. Indeed, the transition was noticed at the sliding speed of 1.061 m/s. Out of the six experiments performed at this speed, three showed the presence of wustite in the wear debris particles.

The speed range of 0.965 m/s to 1.158 m/s was, therefore, selected for further investigations. The appearance of FeO at a certain speed led to the postulation of a heat flow model which could be calibrated by the fact that FeO appears at 570°C.

10.1.1. Heat Source Model

The heat produced at an asperity contact, flows into the two rubbing specimens increasing the mean surface and the ambient temperatures of specimens.

An electrical analogy for heat flow is given in Fig 10.1. θ_S is the 'SOURCE' temperature. By this is meant the temperature on an envelop, enclosing what may be regarded as the source of heat and FeO. The significance of this will be apparent below, when θ_S is taken to be the temperature of formation of FeO, for the experiments in which FeO just appears. It is realised, as discussed later, that the effective oxidation may take place some little distance from the actual points of contact.

θ_A is the ambient temperature. The ambient temperature is taken to be the temperature of the face of specimen holder, as indicated by specimen holder thermocouples (placed there to control the specimen holder heaters but indicated this temperature, whether the heaters were on or not). R_S is the resistance experienced by frictional heat as it spreads from the sources over the general surface of the specimens.

θ_B is the mean surface temperature, defined as what would be the temperature of the surface, if the heat were generated uniformly over the whole surface, instead of at the contact points within the heat 'sources'. R_B is the resistance between the specimen surface and the location where θ_A is recorded.

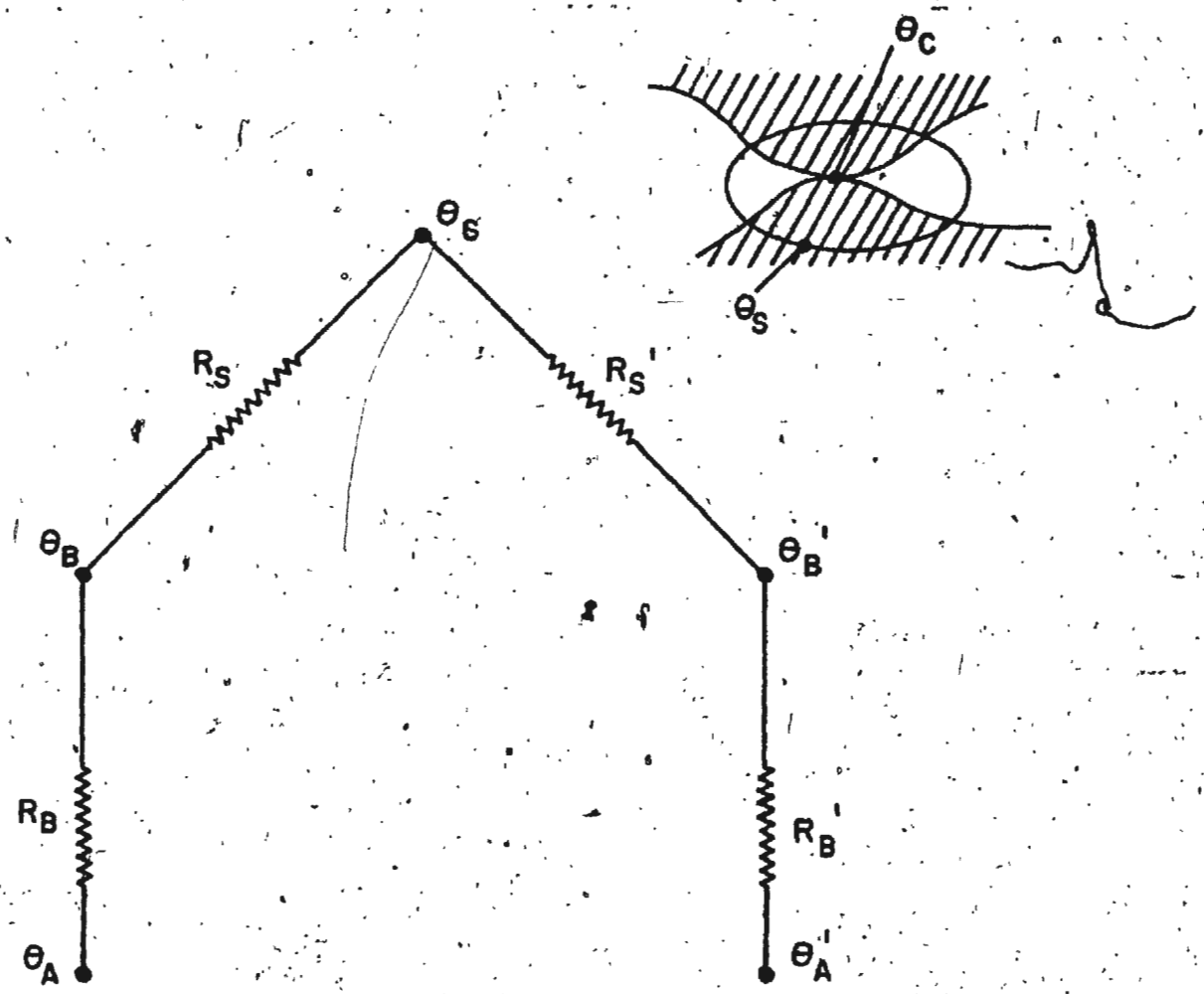

FIG. 10.1
HEAT FLOW MODEL

Θ_B, Θ_A, R_S and R_B refer to the rotating specimen while Θ_B', Θ_A', R_S' and R_B' refer to the stationary specimen.

The ratio of the resistances are given by

$$\frac{R_S}{R_B} = \frac{\Theta_S - \Theta_B}{\Theta_B - \Theta_A} \qquad 10.1$$

and $$\frac{R_S'}{R_B'} = \frac{\Theta_S - \Theta_B}{\Theta_B' - \Theta_A'} \qquad 10.2$$

For the experiments where FeO just appears (indicating $\Theta_S = 570^\circ$) values of (R_S/R_B) and (R_S'/R_B') can be calculated from the experimental values of Θ_B, Θ_A, Θ_B' and Θ_A'.

The ratio of resistances can then be used to estimate Θ_S, for experiments which are almost similar to the experiment for which Θ_S is assumed.

An example of this estimation is given below.

For experiments with the sliding speed of 0.965 m/s and mean normal load of 490 N, the mean surface temperature of the rotating specimen (Θ_B) was estimated as 250°C and temperature behind the specimens, in the specimen holder block (Θ_A) was 100°C. When the speed was increased to 1.158 m/s, keeping all the other variables the same as for the 0.965 m/s experiment, FeO appeared, indicating Θ_S ($= 570^\circ$C). The estimated surface temperature (Θ_B) was 300°C and Θ_A (measured at the same location as in 0.965 m/s experiment) was 130°C.

It seemed that it might be possible to produce FeO at 0.965 m/s, either by raising Θ_A by 30°C to make it the same as at 1.158 m/s or by raising Θ_A by 50°C to make Θ_B the same as at 1.158 m/s, or by raising

θ_A sufficiently to make θ_S the same as in the experiment at 1.158 m/s, this third alternative being the important temperature according to this model.

For the experiments at 1.158 m/s,

$$\frac{R_S}{R_B} = \frac{570 - 300}{300 - 130} = 1.59$$

By using this value of (R_S/R_B) for the 0.965 m/s experiment

$$\frac{R_S}{R_B} = \frac{\theta_S - 250}{250 - 100} = 1.59$$

or $\theta_S = 488^{\circ}C$

which shows that for θ_S to be 570°C, the source temperature has to be increased at least by 90°C. Experiments were designed where the specimen holder temperature (i.e. θ_A) was increased. Details of these experiments are described earlier in Section 8.3.

For an increase of 50°C, no FeO appeared. It was found that when the temperature was increased by 100°C (to bring θ_A to 200°C) FeO appeared, confirming the heat source model.

10.1.2. General Surface Oxidation versus Hot Spot Oxidation:

When FeO was noticed at the sliding speed of 1.061 m/s the mean surface temperature of the rotating specimen was in the range of 315 to 315°C (DWTE 69, 70 & 71) while the mean temperature of the stationary specimen surface temperature was between 325 to 330°C. These temperatures are far below 570°C, the significant temperature for the formation of FeO. Even for the experiments at higher sliding speeds, where FeO was present in the wear debris particles, the mean surface

temperature never exceeded 340°C.

The theory that "The total bulk temperature is representative of effective surface temperature controlling the wear mechanism" does not seem to be true for the observations made in the present series of experiments.

If, on the other hand, it is assumed that the temperature expected to occur at the contacting asperities is the significant temperature for the formation of FeO, the appearance of FeO, at a sliding speed of 1.158 m/s irrespective of load (295N, 490N, or 980N) is difficult to explain. For a load of 980N, FeO appeared at 1.158 m/s and did not appear at lower speeds (see Fig 9.5). If the temperatures of the hot spots are, in fact, 570°C, it will be reasonable to believe that when the load is decreased to 295N the hot spots for the same speed 1.158 m/s^{-1} must be at a temperature lower than 570°C. However, FeO was present at this speed and load.

It appears likely that the wear rate is governed by oxidation of an area a little larger than the hot spots and not by hot spots or the general surface itself. The pertinent source area could then vary with the applied load producing a constant proportion of FeO in relation to the total wear debris. The area in question could, in fact, be on the metal oxide interface, which is the most plausible location for the formation of FeO in a multilayer oxide. To substantiate this statement, a wear model has been proposed and discussed in section 10.1.9, in addition to the arguments put forth in the preceding paragraphs.

10.1.3. Wear rate of the rubbing specimens and the accessibility of gas:

The effect of forcing air between the surfaces, shown in Figs 9.3(a) and 9.3(b) is interpreted as follows. At low speeds metallic adhesion seemed to predominate and it appears that the presence of loose debris when there is no air flow, reduces this severe wear mechanism. On the other hand, at high speeds, oxidation is a major element in the wear process and the oxide debris may be quite abrasive. The presence of loose debris would, therefore, increase the wear rate.

The removal of loose debris, soon after its formation must reduce any abrasion or other effects of the debris and simplify the interpretation of the wear process.

Whatever the role of the loose debris, its effects must depend on the length of time such debris remains trapped between the rubbing surfaces and, therefore, very much dependent on the equipment concerned, in particular, on the size of the rubbing surfaces. Quick removal of the debris is clearly an advantage in a study in which it is desired to study as few variables as possible at any time.

The propensity for debris to be air borne, so that as much as 70% of all debris produced can escape collection on a tray below test objects indicates that some doubt must be thrown upon any quantitative analysis of the debris composition, in which it has not been verified that the debris analysed is representative of all the debris produced. This means that almost all the debris produced must be collected even if the debris is air borne.

In Fig 9.3(a), changes in slopes of sliding speed versus wear volume per unit distance plot were observed at sliding speeds of 0.772 m/s and 1.158 m/s. The wear debris particles were identified as mostly α-Fe and α-Fe_2O_3 upto a speed of 0.386 m/s. Traces of Fe_3O_4 were found at 0.386 m/s, however the intensity of diffraction lines were fairly weak (never exceeding 10% of the maximum intensity (100%) observed for α Fe). For 0.772 m/s, Fe_3O_4 was present in the wear debris particles. When speed was increased from 0.772 m/s to 1.061 m/s, the colour of the wear debris particles changed from dark brown to almost black. However, the wear debris particles were identified as α-Fe, α-Fe_2O_3 and Fe_3O_4 for all these runs. At a speed of 1.158 m/s, where the second change in the slope is noticed, FeO was found in the wear debris particles.

It seemed logical to assume that the oxidation of the wearing surfaces is affecting these changes in slope of the plots of sliding speed versus wear rate (expressed as wear volume per unit distance). Since oxidation is a function of time, rather than sliding distance the wear rate value, expressed as wear mass per unit time is plotted against the sliding speed as shown in Fig 9.3(b).

Upto a sliding speed of 0.772 m/s (see Fig 9.3(b)) with an increase in the sliding speed, a decrease in the wear rate and coefficient of friction (Table 9.4) was noted. However, the total heat generated at the wearing surfaces, which is proportional to the product of the coefficient of friction (f) and the sliding speed (V_s), at a given load, showed an increase. The extrapolated surface temperatures

(ref Table 9.5) increased with the increase in sliding speed which was as expected, since the total heat produced at the wearing surface had increased.

At 0.772 m/s, Fe_3O_4 appeared at the surface. Fe_3O_4 has a spinel structure and a lower shear strength than $\alpha \cdot Fe_2O_3$ which has an orthorombic structure, making Fe_3O_4 more plastic than $\alpha \cdot Fe_2O_3$. For this reason, the hardness of Fe_3O_4 is 645 kg/mm^2 against 1145 kg/mm^2 of $\alpha \cdot Fe_2O_3$. Once Fe_3O_4 has formed on the surface it acts to some extent like a lubricant while $\alpha \cdot Fe_2O_3$, which is the predominant oxide at the lower speeds, acts like an abrasive.

The low values of the coefficient of friction at 0.772 m/s can be attributed to the lubricating properties of Fe_3O_4. The increase in the extrapolated surface temperature is in line with increase in the product of coefficient of friction (f) and sliding velocity (V_s), ($f \times V_s$), the quantity proportional to the toal heat generated at a given load.

In fully oxidative wear, the wear rate must equal the oxidation rate. With a parabolic oxidation law it is possible in standard oxidation experiments to have two similar slopes for oxidation taking place at two different temperatures if the thickness of the oxide film corresponding to the oxidation at a higher temperature is greater than the thickness of the film corresponding to a lower temperature (ref. Fig 10.2). The growth and removal of oxides from wearing surfaces for the wear tests is a different situation from oxidation experiments. Nevertheless, a comparsion of the topography of the wear surfaces produced at speeds of 1.061 m/s and 0.772 m/s does show that for worn surfaces obtained at a

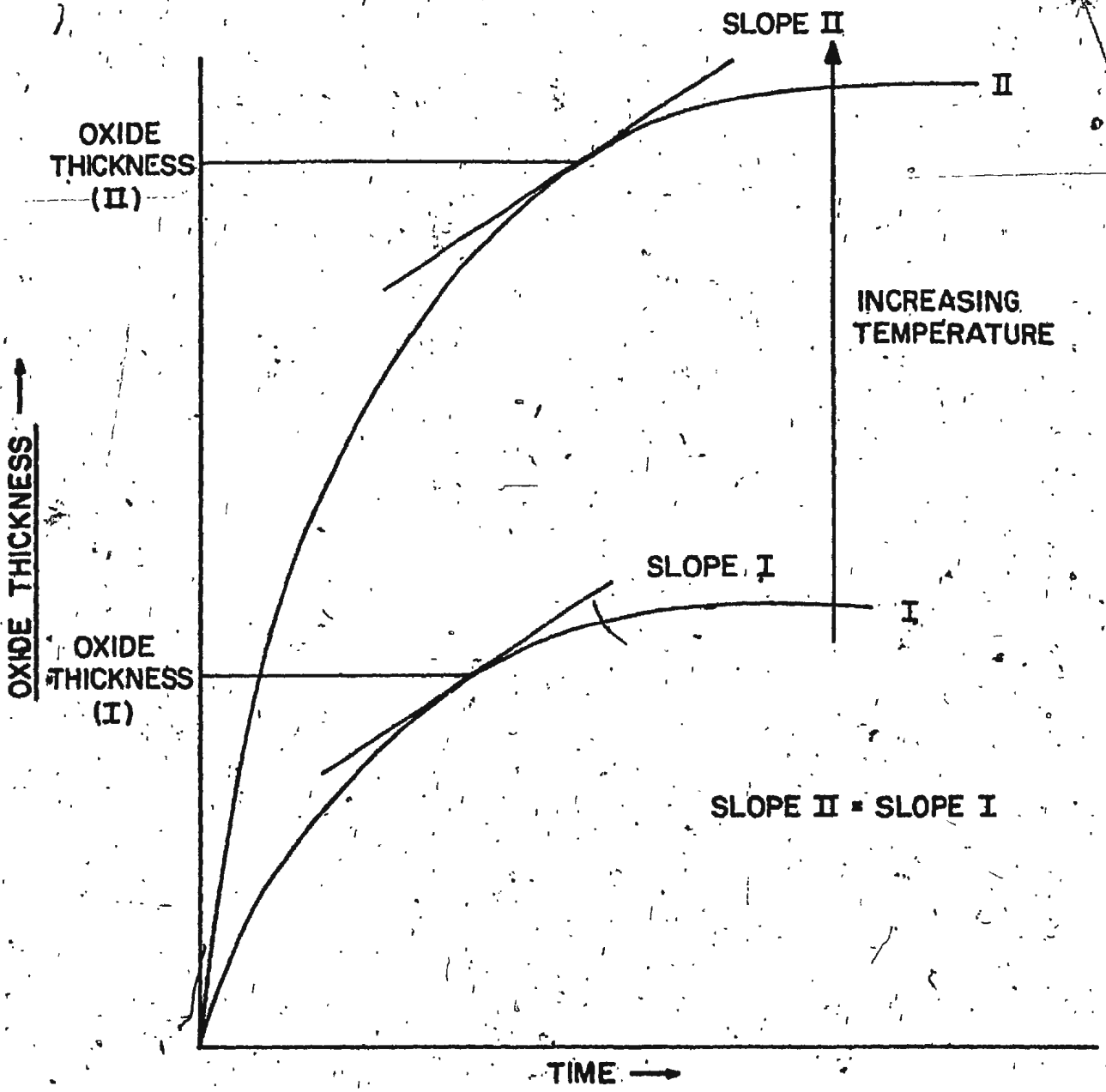

FIG. 10.2

PLOT OF OXIDE THICKNESS AGAINST TIME FOR OXIDATION (FOLLOWING A PARABOLIC OXIDATION LAW)

speed of 1.061 m/s there were thicker oxides, and a relatively larger area was covered by oxides.

The increased thickness of oxide layers at high temperatures (e.g. at 1.061 m/s) could very well correspond to oxidation rates similar to those occurring with the relatively thin oxide layers at lower temperatures (e.g. at 0.965 m/s and 0.772 m/s).

The observation of the change in colour of the wear debris particles from dark brown at a speed of 0.772 m/s to almost black at a speed of 1.061 m/s can be interpretted as increasing proportion of Fe_3O_4 in the total debris particles collected.

When the sliding speed was increased to 1.158 m/s from 1.061 m/s there was an abrupt increase in the coefficient of friction (see Table 9.4) and the extrapolated surface temperature (see Table 9.5) and FeO appeared in the wear debris particles (see Table 9.6). The explanation for this sudden rise in the coefficient of friction is attributed to friction between identical oxides. With an increase in the sliding speed from 0.772 m/s to 1.158 m/s, the proportion of Fe_3O_4 on the wear surfaces will increase until both the surfaces are almost fully covered with Fe_3O_4. The observation of a change in colour of the wear debris particles in an evidence in favour of this argument. The identical oxide layers, will then be rubbing against each other giving rise to adhesion and hence a high coefficient of friction, which in turn will result in high heat generated at the surface.

The product of the coefficient of friction (f) and the sliding speed (V_s), the function proportional to the heat generated at a given load, increased by almost 25% at 1.158 m/s from the corresponding value for 1.061 m/s experiment. This increase in the total heat produced, could have caused the temperatures of certain areas to rise above 570°C and hence FeO was noticed in the wear debris particles.

Out of the three stable oxides of iron, FeO, Fe_3O_4 and α-Fe_2O_3, FeO is the most plastic oxide. It has a cubic structure and its hardness of 540 kg/mm^2 is the least of the hardness of the three oxides. When the sliding speed was increased to 1.544 m/s from 1.158 m/s, a layer of FeO, thicker than the layer produced at 1.158 m/s could have been produced. Caplan and Cohen (1966) observed that for oxidation of iron (abraded with 8 μm size diamond powder) the thickness of FeO film increased from about 2 μm to 38 μm when the temperature was raised from 580°C to 650°C.

Even though the extrapolated surface temperature of the specimens, at this speed, does not indicate any significant change, the product of the coefficient of friction (f) and the sliding speed (V_s), ($f \times V_s$), the function proportional to heat produced at the surface at a given load, has increased by about 25% from the 1.158 m/s value. In photograph , the thin layer of the oxide, completely smeared on the surface and almost a wear track free surface, can be seen.

Thus the highly plastic oxide, FeO, present at the surface at the sliding speed of 1.544 m/s could be affecting the reduced wear rate at this speed.

The product of the coefficient of friction (f) and the sliding speed (V_s), the function proportional to the heat generated at a given load, increased by almost 25% at 1.158 m/s from the corresponding value for 1.061 m/s experiment. This increase in the total heat produced, could have caused the temperatures of certain areas to rise above 570°C and hence FeO was noticed in the wear debris particles.

Out of the three stable oxides of iron, FeO, Fe_3O_4 and αFe_2O_3, FeO is the most plastic oxide. It has a cubic structure and its hardness of 540 kg/mm^2 is the least of the hardness of the three oxides. When the sliding speed was increased to 1.544 m/s from 1.158 m/s, a layer of FeO, thicker than the layer produced at 1.158 m/s could have been produced. Caplan and Cohen (1966) observed that for oxidation of iron (abraded with 8 μm size diamond powder) the thickness of FeO film increased from about 2 μm to 38 μm when the temperature was raised from 580°C to 650°C.

Even though the extrapolated surface temperature of the specimens, at this speed, does not indicate any significant change, the product of the coefficient of friction (f) and the sliding speed (V_s), ($f \times V_s$), the function proportional to heat produced at the surface at a given load, has increased by about 25% from the 1.158 m/s value. In photograph , the thin layer of the oxide, completely smeared on the surface and almost a wear track free surface, can be seen.

Thus the highly plastic oxide, FeO, present at the surface at the sliding speed of 1.544 m/s could be affecting the reduced wear rate at this speed.

10.1.4. Effect of the gas mixture:

Changing oxygen/argon gas ratios in the forced gas flow does hold some promise as a tool for elucidation of the role of gaseous environment upon wear processes.

The effect of oxygen partial pressure upon oxidation rate, determined in the traditional oxidation experiments, depends some what on the temperature. The results of Fig 9.6 and 9.7 are believed to relate to temperatures in the range of 450 to 650°C.

The interpretation of data, such as that in Figs 9.6, 9.7 and Tables C-29 and C-30, depends on the model adopted for the wear process, which undoubtedly involves a number of interrelated mechanism. For the present discussion it will suffice to indicate that the observations on the effect of the oxygen content of the environment on the wear rate as shown in Figs 9.6 and 9.7 and Tables C-29 and C-30 are reasonable and potentially useful. With a reduction in the oxygen content from 20% down to 2% there was no significant change in the wear rate value. However, below 2% to 0.02% it appears that the oxygen content controls the wear rate value. The relationship between the oxygen content and wear rate indicates that the oxidation of the surfaces is a linear function of time, as this is usually the case when oxidation rates depend upon oxygen pressure.

Pfeiffer and Laubmeyer (1955) in their studies of oxidation of iron at various partial pressures of oxygen and at 1000°C observed that for a partial pressure of oxygen greater than 10 torr (i.e. 1.4%) there was no effect of the partial pressure of oxygen on the oxidation

rate. Below 10 torr, the oxidation of the surfaces followed the linear rate equation and the linear rate constant (k_l) was related to the partial pressure of oxygen by the equation

$$k_l = \text{constant} \quad P_{O2}^{0.70}$$

where K_l: linear rate constant

& PO_2: partial pressure of oxygen

Rahmel & Engell (1959) in their study of oxidation of pure iron in Ar-O_2 mixtures at temperatures of 700°C, 800°C and 950°C observed that the partial pressure of oxygen does not affect the oxidation rate for PO_2 values of 1%, 1.1% and 2% at temperatures of 700°C, 800°C and 950°C respectively.

As mentioned earlier, the results of Figs 9.6 and 9.7 are believed to relate to temperature in the range of 450 to 650°C. There is not enough data in the available literature on this static oxidation experiments performed to study the effect of the partial pressure of oxygen in this temperature zone. However, the results seem to coincide with the findings of Pfeiffer & Laubmeyer (1955) and Rahmel & Engell (1959), even though the temperature ranges in the oxidation experiments are different.

10.1.5. The difference in the mean surface temperature of the two rubbing specimens and its influence on the wear rate of each specimen:

The extrapolated surface temperature of the stationary specimen was always higher than that of the rotating specimen. However, this difference never exceeded 35°C. Another interesting observation was that the wear rate of the stationary specimen was always lower than

the wear rate of the rotating specimens. The reduced wear rate of the stationary specimen could be attributed to a harder surface layer about 75 μm thick in the stationary specimen. Both rotating and the stationary specimen were covered with this hard layer (see Figs 9.43 and 9.44) but in the first transition zone, the stationary specimen was always harder than the rotating specimen.

A hard surface layer has been noticed before sometimes seen as a 'white layer' (e.g. Welsh(1965), Eyre(1971)). In these tests the surface layer did not etch white, but is obviously hard.

To correlate the higher temperature of the stationary specimen surface with the increased hardness and reduced wear, more work is needed. However, the trend of lower wear rates at higher temperature are noticeable in all the graphs where a reduction in wear rate is noticed with increase in the sliding speed.

10.1.6. Calculation of the Activation Energy

In the speed range of 0.772 m/s to 1.061 m/s where oxidation is clearly well established, (ref. Fig 9.3(b)), wear rate is constant with temperature going up. Between 1.158 m/s and 1.544 m/s, the wear rate drops while temperature stays constant or increases slightly.

This is contrary to results of usual oxidation experiment. Several wear researchers have equated wear rate to oxidation rate and have derived activation energy. Equating wear rate to oxidation rate in these two ranges will give negative activation energies whereas standard oxidation experiments give positive values of activation energy in the order of 20-40 kCal/mole.

Only in the interval between 1.061 m/s and 1.158 m/s is there a rise in wear rate with an increase in temperature. The virtue of choosing 1.061 m/s and 1.158 m/s for a calculation of activation energy is that we are dealing with two speeds which are practically the same and all other conditions are similar and it is implicit in the analysis that the thickness of oxide layer is the same in both due to similar mechanical circumstances.

For the experiments with air forced through the specimens and a constant load of 490 N, for a sliding speed of 1.061 m/s no FeO was noticed; however, FeO was noticed at a speed of 1.158 m/s.

Using the model described in the previous section, the source temperature (θ_s), at the speed of 1.061 m/s, was estimated as 525°C.

By using Quinn's model for the parabolic oxidation (Equation 3.4) and inserting wear rates, sliding speeds and calculated source temperatures for the speeds of 1.061 m/s and 1.158 m/s, an activation energy was calculated.

Three values of θ_s, for experiments at 1.158 m/s were tried, 550°C, 570°C and 600°C (as per oxidation theory FeO appears at 570°C but there may be some uncertainty under these conditions).

The values of activation energy corresponding to these temperatures are given below.

Assumed source temperature for 1.158 m/s experiment (°C)	Activation Energy (K Cal/mole)
550	23
570	32
600	60

The value of the activation energy for oxidation of Fe has been found as 24 K Cal/mode in the temperature range of 450°C-580°C and 31 K Cal/mode in the temperature range of 580°C-650°C by Kaplan(1966).

10.1.7. Particle Size

The wear debris particles were analysed to see if there was any significance. It was thought that there might be a correlation between the mean particle size and the oxide formed at the rubbing surface. However, no such correlation was found.

The mean size of the particles was of the order of 1 μm. Using Rabinowicz Particle Size Equation (Rabinowicz, 1965) the average particle size for Fe_2O_3 particles was estimated as 2 μm. Rabinowicz in his dry wear experiments found the average size as 1 μm for the wear debris particles which were predominantly Fe_2O_3.

10.1.8. Comparision of these wear results with the results of some other workers

Most of the experiments by Earles were performed at high sliding speeds (5 m/s - 150 m/s) and low loads (2.2 N - 176 N). Also in his work Earles has used the function ($(LOAD)^{1/2}$. VELOCITY) to correlate with various parameters. It is hardly possible to compare the present work with Earles since greater emphasis, in the present work, was on varying speed rather than load.

In the experiment by Welsh (1965) the range of the load applied was from 0.1 N to 400 N and the speed was varied from 0,002 m/s to 2.66 m/s. Mostly variation of load was studied. It would appear that most of my work used loads and speeds above Welsh's T_2 transition loads

for which wear rates were 1×10^{-11} m^3/m of sliding for a load of 400 N and a speed of 1 m/s for SAE1078 steel and 0.8×10^{-11} m^3/m of sliding for a load of 400 N and a speed of 2 m/s for SAE1078 steel. This wear rate is of the same order as the wear rates observed here.

In the experiments by Grosberg and Molgaard (1967) a similar variation of wear rate, with the black oxide debris formed on the surface, was noticed. Rubbing speeds were generally higher than 2 m/s with wear rate in the range of 1 to 1.5×10^{-13} m^3/m of sliding for a load of 3 N, but the specimen sizes used were an order lower.

All these experiments were with Pin on Disc or Ring tests and, therefore, asymmetrical.

10.1.9. Possible Wear Model

Most of the effort, in the present investigation, was channeled into developing the test equipment. The data obtained from these experiments are not enough to make it possible yet a definite picture of the wear process over a wide range of conditions.

The appearance of the wear specimens, in particular, suggest that oxidation and the transfer of oxide is important, together with some abrasion in the speed range 0.77 - 1.344 m/s.

The appearance of FeO indicated that the significant temperature was between 550 and 600°C (oxidation theory indicates 570°C) at the speed of 0.965 m/s and a load of 490 N, which was clearly above the mean surface temperature.

A simple application of Archard's treatment to calculate the theoretical hot spot temperature, assuming only one hot spot, gives a temperature of 2675°C, ignoring any oxide layers which would make the contact temperature even higher on the surface of the oxide.

For a larger number of points of contact, lower hot spot temperatures were obtained using Grosberg and Molgaard's treatment (1966).

Assumed Number of Contacts	Estimated Hot Spot Temperature (°C)
10	1290
100	570
500	300

However, it seems unreasonable that oxygen has access to the contacting points during contact. Also, it's unreasonable to assume that oxidation takes place at the outer surface of an oxide.

Oxidation is a diffusion controlled process, therefore, diffusion at the oxide-metal interface is likely to be rate controlling, as this is the cooler side of an oxide layer during sliding. Also, the diffusion of iron is thought to be the rate controlling mechanism in the formation of FeO and Fe_3O_4.

A simple picture would seem to be, that an oxide layer forms, parts of it may be transferred and perhaps retransferred between the specimens, increasing the layer thickness locally. Further oxidation may occur 'below' these transferred layers, ie. by diffusion of iron ions through the layers and the effective temperature of oxidation is

that of an extended region below the points of contact. Wear occurs both by abrasion of the surface and by local detachment of parts of the oxide layer, probably previously transferred portions.

More work is needed to substantiate this picture and to verify the possible interpretations of the results of Figs 9.3(a), 9.3(b), 9.6 and 9.7, discussed in sections 10.1.3. and 10.1.4. Additional information on the thickness of the oxide film, morphology of the oxide and the proportional analysis of all the constituents in the wear debris particles is needed to support the most plausible picture of the wear process.

CHAPTER 11

DISCUSSION OF THE WEAR TEST MACHINE & SUGGESTIONS FOR FURTHER WORK

11.1. Performance of the Wear-Test Machine

With the exception of design criteria set forth for vibration, all other design criteria described in Chapter 4 were met.

Vibration was reduced during development of the equipment by increasing the stiffness of the system on the stationary side. However at the bearings in the lathe head stock, higher vibration was recorded than on the stationary specimen mounting. Also, vibration of the crossbeam, because of a heavy mass, affects the overall vibration of the machine during wear tests.

The record of a widely fluctuating force of reaction between the rubbing objects causes some concern. This is an apparatus dependent effect. The stiffer the suspension, the less the amplitude of vibration will be, but on the other hand the greater the normal reaction fluctuations will be. From the point of view of interpreting wear studies, the force fluctuations represent a complication, a departure from an ideal steady normal force.

It is preferable to have as stiff a test equipment as is feasible, with both vibration and the normal reaction recorded, as was attempted in this work. It then becomes necessary to include the force fluctuations and vibration, along with oxidation and other aspects, in the interpretation of wear studies.

A wear tester has been developed which controls the environment as close as it is possible to get to the rubbing surface. The apparatus also incorporates some control over test surface temperatures. In addition, vibration generated in the equipment is recorded.

The various parts of the equipment are not novel. Nevertheless, as a unit, this represents an approach to the most appropriate technique for a general study of oxidative wear under conditions which come close to practical circumstances of sliding metal surfaces in machinery, yet allow for evaluation of role of several parameters affecting oxidative wear.

11.2. Suggestions for Further Work

As mentioned in a previous section, more work is needed to provide a definite picture of the wear process over a wide range of conditions.

The following suggestions are made for further work to provide answers to some of the questions posed by this work.

The surface layers on both the stationary and the rotating specimen need to be analysed - quantitatively and reliable measurements made of the thickness of the oxide layers. The proportion of the different oxides, either embedded in the surface or smeared on the surface, seem to influence the wear rate. This can only be determined by much more detailed analysis of the transferred layer on the surface.

The effect of changing the stiffness of the system, by providing variable damping, need to be studies. Vibration in the machine at high loads and speeds is still a constraint, limiting the performance of the machine.

On the instrumentation side, there is a need for recording continuous flow rate of the air or gas mixture flowing through the specimen interface, in order to get a quantitive estimate of the effect of flow rate on wear.

CHAPTER 12

CONCLUSIONS

The objectives set forth for the work have been achieved in general terms.

It appears likely that wear rate is governed by oxidation of an area at a little distance from the hot spot and not by the hot spot or general surface itself. The area in question could, in fact, be on the metal-oxide interface. (Section 10.1.2)

A correlation has been found between the sliding speed, which in turn affects the surface temperature, with the wear rate. The appearance of FeO is associated with a jump in the wear rate. The surface topography is shown to be a function of speed. (Section 10.1.3)

In an atmosphere of an inert gas, wear is of a severe type. When different mixtures of oxygen and argon gas are forced through the specimen, a significant change in the wear rate is observed which is similar to observations in static oxidation tests. (Section 10.1.4)

The wear rate of the specimens is affected by forcing air through the specimens. At low sliding speeds the wear rate is increased, while at high sliding speeds it decreases. Air provides a surface free of loose oxide debris at lower speeds and hence the sliding surfaces more readily come into direct contact protected inadequately by very thin oxide layers. However, at higher speeds the removal of oxide debris particles lessens the abrasive action of the debris. Contact is then between thick

oxides which remain intact for longer periods. (Section 10.1.3)

The difference in mean temperature of the two rubbing specimens influences the wear rate. The specimen at higher temperature shows lower wear rate, except where the higher temperature is such that FeO is likely to be produced, while the lower temperature is below this value. (Section 10.1.5)

REFERENCES

Report 1 (1969); "Lubrication of the Antifriction Bearings", Naval Engineering Test Establishment, Lasalle, Quebec, No. 16/69.

Report 2 (1969); "Corrosion Problems in Antifriction Bearings", Naval Engineering Test Establishment, Lasalle, Quebec, No. 32/69.

Report 3 (1970); "The Antifriction Bearing Investigation", Naval Engineering Test Establishment, Lasalle, Quebec, No. 14/70.

Archard, J.F. (1953); "Contact and Rubbing of Flat Surfaces", J. Appl. Phys., V.24, p.981.

Archard, J.F. (1959); "Temperature of Rubbing Surfaces Wear", V.2, p.438.

Archard, J.F. (1968); "Wear" in P.M. Ku(ed), Interdisciplinary Approach to Friction and Wear, NASA SP-181, p.267.

Archard, J.F. and W. Hirst (1957); "An Examination of Mild Wear Process", Proc. Roy. Soc., A, V.238, p.515.

Barber, J.R. (1967); "Distribution of Heat between Sliding Surfaces", J.I. Mech.Engrg.Sc. V.9, p.16.

Caplan, D & M. Cohen (1966); "Effect of Cold Work on the Oxidation of Iron from 400 - 650°C.", Corrosion Science, Vol. 6 p.321.

Caplan, D., G.I. Sproute & R.J. Hussey (1970);	"Comparison of Kinetics of high temperature oxidation of Fe as Influenced by Metal Purity & Cold Work", Corrosion Science, Vol. 10, p.9.
Clark, W.T.; C. Prichard and J.M. Midgley (1968);	"Mild Wear of Unlubricated Hard Steels in Air and Carbon-Dioxide", Proc. Instn. Mech. Engrs., V.182, pt.3N, p.97.
Cocks, M. (1957);	"Role of Atmospheric Oxidation in High Speed Sliding Phenomena", J. Appl. Phy., V.28, P.835.
Dautzenberg, J.H. and Zaat, J.H. (1973);	"Quantitative Determination of Deformation by Sliding Wear", Wear, V.23, p.9.
deGee, A.W.G. (1967);	"Material Pruefung", Materiaux, U.9, n.6, p.166.
Earles, S.W.E., M.G. Hayler and D.G. Powell (1970);	"A comparison of Surface Temperature Theories and Experimental Results for High Speed Dry Sliding", ASME/ASLE Lubrication Conference, Cincinnati, Ohio.
Earles, S.W.E. and M.J. Kadhim (1967);	"Unlubricated Sliding at High Speeds between Copper and Steel Surfaces, Proc. Instn. Mech. Engrs., V.181, pt. 30 p.25.
Earles, S.W.E. and D.G. Powell (1967-a);	"Variation in Friction and Wear between Unlubricated Steel Surfaces", Proc. Instn. Mech. Engrs., V.18, pt.30, p.16.
Earles, S.W.E. and D.G. Powell (1967-b);	"Wear of Unlubricated Steel Surfaces in Sliding Contact", ASME/ASLE Lubrication Conference, Chicago, Illinois.
Earles, S.W.E. and D.G. Powell (1968);	"Stability of Self Generated Oxide Films on Unlubricated En 1A steel Surfaces", Proc. Inst. Mech. Engrs., Tribology Convention, paper 20.

Earles, S.W.E. and N. Tenwick (1971);	"A simplified Theory for the Oxidative Wear of Steels", Wear, V.18, p.381.
Eyre, T.S. and D. Maynaard (1971);	"Surface Aspects of Unlubricated Metal-to-Metal Wear", Wear, V.18, p.301.
Fink, M. and U. Hoffman (1932);	"Zur Theorie der Reiboxydation", Archiv. f. d. Eisenhilt tenwese, V.6, N.4, p.161.
Finkin, E.F. (1964);	"The Wear of Copper, Aluminum, Mild Steel and Zinc and their Wear Particle Shape Factors", A.S.L.E. Trans., V.7, p.377.
Jaeger, J.C. (1942);	"Moving Sources of Heat and Temperature at Sliding Contacts", Proc. Roy. Soc. NSW, V.76, p.203.
Johnson, R.L., M. Swickert and E. Bisson (1957);	"Friction, Wear and Surface Damage of Metals as affected by Solid Surface Films" - A Review of N.A.S.A. Research Proc. Conf. on Lub. and Wear, paper 31, p.384.
Kerridge, M. (1955);	"Metal Transfer and the Wear Process", Proc. Phy. Soc., B 68, p.400.
Kerridge, M. and J.K. Lancaster (1957);	"The Stages in Process of Severe Wear", Proc. Roy. Soc. A, V.236, p.250.
Kubachewski, O. and B.E. Hopkins (1962);	"Oxidation of Metals and Alloys", Butterworth.
Lancaster, J.K. (1957);	"The Influence of Temperature on Metallic Wear", Proc. Phy. Soc., B, V.70, p.112.
Molgaard, J.M. and P. Grosberg (1967);	"Aspects of Wear of Spinning Travellers: The Division of Heat at the Rubbing Surfaces", Proc. Instn. Mech. Engrs., V.181, pt.3-L, p.16.

Nault, A.J. Lander and Edgar (1954); "The Effect of Surface Temperatures on the Wear of Diesel Engine Cylinders and Rings", S.A.E., paper 340.

Neale, M.J. (1971); "Piston Ring Scuffing - A Broad Survey of Problems and Practice", Tribology group Chairman's Address - Instn. Mech. Engrs. V.185, p.2/71.

Pfeiffer Von H. & C. Laubmeyer (1955); "Uber die Sauerstoff-druckabhanglgKeit der Eisenoxydation bei 1000°C. und das problem des Materietransports in Eisenoxyd", Zeitschrift fur Electrochemie, Bd59, Nr6.

Rahmel Von A. & Hans - Jurgen Engell (1959); Ueber den EinfluB des Sauerstoffdrucko auf die Oxydationsgeschwindigkeit Von Reinem Eisen, Archiv fur das Eisenhuttenwesen.

Palmer, P.B. (1970); "Medium and High Speed Diesel Engines in Fishing Vessels", Canadian Fisheries Report No. 15, Proc. Conf. on Automation & Mechanisation in Fishing Industry.

Quinn, T.F.J. (1962); "Role of Oxidation in the Mild Wear of Steel", J. Appl. Phy., V.13, p.33.

Quinn, T.F.J. (1968); "Dry Wear of Steel as revealed by Electron Microscopy & X-Ray Diffraction", Proc. Instn. Mech. Engrs., V.182, pt.3N p.201.

Quinn, T.F.J. (1969); "An Experimental Study of the Thermal Aspects of Sliding Contracts and their Relation to the Unlubricated Wear of Steel", Proc. Instn. Mech. Engrs., V.183, pt.3P, p.129.

Quinn, T.F.J. (1971); "Oxidational Wear", Wear, V.18, p.413.

Rowe, C.N. (1968); "Wear", in P.M. Ku (ed), Interdisciplinary Approach to Friction and Wear, NASA SP-181, p.308.

Sreenath, A.V. and S. Venkatesh (1970); "Experimental Studies of Wear of Engine Components", Wear, V.16,p.245.

Suh, N.P. (1973); "The Delamination Theory of Wear", Wear V.25, p.111.

Suh, N.P. S. Jahanmir and P. Abrahamson (1974); "Microscopic Observation of the Wear Sheet Formation by Delamination", Wear, V.28, p.235.

Welsh, N.C. (1965); "The Dry Wear of Steels", Phil-Trans. Roy. Soc., V.257, A, N.1077, p.31.

Yoshimoto, G and T. Tsukizoe (1958); "On the Mechanism of Wear between Metal Surfaces", Wear, V.1, p.472.

APPENDICES

APPENDIX A

Extrapolation of Mean Surface Temperature From the Recorded Body Temperatures

For Rotating Specimen

For simplicity of calculations the rubbing surface is assumed perpendicular to the longitudinal axis of the specimen.

In figs. A-1 and A-2, actual and simplified geometry of the rotating specimen surface are shown.

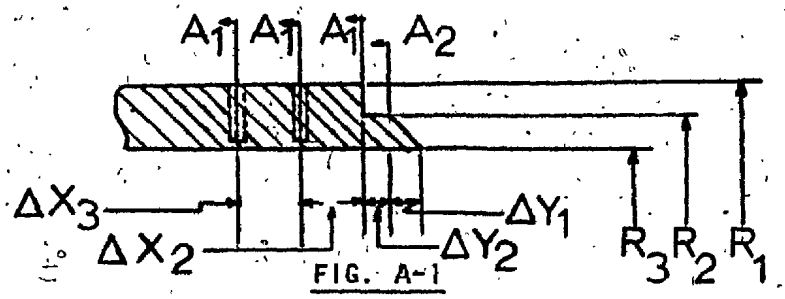

FIG. A-1

ACTUAL GEOMETRY OF THE SPECIMEN

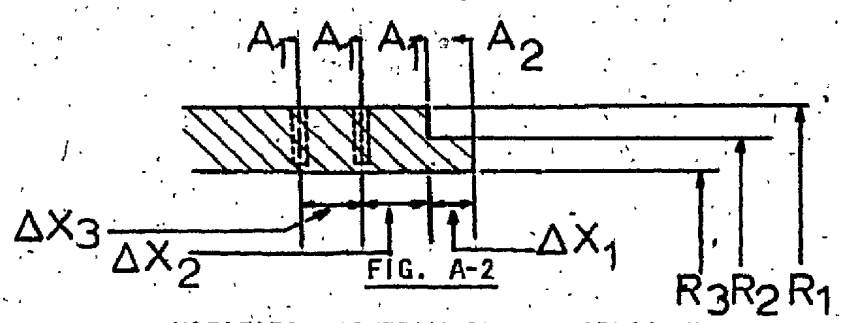

FIG. A-2

MODIFIED GEOMETRY OF THE SPECIMEN

$$\Delta X_1 = \Delta Y_2 + \frac{1}{2}\Delta Y_1$$

A.2

R_1, R_2 & R_3 are the radii of the outermost surface of the specimen, the outside surface of wear face and the inside surface of the wear face. A_1 & A_2 are areas normal to the axis of the specimen at radii R_1 and R_2 respectively, as shown in Figs. A-1 and A-2.

An equivalent analogy for heat flow is given in Fig. A-3.

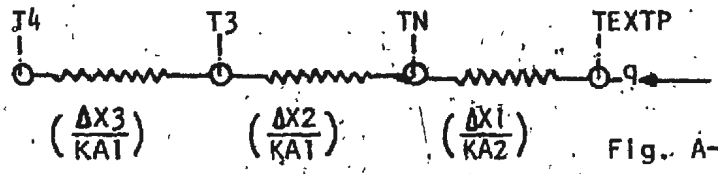

Fig. A-3

where q is heat flowing into the specimen, K is the thermal conductivity of the material of test specimens, T3 and T4 are the temperatures recorded by the thermocouples. TN is the temperature at step in the specimen & T EXTP is the surface temperature, which is to be extrapolated.

An estimation of heat lost by specimen surface over the distance $(\Delta X_1 + \Delta X_2 + \Delta X_3)$ indicated that a maximum of 3% of heat could be lost. Since, the loss of heat would be a function of sliding speed, normal load and gas through the rubbing specimens, it was assumed that in steady state the heat lost by specimen over this distance (maximum 3% of total produced) is small and could be neglected.

The heat flowing through the specimen (q) is given by:

$$q = \frac{TEXTP-TN}{(\frac{\Delta X1}{KA2})} = \frac{TN-T3}{(\frac{\Delta X2}{KA1})} = \frac{T3-T4}{(\frac{\Delta X3}{KA1})} \quad \ldots\ldots\ldots \text{(Eq}^{n}\text{ A-1)}$$

A.3

From Equation (A-1):

$$\frac{TN-T3}{(\frac{\Delta X2}{KA1})} = \frac{T3-T4}{(\frac{\Delta X3}{KA1})}$$

or, $$TN = T3 + \frac{\Delta X2}{\Delta X3}(T3-T4) \qquad (Eq^n\ A-2)$$

also $$\frac{TEXTP-TN}{(\frac{\Delta X1}{KA2})} = \frac{T3-T4}{(\frac{\Delta X3}{KA1})}$$

or, $$TEXTP = TN + \frac{\Delta X2}{\Delta X3} \cdot \frac{A1}{A2} \cdot (T3-T4)$$

From geometry of the specimen $\frac{A1}{A2} = 2.15$

or, $$TEXTP = TN + \frac{\Delta X1}{\Delta X3} \cdot (2.15)(T3-T4)$$

$$TEXTP = T3 + \frac{1}{\Delta X3}(\Delta X2 + 2.15\Delta X1)(T3-T4) \qquad (Eq^n\ A-3)$$

For the Stationary Specimen

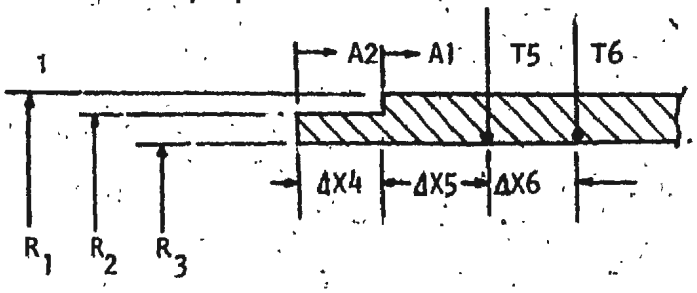

FIG. A-4

MODIFIED GEOMETRY OF STATIONARY SPECIMEN

Working along the same lines as for the rotating specimen the extrapolated surface temperature (TEXTP') for the stationary specimen

$$TEXTP' = T5 + \frac{1}{\Delta X6}(\Delta X5 + 2.15\Delta X4)(T5-T6) \qquad (Eq^n\ A-4)$$

A.4

For new specimens (i.e. specimens which were not refaced and repolished from a previous run), $\Delta X4 = \Delta X_1$, $\Delta X_5 = \Delta X_2$ and $\Delta X_6 = \Delta X_3$ and the equation (A-4) modifies to

$$TEXTP' = T5 + \frac{1}{\Delta X3} (\Delta X_2 + 2.15\, \Delta X_1)(T5-T6) \quad (Eq^n\ A\text{-}5)$$

APPENDIX B

Estimation of mean value of a parameter from the records obtained at various number of revolutions

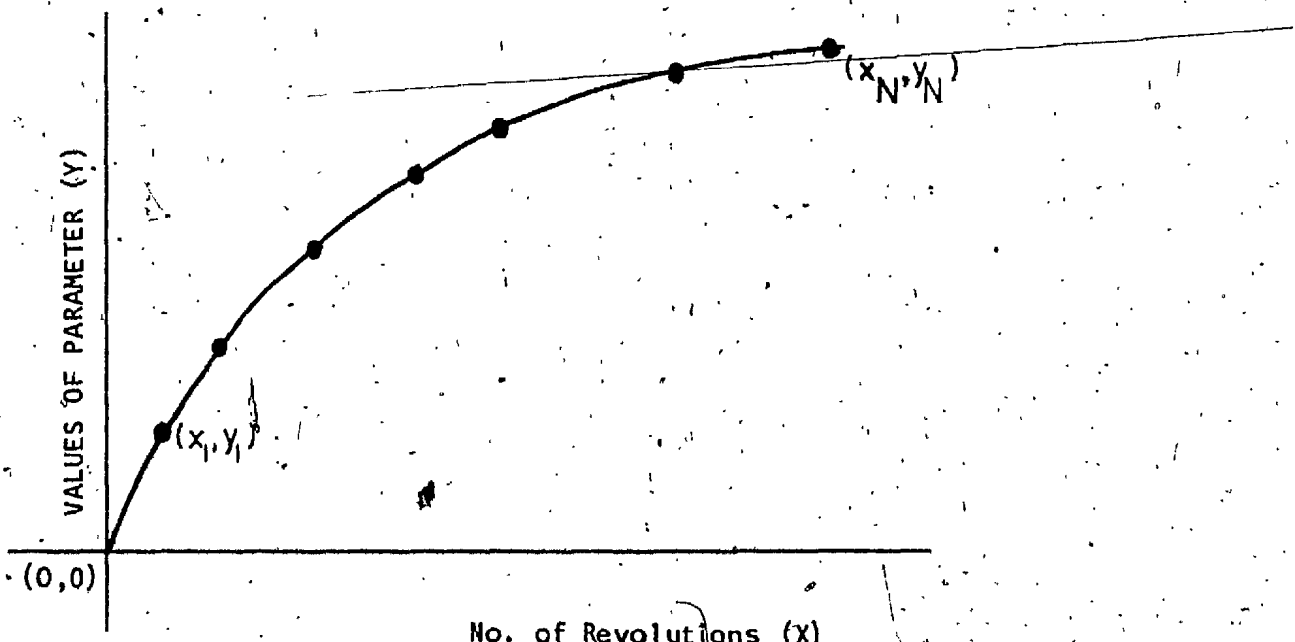

$$\text{Y Mean} = \frac{1/2 \sum_{N=1}^{N} (Y_{N-1} + Y_N) \cdot (X_N - X_{N-1})}{(X_N - X_1)}$$

Where Y Mean = Mean value of the parameter over the entire duration of the run

X_1, X_2 X_N are number of revolutions where record was made and

Y_1, Y_2, Y_N are values of the parameter at X_1, X_2, X_N revolutions

APPENDIX C

TABLES OF RESULTS

TABLE C-1

MEAN VALUES AND STANDARD DEVIATION OF WEAR RATE, COEFFICIENT OF FRICTION & EXTRAPOLATED SURFACE TEMPERATURE

UNHEATED SPECIMENS, NO AIR, NORMAL LOAD: 49ON

SPEED	WEAR RATE								COEFFICIENT OF FRICTION		EXTRAPOLATED SURFACE TEMPERATURE			
	VOLUME/UNIT DISTANCE			MASS/UNIT TIME			S.D/MEAN				ROTATING SIDE		STATIONARY SIDE	
	ROTATING SPECIMEN	STATIONARY SPECIMEN	TOTAL WEAR	ROTATING SPECIMEN	STATIONARY SPECIMEN	TOTAL WEAR	ROTATING SPECIMEN	STATIONARY SPECIMEN	MEAN	S.D.	MEAN	S.D.	MEAN	S.D.
ms^{-1}	$(X10^{-11} m^3/m$ of sliding)			$(X10^{-6}$ kg/min)			%	%			^oC		^oC	^oC
0.193	8.20	6.35	14.55	7.4	5.8	13.2	3.3	3.3	0.55	0.02	105	6	120	7
0.386	3.15	2.95	6.10	5.7	5.4	11.1	4.9	6.0	0.51	0.01	150	6	160	6
0.772	1.45	1.00	2.45	5.3	3.7	9.0	11.0	11.4	0.44	0.01	225	4	240	8
0.965	1.30	0.90	2.20	5.9	4.0	9.9	3.3	4.3	0.46	0.01	250	4	265	0
1.061	1.25	0.89	2.14	6.2	4.5	10.7	6.5	6.0	0.45	0.01	240	4	260	3
1.061	1.95	1.65	3.60	9.7	8.2	17.9	4.2	2.2	0.62	0.01	320	4	330	4
1.158	1.65	1.35	3.00	8.9	7.3	16.2	11.1	5.5	0.65	0.01	300	8	330	4
1.544	0.77	0.60	1.37	5.6	4.4	10.0	28.3	7.5	0.58	0.00	310		335	4

TABLE C-2

EFFECT OF SLIDING SPEED ON WEAR RATE, COEFFICIENT OF FRICTION & EXTRAPOLATED SURFACE TEMPERATURE

UNHEATED SPECIMENS, NO AIR, NORMAL LOAD: 490N

SLIDING SPEED	TEST NO.	WEAR RATE						COEFFICIENT OF FRICTION	EXTRAPOLATED SURFACE TEMPERATURE	
		WEAR VOLUME PER UNIT DISTANCE			WEAR MASS PER UNIT TIME					
		ROTATING SPECIMEN	STATIONARY SPECIMEN	TOTAL WEAR	ROTATING SPECIMEN	STATIONARY SPECIMEN	TOTAL WEAR		ROTATING SPECIMEN	STATIONARY SPECIMEN
ms^{-1}		($X10^{-11}$ M^3/M OF SLIDING)			($X10^{-6}$ Kg/min)				^0C	
0.193	22	8.70	6.65	15.35	7.9	6.0	13.9	0.57	110	130
	23	8.15	6.37	14.52	7.4	5.8	13.2	0.53	105	115
	24	8.05	6.30	14.35	7.3	5.7	13.0	-	100	120
	25	7.90	6.00	13.90	7.2	5.4	12.6	0.55	95	110
	41	8.20	6.43	14.63	7.4	5.8	13.2	0.55	110	125
0.386	27	3.15	2.90	6.05	5.7	5.3	11.0	0.51	155	160
	28	3.25	2.85	6.10	5.9	5.2	11.1	0.51	155	165
	29	2.90	2.80	5.70	5.3	5.1	10.4	0.52	140	150
	40	3.30	3.25	6.55	6.0	5.9	11.9	0.50	150	165
0.772	30	1.30	0.82	2.12	4.8	3.0	7.8	-	220	235
	31	1.64	1.01	2.65	6.0	3.7	9.7	0.45	230	240
	32	1.34	0.97	2.31	4.9	3.6	8.5	0.44	225	230
	33	1.39	1.05	2.44	5.1	3.9	9.0	0.44	-	245
	34	1.33	0.95	2.28	4.9	3.5	8.4	0.42	220	225
	42	1.70	1.20	2.90	6.2	4.4	10.6	0.46	230	245

TABLE C-2 (cont'd)

EFFECT OF SLIDING SPEED ON WEAR RATE, COEFFICIENT OF FRICTION & EXTRAPOLATED SURFACE TEMPERATURE

UNHEATED SPECIMENS, NO AIR, NORMAL LOAD: 490N

SLIDING SPEED	TEST NO.	WEAR RATE						COEFFICIENT OF FRICTION	EXTRAPOLATED SURFACE TEMPERATURE	
		WEAR VOLUME PER UNIT DISTANCE			WEAR MASS PER UNIT TIME					
		ROTATING SPECIMEN	STATIONARY SPECIMEN	TOTAL WEAR	ROTATING SPECIMEN	STATIONARY SPECIMEN	TOTAL WEAR		ROTATING SPECIMEN	STATIONARY SPECIMEN
ms^{-1}		($\times 10^{-11}$ m^3/m OF SLIDING)			($\times 10^{-6}$ Kg/min)				^0C	
0.965	63	1.34	0.94	2.28	6.1	4.2	10.3	0.46	255	265
	64	1.32	0.92	2.24	6.0	4.1	10.1	0.45	250	265
	65	1.24	0.84	2.08	5.6	3.8	9.4	0.45	245	265
1.061	68	1.15	0.82	1.97	5.7	4.1	9.8	0.44	240	260
	69	1.85	1.62	3.47	9.2	8.0	17.2	0.61	315	325
	70	1.95	1.63	3.58	9.7	8.1	17.8	0.62	320	330
	71	2.05	1.70	3.75	10.2	8.4	16.6	0.63	325	335
	72	1.35	0.95	2.30	6.7	4.7	11.4	0.46	245	265
	73	1.25	0.90	2.15	6.2	4.5	10.7	0.45	235	260
1.158	35	1.62	1.36	2.96	8.7	7.3	16.0	0.64	300	-
	36	1.46	1.24	2.70	7.9	6.7	14.5	0.64	295	330
	37	1.57	1.35	2.92	8.5	7.3	15.8	0.65	-	325
	43	1.95	1.45	3.40	10.5	7.9	18.4	0.66	305	335
1.544	44	1.01	0.64	1.65	7.4	4.7	12.1	0.58	320	340
	45	0.80	0.65	1.45	5.8	4.7	10.5	0.59	315	330
	46	0.63	0.55	1.18	4.6	4.0	8.6	0.58	305	335
	47	0.64	0.56	1.20	4.7	4.1	8.8	0.58	300	335

TABLE C-3

EFFECT OF SLIDING SPEED ON COMPOSITION AND SIZE OF WEAR DEBRIS PARTICLES

UNHEATED SPECIMENS, NO AIR, NORMAL LOAD: 490N

SLIDING SPEED ms^{-1}	TEST NO.	COMPOSITION OF WEAR DEBRIS PARTICLES				SIZE OF 80% OF WEAR DEBRIS PARTICLES			
						COLLECTED UNDER THE SPECIMEN		COLLECTED ON FILTER PAPER	
		Fe	FeO	Fe_3O_4	Fe_2O_3	MEDIAN	STANDARD DEVIATION	MEDIAN	STANDARD DEVIATION
						μm		μm	
0.193	22	✓			✓				
	23	✓			✓				
	24	✓			✓				
	25	✓			✓				
	41	✓			✓	2.0	6.0	1.5	5.0
0.386	27	✓			✓	1.5	5.0	1.0	2.5
	28	✓		T	✓				
	29	✓		T	✓				
	40	✓			✓	1.5	4.0	1.0	3.5
0.772	30	✓		✓	✓				
	31	✓		✓	✓				
	32	✓		✓	✓				
	33	✓		✓	✓	1.0	3.5	1.0	3.0
	34	✓		✓	✓				
	42	✓		✓	✓				
0.965	63	✓		✓	✓				
	64	✓		✓	✓			1.0	2.0
	65	✓		✓	✓	1.5	3.5	0.75	2.04
1.061	68	✓		✓	✓				
	69	✓	✓	✓	✓	2.0	6.0	1.5	6.0
	70	✓	✓	✓	✓				
	71	✓	✓	✓	✓				
	72	✓	✓	✓	✓				
	73	✓		✓	✓	2.0	6.0	1.5	4.0
1.158	35	✓	✓	✓	✓				
	36	✓	✓	✓	✓				
	37	✓	✓	✓	✓				
	43	✓	✓	✓	✓	2.0	4.0	1.0	3.0
1.544	44	✓	✓	✓	✓				
	45	✓	✓	✓	✓	0.75	2.5	0.75	2.5
	46	✓	✓	✓	✓				
	47	✓	✓	✓	✓				

TABLE C4

LINEAR DISPLACEMENT (AMPLITUDE) AT LOWEST FREQUENCIES OF VIBRATION & INTEGRATED POWER SPECTRAL DENSITY

LOAD 490N, NO AIR, UNHEATED SPECIMENS, VARIOUS SLIDING SPEEDS

SLIDING SPEED MS^{-1}	TEST NO.	FREQ. OF VIBRATION (HZ)	LINEAR DISPLACEMENT (AMPLITUDE) IN μm FOR ACCELEROMETERAT						PSD $\sum_{20}^{3000} g^2/HZ$	
			A	B	B'	a	b	b'		
0.193	22	270	158*	280*	250*	-	39*	-	A = 3.9	
		480	-	-	-	47*	30	84*	B = 4.4	
		540-560	25	39	15	-	-	-	B' = 4.8	
		800-850	5	8	10	1	-	-	a = 0.7	
		950-1050	3	10	5		4	4	b' = 0.65	
		1250-1350	2	8	-	5	4	3		
	41	240	-	-	-	42*	-	-		
		290-300	159*	126*	-	-	-	134*		
		440-480	38	54	-	30	53*	68		
		550-600	9	27	-	-	-	5		
		700-750	4	5	-	5	-	-		
		950	-	-	-	-	9	-		
0.386	40	290-300	120*	239*		28	21*	89*	A = 3.1	
		400	24	49		-	-	-	B = 4.0	
		450-500	56	53		33*	16	73	a = 0.65	
		670-750	14	20		-	-	7	b' = 0.64	
		800-850	15	13		11	17	-	b = 0.50	
		950-1000	10	15		9	11	-		
	32	230-280	-	118*	80*	-	-	132*	A = 2.50	
		300	-	-	68	-	-		B = 3.55	
		440-450	92*	60	60	30*	-	38	B' = 2.40	
		520--50	33	-	-	17	-	47	a = 0.60	
		670-700	-	24	40	9	-	12	b' = 0.64	
		950-1100	-	15	-	7	-	6		
0.772	34	260-300	34	120*	47*	-	-	27	A = 2.60	
		440-480	-	60	38	30	22*	30*	B = 3.45	
		520	47*	-	-	-	-	-	B' = 2.40	
		670-750	-	28	4	-	10	-	a - 0.64	
		800-950	6	17	-	4	-	11	b' = 0.60	
		1000-1200	5	12	-	-	3	4		

TABLE C-4

LINEAR DISPLACEMENT (AMPLITUDE) AT LOWEST FREQUENCIES OF VIBRATION & INTEGRATED POWER SPECTRAL DENSITY.

LOAD 490N, NO AIR, UNHEATED SPECIMENS, VARIOUS SLIDING SPEEDS

SPEED ms^{-1}	TEST NO.	FREQ. OF VIBRATION (HZ)	LINEAR DISPLACEMENT (AMPLITUDE) IN μm FOR ACCELEROMETERAT						PSD $\sum_{20}^{3000} g^2/HZ$	
			A	B	B'	a	b	b'		
0.965	64	210	-	205*		-	-	84*		
		280-300	112*	-		24	34*	-		
		400	39	49		-	22	-		
		480-520	59	75		33*	15	37		
		670-750	18	19		-	9	10		
		950-1300	6	13		5	4	-		
	65	280-290	149*	141*						
		380	-	47						
		475-500	76	56						
		650-680	38	16						
		900-1000	12	11						
		1300	9	-						
1.061	68	270-290	45*	265*		47*	30*	125*		
		480	-	75		47*	26	59		
		650-750	22	30		13	34	13		
		900-950	23	-		15	16	5		
		1050	-	13		-	-	-		
		1200-1300	-	-		7	-	6		
	69	270-280	158*	125*		50*	-	119*		
		440-480	96	85		33	21*	33		
		650-670	-	15		-	10	9		
		850-950	16	10		10	6	9		
		1000-1100	12	10		7	4	-		
		1500	-	4		3	3	6		
	70	280-300	112*	96*		28	30*	94*		
		400	39	49		-	17	-		
		480	47	94		33*	24	42		
		670-700	13	12		6	11	10		
		850-950	-	-		-	6	4		
		1200-1300	7	6		-	-	-		
	73	270-300	178*	119*		30	30*	111*		
		360-400	-	-		16	24	-		
		480-520	66	59		47*	29	33		
		750-800	19	20		8	13	24		
		1000-1050	14	28		11	10	-		
		1300	-	9		6	-	-		

* Highest amplitude at the particular location

TABLE C4

LINEAR DISPLACEMENT (AMPLITUDE) AT LOWEST FREQUENCIES OF VIBRATION & INTEGRATED POWER SPECTRAL DENSITY

LOAD 490N, NO AIR, UNHEATED SPECIMENS, VARIOUS SLIDING SPEEDS

SLIDING SPEED MS^{-1}	TEST NO.	FREQ. OF VIBRATION (HZ)	LINEAR DISPLACEMENT (AMPLITUDE) INμm FOR ACCELEROMETERAT A	B	B'	a	b	b'	PSD 3000_{20} g^2/HZ	
	42	320-340	44*	28	-	-	-	24*		
		480	-	53*	-	-	-	-		
		560	42	-	-	21*	17*	15		
		750-850	-	9	-	14	7	4		
		900	6	-	-	-	-	-		
		1200-1300	6	9	-	3	3	2		
	35	260-280	61	42	64	-	20	76*	A 2.70	
		440-450	76*	76*	76*	38*	25*	58	B -	
		600	-	20	30	-	-	-	B' 1.25	
		850-900	20	18	15	5	5	-	a 0.54	
		1200-1300	8	10	3	2	2	-	b -	
									b' 0.54	
1.158	36	235-275	-		61	-	-	69*		
		425-460	80*		96*	43*	15*	32		
		700-800	15		15	-	-	11		
		850	13		10	7	7	-		
		1250-1300	4		-	3	2	-		
	37	330-340	89*			-	-	52*		
		460	-			-	-	35		
		540-560	84			28*	12*	30		
		850-875	9			8	10	7		
		1100-1300	8			2	2	-		
	43	240-280	250*	211*		24	35	75*	A 2.90	
		400	-	55		-	-	-	B 1.45	
		480	75	94		33*	42*	53	B' -	
		670-750	15	20		-	-	7	a 0.58	
		800	-	-		4	15	-	b -	
		1000-1200	5	10		3	4	14	b' 0.58	

TABLE C4

LINEAR DISPLACEMENT (AMPLITUDE) AT LOWEST FREQUENCIES OF VIBRATION & INTEGRATED POWER SPECTRAL DENSITY

LOAD 490N, NO AIR, UNHEATED SPECIMENS, VARIOUS SLIDING SPEEDS

SLIDING SPEED MS^{-1}	TEST NO.	FREQ. OF VIBRATION (HZ)	LINEAR DISPLACEMENT (AMPLITUDE) IN μm FOR ACCELEROMETERAT						PSD 3000_{20} g^2/HZ	
			A	B	B'	a	b	b'		
1.544	44	280-320	49*	49*		17	16	44	A 3.4	
		480	42	42		30*	17*	70*	B 2.6	
		670-700	13	13		5	6	12	B' -	
		850-950	-	-		4	4	-	a 0.58	
		1050-1200	5	9		-	-	-	b -	
									b' 0.58	
	45	220	-	270*			-			
		300	76*	-			21*			
		440-520	24	24			-			
		580-660	-	13			13			
		800	12	-			8			
	46	270-300	50	56*		19	-			
		425-500	73*	44		39*	25*			
		670-700	11	21		-	-			
		1000-1100	7	10		4	-			
		1150	-	4		-	-			

TABLE C-5

MEAN VALUES AND STANDARD DEVIATION OF WEAR RATE,

COEFFICIENT OF FRICTION & EXTRAPOLATED SURFACE TEMPERATURE

HEATED SPECIMENS, NO. AIR, NORMAL LOAD: 490N

SLIDING SPEED 0.965 MS^{-1}, VARIOUS SPECIMEN HOLDER TEMPERATURES.

SPECIMEN HOLDER TEMPERATURE	WEAR RATE								COEFFICIENT OF FRICTION		EXTRAPOLATED SURFACE TEMPERATURE			
	VOLUME/UNIT DISTANCE			MASS/UNIT TIME			S.D/MEAN				ROTATING SIDE		STATIONARY SIDE	
	ROTATING SPECIMEN	STATIONARY SPECIMEN	TOTAL WEAR	ROTATING SPECIMEN	STATIONARY SPECIMEN	TOTAL WEAR	ROTATING SPECIMEN	STATIONARY SPECIMEN	MEAN	S.D.	MEAN	S.D.	MEAN	S.D.
°C	($X10^{-11}$ m^3/mofsliding)			($X10^{-6}$ kg/min)			%	%			°C		°C	
100	1.10	1.00	2.10	5.0	4.5	9.5	2.0	3.0	0.45	-	250	-	265	-
150	1.27	1.13	2.40	5.7	5.0	10.7	2.0	5.1	0.48	0.01	295	5	310	-
200	1.72	1.53	3.25	7.7	6.9	14.6	2.3	3.3	0.59	-	-	-	-	-

TABLE C-6

EFFECT OF SPECIMEN HOLDER TEMPERATURE ON WEAR RATE, COEFFICIENT OF FRICTION & EXTRAPOLATED SURFACE TEMPERATURE

HEATED SPECIMENS, NO AIR, NORMAL LOAD 490N

SLIDING SPEED 0.965 MS^{-1}

SPECIMEN HOLDER TEMPERATURE HOLDER ^{o}C	TEST NO.	WEAR RATE						COEFFICIENT OF FRICTION	EXTRAPOLATED SURFACE TEMPERATURE	
		WEAR VOLUME PER UNIT DISTANCE			WEAR MASS PER UNIT TIME					
		ROTATING SPECIMEN	STATIONARY SPECIMEN	TOTAL WEAR	ROTATING SPECIMEN	STATIONARY SPECIMEN	TOTAL WEAR		ROTATING SPECIMEN	STATIONARY SPECIMEN
		($X10^{-11}$ M^3/M OF SLIDING)			($X10^{-6}$ Kg/min)				^{o}C	
100	56	1.12	1.03	2.15	5.0	4.6	9.6	0.45	250	265
	81	1.08	0.97	2.05	4.9	4.3	9.2	0.45		
150	58	1.29	1.08	2.37	5.8	4.9	10.7	0.47	290	310
	60	1.25	1.18	2.43	5.6	5.3	10.9	0.49	300	310
200	79	1.76	1.48	3.24	7.9	6.6	14.5	0.59		
	80	1.68	1.58	3.26	7.5	7.1	14.6			

TABLE C-7

EFFECT OF SPECIMEN HOLDER TEMPERATURE ON COMPOSITION

HEATED SPECIMENS, NO AIR, NORMAL LOAD: 490N

SLIDING SPEED: $0.965 MS^{-1}$

SPECIMEN HOLDER TEMPERATURE	TEST NO.	COMPOSITION OF WEAR DEBRIS PARTICLES				SIZE OF 80% OF WEAR DEBRIS PARTICLES			
						COLLECTED UNDER THE SPECIMEN		COLLECTED ON FILTER PAPER	
		Fe	FeO	Fe_3O_4	E_2O_3	MEDIAN	STANDARD DEVIATION	MEDIAN	STANDARD DEVIATION
°C						μm		μm	
100	56	✓		✓	✓				
	81	✓		✓	✓				
150	58	✓		✓	✓				
	60	✓		✓	✓	1.5	10	2.0	12.0
200	79	✓		✓	✓				
	80	✓		✓	✓	1.5	6	2.0	10.0

TABLE C-8

MEAN VALUES AND STANDARD DEVIATION OF WEAR RATE,

COEFFICIENT OF FRICTION & EXTRAPOLATED SURFACE TEMPERATURE

UNHEATED SPECIMENS, WITH AIR, NORMAL LOAD: 490N

FLOW RATE OF AIR $75 \times 10^{-6} m^3 s^{-1}$

SPEED	WEAR RATE								COEFFICIENT OF FRICTION		EXTRAPOLATED SURFACE TEMPERATURE			
	VOLUME/UNIT DISTANCE			MASS/UNIT TIME			S.D/MEAN				ROTATING SIDE		STATIONARY SIDE	
	ROTATING SPECIMEN	STATIONARY SPECIMEN	TOTAL WEAR	ROTATING SPECIMEN	STATIONARY SPECIMEN	TOTAL WEAR	ROTATING SPECIMEN	STATIONARY SPECIMEN	MEAN	S.D.	MEAN	S.D.	MEAN	S.D.
ms^{-1}	$(\times 10^{-11} m^3/m$ of sliding)			$(\times 10^{-6}$ kg/min)			%	%			°C	°C	°C	°C
0.193	47.50	35.96	83.46	-	-	-	-	-	0.70	-	80	-	90	-
0.386	4.60	3.90	8.50	8.4	7.0	15.4	2.6	2.3	0.55	.01	115	0	125	5
0.772	0.90	0.65	1.55	3.3	2.4	5.7	14.6	12.5	0.40	.02	205	5	220	5
0.965	0.75	0.50	1.25	3.4	2.3	5.7	9.4	7.1	0.45	.02	230	0	245	0
1.061	0.64	0.51	1.15	3.2	2.5	5.7	1.1	1.1	0.45	.01	225	2	235	0
1.158	1.15	0.77	0.92	6.3	4.2	10.5	5.9	15.2	0.50	.02	275	4	285	4
1.544	0.41	0.25	0.67	3.0	1.8	4.8	-	-	0.46	-	280	-	300	-

TABLE C-9

EFFECT OF SLIDING SPEED ON WEAR RATE, COEFFICIENT OF FRICTION

& EXTRAPOLATED SURFACE TEMPERATURE

UNHEATED SPECIMENS, WITH AIR, NORMAL LOAD 490N

FLOW RATE OF AIR 75 x $10^{-6} M^3/s^{-1}$

SLIDING SPEED	TEST NO.	WEAR RATE						COEFFICIENT OF FRICTION	EXTRAPOLATED SURFACE TEMPERATURE	
		WEAR VOLUME PER UNIT DISTANCE			WEAR MASS PER UNIT TIME					
		ROTATING SPECIMEN	STATIONARY SPECIMEN	TOTAL WEAR	ROTATING SPECIMEN	STATIONARY SPECIMEN	TOTAL WEAR		ROTATING SPECIMEN	STATIONARY SPECIMEN
MS^{-1}		($X10^{-11}$ M^3/M OF SLIDING)			($X10^{-6}$ Kg/min)				^0C	
0.193	[redacted]	47.50	35.96	83.46	-	-	-	0.70	80	90
0.386	51	4.72	3.99	8.71	8.6	7.3	15.9	0.56	115	130
	52	4.48	3.81	8.29	8.2	6.9	15.1	0.54	115	120
0.772	48	1.03	0.75	1.78	3.8	2.7	6.5	0.40	-	225
	49-1	0.72	0.55	1.27	2.6	2.0	4.6	0.42	200	215
	49-2	0.95	0.65	1.60	3.5	2.4	5.9	0.38	210	220
0.965	66	0.85	0.55	1.40	3.9	2.5	6.4	0.47	-	-
	67	0.70	0.47	1.17	3.2	2.1	5.3	0.44	230	245
	74	0.70	0.48	1.18	3.2	2.1	5.3	0.44	230	245
1.061	75	0.65	0.50	1.15	3.2	2.5	5.7	0.46	225	235
	76	0.64	0.52	1.16	3.1	2.6	5.7	0.44	222	235

Continued

TABLE C-9

EFFECT OF SLIDING SPEED ON WEAR RATE, COEFFICIENT OF FRICTION

& EXTRAPOLATED SURFACE TEMPERATURE

UNHEATED SPECIMENS, WITH AIR, NORMAL LOAD 490N

FLOW RATE OF AIR $75 \times 10^{-6} M^3 S^{-1}$

SLIDING SPEED	TEST NO.	WEAR RATE						COEFFICIENT OF FRICTION	EXTRAPOLATED SURFACE TEMPERATURE	
		WEAR VOLUME PER UNIT DISTANCE			WEAR MASS PER UNIT TIME					
		ROTATING SPECIMEN	STATIONARY SPECIMEN	TOTAL WEAR	ROTATING SPECIMEN	STATIONARY SPECIMEN	TOTAL WEAR		ROTATING SPECIMEN	STATIONARY SPECIMEN
MS^{-1}		($\times 10^{-11}$ M^3/M OF SLIDING)			($\times 10^{-6}$ Kg/min)				^0C	
1.158	53	1.06	0.74	1.80	5.8	4.0	9.8	0.52	275	280
	54	1.25	0.92	2.17	6.8	5.0	11.8	0.48	270	285
	77	1.13	0.60	1.73	6.2	3.3	9.5	0.49	280	290
	78	1.16	0.82	1.98	6.3	4.5	10.8	0.51	-	285
1.544	55	0.41	0.25	0.67	3.0	1.8	4.8	0.46	280	300

TABLE G-10

EFFECT OF SLIDING SPEED ON COMPOSITION

AND SIZE OF WEAR DEBRIS PARTICLES

UNHEATED SPECIMENS, WITH AIR, NORMAL LOAD 490N

FLOW RATE OF AIR 75 x $10^{-6} M^3/S$

SLIDING SPEED	TEST NO.	COMPOSITION OF WEAR DEBRIS PARTICLES				SIZE OF 80% OF WEAR DEBRIS PARTICLES			
						COLLECTED UNDER THE SPECIMEN		COLLECTED ON FILTER PAPER	
		Fe	FeO	Fe_3O_4	Fe_2O_3	MEDIAN	STANDARD DEVIATION	MEDIAN	STANDARD DEVIATION
MS^{-1}						μm		μm	
0.193	50	✓			✓				
0.386	51	✓		T	✓	2.0	5.5	1.5	5.0
	52	✓		T	✓				
0.772	48	✓		✓	✓				
	49-1	✓		✓	✓	2.5	6.0	2.0	6.5
	49-2	✓		✓	✓				
0.965	66	✓		✓	✓	1.5	2.5	1.0	2.5
	67	✓		✓	✓				
	74	✓		✓	✓				
1.061	75	✓		✓	✓	1.5	2.5	1.0	2.0
	76	✓		✓	✓				

TABLE 10

EFFECT OF SLIDING SPEED ON COMPOSITION AND SIZE OF WEAR DEBRIS PARTICLES

UNHEATED SPECIMENS, WITH AIR, NORMAL LOAD 490N

FLOW RATE OF AIR 75 x $10^{-6} M^3 S^{-1}$

SLIDING SPEED MS^{-1}	TEST NO.	COMPOSITION OF WEAR DEBRIS PARTICLES				SIZE OF 80% OF WEAR DEBRIS PARTICLES			
						COLLECTED UNDER THE SPECIMEN		COLLECTED ON FILTER PAPER	
		Fe	FeO	Fe_3O_4	Fe_2O_3	MEDIAN	STANDARD DEVIATION	MEDIAN	STANDARD DEVIATION
						μm		μm	
1.158	53	✓	✓	✓	✓				
	54	✓	✓	✓	✓	1.5	3.5	1.0	3.0
	77	✓	✓	✓	✓	1.0	3.0	0.75	2.5
	78	✓	✓	✓	✓				
1.544	55	✓	✓	✓	✓	0.75	2.0	1.0	1.5

TABLE C II

LINEAR DISPLACEMENT (AMPLITUDE) AT LOWEST FREQUENCIES OF VIBRATION & INTEGRATED POWER SPECTRAL DENSITY

LOAD 490N, WITH AIR, UNHEATED SPECIMENS, VARIOUS SLIDING SPEEDS

SLIDING SPEED MS^{-1}	TEST NO.	FREQ. OF VIBRATION (HZ)	LINEAR DISPLACEMENT (AMPLITUDE) IN μm FOR ACCELEROMETER AT A	B	B'	a	b	b'	PSD 3000_{20} g^2/HZ	
0.386	52	300	68*	48*	19	-	87*	31*		
		480	47	42	-	-	30	-		
		520-560	-	-	53*	21*	-	19		
		650	-	17	-	-	-	-		
		850	10	16	22	7	5	13		
0.772	49-1	210	-		182*	-	-			
		310-360	67		57	-	-			
		480	83*		-	10*	37*			
		650	-		-	-	-			
		950	12		-	7	7			
		1300	8		-	8	8			
	49-2	270-290	90*	110*	195*	-	-			
		480	80	60	63	10*	27*			
		650	-	30	-	-	-			
		800-850	15	5	13	6	17			
		950-1050	9	-	1	3	7			
0.965	66	300-320	69*	53*		21	38*	85*	A = 2.1	
		400-480	49	49		-	21	37	B = 2.8	
		520-560	42	42		33*	-	-	B' - -	
		670-700	-	-		-	12	7	a = 0.4	
		750-850	8	15		-	5	5	b = 0.29	
		1000-1100	9	19		8	-	3		
	67	260-280	140*	133*		35	30*	105*	A = 2.3	
		460-480	100	84		36*	26	50	B = 3.2	
		650	27	15		9	-	7	B' - -	
		750	-	11		-	-	-	a = 0.8	
		850-950	-	10		8	-	-	b = 0.27	
									b' = 0.65	
	74	270-280	21*	118*		-	-	99*		
		480	11	66		9	9	33		
		670	-	-		-	-	10		
		800-850	10	10		11*	10*	11		
		1200-1400	-	8		-	-	2		

TABLE C11

LINEAR DISPLACEMENT (AMPLITUDE) AT LOWEST FREQUENCIES OF VIBRATION & INTEGRATED POWER SPECTRAL DENSITY

LOAD 490N, WITH AIR, UNHEATED SPECIMENS, VARIOUS SLIDING SPEEDS

SLIDING SPEED MS^{-1}	TEST NO.	FREQ. OF VIBRATION (HZ)	LINEAR DISPLACEMENT (AMPLITUDE) IN μm FOR ACCELEROMETERAT						PSD 3000_{20} g^2/HZ	
			A	B	B'	a	b	b'		
1.061	76	270-280	100*	149*		23	42*	88*		
		360	41	-		-	26	-		
		440-460	76	112		30*	32	45		
		650-670	17	14		-	7	8		
		750	10	-		-	7	-		
		850-900	-	12		-	5	4		
	53	300	76*	85*	-		-			
		480	53	42	-		-			
		600	27	-	24*		10*			
		800	-	15	-		-			
		1100-1200	7	15	3		2			
1.158	54	210	-	52		-	-		A = 2.1	
		300-320	27	85*		-	-		B = 3.2	
		560	50*	55		-	19*		B' = -	
		650	13	13		-	-		a = -	
		800	12	-		-	7		b' = .42	
		1100-1150	7	13		-	-			
	78	280	133	133		26	38	75		
		460-480	59	59		45	25	37		
		650-660	19	16		5	13	-		
		750	-	-		-	-	7		
		950	6	8		4	5	-		
		1100-1400	5	13		2	2	2		

TABLE C-12

EFFECT OF PREHEATING AIR TO 200°C ON WEAR RATE, COEFFICIENT OF FRICTION & EXTRAPOLATED SURFACE TEMPERATURE

UNHEATED SPECIMENS, VARIOUS SLIDING SPEEDS, NORMAL LOAD 490N

FLOW RATE OF PREHEATED AIR = 75×10^{-6} $M^3 S^{-1}$

SLIDING SPEED	TEST NO.	WEAR RATE						COEFFICIENT OF FRICTION	EXTRAPOLATED SURFACE TEMPERATURE	
		WEAR VOLUME PER UNIT DISTANCE			WEAR MASS PER UNIT TIME					
		ROTATING SPECIMEN	STATIONARY SPECIMEN	TOTAL WEAR	ROTATING SPECIMEN	STATIONARY SPECIMEN	TOTAL WEAR		ROTATING SPECIMEN	STATIONARY SPECIMEN
MS^{-1}		($\times 10^{-11}$ M^3/M OF SLIDING)			($\times 10^{-6}$ Kg/min)				°C	
0.386	62	2.90	2.30	5.20	5.3	4.2	9.5	-	-	137
0.772	61	1.21	0.49	1.70	4.4	1.8	6.2	-	215	235
0.965	68.2	0.65	0.45	1.10	2.9	2.0	4.9	0.46	225	235
1.158	57	1.05	0.98	2.03	5.71	5.3	11.0	0.48	-	265

TABLE C-13

EFFECT OF PREHEATING AIR TO 200°C ON COMPOSITION

AND SIZE OF WEAR DEBRIS PARTICLES

UNHEATED SPECIMENS, NORMAL LOAD: 49ON

VARIOUS SLIDING SPEEDS, FLOW RATE OF PREHEATED AIR = $75 \times 10^{-6} M^3 S^{-1}$

SLIDING SPEED MS^{-1}	TEST NO.	COMPOSITION OF WEAR DEBRIS PARTICLES				SIZE OF 80% OF WEAR DEBRIS PARTICLES			
						COLLECTED UNDER THE SPECIMEN		COLLECTED ON FILTER PAPER	
		Fe	FeO	Fe_3O_4	Fe_2O_3	MEDIAN	STANDARD DEVIATION	MEDIAN	STANDARD DEVIATION
						μm	μm	μm	μm
0.386	62	✓		✓	✓				
0.772	61	✓		✓	✓				
0.965	68-2	✓		✓	✓			1.5	6
1.158	57	✓	✓	✓	✓				

TABLE C-14

MEAN VALUES AND STANDARD DEVIATION OF WEAR RATE,

COEFFICIENT OF FRICTION & EXTRAPOLATED SURFACE TEMPERATURE

UNHEATED SPECIMENS, AIR, NORMAL LOAD: 49ON

FLOW RATE $75 \times 10^{-6} M^3/S$ DIFFERENT GAS MIXTURES SLIDING SPEED 0.965 MS^{-1}

PERCENT	WEAR RATE								COEFFICIENT OF FRICTION		EXTRAPOLATED SURFACE TEMPERATURE			
	VOLUME/UNIT DISTANCE			MASS/UNIT TIME			S.D/MEAN				ROTATING SIDE		STATIONARY SIDE	
(V/V) O_2 in Ar	ROTATING SPECIMEN	STATIONARY SPECIMEN	TOTAL WEAR	ROTATING SPECIMEN	STATIONARY SPECIMEN	TOTAL WEAR	ROTATING SPECIMEN	STATIONARY SPECIMEN	MEAN	S.D.	MEAN	S.D.	MEAN	S.D.
	($X10^{-11} m^3$/mofsliding)			($X10^{-6}$ kg/min)			%	%	—		°C	°C	°C	°C
0 (Pure Ar)	1.84	-0.37	1.47	-	-	-			1.65	0	400		-	
0.02	0.15	0.03	0.18	0.7	0.1	0.8	6.6	0	0.54	0	305	5	315	5
0.20	0.42	0.28	0.70	1.9	1.3	3.2	14.6	5.1	0.51	.01	290	5	300	0
2.00	0.95	0.55	1.50	4.3	2.5	6.8	0.9	6.5	0.48	.01	260	5	275	4
20.0 (Air)	0.75	0.50	1.25	3.4	2.3	5.7	9.4	7.1	0.45	.02	230	0	245	0

TABLE C-15

EFFECT OF DIFFERENT GAS MIXTURES ON WEAR RATE, COEFFICIENT OF FRICTION & EXTRAPOLATED SURFACE TEMPERATURE

UNHEATED SPECIMENS, NORMAL LOAD 490N

FLOW RATE: $75 \times 10^{-6} M^3 s^{-1}$ SLIDING SPEED $0.965 MS^{-1}$

PERCENT (O_2 in Ar) (V/V)	TEST NO.	WEAR RATE						COEFFICIENT OF FRICTION	EXTRAPOLATED SURFACE TEMPERATURE	
		WEAR VOLUME PER UNIT DISTANCE			WEAR MASS PER UNIT TIME					
		ROTATING SPECIMEN	STATIONARY SPECIMEN	TOTAL WEAR	ROTATING SPECIMEN	STATIONARY SPECIMEN	TOTAL WEAR		ROTATING SPECIMEN	STATIONARY SPECIMEN
		($\times 10^{-11}$ M^3/M OF SLIDING)			($\times 10^{-6}$ Kg/min)				^0C	
0 (Pure Ar)	86	1.84	-0.37	1.47	-	-		1.65	400	-
0.02	94	0.16	0.03	0.19	0.7	0.1	0.8	0.54	300	310
	95	0.14	0.03	0.17	0.6	0.1	0.7	0.54	310	320
0.20	90	0.46	0.28	0.74	2.1	1.3	3.4	0.52	-	300
	91	0.48	0.30	0.78	2.2	1.3	3.5	0.51	-	-
	92	0.42	0.26	0.58	1.4	1.2	2.6	0.50	295	-
	93	0.42	0.28	0.70	1.9	1.3	3.2	0.52	285	300
2.00	88	0.95	0.52	1.47	4.3	2.4	6.7	0.47	265	275
	89-1	0.96	0.60	1.56	4.4	2.7	7.1	0.49	255	270
	89-2	0.94	0.53	1.47	4.3	2.4	6.7	0.48	-	280

TABLE C-16

EFFECT OF DIFFERENT GAS MIXTURES ON COMPOSITION AND SIZE OF WEAR DEBRIS PARTICLES

UNHEATED SPECIMENS, NORMAL LOAD: 490N

FLOW RATE: $75 \times 10^{-6} M^3 S^{-1}$ SLIDING SPEED: $0.965 MS^{-1}$

PERCENT (V/V) O_2 in Ar	TEST NO.	COMPOSITION OF WEAR DEBRIS PARTICLES				SIZE OF 80% OF WEAR DEBRIS PARTICLES			
						COLLECTED UNDER THE SPECIMEN		COLLECTED ON FILTER PAPER	
		α Fe	FeO	Fe_3O_4	αFe_2O_3	MEDIAN	STANDARD DEVIATION	MEDIAN	STANDARD DEVIATION
						μm		μm	
0 (Pure Ar)	86	✓							
0.02	94	✓	✓						
	95	✓	✓			2.0	10.0	2.0	8.0
0.20	90	✓	✓	✓					
	91	✓	✓	✓					
	92	✓	✓	✓					
	93	✓	✓	✓		2.5	12.0	2.0	7.0
2.00	88	✓	✓	✓	✓				
	89-1	✓	✓	✓	✓	1.5	10.0	1.0	5.0
	89-2	✓	✓	✓	✓	1.5	8.0	1.0	5.0

TABLE C-17

LINEAR DISPLACEMENT (AMPLITUDE) AT LOWEST FREQUENCIES OF VIBRATION & INTEGRATED POWER SPECTRAL DENSITY

LOAD 490N, UNHEATED SPECIMENS, SPEED 0.965MS^{-1} VARIOUS GAS MIXTURES

(%)V/V O_2 in Ar	TEST NO.	FREQ. OF VIBRATION (HZ)	LINEAR DISPLACEMENT (AMPLITUDE) IN mM FOR ACCELEROMETERAT						PSD 3000 M_{20} g^2/HZ	
			A	B	B'	a	b	b'		
0.02	94	300	7*	25*		-	1*	4*		
		480-520	3	13		1*	1	-		
		650-670	-	2		-	-	1		
		800-850	1	-		-	-	-		
		950-1100	-	3		-	-	-		
		1300-1700	1	1		-	-	-		
	95	210-270	14*	35*		-	-	8	A 0.06	
		310-340	9	-		4*	2	11*	B 1.70	
		480	-	21		-	-	4	B' -	
		520-600	5	-		4	5	4	a 0.01	
		650-700	1	6		1	2	2	b -	
		900-1000	1	4		1	1	1	b' 0.01	
		1300-1400	-	1		-	-	1		
0.20	90	290-300	-	9*			-	22*		
		320	4*	-			-	-		
		400-480	-	4			1*	4		
		520	4*	4			-	-		
		670-700	1	1			1	-		
		850	-	-			-	-		
	91	300-360	3*	7		1	-			
		520-560	2	11*		-	1*			
		600-650	-	2		1*	1			
		800	-	-		-	-			
		950	-	-		-	-			
		1050-1100	-	2		-	-			
	92	210	14	4		4	-	4	A 0.10	
		300-320	24*	13		3	2.4	5	B 1.90	
		480-520	18	23*		11*	5*	5*	a 0.05	
		650-750	3	4		1	2	1	b 0.03	
		1050	2	8		-	-	-	b' 0.07	

Continued...

TABLE C-17

	TEST NO.	FREQ. OF VIBRATION (HZ)	LINEAR DISPLACEMENT (AMPLITUDE) IN μm FOR ACCELEROMETERAT						PSD $\frac{3000}{20}$ g^2/HZ	
			A	b	b'	a	b	b'		
	93	280	-	25*		-	-			
		340	17*	-		2	-			
		480-520	-	12		5*	-			
		560	11	-		-	1*			
		800	-	-		-	-			
		1100-1300	3	3		1	-			
2.0	89-1	290-320	38*	52*	-	15*	-	-	A = 2.20	
		420	16	-		-	4*	15*	B = 3.00	
		560	26	30		-		-	a = 1.8	
		670-750	8	8		10	3	12	b = 0.08	
		1100	-	9		-	-	-	b'= 1.7	
		1300	4	7		6	1	2		

TABLE C-18

MEAN VALUES AND STANDARD DEVIATION OF WEAR RATE, COEFFICIENT OF FRICTION & EXTRAPOLATED SURFACE TEMPERATURE

UNHEATED SPECIMENS, NORMAL LOAD: 49ON

DIFFERENT GAS MIXTURES SLIDING SPEED 1.158 MS^{-1}

PERCENT (V/V) O_2 IN Ar	WEAR RATE								COEFFICIENT OF FRICTION		EXTRAPOLATED SURFACE TEMPERATURE			
	VOLUME/UNIT DISTANCE			MASS/UNIT TIME			S.D/MEAN				ROTATING SIDE		STATIONARY SIDE	
	ROTATING SPECIMEN	STATIONARY SPECIMEN	TOTAL WEAR	ROTATING SPECIMEN	STATIONARY SPECIMEN	TOTAL WEAR	ROTATING SPECIMEN	STATIONARY SPECIMEN	MEAN	S.D.	MEAN	S.D.	MEAN	S.D.
	($X10^{-11}$ m^3/mofsliding)			($X10^{-6}$ kg/min)			%	%			^oC	^oC	^oC	^oC
0 (Pure Ar)	1.03	0.54	1.57	-	-	-	-	-	1.60		400		-	
0.02	0.30	0.28	0.58	1.6	1.5	3.1	2.7	2.8	0.64	.01	355	4	365	3
0.20	0.58	0.41	0.99	3.1	2.2	5.4	5.3	8.3	0.60	.01	340	0	355	3
2.00	0.97	0.65	1.62	5.3	3.5	8.8	1.7	3.5	0.54	.01	310	-	315	0
20.0 (Air)	1.15	0.77	1.95	6.3	4.2	10.5	5.9	15.2	0.50	.02	275	4	285	4

TABLE C-19

EFFECT OF VARIOUS GAS MIXTURES ON WEAR RATE, COEFFICIENT OF FRICTION & EXTRAPOLATED SURFACE TEMPERATURE

UNHEATED SPECIMENS, NORMAL LOAD 49ON

FLOW RATE: 75×10^{-6} $M^3 S^1$ SLIDING SPEED: 1.158 MS-1

PERCENT (V/V) O_2 in Ar	TEST NO.	WEAR RATE						COEFFICIENT OF FRICTION	EXTRAPOLATED SURFACE TEMPERATURE	
		WEAR VOLUME PER UNIT DISTANCE			WEAR MASS PER UNIT TIME					
		ROTATING SPECIMEN	STATIONARY SPECIMEN	TOTAL WEAR	ROTATING SPECIMEN	STATIONARY SPECIMEN	TOTAL WEAR		ROTATING SPECIMEN	STATIONARY SPECIMEN
		($X10^{-11}$ M^3/M OFSLIDING)			($X10^{-6}$ Kg/min)				^0C	
0 (Pure Ar)	87	1.03	0.54	1.57	-	-	-	1.60	400	-
0.02	96	0.29	0.27	0.56	1.6	1.5	3.1	0.64	350	360
	97-1	0.31	0.29	0.60	1.7	1.6	3.3	0.65	355	365
	97-2	0.30	0.28	0.58	1.6	1.5	3.1	0.63	360	365
0.20	98-1	0.55	0.36	0.91	3.0	2.0	5.0	-	-	-
	98-2	0.60	0.43	1.03	3.3	2.3	5.6	-	340	350
	99-1	0.62	0.45	1.07	3.4	2.4	5.8	0.61	340	355
	99-2	0.55	0.40	0.95	3.0	2.1	5.1	0.59	-	355
2.0	100-1	0.95	0.66	1.61	5.2	3.6	8.8	0.55	-	-
	100-2	0.99	0.670	1.66	5.4	3.6	9.0	0.53	-	315
	100-3	0.97	0.62	1.59	5.3	3.4	8.7	0.54	310	315

TABLE C-20

EFFECT OF VARIOUS GAS MIXTURES ON COMPOSITION AND SIZE OF WEAR DEBRIS PARTICLES

UNHEATED SPECIMENS, NORMAL LOAD: 490N

FLOW RATE: $75 \times 10^{-6} M^3 S^{-1}$ SLIDING SPEED $1.158 MS^{-1}$

PERCENT (V/V) O_2 in Ar	TEST NO.	COMPOSITION OF WEAR DEBRIS PARTICLES.				SIZE OF 80% OF WEAR DEBRIS PARTICLES.			
						COLLECTED UNDER THE SPECIMEN		COLLECTED ON FILTER PAPER	
		Fe	FeO	Fe_3O_4	Fe_2O_3	MEDIAN	STANDARD DEVIATION	MEDIAN	STANDARD DEVIATION
						μm		μm	
0 (Pure Ar)	87	✓	✓	✓	✓	-	-	-	-
0.02	96	✓	✓	✓	✓	1.5	5.5	1.0	4.0
	97-1	✓	✓			2.0	5.0	1.5	4.0
	97-2	✓	✓						
0.20	98-1	✓	✓	✓					
	98-2	✓	✓	✓					
	99-1	✓	✓	✓		2.5	6.0	2.0	5.0
	99-2	✓	✓	✓		2.5	6.0	2.0	5.5
2.0	100-1	✓	✓	✓	✓				
	100-2	✓	✓	✓	✓				
	100-3	✓	✓	✓	✓	2.0	6.0	1.0	5.0

TABLE C-21

LINEAR DISPLACEMENT (AMPLITUDE) AT LOWEST FREQUENCIES OF VIBRATION & INTEGRATED POWER SPECTRAL DENSITY

LOAD 490N, UNHEATED SPECIMENS, SPEED 1.158MS^{-1}, VARIOUS GAS MIXTURES.

% (V/V) O_2 in Ar	TEST NO.	FREQ. OF VIBRATION (HZ)	LINEAR DISPLACEMENT (AMPLITUDE) IN μm FOR ACCELEROMETER AT						PSD $\sum_{20}^{3000} g^2/HZ$	
			A	b	b'	a	b	b'		
0.02	96	210	14*	-		-	-	9*		
		250-280	-	35*		-	14*	-		
		320-340	10	-		4	4	8		
		480-520	13	13		6*	3	-		
		650	-	-		1	-	4		
		700-800	3	2		1	-	1		
		1100-1300	1	2		1	1	-		
	97-1	320	20*	10		-	2	2*		
		550	13	11*		1*	4*	1		
		700-750	-	-		-	1	-		
		1100-1150	1	2		-	-	-		
		1300	1	2		-	-	-		
		1400-1700	1	1		-	-	-		
0.20	98-1	270-300	34*	1		-	-			
		400-440	27	2*		-	-			
		480	-	-		4*	1*			
		700-750	2	-		-	1			
		800-850	1	1		1	-			
		1100	-	-		-	-			
	99-1	210	25	-		-	-	3		
		300-320	41*	48*		1*	-	3*		
		400-440	14	15		1	1	1		
		520	26	26		-	1	-		
		700-725	3	4		-	-	-		
		1050-1200	2	4		-	1	-		
2.00	100-1	280	-	22*		-	5			
		320-340	19*	-		3	-			
		550	13	10		6*	-			
		675	4	-		-	-			
		775	-	2		-	2			
		950	-	-		1	-			

TABLE C-22

MEAN VALUES AND STANDARD DEVIATION OF WEAR RATE, COEFFICIENT OF FRICTION & EXTRAPOLATED SURFACE TEMPERATURE

UNHEATED SPECIMENS, NO. AIR, NORMAL LOAD: 295N

SLIDING SPEED 0.965 MS^{-1}, VARIOUS SPECIMEN HOLDER TEMPERATURES.

SPEED	WEAR RATE								COEFFICIENT OF FRICTION		EXTRAPOLATED SURFACE TEMPERATURE			
	VOLUME/UNIT DISTANCE			MASS/UNIT TIME			S.D/MEAN				ROTATING SIDE		STATIONARY SIDE	
	ROTATING SPECIMEN	STATIONARY SPECIMEN	TOTAL WEAR	ROTATING SPECIMEN	STATIONARY SPECIMEN	TOTAL WEAR	ROTATING SPECIMEN	STATIONARY SPECIMEN	MEAN	S.D.	MEAN	S.D.	MEAN	S.D.
MS^{-1}	($X10^{-11} m^3$/mofsliding)			($X10^{-6}$ kg/min)			%	%			°C		°C	
0.965	0.55	0.50	1.05	2.5	2.3	4.8	4.5	3.3	0.37	0.01	140	-	145	4
1.158	0.83	0.77	1.60	4.5	4.1	8.6	18.6	12.3	0.64	0.02	195	-	210	4
1.544	0.44	0.36	0.80	3.2	2.7	5.9	9.1	5.6	0.55	0.01	207	3	220	0

TABLE C-23

EFFECT OF SLIDING SPEED ON WEAR RATE, COEFFICIENT OF FRICTION & EXTRAPOLATED SURFACE TEMPERATURE

UNHEATED SPECIMENS, NO AIR, NORMAL LOAD: 295N

SLIDING SPEED	TEST NO.	WEAR RATE						COEFFICIENT OF FRICTION	EXTRAPOLATED SURFACE TEMPERATURE	
		WEAR VOLUME PER UNIT DISTANCE			WEAR MASS PER UNIT TIME					
		ROTATING SPECIMEN	STATIONARY SPECIMEN	TOTAL WEAR	ROTATING SPECIMEN	STATIONARY SPECIMEN	TOTAL WEAR		ROTATING SPECIMEN	STATIONARY SPECIMEN
MS^{-1}		($X10^{-11}$ M^3/M OF SLIDING)			($X10^{-6}$ Kg/min)				^{o}C	
0.965	111-1	0.58	0.52	1.10	2.6	2.4	5.0	0.35	140	145
	111-2	0.52	0.48	1.00	2.4	2.2	4.6	0.37	-	150
	111-3	0.55	0.50	1.05	2.5	2.3	4.8	0.39	-	140
1.158	112-1	0.85	0.80	1.65	4.5	4.3	8.8	0.65	-	-
	112-2	1.00	0.90	1.90	5.4	4.8	10.2	0.66	-	205
	112-3	0.72	0.64	1.36	3.9	3.4	7.3	0.63	-	215
	113-1	0.75	0.74	1.49	4.0	4.0	8.0	0.62	195	210
1.544	114-1	0.48	0.38	0.86	3.5	2.8	6.3	0.54	205	220
	114-2	0.40	0.34	0.74	2.9	2.5	5.4	0.56	210	220

TABLE C-24

EFFECT OF SLIDING SPEED ON COMPOSITION

AND SIZE OF WEAR DEBRIS PARTICLES

UNHEATED SPECIMENS, NO AIR, NORMAL LOAD: 295N

SLIDING SPEED ms^{-1}	TEST NO.	COMPOSITION OF WEAR DEBRIS PARTICLES				SIZE OF 80% OF WEAR DEBRIS PARTICLES			
						COLLECTED UNDER THE SPECIMEN		COLLECTED ON FILTER PAPER	
		Fe	FeO	Fe_3O_4	Fe_2O_3	MEDIAN	STANDARD DEVIATION	MEDIAN	STANDARD DEVIATION
						μm		μm	
0.965	111-1	✓		✓	✓				
	111-2	✓		✓	✓				
	111-3	✓		✓	✓	1.5	12.0	1.5	10
1.158	112-1	✓	✓	✓	✓				
	112-2	✓	✓	✓	✓	1.5	6.0	1.5	5.0
	112-3	✓	✓	✓	✓	0.75	3.0	1.5	6.0
	113-1	✓	✓	✓	✓	1.00	4.0	1.0	6.0
1.544	114-1	✓	✓	✓	✓	0.75	3.0	1.0	6.0
	114-2	✓	✓	✓	✓				

TABLE C-25

MEAN VALUES AND STANDARD DEVIATION OF WEAR RATE,

COEFFICIENT OF FRICTION & EXTRAPOLATED SURFACE TEMPERATURE

UNHEATED SPECIMENS, WITH AIR, NORMAL LOAD: 295N

FLOW RATE OF AIR 75 x 10^{-6} M^3 s^{-1}

SPEED	WEAR RATE								COEFFICIENT OF FRICTION		EXTRAPOLATED SURFACE TEMPERATURE			
	VOLUME/UNIT DISTANCE			MASS/UNIT TIME			S.D/MEAN				ROTATING SIDE		STATIONARY SIDE	
	ROTATING SPECIMEN	STATIONARY SPECIMEN	TOTAL WEAR	ROTATING SPECIMEN	STATIONARY SPECIMEN	TOTAL WEAR	ROTATING SPECIMEN	STATIONARY SPECIMEN	MEAN	S.D.	MEAN	S.D.	MEAN	S.D.
MS^{-1}	($X10^{-11}$ m^3/mofsliding)			($X10^{-6}$ kg/min)			%	%			°C	°C	°C	°C
0.965	0.46	0.44	0.90	2.1	2.0	4.1	9.4	3.7	0.39	0	135	5	145	5
1.158	0.48	0.47	0.95	2.6	2.5	5.1	3.4	1.7	0.45	0	175	4	185	4
1.544	0.27	0.23	0.50	2.0	1.7	3.7	15.1	9.4	0.40	.01	180	4	195	2

TABLE C-25

MEAN VALUES AND STANDARD DEVIATION OF WEAR RATE, COEFFICIENT OF FRICTION & EXTRAPOLATED SURFACE TEMPERATURE

UNHEATED SPECIMENS, WITH AIR, NORMAL LOAD: 295N

FLOW RATE OF AIR 75 x 10^{-6} M^3 S^{-1}

SPEED	WEAR RATE								COEFFICIENT OF FRICTION		EXTRAPOLATED SURFACE TEMPERATURE			
	VOLUME/UNIT DISTANCE			MASS/UNIT TIME			S.D/MEAN				ROTATING SIDE		STATIONARY SIDE	
	ROTATING SPECIMEN	STATIONARY SPECIMEN	TOTAL WEAR	ROTATING SPECIMEN	STATIONARY SPECIMEN	TOTAL WEAR	ROTATING SPECIMEN	STATIONARY SPECIMEN	MEAN	S.D.	MEAN	S.D.	MEAN	S.D.
MS^{-1}	($X10^{-11}$ m^3/mofsliding)			($X10^{-6}$ kg/min)			%	%			°C	°C	°C	°C
0.965	0.46	0.44	0.90	2.1	2.0	4.1	9.4	3.7	0.39	0	135	5	145	5
1.158	0.48	0.47	0.95	2.6	2.5	5.1	3.4	1.7	0.45	0	175	4	185	4
1.544	0.27	0.23	0.50	2.0	1.7	3.7	15.1	9.4	0.40	.01	180	4	195	2

TABLE C-26

EFFECT OF SLIDING SPEED ON WEAR RATE, COEFFICIENT OF FRICTION

& EXTRAPOLATED SURFACE TEMPERATURE

UNHEATED SPECIMENS, WITH AIR, NORMAL LOAD: 295N

FLOW RATE OF AIR 75×10^{-6} M/S

SLIDING SPEED	TEST NO.	WEAR RATE						COEFFICIENT OF FRICTION	EXTRAPOLATED SURFACE TEMPERATURE	
		WEAR VOLUME PER UNIT DISTANCE			WEAR MASS PER UNIT TIME					
		ROTATING SPECIMEN	STATIONARY SPECIMEN	TOTAL WEAR	ROTATING SPECIMEN	STATIONARY SPECIMEN	TOTAL WEAR		ROTATING SPECIMEN	STATIONARY SPECIMEN
MS^{-1}		($X10^{-11}$ M^3/M OF SLIDING)			($X10^{-6}$ Kg/min)				^0C	
0.965	105-1	0.50	0.46	0.96	2.3	2.1	4.4	-	130	140
	105-2	0.40	0.42	0.82	1.8	1.9	3.7	0.39	140	150
	105-3	0.48	0.44	0.92	2.2	2.0	4.2	0.39	135	145
1.158	104-1	0.46	0.47	0.92	2.5	2.5	5.0	0.45	180	190
	104-2	0.50	0.48	0.98	2.1	2.6	5.3	0.45	170	180
	104-3	0.48	0.47	0.95	2.6	2.5	5.1	0.45	175	185
1.544	106-1	0.22	0.20	0.42	1.6	1.5	3.1	0.41	185	195
	106-2	0.32	0.25	0.57	2.3	1.9	4.2	0.40	175	193
	106-3	0.27	0.24	0.51	2.0	1.8	3.8	0.40	180	195

TABLE C-27

EFFECT OF SLIDING SPEED ON COMPOSITION AND SIZE OF WEAR DEBRIS PARTICLES

UNHEATED SPECIMENS, WITH AIR, NORMAL LOAD: 295N

FLOW RATE OF AIR 75×10^{-6} M^3/S

SPEED	TEST NO.	COMPOSITION OF WEAR DEBRIS PARTICLES				SIZE OF 80% OF WEAR DEBRIS PARTICLES			
						COLLECTED UNDER THE SPECIMEN		COLLECTED ON FILTER PAPER	
		Fe	FeO	Fe_3O_4	Fe_2O_3	MEDIAN	STANDARD DEVIATION	MEDIAN	STANDARD DEVIATION
MS^{-1}						μm		μm	
0.965	105-1	✓		✓	✓				
	105-2	✓		✓	✓	1.5	4.0	1.0	4.5
	105-3	✓		✓	✓				
1.158	104-1	✓	✓	✓	✓				
	104-2	✓	✓	✓	✓				
	104-3	✓	✓	✓	✓	1.0	4.5	1.0	3.5
1.544	106-1	✓	✓	✓	✓				
	106-2	✓	✓	✓	✓				
	106-3	✓	✓	✓	✓	1.0	3.0	0.75	3.0

TABLE C-28

LINEAR DISPLACEMENT (AMPLITUDE) AT LOWEST FREQUENCIES OF VIBRATION & INTEGRATED POWER SPECTRAL DENSITY

LOAD 295N, WITH AIR, UNHEATED SPECIMENS, VARIOUS SLIDING SPEEDS

SLIDING SPEED	TEST NO.	FREQ. OF VIBRATION (HZ)	LINEAR DISPLACEMENT (AMPLITUDE) IN μm FOR ACCELEROMETERAT						PSD $\sum_{20}^{3000} g^2/HZ$	
			A	B	B'	a	b	b'		
MS^{-1}										
		290	29	33		4	-	15	A - 1.8	
		360-380				4	3	-	B - 3	
1.158	104.2	460-480	19	19		7	-	5	B'- -	
		520	-	-		-	6	-	a - .36	
		650-670	5	4		1	1	2	b - .22	
		750-850	1	2		-	1	-	b'- .23	
		950-1100	2	2		1	1	1		
		280	31	31		3	10	16		
		475-500	14	22		7	4	7		
		650-680	7	-		1	4	7		
1.544	106-1	750-850	2	-		-	1	-		
		900-1000	-	-		1	1	1		
		1150-1300	1	2		1	-	-		

TABLE C-29

MEAN VALUES AND STANDARD DEVIATION OF WEAR RATE,

COEFFICIENT OF FRICTION & EXTRAPOLATED SURFACE TEMPERATURE

UNHEATED SPECIMENS, NORMAL LOAD: 295N

DIFFERENT GAS MIXTURES SLIDING SPEED 1.158MS^{-1}

PERCENT (V/V)	WEAR RATE								COEFFICIENT OF FRICTION		EXTRAPOLATED SURFACE TEMPERATURE			
	VOLUME/UNIT DISTANCE			MASS/UNIT TIME			S.D/MEAN				ROTATING SIDE		STATIONARY SIDE	
O_2 in Ar	ROTATING SPECIMEN	STATIONARY SPECIMEN	TOTAL WEAR	ROTATING SPECIMEN	STATIONARY SPECIMEN	TOTAL WEAR	ROTATING SPECIMEN	STATIONARY SPECIMEN	MEAN	S.D.	MEAN	S.D.	MEAN	S.D.
	($\times 10^{-11}$ m^3/mofsliding)			($\times 10^{-6}$ kg/min)			%	%			°C	°C	°C	°C
0 (Pure Ar)	0.33	-0.14	0.19	-	-	-	-	-	175	-	375	-	-	-
0.02	0.28	0.25	0.53	1.5	1.3	2.8	2.1	3.3	0.60	.01	290	4	305	4
0.20	0.30	0.26	0.56	1.6	1.4	3.0	8.4	5.4	0.48	.03	246	5	255	4
2.00	0.44	0.38	0.82	2.4	2.1	4.5	3.7	2.1	0.47	.01	220	0	230	4
20.00 (Air)	0.48	0.47	0.95	2.6	2.5	5.1	3.4	1.7	0.45	0	175	4	180	4

TABLE C-30

EFFECT OF DIFFERENT GAS MIXTURES ON WEAR RATE, COEFFICIENT OF FRICTION & EXTRAPOLATED SURFACE TEMPERATURE

UNHEATED SPECIMENS, NORMAL LOAD 295N

FLOW RATE: $75 \times 10^{-6} M^3 s^{-1}$ SLIDING SPEED 1.158 MS^{-1}

PERCENT (V/V) O_2 in Ar	TEST NO.	WEAR RATE						COEFFICIENT OF FRICTION	EXTRAPOLATED SURFACE TEMPERATURE	
		WEAR VOLUME PER UNIT DISTANCE			WEAR MASS PER UNIT TIME					
		ROTATING SPECIMEN	STATIONARY SPECIMEN	TOTAL WEAR	ROTATING SPECIMEN	STATIONARY SPECIMEN	TOTAL WEAR		ROTATING SPECIMEN	STATIONARY SPECIMEN
		($X10^{-11}$ M^3/M OF SLIDING)			($X10^{-6}$ Kg/min)				^0C	
0 (Pure Ar)	85	0.33	-0.14	0.19	-	-	-	1.75	375	-
0.02	107-1	0.27	0.25	0.52	1.5	1.3	2.8	0.60	290	305
	107-2	0.30	0.26	0.56	1.6	1.4	3.0	0.59	285	300
	107-3	0.27	0.24	0.51	1.5	1.3	2.8	0.61	295	310
0.20	108-1	0.27	0.24	0.51	1.5	1.3	2.8	0.50	245	255
	108-2	0.32	0.27	0.59	1.7	1.5	3.2	0.44	244	255
	108-3	0.31	0.25	0.56	1.7	1.3	3.0	0.52	255	260
	109-1	0.27	0.26	0.53	1.5	1.4	2.9	0.50	240	250
	109-2	0.33	0.28	0.61	1.8	1.5	3.3	0.44	-	-
2.00	110-1	0.44	0.39	0.83	2.4	2.1	4.5	-	-	235
	110-2	0.42	0.37	0.79	2.3	2.0	4.3	0.46	220	230
	110-3	0.46	0.38	0.84	2.5	2.1	4.6	0.48	220	240

TABLE C-31

EFFECT OF DIFFERENT GAS MIXTURES ON COMPOSITION AND SIZE OF WEAR DEBRIS PARTICLES

UNHEATED SPECIMENS, NORMAL LOAD: 295N

FLOW RATE: $75 \times 10^{-6} M^3 S^{-1}$

SLIDING SPEED: $1.158 MS^{-1}$

PERCENT (V/V) O_2 in Ar	TEST NO.	COMPOSITION OF WEAR DEBRIS PARTICLES				SIZE OF 80% OF WEAR DEBRIS PARTICLES			
						COLLECTED UNDER THE SPECIMEN		COLLECTED ON FILTER PAPER	
		Fe	FeO	Fe_3O_4	Fe_2O_3	MEDIAN	STANDARD DEVIATION	MEDIAN	STANDARD DEVIATION
						μm		μm	
0 (Pure Ar)									
0.02	107-1	✓	✓			2.0	6.0	1.5	3.0
	107-2	✓	✓						
	107-3	✓	✓						
0.20	108-1	✓	✓	✓		2.5	7.0	2.0	5.0
	108-2	✓	✓	✓					
	108-3	✓	✓	✓		2.0	6.0	2.0	5.0
	109-1	✓	✓	✓		2.0	6.0	2.0	4.5
	109-2	✓	✓	✓					
2.0	110-1	✓	✓	✓	✓	1.5	5.0	1.0	4.0
	110-2	✓	✓	✓	✓				
	110-3	✓	✓	✓	✓	1.0	4.0	1.0	3.5

TABLE C-32

LINEAR DISPLACEMENT (AMPLITUDE) AT LOWEST FREQUENCIES OF VIBRATION & INTEGRATED POWER SPECTRAL DENSITY

LOAD 295N, UNHEATED SPECIMENS, SPEED 1.158MS^{-1}, VARIOUS GAS MIXTURES

% (V/V) O_2 in Ar	TEST NO.	FREQ. OF VIBRATION (HZ)	LINEAR DISPLACEMENT (AMPLITUDE) IN μm FOR ACCELEROMETERAT						PSD $\sum_{20}^{3000} g^2$/HZ	
			A	B	B'	a	b	b'		
0.02	107-1	290-300	24	29		4	5			
		500	22	16		7	6			
		650-675	7	4		3	3			
		1200-1400	2	1		1	-			
		1700	1	1		-	1			
		2100-2300	-	-		-	-			
	108-1	280-335	20	16		4	4	5		
		475-550	15	23		20	4	2		
		675-725	4	4		1	2	1		
		1000-1150	-	2		1	1	1		
		1300-1400	2	-		-	-	-		
	109-1	280-320	6	12		4	-	7		
		440	12	-		-	2	-		
		520-540	-	6		3	2	3		
		650-700	2	3		1	1	1		
		800-850	1	-		1	1	-		
		1050-1200	2	2		-	-	-		
2.00	110-2	300-320	1	2		1	1	4		
		440	3	2		-	-	-		
		650	22	7		3	3	2		
		800-850	1	2		1	1	2		
		1300-1400	3	1		1	1	1		

TABLE C-33

MEAN VALUES AND STANDARD DEVIATION OF WEAR RATE,

COEFFICIENT OF FRICTION & EXTRAPOLATED SURFACE TEMPERATURE

UNHEATED SPECIMENS, NO AIR, NORMAL LOAD: 980N

SPEED	WEAR RATE								COEFFICIENT OF FRICTION		EXTRAPOLATED SURFACE TEMPERATURE			
	VOLUME/UNIT DISTANCE			MASS/UNIT TIME			S.D/MEAN				ROTATING SIDE		STATIONARY SIDE	
	ROTATING SPECIMEN	STATIONARY SPECIMEN	TOTAL WEAR	ROTATING SPECIMEN	STATIONARY SPECIMEN	TOTAL WEAR	ROTATING SPECIMEN	STATIONARY SPECIMEN	MEAN	S.D.	MEAN	S.D.	MEAN	S.D.
ms^{-1}	($\times 10^{-11} m^3$/mofsliding).			($\times 10^{-6}$ kg/min)			%	%			°C		°C	°C
0.772	2.02	1.93	3.95	7.4	7.1	14.5	3.5	6.3	0.46	.01	330	-	340	5
0.965	1.53	1.47	3.00	7.0	6.7	13.7	6.2	1.5	0.48	-	450	11	475	15
1.158	1.80	1.70	3.50	9.8	9.3	19.1	-	-	0.70	-	600	-	620	-

TABLE C-34

EFFECT OF SLIDING SPEED ON WEAR RATE, COEFFICIENT OF FRICTION & EXTRAPOLATED SURFACE TEMPERATURE

UNHEATED SPECIMENS, NO AIR NORMAL LOAD 98ON

SLIDING SPEED	TEST NO.	WEAR RATE						COEFFICIENT OF FRICTION	EXTRAPOLATED SURFACE TEMPERATURE	
		WEAR VOLUME PER UNIT DISTANCE			WEAR MASS PER UNIT TIME					
		ROTATING SPECIMEN	STATIONARY SPECIMEN	TOTAL WEAR	ROTATING SPECIMEN	STATIONARY SPECIMEN	TOTAL WEAR		ROTATING SPECIMEN	STATIONARY SPECIMEN
ms^{-1}		($X10^{-11}$ M^3/M OFSLIDING)			($X10^{-6}$ Kg/min)				^0C	
0.772	115-1	2.02	1.98	4.00	7.4	7.3	14.7	0.47	-	345
	115-2	2.05	1.95	4.00	7.5	7.2	14.7	0.45	-	335
	115-3	1.91	1.73	3.64	7.0	6.3	13.3	-	-	345
	115-4	2.10	2.06	4.16	7.7	7.5	15.2	0.46	330	335
0.965	116-1	1.62	1.50	3.12	7.4	6.8	14.2	0.48	435	-
	116-2	1.40	1.45	2.85	6.4	6.6	13.0	-	460	460
	116-3	1.57	1.46	3.03	7.1	6.7	13.8	-	455	490
1.158	117-1	1.80	1.70	3.50	9.8	9.3	19.1	0.7	600	620

TABLE C-35

EFFECT OF SLIDING SPEED ON COMPOSITION AND SIZE OF WEAR DEBRIS PARTICLES

UNHEATED SPECIMENS, NO AIR, NORMAL LOAD: 980N

SLIDING SPEED ms^{-1}	TEST NO.	COMPOSITION OF WEAR DEBRIS PARTICLES				SIZE OF 80% OF WEAR DEBRIS PARTICLES			
						COLLECTED UNDER THE SPECIMEN		COLLECTED ON FILTER PAPER	
		Fe	FeO	Fe_3O_4	Fe_2O_3	MEDIAN	STANDARD DEVIATION	MEDIAN	STANDARD DEVIATION
						μm		μm	
0.772	115-1	✓		✓	✓				
	115-2	✓		✓	✓				
	115-3	✓		✓	✓				
	115-4	✓		✓	✓				
0.965	116-1	✓		✓	✓				
	116-2	✓		✓	✓				
	116-3	✓		✓	✓				
1.158	117-1	✓	✓	✓	✓				

TABLE C-36

MEAN VALUES AND STANDARD DEVIATION OF WEAR RATE,

COEFFICIENT OF FRICTION & EXTRAPOLATED SURFACE TEMPERATURE

HEATED SPECIMENS, WITH AIR, NORMAL LOAD: 98ON

FLOW RATE OF AIR 75×10^{-6} $m^3 s^{-1}$

SPEED	WEAR RATE								COEFFICIENT OF FRICTION		EXTRAPOLATED SURFACE TEMPERATURE			
	VOLUME/UNIT DISTANCE			MASS/UNIT TIME			S.D/MEAN				ROTATING SIDE		STATIONARY SIDE	
	ROTATING SPECIMEN	STATIONARY SPECIMEN	TOTAL WEAR	ROTATING SPECIMEN	STATIONARY SPECIMEN	TOTAL WEAR	ROTATING SPECIMEN	STATIONARY SPECIMEN	MEAN	S.D.	MEAN	S.D.	MEAN	S.D.
ms^{-1}	($X10^{-11}$ m^3/mofsliding)			($X10^{-6}$ kg/min)			%				°C		°C	
0.772	1.71	1.39	3.10	6.3	5.1	11.4			0.42		300		305	
0.965	0.60	0.45	1.05	2.7	2.1	4.8			0.47		440		450	
1.158	0.57	0.53	1.10	3.1	2.9	6.0			0.63		550		565	

TABLE C-37

EFFECT OF SLIDING SPEED ON WEAR RATE, COEFFICIENT OF FRICTION & EXTRAPOLATED SURFACE TEMPERATURE

UNHEATED SPECIMENS, WITH AIR, NORMAL LOAD 98ON

FLOW RATE OF AIR, 75×10^{-6} $m^3 s^{-1}$

SLIDING SPEED	TEST NO.	WEAR RATE						COEFFICIENT OF FRICTION	EXTRAPOLATED SURFACE TEMPERATURE	
		WEAR VOLUME PER UNIT DISTANCE			WEAR MASS PER UNIT TIME					
		ROTATING SPECIMEN	STATIONARY SPECIMEN	TOTAL WEAR	ROTATING SPECIMEN	STATIONARY SPECIMEN	TOTAL WEAR		ROTATING SPECIMEN	STATIONARY SPECIMEN
ms^{-1}		($X10^{-11}$ M^3/M OF SLIDING)			($X10^{-6}$ Kg/min)				^0C	
0.772	102-1	1.52	1.31	2.83	5.6	4,8	10.4	-	-	-
	102-2	1.70	1.35	3.05	6.2	5.0	11.2	0.43	-	-
	102-3	1.80	1.40	3.20	6.6	5.1	11.7	0.42	-	305
	102-4	1.82	1.50	3.32	6.7	5.5	12.2	0.42	300	305
0.965	101-1	0.55	0.40	0.95	2.5	1.8	4.3	0.47	445	460
	101-2	0.67	0.48	1.15	3.0	2.2	5.2	0.47	435	440
	101-3	0.58	0.47	1.05	2.6	2.1	4.7	0.48	440	450
1.158	103-1	0.57	0.53	1.10	3.1	2.9	6.0	0.63	550	565

TABLE C-38

EFFECT OF SLIDING SPEED ON COMPOSITION AND SIZE OF WEAR DEBRIS PARTICLES

UNHEATED SPECIMENS, WITH AIR, NORMAL LOAD: 98ON

FLOW RATE OF AIR 75 x 10^{-6} $m^3 s^{-1}$

SLIDING SPEED ms^{-1}	TEST NO.	COMPOSITION OF WEAR DEBRIS PARTICLES				SIZE OF 80% OF WEAR DEBRIS PARTICLES			
						COLLECTED UNDER THE SPECIMEN		COLLECTED ON FILTER PAPER	
		Fe	FeO	Fe_3O_4	Fe_2O_3	MEDIAN	STANDARD DEVIATION	MEDIAN	STANDARD DEVIATION
						μm		μm	
0.772	102-1	✓		✓	✓				
	102-2	✓		✓	✓				
	102-3	✓		✓	✓				
	102-4	✓		✓	✓				
0.965	101-1			✓	✓				
	101-2			✓	✓				
	101-3	✓		✓	✓				
1.158	103-1	✓	✓	✓	✓				

TABLE C-39

LINEAR DISPLACEMENT (AMPLITUDE) AT LOWEST FREQUENCIES OF VIBRATION & INTEGRATED POWER SPECTRAL DENSITY

LOAD 98ON WITH AIR UNHEATED SPECIMENS, VARIOUS SLIDING SPEEDS

SLIDING SPEED ms^{-1}	TEST NO.	FREQ. OF VIBRATION (HZ)	LINEAR DISPLACEMENT (AMPLITUDE) IN μm FOR ACCELEROMETERAT						PSD $\sum_{20}^{3000} g^2/HZ$	
			A	B	B'	a	b	b'		
0.772	102-1	290-300	24*	52*		12*	7*	17*		
		480	21	-		-	-	6		
		520	-	16		-	4	-		
		600	-	-		5	-	-		
		750-950	-	-		2	3	1		
		1200-1300	3	3		1	-	1		
0.965	101-1	480	-	15		-	-	-		
		580	-	-		-	3	-		
		650-670	11*	19*		1	4*	-		
		800	-	2		-	-	-		
		1300-1400	5	3		1	1	-		
1.158	103-1	210	-	9		-	-	-	A-9	
		270-290	85*	-		23*	7*	47*	B-3.4	
		340	-	13*		-	5	-	a-5	
		440-480	51	-		22	-	8	b-2.4	
		560-650	-	16		3	6	-	b'-1.8	
		700-750	7	4		-	6	-		
		900-1200	4	4		3	2	2		